9. SITE 638[1]

Shipboard Scientific Party[2]

HOLE 638A

Date occupied: 5 May 1985

Date departed: 6 May 1985

Time on hole: 18 hr

Position: 42°09.2′N, 12°11.8′W

Water depth (sea level, corrected m, echo-sounding): 4661

Water depth (rig floor, corrected m, echo-sounding): 4671

Bottom felt (m, drill pipe): 4673

Penetration (m): 44

Number of cores: None

Total length of cored section (m): 0

Total core recovered (m): 0

Core recovery (%): 0

HOLE 638B

Date occupied: 6 May 1985

Date departed: 12 May 1985

Time on hole: 6 days, 21 hr

Position: 42°09.2′N, 12°11.8′W (100 m east of Hole 638A)

Water depth (sea level, corrected m, echo-sounding): 4661

Water depth (rig floor, corrected m, echo-sounding): 4671

Bottom felt (m, drill pipe): 4673

Penetration (m): 431.1

Number of cores: 45

Total length of cored section (m): 431.1

Total core recovered (m): 210.5

Core recovery (%): 49

Deepest sedimentary unit cored:
Depth sub-bottom (m): 431.1
Nature: sandstone and claystone
Age: late Valanginian
Measured vertical sound velocity (km/s): 4.0 and 2.2, respectively

HOLE 638C

Date occupied: 12 May 1985 (1); 1 June 1985 (2)

Date departed: 23 May 1985 (1); 3 June 1985 (2)

Time on hole: 12 days, 16 hr

Position: 42°09.2′N, 12°11.8′W (100 m east and 30 m south of Hole 638A)

Water depth (sea level, corrected m, echo-sounding): 4661

Water depth (rig floor, corrected m, echo-sounding): 4671

Bottom felt (m, drill pipe): 4673

Penetration (m): 547.2

Number of cores: 14

Total length of cored section (m): 135.3

Total core recovered (m): 37.7

Core recovery (%): 28

Deepest sedimentary unit cored:
Depth sub-bottom (m): 547.2
Nature: sandstone and claystone
Age: Valanginian
Measured vertical sound velocity (km/s): 4.4 and 2.5, respectively

Principal results: Three holes were drilled at Site 638: Hole 638A as an engineering test hole, Hole 638B as a pilot hole to prepare for reentry operations, and Hole 638C as a multiple reentry hole.

The stratigraphic column, combining data from Holes 638B and 638C, to a depth of 547.2 meters below seafloor (mbsf), shown graphically in Figure 1, consists of the following intervals:

1. 0–183.6 m: upper Miocene to Pleistocene nannofossil ooze and chalk, occurring as a submarine valley fill.
2. 183.6–212.6 m: upper Barremian bioturbated micrite and couplets of laminated claystone and marlstone.

[1] Boillot, G., Winterer, E. L., Meyer, A. W., et al., *Proc. Init. Repts. (Pt. A), ODP*, 103.

[2] Gilbert Boillot (Co-Chief Scientist), Laboratoire de Géodynamique Sous-Marine, Université Pierre et Marie Curie, B.P. 48, 06230, Villefranche-sur-Mer, France; Edward L. Winterer (Co-Chief Scientist), Graduate Research Division A-012-W, Scripps Institution of Oceanography, La Jolla, CA 92093; Audrey W. Meyer (ODP Staff Scientist), Ocean Drilling Program, Texas A&M University, College Station, TX 77843-3469; Joseph Applegate, Department of Geology, Florida State University, Tallahassee, FL 32306; Miriam Baltuck, Department of Geology, Tulane University, New Orleans, LA 70118 (current address: NASA Headquarters, Code EEL, Washington, D.C. 20546); James A. Bergen, Department of Geology, Florida State University, Tallahassee, FL 32306; M. C. Comas, Departamento Estratigrafia y Paleontologia, Facultad de Ciencias, Universidad de Granada, 18001 Granada, Spain; Thomas A. Davies, Institute for Geophysics, University of Texas at Austin, 4920 North IH 35, Austin, TX 78751; Keith Dunham, Department of Atmospheric and Oceanic Sciences, University of Michigan, 2455 Hayward Avenue, Ann Arbor, MI 48109 (current address: P.O. Box 13, Pequat Lakes, MN 56478); Cynthia A. Evans, Department of Geology, Colgate University, Hamilton, NY 13346 (current address: Lamont-Doherty Geological Observatory, Palisades, NY 10964); Jacques Girardeau, Laboratoire de Materiaux Terrestres, I.P.G., 4 Place Jussieu, 75252 Paris Cedex 05, France; David Goldberg, Lamont-Doherty Geological Observatory, Palisades, NY 10964; Janet Haggerty, Department of Geology, University of Tulsa, 600 S. College Avenue, Tulsa, OK 74104; Lubomir F. Jansa, Atlantic Geoscience Center, Bedford Institute of Oceanography, Dartmouth, Nova Scotia B2Y 4A2, Canada; Jeffrey A. Johnson, Department of Earth and Space Sciences, University of California, Los Angeles, CA 90024 (current address: 9449 Briar Forest Drive, No. 3544, Houston, TX 77063); Junzo Kasahara, Earthquake Research Institute, University of Tokyo, 1,1,1 Yayoi, Bunkyo, Tokyo 113, Japan (current address: Nippon Schlumberger K.K., 2-1 Fuchinobe, 2-Chome, Sagamihara-shi, Kanagawa-Ken, 229, Japan); Jean-Paul Loreau, Laboratoire de Géologie, Museum National D'Histoire Naturelle, 43 Rue Buffon, 75005 Paris, France; Emilio Luna, Hispanoil, Pez Volador No. 2, 28007 Madrid, Spain; Michel Moullade, Laboratoire de Géologie et Micropaleontologie Marines, Université de Nice, Parc Valrose, 06034 Nice Cedex, France; James Ogg, Geological Research Division A-012, Scripps Institution of Oceanography, La Jolla, CA 92093 (current address: Dept. Earth and Atmospheric Sciences, Purdue University, W. Lafayette, IN 47907); Massimo Sarti, Istituto di Geologia, Universitá di Ferrara, Corso Ercole d'Este, 32, 44100 Ferrara, Italy; Jürgen Thurow, Institut und Museum für Geologie und Paleontologie, Universität Tübingen, Sigwartstr. 10, D-7400 Tübingen, Federal Republic of Germany; Mark A. Williamson, Atlantic Geoscience Centre, Geological Survey of Canada, Bedford Institute of Oceanography, Box 1006, Dartmouth, Nova Scotia B2Y 4A2, Canada (current address: Shell Canada Ltd., P.O. Box 100, Stn. M, Calgary, Alberta T2P 2H5, Canada).

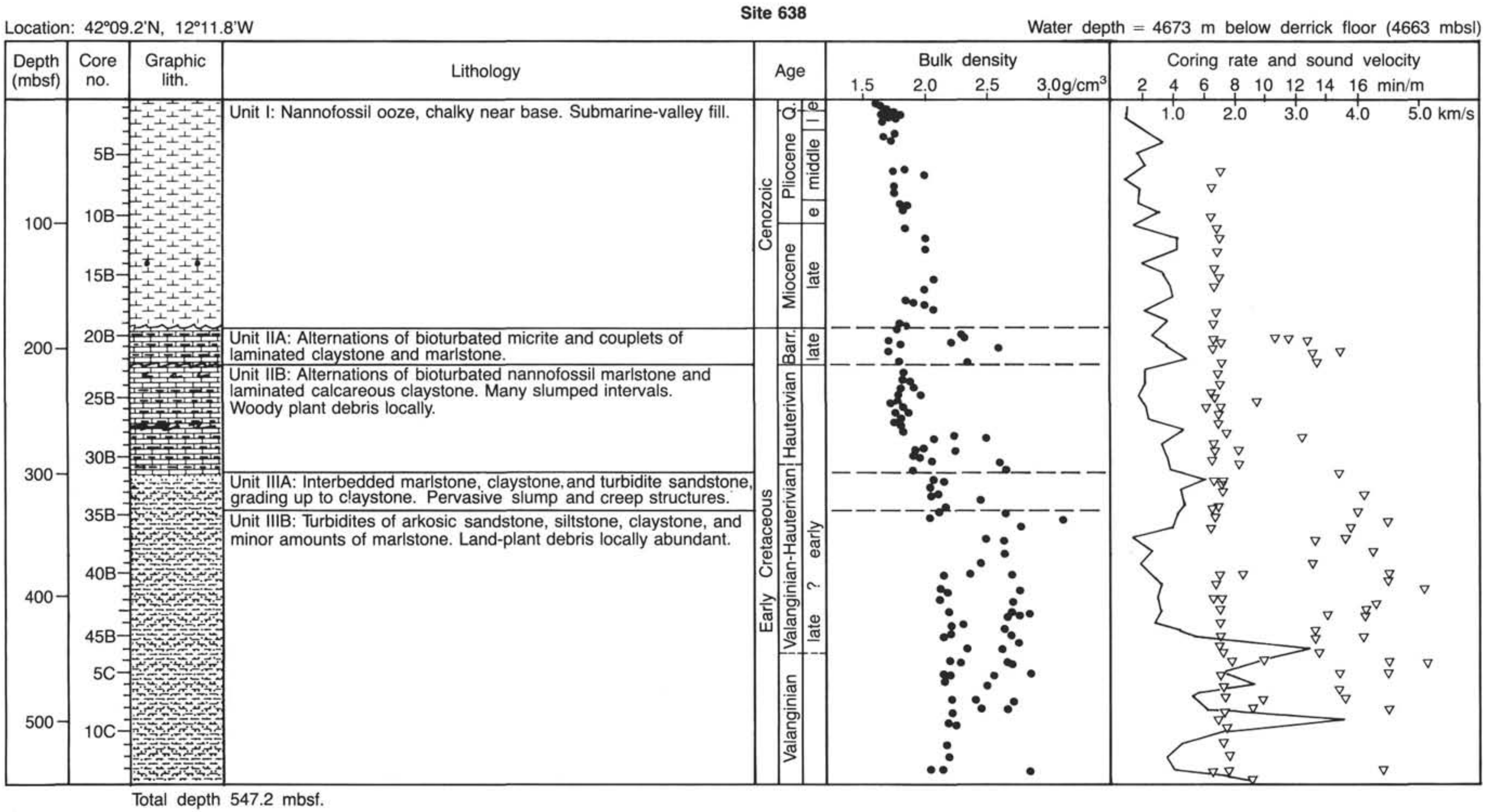

Figure 1. Stratigraphic summary log of Site 638 (Holes 638B and 638C).

3. 212.6–298.4 m: Hauterivian; alternations of bioturbated nannofossil marlstone and laminated calcareous claystone, with many slumped intervals. Woody plant debris is abundant locally.

4. 289.4–329.9 m: upper Valanginian to lower Hauterivian. Interbedded marlstone, claystone, and turbidite sandstone, grading up to claystone, with pervasive slump and creep structures.

5. 329.9–547.2 m: upper Valanginian to lower Hauterivian turbidites of arkosic sandstone, siltstone, and claystone, with minor amounts of marlstone. Land-plant debris is locally abundant.

Downhole logs of gamma ray, resistivity, sonic velocity, and density were taken over the interval from about 105 to 270 mbsf. These, in combination with laboratory measurements of velocity and density, provide an estimated thickness of about 40–75 m between the bottom of Hole 638C and the top of the carbonate platform, later drilled at Site 639 (see Site 639 chapter, this volume).

Finding Lower Cretaceous turbidite beds beneath the seismic reflector previously identified as the top of the pre-rift carbonate platform further illuminates the history of the Galicia margin, extending the syn-rift period back to at least the Valanginian and necessitating a reassessment of the regional seismic stratigraphy.

BACKGROUND AND OBJECTIVES

In addition to the general information on regional geology of the Galicia margin contained in the "Introduction, Objectives, and Principal Results" chapter (this volume), some data are pertinent from dredging near Site 638 at Stations DRO1 and DRO3 (Figs. 2 and 3) (Mougenot et al., 1985). Station DRO3 is only about 6 km northwest of Site 638, on the steep escarpment that exposes the lower part of the stratigraphic sequence scheduled for coring at the drill site (Fig. 3). The single dredge haul at station DRO3 contained fragments of many rock types: (1) crystalline rocks from the basement, including quartz monzonite, mylonitized granodiorite, and fresh basalt; (2) schist and argillite, tentatively assigned to the Lower Paleozoic; (3) litharenite and graywacke, resembling rocks from the Permian–Carboniferous, or perhaps from the Triassic or Ordovician sandstones in Portugal; (4) red sandstone, without fossils but resembling certain sandstones from the Triassic of Portugal; and (5) limestone of shallow-water facies, assigned to the Upper Jurassic or Lower Cretaceous.

The dredge data led Mougenot et al. (1985) and Boillot (pers. comm., 1985) to interpret seismic Unit 5 (Figs. 2 and 3) as being pre-rift carbonate-platform rocks, either resting directly on basement ("S" in Fig. 3) or occurring with Triassic sandstone between the limestone and basement. This in turn led to the interpretation of seismic Unit 4 as being a sequence of Lower Cretaceous syn-rift strata.

The fundamental processes, such as lithospheric thinning, faulting, and subsidence, that control the evolution of a passive continental margin cannot be clearly understood without a knowledge of the timing of these events. Cores from Site 638 were collected (1) to yield reliable data about the early history of the margin and about the timing of rifting and (2) to provide important information on the timing of the paleoenvironmental changes in this North Atlantic region. Specific problems investigated include the following:

1. The petrology and mutual relations of the rocks of the crystalline basement and the relations of these rocks to those exposed on the mainland of Iberia.

2. The rates and amounts of subsidence from the Triassic to the Late Jurassic, as clues to the history of crustal thinning before the onset of oceanic-crustal accretion.

3. The timing of the first appearance of marine waters, in what later became the oceanic rift, and the provincial relations of the biota in those waters.

4. The timing and drowning rates of the Jurassic carbonate platform.

5. The timing of significant transgressions and regressions, shifts in coastal onlap relations, and development of unconformities to evaluate the effects of eustasy and vertical tectonic movements on the stratigraphy of this margin.

6. The determination of the age and physical significance of the many key seismic reflectors, as a prerequisite to regional interpretation of the observed seismic stratigraphy.

7. The timing of significant changes in major oceanographic variables such as temperature, oxygenation, fertility, bottom-current activity, and dissolution of carbonates.

The combination of continuous cores and downhole logs from Site 638, traversing the syn-rift and pre-rift sedimentary strata into the basement (Fig. 2), should reveal nearly the entire history of the margin, from the succession of rifting phases during the Mesozoic through the drowning of the carbonate platform and the progressive or sudden changes in the environment during the initiation of seafloor spreading.

OPERATIONS

Approach to Site 638

The transit to Site 638 began at 2105 hr on 4 May 1985, when *JOIDES Resolution* got under way from Site 637. We immediately learned how seismic-profiling procedures on this vessel are different from those used for so many years on *Glomar Challenger.* The *Resolution* steamed south at slow speed until the seismic-profiling gear was streamed. Then the ship turned back to head due north in the customary attempt to cross over the acoustic beacon on the seafloor at Site 637, a procedure that provides a sure seismic-reflection picture directly over the drill site. When *JOIDES Resolution* steams at speeds of more than about 1 kt, the hydrophones that receive the beacon signal are withdrawn for protection into wells within the hull, but because of the turbulence across the mouth of the wells, these signals are blocked out. We could only thus estimate our position with respect to the unheard beacon. Clearly, this experiment indicates that any seismic profiling done from the drill ship to establish the acoustic stratigraphy at a drill site must be done at the same time the beacon is dropped, while the ship is underway.

The ship continued north from Site 637 until our track intersected the track of multichannel seismic line GP-101, made by the Institut Français du Pétrole, that runs eastward across the planned location of Site 638 (Fig. 2B, this chapter). The ship then turned due east, and we attempted to follow this seismic line to the site. In fact, the ship had drifted somewhat south of the planned track; therefore, we changed course to a heading of about 070°. By the time we neared the area of Site 638 (Fig. 4), a satellite fix indicated that we were about 2 km north of line GP-101. This was quickly confirmed when the ship crossed the axis of the broad submarine valley at a depth shallower than was expected at the planned location of the site (at shotpoint 3095 on GP-101).

Next we made a back-and-forth survey to place ourselves either at shotpoint 3095 or at a place similar to it in the seismic stratigraphy. Concurrently, we used the 3.5-kHz echo-sounder to confirm that we would drop the acoustic beacon where a cover of soft sediments was sufficiently thick (about 100 m) to protect the bottom-hole assembly (BHA). A combination of wind and current caused the ship to drift appreciably, as apparent in the difference in width of the submarine valley on the echo-sounder records as we steamed on reciprocal courses. Because of infrequent satellite fixes, our dead reckoning was inadequate to position ourselves with much certainty; we, therefore, concentrated on finding a site appearing as much as possible like shotpoint 3095 (Fig. 5), even though arrival at the exact shotpoint seemed unlikely. At 0613 hr on 5 May 1985, we dropped a beacon where the reflection profile met the requirements we had set. We continued the profile well beyond the site of the dropped

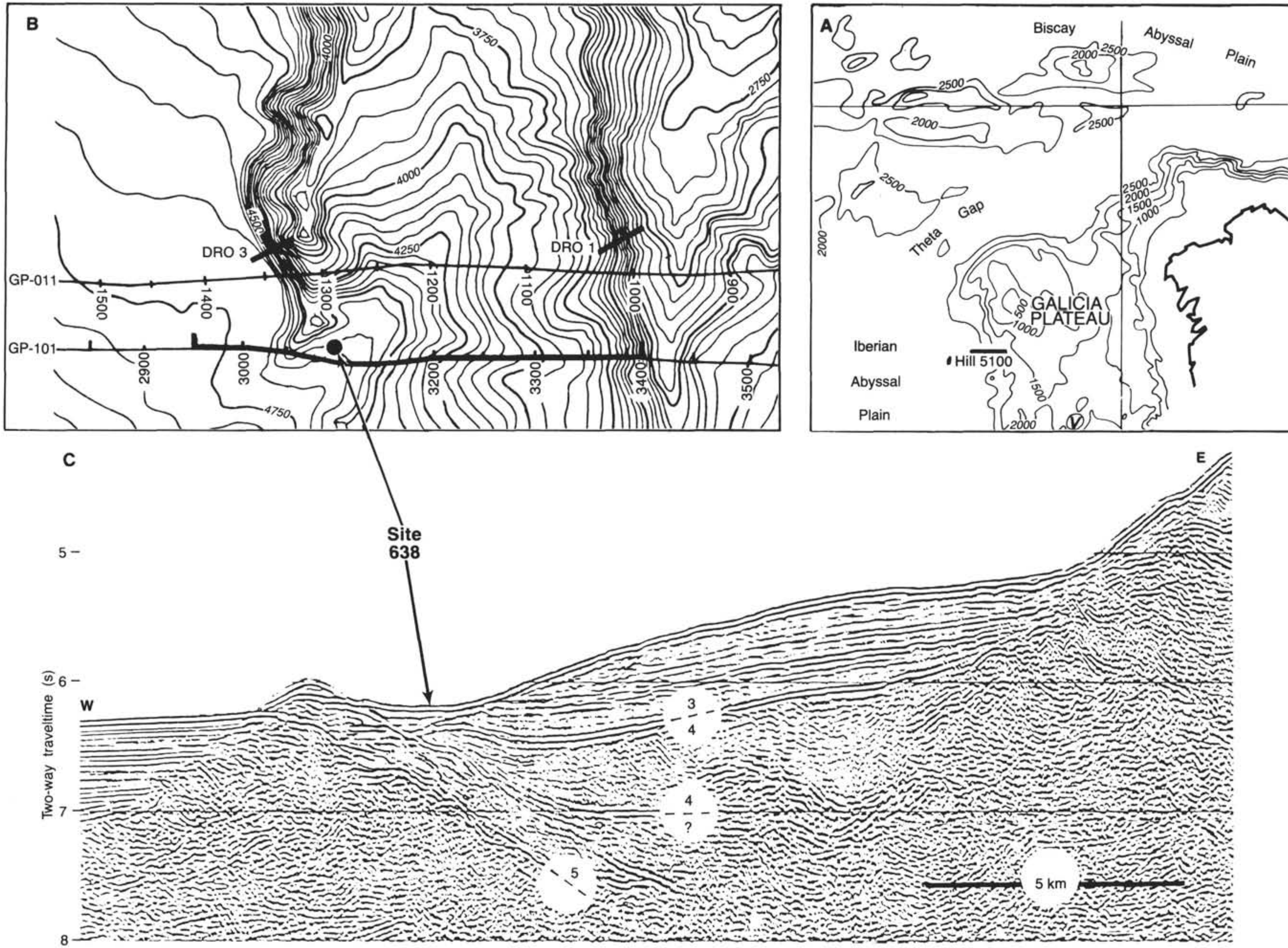

Figure 2. A. West Galicia margin. B. Map location of Site 638 and dredge sites DR01 and DR03 on Sea Beam map by Sibuet et al. (this volume). C. Location of Site 638 on multichannel seismic profile GP-101 (profile courtesy of L. Montadert). Post-rift strata, 3; syn-rift strata, 4; and pre-rift strata, 5 (interpretation before drilling). Vertical exaggeration, about ×2.

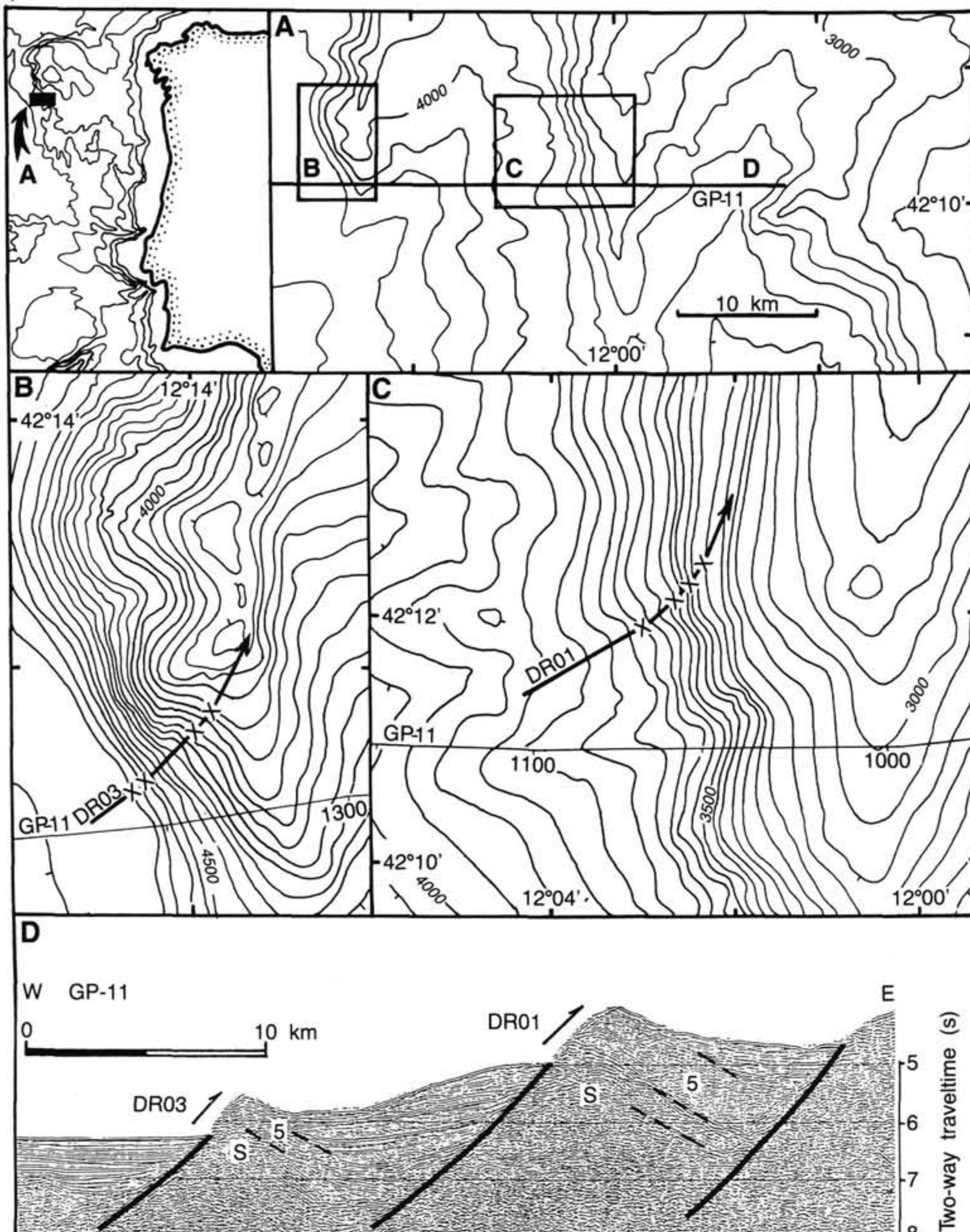

Figure 3. Locations of dredge Stations DR01 and DR03 on the Sea Beam map (courtesy of J. C. Sibuet) and on seismic profile GP-11 (courtesy of L. Montadert). Seismic units 5, pre-rift; and S, basement (interpretation before drilling). Vertical exaggeration, about ×2. After Mougenot et al. (1985).

beacon, and after study of the record, we elected to drill the pilot hole for Site 638 at a location 200 m due east of the beacon. Here the seismic record appeared much like the record at shotpoint 3095, and the 3.5-kHz record (Fig. 5) revealed a flat terrace that on all previous crossings of the valley also showed subbottom reflectors indicating soft sediments. As depicted in Figure 4, the beacon was dropped slightly more than 1 km north and a bit east of shotpoint 3095.

After we had retrieved the seismic gear, the ship moved back over the beacon and stationed itself 200 m east of the beacon. Meanwhile, preparations were made for drilling a pilot hole at Site 638 to prepare for subsequent drilling of a reentry hole through the entire sedimentary section and into crystalline basement rocks.

Drilling, Coring, and Logging Operations

Hole 638A

First, the depth of the seafloor was established at Site 638. The echo-sounder gave a depth of 4671 m below the derrick floor, but the weight indicator for the drill string measured a firm bottom at 4673 m. We accepted this latter depth.

Next, the Hole 638A was spudded at 2145 hr on 5 May and opened to a depth of 44 mbsf by rotating the pipe and circulating at about 90 strokes per min (spm) at a pressure of about 650 psi. The ODP operations superintendent and the SEDCO drilling superintendent agreed that this "jet-in" test showed that a reentry cone and 44 m of 16-in. casing could be emplaced at this spot. The pipe was then pulled up to a level slightly above the

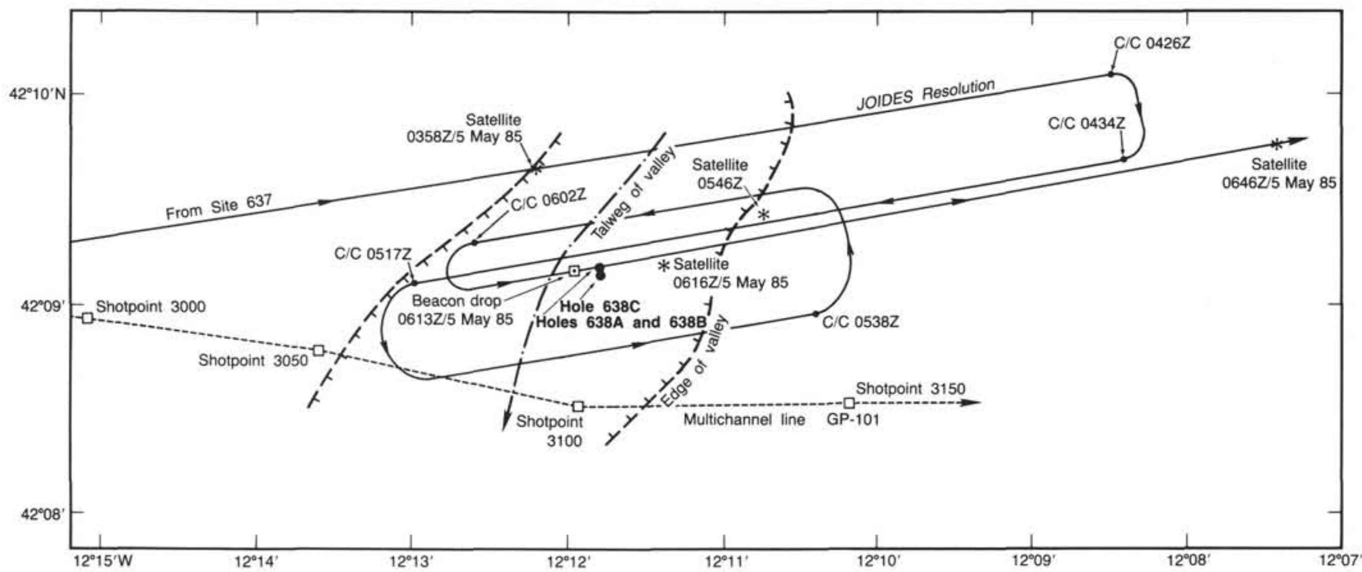

Figure 4. Approach to Site 638, showing location of Holes 638A, 638B, and 638C with respect to the acoustic beacon, and track of multichannel seismic line GP-101. Position of Hole 638B based on weighted average of 26 good-quality satellite fixes. Approximate position of the thalweg and of the change in slope at edges of the submarine valley in which the site is located are shown.

seafloor, and we were ready to begin the pilot hole, which would enable us to decide what length of casing, if any, was required in the reentry hole.

Hole 638B

Hole 638B, spudded at 0215 hr on 6 May, was continuously cored from the seafloor to a depth of 431.1 mbsf, recovering a total of 45 cores, in which the average recovery rate was 49%. Details of the coring record are shown in Table 1.

The coring proceeded without any serious difficulty and at satisfactory rates. The coring rate, in minutes per meter, for each core is graphed on Figure 1, which shows that little systematic change in rates occurred until the drill began coring the well-cemented sandstone layers in the Lower Cretaceous. Even here the average rates were not much slower than in the overlying marlstone.

The customary drilling disturbances were seen in the cores of Neogene ooze; the squeezing, diapirlike effects in the upper cores give way downward to better preservation of original structures but with the concomitant appearance of "drilling cakes," in which short sections of undisturbed core are separated by a drilling paste. The number of such cakes in a core generally correlates well with the number of heaves of the vessel during the cutting of a core. (This same observation was often made by scientists viewing cores taken by *Glomar Challenger*, but we did not expect to see these drilling cakes develop in cores taken with what appears to be an effective heave-compensation system on *JOIDES Resolution*.) In the Cretaceous marlstone, the drilling cakes are not separated by a layer of paste but rather are in close contact, their presence being signaled by the abrupt changes in apparent dip of inclined bedding or the termination of burrows and other internal sedimentary structures. We suggest that the lower end of the drill string, at the bit, still moves up and down enough to disturb cores, even as the heave compensator is operating.

In the lower 100 m of the hole, the recovery rate in the Lower Cretaceous turbidite sandstone unit was disappointing. Generally, only well-cemented sandstone was recovered, and we had no sure way of estimating what the unrecovered portions might be: poorly cemented sandstone or mudstone. As a compensation for the poor rate of recovery in the sandstone, the recovered pieces were virtually free of drilling-disturbed original structures.

The last few sandstone cores began to show that the drill bit might have been worn; the diameter of the cores became progressively smaller. Although the hard fingers of the core catchers scraping off friable sand could account for some of this, we decided that to stop drilling would be wise. As the coring rate in the sandstone was slowing, we also thought that the most efficient way to advance the drill would probably be to recore this interval in the planned reentry hole. We, therefore, terminated coring in Hole 638B at 0145 hr on 11 May and prepared to log the hole.

A serious concern during operations in Hole 638B was that the hole was not vertical, thus possibly causing difficulties during logging operations—a concern that proved well justified. A measurement at about 130 mbsf showed a deviation of 2°; another at about 295 mbsf gave a reading of 4.5°, and a last one at about 350 mbsf read 4.75°.

To prepare for logging, the hole was conditioned by circulating fresh-water drilling mud and by cleaning the hole by running the drill pipe up and down to remove any obstructions. A go-devil was pumped down, and the bit was released hydraulically. The hole was then filled with mud as the drill bit was pulled back up to a depth of about 100 mbsf. At 1830 hr on 11 May, the rig floor was free to begin rigging for logging.

The first set of instruments used included gamma-ray, sonic, resistivity, and caliper tools, which were lowered into the hole but could go no deeper than 278 mbsf. The tools were raised and lowered, each lowering at an increasing speed of descent, seven different times, with no sign of progress. The depth at which the tools stopped was near the depth where coring encountered rather brittle marlstone that fractured severely during the coring process and near the depth where a hole deviation of 4.5° was measured.

Whether the main obstruction to logging was the presence of "bridges" of rock jutting out into the hole or a bend in the hole or some combination of these two conditions is uncertain. We suspect that the use of fresh-water-base mud in the hole may lead to swelling and disintegration of clay and clayey rocks. The beneficial effects of the mud, in helping to suspend cuttings,

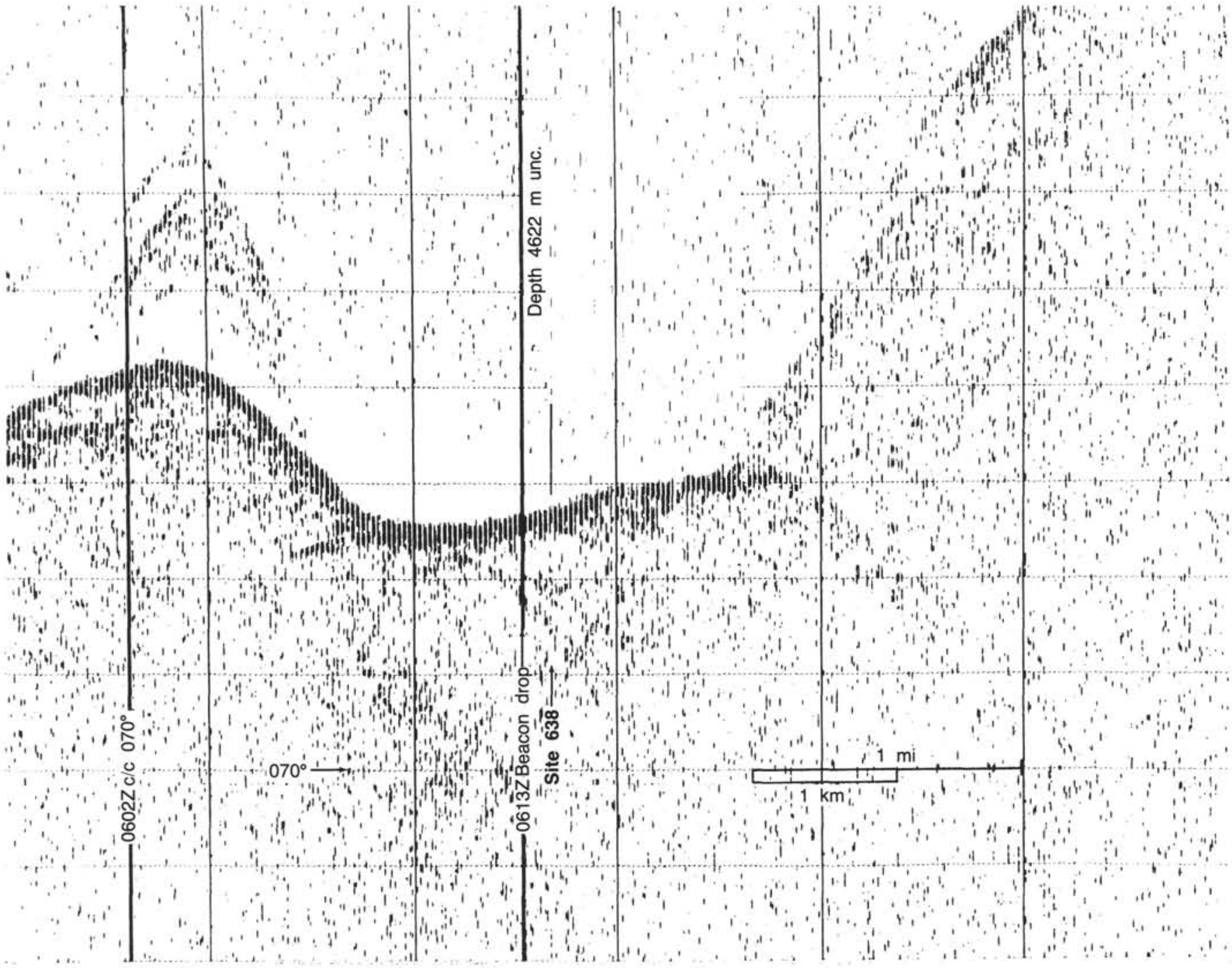

Figure 5. The 3.5-kHz echo-sounding record made from *JOIDES Resolution* during the approach to Site 638, showing place where the beacon dropped. Site 638 is located about 200 m east of the beacon.

has to be balanced against its possible deleterious effects. In any event, the hole was logged from the blocking depth back up to the base of the BHA. We regretted not having been able to obtain logs from the deeper levels of the hole to provide a basis for estimating the average velocity of sound in the sandstone unit. This estimate is prerequisite to estimating the depth to the seismic reflector identified as the top of the carbonate platform.

For the second logging run, we elected to use the L-DGO multichannel sonic tool, reasoning that its short length (only about 6 m) might enable it to pass the obstruction that had blocked the other, longer (20-m) set of tools. Yet this shorter tool could not be lowered any deeper than 164 mbsf, which is still well within the Neogene nannofossil ooze. Because the tool weighs only about 200 kg, compared to about 900 kg for the first set of tools run, even a minor bridge could stop it. A log was obtained for the 64 m from the blocking depth back up to the BHA; then the logging tools were cleared from the hole and the drill string pulled out. The final piece of pipe was on deck at 2245 hr on 12 May, and we began preparations to establish a reentry hole.

One last, helpful piece of information came from inspection of the shank of the center bit, which was deeply grooved by the cones in the bit grinding against it. The bearings for the cones were loose and the bit was, therefore, near the end of its usefulness when it was released. The bit had rotated for about 21.5 hr, counting only the actual times that the bit was turning and advancing downward.

Hole 638C

On 13 May, beginning just after midnight, a reentry cone, having 40 m of 16-in. casing hung below, was assembled for lowering to the seafloor to establish Hole 638C. Just before the lowering, the ship moved to a position 30 m due south of Hole 638B, about 200 m in a direction about 100° from the acoustic beacon. To provide continual beacon signals, a new, second beacon was dropped near the reentry cone. This beacon can be switched on or off by command from the surface; as soon as it reached the seafloor and was heard, it was turned off for future use.

The cone and casing were lowered to the seafloor. A hole 44 m deep was drilled using a 14⅞-in. bit; the casing and cone were unlatched from the drill string, and the pipe was pulled out of the hole. The drill bit arrived on deck at 2145 hr on 14 May, nearly a full day after the cone-setting operation had begun.

By 0630 hr the next morning, 15 May, the drill string, now equipped with a 9⅞-in. bit, was poised about 4 m above the

Table 1. Coring summary, Site 638. No cores were recovered from Hole 638A.

Core no.	Date (May 1985)	Time (hr)	Sub-bottom top (m)	Sub-bottom bottom (m)	Length cored (m)	Length recovered (m)	Percentage recovered
				Hole 638B			
1R	6	0345	0.0	6.4	6.4	6.4	100.0
2R	6	0600	6.4	16.0	9.6	9.2	95.0
3R	6	0830	16.0	25.5	9.5	2.0	20.0
4R	6	1045	25.5	35.2	9.7	9.7	100.0
5R	6	1445	35.2	44.8	9.6	0.0	0.0
6R	6	1710	44.8	54.4	9.6	TR	TR
7R	6	1930	54.4	64.1	9.7	3.7	37.0
8R	6	2215	64.1	73.6	9.5	9.7	102.0
9R	7	0100	73.6	84.1	10.5	0.1	1.0
10R	7	0315	84.1	93.7	9.6	3.7	38.0
11R	7	0535	93.7	103.4	9.7	3.4	34.0
12R	7	0815	103.4	113.1	9.7	1.6	16.0
13R	7	1030	113.1	122.9	9.8	4.0	40.0
14R	7	1315	122.9	132.6	9.7	4.6	47.0
15R	7	1555	132.6	142.2	9.6	5.6	57.0
16R	7	1850	142.2	151.8	9.6	3.9	40.0
17R	7	2130	151.8	161.5	9.7	0.5	4.0
18R	8	0015	161.5	171.1	9.6	7.4	77.0
19R	8	0300	171.1	180.6	9.5	0.5	5.0
20R	8	0515	180.6	190.1	9.5	3.7	39.0
21R	8	0800	190.1	199.7	9.6	8.4	87.0
22R	8	1045	199.7	209.3	9.6	7.7	79.0
23R	8	1320	209.3	218.8	9.5	8.4	88.0
24R	8	1545	218.8	228.4	9.6	8.0	83.0
25R	8	1810	228.4	238.1	9.7	8.8	90.0
26R	8	2100	238.1	247.7	9.6	8.5	88.0
27R	8	2345	247.7	257.3	9.6	9.7	101.0
28R	9	0230	257.3	267.0	9.7	9.8	100.0
29R	9	0445	267.0	276.7	9.7	4.8	49.0
30R	9	0745	276.7	286.3	9.6	6.3	65.0
31R	9	1015	286.3	296.0	9.7	6.1	63.0
32R	9	1325	296.0	305.6	9.6	3.2	32.0
33R	9	1615	305.6	315.3	9.7	6.2	63.0
34R	9	1915	315.3	324.9	9.6	5.0	51.0
35R	9	2150	324.9	334.5	9.6	5.7	59.0
36R	10	0045	334.5	344.2	9.7	3.5	36.0
37R	10	0315	344.2	353.8	9.6	1.2	12.0
38R	10	0530	353.8	363.5	9.7	1.0	10.0
39R	10	0745	363.5	373.1	9.6	0.5	5.0
40R	10	1030	373.1	382.8	9.7	0.7	6.0
41R	10	1315	382.8	392.5	9.7	2.2	22.0
42R	10	1602	392.5	402.2	9.7	2.3	23.0
43R	10	1930	402.2	411.9	9.7	3.0	31.0
44R	10	2215	411.9	421.5	9.6	3.7	38.0
45R	11	0145	421.5	431.1	9.6	4.3	44.0
				Hole 638C			
1R	18	1130	411.9	421.5	9.6	3.5	36.0
2R	19	0500	421.5	431.2	9.7	0.2	2.0
3R	20	0945	431.2	440.9	9.7	4.0	41.0
4R	20	1315	440.9	450.5	9.6	5.3	55.0
5R	20	1615	450.5	460.2	9.7	3.0	30.0
6R	20	2030	460.2	469.9	9.7	4.0	41.0
7R	20	2315	469.9	479.5	9.6	3.6	37.0
8R	21	0300	479.5	489.2	9.7	2.6	27.0
9R	21	0735	489.2	498.9	9.7	3.7	38.0
10R	21	1045	498.9	508.5	9.6	3.1	31.0
11R	21	1345	508.5	518.2	9.7	0.0	0.0
12R	21	1705	518.2	527.9	9.7	1.1	11.0
13R	21	2115	527.9	537.5	9.6	0.7	7.0
14R	22	0635	537.5	547.2	9.7	2.8	28.0

depth of the top of the cone, and a sonar tool made by Mesotech was lowered through the pipe and just out of the end of the bit, where it began scanning. After about 45 min of scanning and some maneuvering of the ship, the sonar image, displayed in color on a television screen, showed the four reflectors mounted around the rim of the cone as four bright targets around the sonar tool. Word went immediately to the drill floor to stab in the pipe. Because the sonar tool had no sound pick-up, we had no accurate way of confirming that the drill string had entered the cone and casing unless we advanced the drill string downward to the 44 mbsf depth drilled during the emplacement of the cone. We therefore retrieved the sonar tool, dropped a center bit into the string to enable us to drill ahead, and lowered the drill string slowly, exploring for firm sediment. We were dismayed to find firm sediment only 20 m below the seafloor, rather than at 44 m. We drilled ahead to 44 m in firm material, proving that we were not dealing here with some accidental and virtually unexplainable fill material inside the casing. We concluded that we had not reentered Hole 638C but had instead drilled a short hole outside the cone.

It was now 1800 hr on 15 May, and we began preparations for a second try at reentry. By midnight, the Mesotech sonar tool was again in position and scanning. This time the approach was slower, and it was not until 0600 hr on 16 May that the centered image of the reflectors again presented itself on the screen and the pipe was again stabbed into the cone. Again, the drill hit firm sediments at 20 mbsf, and we were again forced to conclude that we had missed the cone.

For the third and final try, we used a sonar tool made by Edo, which although not giving a color image, did have a sound pick-up. Just after midnight on 16 May, the Edo tool began its search, and at 0130 hr the reflectors showed a symmetrical pattern surrounding the tool; the drill string was again stabbed into the cone. Faint rattling noises and a loud click, as made by a tool joint going into the casing, led us to hope that we were at last truly and properly reentered. After the sonar returned to the derrick floor, a center bit was dropped and the pipe advanced 44 m without any resistance. We had indeed reentered Hole 638C.

One interesting piece of geological information resulted from all the sonar scanning: the depth of the seafloor in the immediate vicinity of the cone is about 6 m shallower than indicated by the weight change of the drill string. We decided that we would continue to operate *as if* the seafloor were at 4673 m below the derrick floor, but we would take a core right at the seafloor just after the drill pipe was pulled up through the level of the cone during one of the future round trips for reentry into this hole.

By 2230 hr on 16 May, we started drilling ahead without taking any cores but pausing to make surveys of the deviation from vertical of the hole. The deviation at 180 mbsf was 1°, at 265 mbsf it was 0.75°, and at 334 mbsf it was only 0.5°. At 0900 hr on 17 May, about 6½ days after we retrieved the last core from Hole 638B at a depth of 431 mbsf, we were ready to cut the first core in Hole 638C, to a depth of 421 mbsf.

For a long time, the first core was our only core. Because it showed that we were essentially at our anticipated stratigraphic level, but that the drilling disturbance of the core was significantly less than that of the final cores from Hole 638B, we waited expectantly for the second core, which did not return easily. When the overshot device used to retrieve core barrels arrived on deck, it arrived with only the topmost part of the barrel assembly, the main, lower part having unscrewed itself from the upper part at a joint that functions as a "quick-release" mechanism. Why or how it released itself was unclear, but we knew from watching the pump gauges that the barrel was seated in its normal place above the bit. To retrieve it we could either fish it out or pull out of the hole.

A suitable fishing tool was found and pumped down the hole, and then the overshot device was sent down to bring back the tool and the core barrel. The overshot device found the fishing tool but not at the top of the barrel; it was stuck at a depth 581 m *above* the seafloor. For the next try, the tool was sent down with the overshot device for added weight to aid in advancing the tool beyond the depth where it had stopped before. This time, the tool was stopped at a depth about 80 m higher up than the first time. We surmised that some foreign object, such as a rag or glove, which might have been introduced accidentally into the drill string, had floated up to this depth and was blocking the tools. Whatever the cause had been, we decided that the most efficient action would be to pull out of the hole, since we would be forced under any circumstances to make a reentry soon because the rotation time on the drill bit was now about 20 hr. During pull out from the hole, several pieces of sandstone and mudstone were discovered wedged into the drill pipe about 1165 m above the bit; evidently the top of the core barrel had opened when it separated into two parts, and pieces of core escaped upward into the drill string, causing the tool blockage.

The complete drill string was back on deck by about 0600 hr on 19 May. After a delay of about 2 hr for the routine cutting of about 50 m of the main drilling line that runs from the draw works and over the crown block and traveling block (this must be done after each 3500 "ton-miles" of drilling-line use), we began running pipe back to the seafloor to make the second reentry. At 2000 hr that same evening, the sonar tool began searching for the cone. The approach to the cone took more than 3 hr, but the reentry was successful on the first try. During the approach to the cone, we repeatedly saw a phantom reflector, located opposite the cone and at an equal distance from the sonar tool. This phantom, mirror image could have easily been confused with a real reflection at close range and may account for our having missed the cone twice during the first reentry in Hole 638C.

Coring continued normally from Cores 103-638C-3R through 103-638C-10R. The bottom few meters of Core 103-638C-11R cut quickly, but when we retrieved the barrel it was empty. Cores 103-638C-12R and 103-638C-13R cut quickly also, and each recovered only about 1 m of turbidite sandstone and claystone. Some of the sandstone beds are poorly cemented, and we speculated that uncemented sand layers might be common in the interval cored but that we were not recovering them. Core 103-638C-14R cut at a more normal rate, but while the overshot tool was coming up with the core, the pipe suddenly would not rotate or move up or down; it was firmly stuck. During the core-retrieval process, the driller had raised the bit up to a point about 7 m off the bottom of the hole to avoid any cuttings that might clog the water holes in the drill bit. We guessed that some loose sand might have collapsed into the hole and wedged against the drill string, most likely at about the place where we had cut Core 103-638C-11R, about 508–518 mbsf.

We recovered Core 103-638C-14R, and spent several hours trying unsuccessfully to free the pipe by pulling it up with a force of about 80,000 lb. We then lowered a severing tool, loaded with explosive pellets for firing and splitting the pipe. We placed the tool within one of the heavy drill collars about 44 m above the drill bit, at a depth of about 496 mbsf, which we assumed should be above the interval where the pipe was stuck. The explosives fired, but the pipe still could not be freed. Was it not severed or was the pipe stuck at a higher level in the hole? While pulling upward on the pipe while waiting to prepare a new explosive charge, the driller determined from the change on the weight indicator that the pipe had unexpectedly freed itself and that the whole BHA was still suspended from the draw works.

After filling the hole with mud, in anticipation of our returning later for logging, we pulled out of the hole and recovered the drill collar in which the explosives had fired. The explosion opened several gashes about 1 m long through the pipe and bulged it out about 3 cm; apparently the explosive was not designed to sever a thick-walled drill collar.

Considering the risk entailed in attempting to deepen Hole 638C and weighing the scientific priorities of Leg 103, we decided to abandon the hole and to try to drill at a place a few km to the west, where the strong seismic reflector, believed to be the top of a Jurassic carbonate platform, is near the seafloor. We departed Site 638 at 0635 on 23 May 1985 and went to Site 639.

On 1 June, after drilling four holes at Site 639, the ship returned to Hole 638C for additional logging. The transit from Site 639 was made by steaming slowly between the acoustic beacons at the two sites, using the thrusters, while concurrently making a complete round trip with the drill string, so as to change to a logging bit that would allow us to clean out Hole 638C and to pass the logging tools through the bit. The reentry took about 5 hr from the time the sonar tool began scanning until the pipe stabbed into the cone, at 2307 hr on 1 June. A full day was consumed cleaning out the hole in preparation for logging, since we knew from our previous experience that bridges would probably be in the hole. By 2115 hr on 2 June, the hole had been cleaned as much as possible, filled with mud, and the drill string raised so that the logging bit was at a depth of 99 mbsf.

For the first logging run, the string of tools, which comprised the gamma-ray, caliper, sonic, and lateral-induction devices, could not be lowered deeper than 287 mbsf because of a bridge or a narrow obstruction in the hole. The logs obtained from 272 to 105 mbsf were of good quality; thus a second run was begun, using the gamma and density tools. This time, a bridge stopped the tools at 250 mbsf, but a good record was taken from there up to 105 m.

During the pulling out of Hole 638C, the threaded connections between drill collars and other connections in the BHA were inspected by the "magnaflux" technique (one of the many essential, but time-consuming procedures that subtract from the effective drilling time during a leg). At 2030 hr on 3 June, *JOIDES Resolution* departed Site 638, headed for Site 640.

SEDIMENT LITHOLOGY

The sedimentary section at Site 638 (Table 2) consists of 184 m of Cenozoic pelagic ooze (Unit I), overlying 364 m of Early Cretaceous marl and limestone (Unit II) and alternating claystone, marlstone, and sandstone (terrigenous turbidites) (Unit III).

Lithologic Unit I (0–183.6 m: Core 103-638B-1R through Sample 103-638B-20R-3, 3 cm)

Unit I, recovered only in Hole 638B, is 183.6 m thick and consists of white, pale-gray, and pale greenish gray nannofossil ooze and clayey nannofossil ooze. The sediment is generally soft, although Cores 103-638B-19R and 103-638B-20R contain material sufficiently indurated to be termed chalk. Core recovery was poor, and the recovered sediments were extremely deformed by drilling, so that any original internal structure is almost totally obliterated. Nonetheless, in some cores, original mottling and faint, diffuse lamination are observed. In Cores 103-638B-19R and 103-638B-20R, faint laminations in the chalk appear to dip at approximately 15°. The unit probably has been extensively bioturbated.

The sediment is composed of nannofossils with subordinate amounts of clay and minor amounts of foraminifers. Trace amounts of pyrite and scattered mineral grains, principally quartz, are ubiquitous. The carbonate content (see "Inorganic Geochemistry" section, this chapter) of the ooze ranges from 68% to 79% in Cores 103-638B-1R through 103-638B-6R, 68% to 93% in Cores 103-638B-7R through 103-638B-10R, and 81% to 99% in Cores 103-638B-11R through 103-638B-20R. Thus, the carbonate content increases downhole. Exceptions to the generally high carbonate contents are Samples 103-638B-10R-2, 90–105 cm, and 103-638B-18R-1, 0–65 cm, which consist of firm clay with less than 5% carbonate. In Core 103-638B-10R, the clay is green with black, zeolite-rich laminae. Clay in Core 103-638B-18R is reddish brown. In each of these occurrences, the lower part of the clay interval consists of nannofossil ooze and a jumble of hard, black, brown, and green clay clasts. These jumbles have the appearance of a debris flow (Fig. 6). Similar sediments, occurring as cuttings in Cores 103-638B-14R and 103-638B-15R, could be either cavings from the hole or debris flows. Certainly, the clay has been redeposited, because it contains Cretaceous microfossils (see "Biostratigraphy" section, this chapter).

Manganese-coated limestone (skeletal wackestone/packstone) pebbles occur in Sample 103-638B-1R-2, 80 cm, Core 103-638B-6R, and Sample 103-638B-11R-2, 118–123 cm. The base of Core 103-638B-17R contains a coarse-sandstone pebble. These exotic pebbles were probably eroded from nearby slopes. However, given the conditions of the hole, they could have come from any stratigraphic interval between the seafloor and the depth from which they were recovered.

The contact between the Miocene pelagic ooze and the underlying Cretaceous sediments, recovered in Core 103-638B-20R (see whole-core photograph of Core 638B-20R, this chapter), is sharp with no evidence of a manganese pavement, a lag deposit, or erosion.

Overall, the Cenozoic sediments at Site 638 are typical pelagic sediments deposited above the carbonate compensation depth (CCD). The occurrence of exotic pebbles, the minor but ubiquitous terrigenous component, the occurrence of clay layers appearing as "debris flows," and the site location being in a topographic low suggest that material locally transported from near-

Table 2. Lithologic units recovered at Site 638.

Lithologic unit/ subunit	Lithology	Cores	Meters below seafloor
I	Nannofossil ooze	103-638B-1R-1, 0 cm– 103-638B-20R-3, 3 cm	0–183.6 (186*)
IIA	Bioturbated limestone, marlstone, and claystone/marlstone couplets	103-638B-20R-3, 3cm– 103-638B-23R-3, 27 cm	183.6–212.6 (216*)
IIB	Light-gray, bioturbated nannofossil marlstone	103-638B-23R-3, 27 cm– 103-638B-32R-2, 95 cm	212.6 (216*)–298.4
IIIA	Claystone/marlstone turbidite couplets	103-638B-32R-2, 95 cm– 103-638B-35R-4, 55 cm	298.4–329.9
IIIB	Coarse-grained sandstone turbidites	103-638B-35R-4, 55 cm– 103-638B-45R-CC, 25 cm and 103-638C-1R-1, 0 cm– 103-638C-14R-CC, 30 cm	329.9–431.1 (Hole 638B) and 411.9–547.2 (Hole 638C)

~~~~ Unconformity
==== Unit boundary
– – – – Subunit boundary
* On basis of logging
~~~~

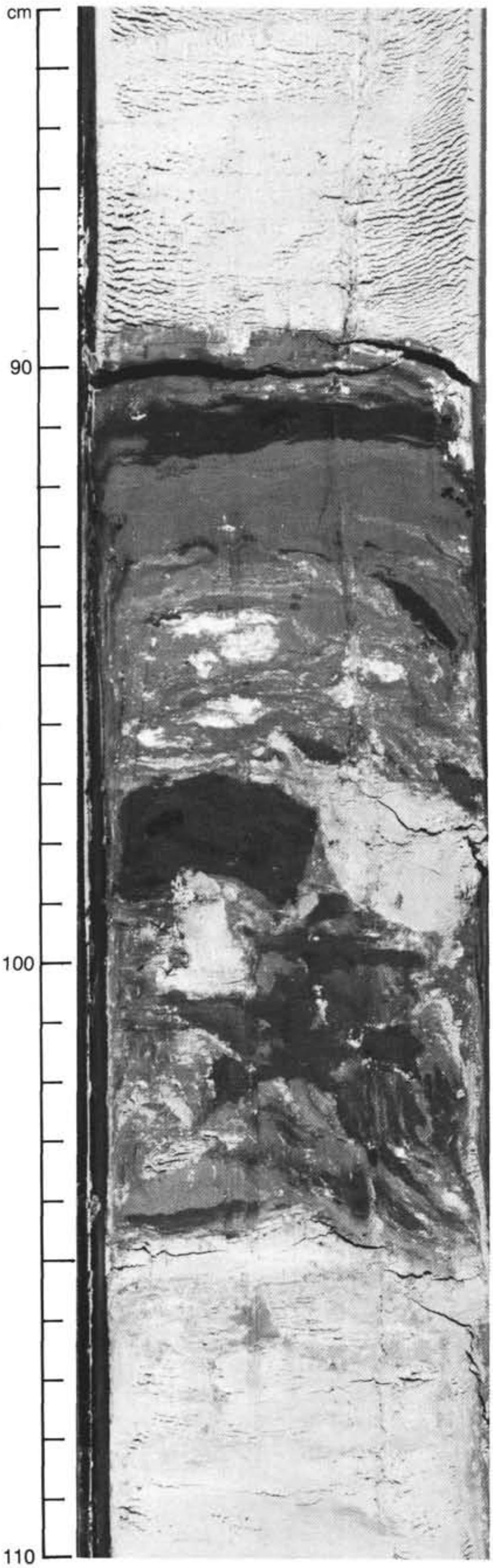

Figure 6. Debris flow of claystone clasts in Cenozoic pelagic ooze (Sample 103-638B-10R-2, 84–110 cm).

by slopes has been mixed with the pelagic sediment. The lower carbonate content of the sediment in the upper part of the sequence presumably results from increased clay sedimentation (or reduced carbonate sedimentation) during Pliocene–Pleistocene glaciation.

Lithologic Unit II (183.6–298.4 m; Samples 103-638B-20R-3, 3 cm, through 103-638B-32R-2, 95 cm)

Unit II consists dominantly of bioturbated nannofossil marlstone, limestone, and calcareous mudstone. It is divided into two subunits: an upper laminated subunit, rich in terrigenous material (Subunit IIA), and a lower, unlaminated, more calcareous subunit (Subunit IIB). The boundary between the two subunits is placed at Core 103-638B-23R-3, 27 cm.

Subunit IIA (183.6–212.6 m; Samples 103-638B-20R-3, 3 cm, through 103-638B-23R-3, 27 cm)

Subunit IIA is 29 m thick and is late Barremian in age (see "Biostratigraphy" section, this chapter). The upper boundary is sharp. Subunit IIA is truncated and unconformably overlain by the Neogene ooze of Unit I. The lower boundary was not recovered but is arbitrarily placed at Core 103-638B-23R-3, 27 cm, which coincides with the top of a slump, which also coincides with a biostratigraphic hiatus. Below this level, the sediments are noticeably more calcareous.

Subunit IIA consists of the following three lithofacies:

1. Light-gray (5Y 7/1) micritic radiolarian limestone and nannofossil marlstone, extensively bioturbated and locally showing faint banding and laminations.
2. Light-gray to gray (5Y 6/1, 5Y 7/1) micritic limestone and calcareous claystone with faint laminations, in places weakly bioturbated.
3. Regularly bedded couplets of gray to dark-olive gray (5Y 4/1, 5Y 3/2, 5Y 4/2), calcareous silt-bearing or silty claystone (mudstone) and light-gray to light-olive and greenish gray (5Y 5/1, 5Y 6/1, 5Y 6/2, 5GY 6/1) marlstone.

Each mudstone/marlstone couplet is typically from 1 to 5 cm thick and shows a gradual change in color from dark-gray claystone at the base to lighter gray, thin marlstone laminae at the top. The carbonate content increases from a few percent to 40%, and the grain size almost imperceptibly decreases upward (Fig. 7). The thickness ratio between the claystone and marlstone is relatively constant at 9:1. A few of the mudstone layers bear discrete silt or fine-sand laminae at the base and display faint parallel lamination. These couplets are probably turbidites, resembling the T_d-T_e beds of the Bouma sequence. The amount of quartz is generally less than 10% but is as much as 30% in silty layers, and mica and feldspar are somewhat less abundant. Zircon, pyrite, and Fe-oxides are present in trace amounts. Zeolites exist in amounts up to 2% in the claystone. The laminae of Lithofacies 3 dip as much as 19°. A drift survey showed the hole to be 4°–5° out of vertical; the true dip of the beds is approximately 15°.

A matrix-supported, inversely graded pebbly bed having elongated clasts occurs in Sample 103-638B-22R-1, 130–150 cm and is interpreted as being a debris flow. In places, the bedding of Lithofacies 3 is contorted and plastically deformed, suggesting slumping (i.e., Samples 103-638B-22R-2, 120 cm, to 103-638B-22R-3, 30 cm).

The three lithofacies alternate over intervals of from 50 to 150 cm, and the boundaries between them are gradational. Lithofacies 1 and 2 are similar and are interpreted as being pelagic sediments deposited above the CCD, in an open-marine environment. Lithofacies 3 consists dominantly of clastic turbidites. Its irregular intercalation within the limestone and marl cycles suggests pulses in the redeposition of terrigenous muds.

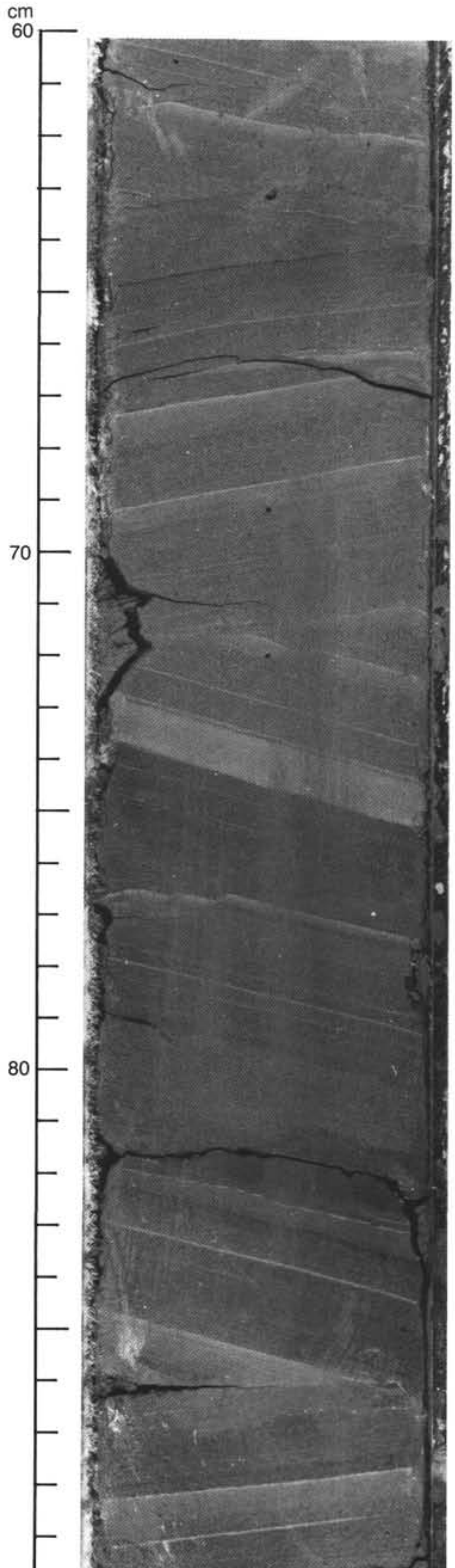

Figure 7. Sequence of centimeter-thick claystone/marlstone turbidites, typical of Subunit IIA (Sample 103-638B-21R-3, 60–90 cm).

Subunit IIB (212.6–298.4 m; Samples 103-638B-23R-3, 27 cm, through 103-638B-32R-2, 95 cm)

Subunit IIB is 86 m thick and is of Hauterivian to early Barremian age (nannofossils) or of Valanginian to late Hauterivian age (foraminifers). The upper boundary of Subunit IIB is placed at the top of a disturbed zone (see Subunit IIA). The lower boundary is gradational and corresponds to the change from dominantly pelagic sedimentation in Subunit IIB to turbidite sedimentation in lithologic Unit III. Owing to poor core recovery, the details of the transition are unknown. We arbitrarily placed the boundary at the lowermost occurrence of white nannofossil limestone (Sample 103-638B-32R-2, 95 cm).

Subunit IIB consists of a monotonous succession of approximately 50-cm-thick intervals of dominantly gray to light-gray (N/5, N/6) and light greenish gray (5Y 5/1 through 7/1, 5GY 5/1 through 7/1) bioturbated nannofossil marlstone that alternate with 10- to 15-cm-thick bands of darker gray (5Y 4/1, 5Y 5/1) more clay-rich nannofossil marlstone. In places, the latter are faintly banded and laminated.

The light-gray nannofossil marlstone contains from 30% to 50% clay and less than a few percent terrigenous, silt-sized material. Very finely divided framboidal pyrite, concentrated in dark-gray specks and blebs, is present.

The dark-gray clay-rich marlstone contains up to 10% terrestrial plant debris and a few percent of terrigenous silt-sized material (quartz, feldspar, mica including biotite, and trace amounts of volcanic glass). As much as 5% zeolites are present, as well as chlorite and glauconite in trace amounts. The carbonate content is typically less than 50%.

The darker gray, clay-rich marlstone beds have an average thickness of 10 to 15 cm, whereas the lighter nannofossil marlstone beds range from 30 to 70 cm. The rhythmic repetition of these sediment types is evident in less disturbed intervals (e.g., Cores 103-638B-24R and 103-638B-25R), but this pattern is mostly masked by either intense drilling disturbance or syn-sedimentary soft-sediment deformation or both. In many places, convolute bedding and plastic deformation of the marlstone layers, as well as crenulated geometry of bedding surfaces, are interpreted as being related to slumping or downslope sediment creep. Slumped beds occur at different intervals in the subunit, but their recognition is difficult because of the intense drilling disturbance. Since a slumped bed is at the top of the subunit (Section 103-638B-23R-3) and sediment deformation is visible throughout the subunit, all Subunit IIB conceivably could have been involved in a single, downslope movement.

Although the sediment in most of Subunit IIB is soft, an increase in lithification of more calcareous beds is noticeable in Cores 103-638B-31R and 103-638B-32R.

Lithologic Unit III (298.4–547.2; Samples 103-638B-32R-2, 95 cm, through 103-638B-45R, CC, 25 cm, and Samples 103-638C-1R-1, 0 cm, through 103-638C-14R, CC, 30 cm)

Unit III, distinguished by the occurrence of abundant terrigenous turbidites, is late Valanginian–Hauterivian in age, according to the study of nannofossils. This unit is divided into two subunits (Table 2). The upper subunit, IIIA, consists of alternating, thin-bedded claystone and marlstone. The lower subunit, IIIB, is characterized by thick beds of terrigenous sandstone.

Subunit IIIA (298.4–329.9 m; Samples 103-638B-32R-2, 95 cm, through 103-638B-35R-4, 55 cm)

The upper boundary of Subunit IIIA is probably gradational and has been highly disturbed by drilling (see Subunit IIB). The lower boundary, which is probably also gradational, corresponds to the lithologic change from dominantly claystone to a sequence containing thick sandstone beds. Arbitrarily, the boundary is placed at Sample 103-638B-35R-4, 55 cm, corresponding to the top of the uppermost thick (i.e., >25 cm) sandstone bed.

Subunit IIIA is 31.5 m thick and consists of irregular, centimeter-scale alternations of thin-bedded, dark-gray (N/4) to gray (5Y 5/1) calcareous silty claystone and greenish (5Y 4/1) to light greenish (5Y 6/1) and olive-gray (5Y 6/2) nannofossil marlstone. The laminae are irregular and wavy. Some are lensoid. The lamination could have been distorted by drilling, which produced intense "biscuiting" and pervasive microfaulting (Fig. 8), or by syn-sedimentary slumping (e.g., Sample 103-638B-33R-2, 30-70 cm). The crenulated geometry of the claystone layers may be the result of shear stress along bedding planes produced by slow, downslope creep or mass sliding. In the less disturbed sections, the dark-gray silty claystone layers have sharp boundaries and locally show faint, normal size grading, more evident where siltstone laminae occur at their base (e.g., Samples 103-638B-34R-2, 40-55 cm, and 103-638B-34R-2, 120-125 cm).

The calcareous claystone generally contains <10%-15% quartz, micas, opaque minerals, and heavy minerals, 10%-25% nannofossils, and trace amounts of zeolites, Fe-oxides, and pyrite, the remainder being clay.

The marlstone comprises nannofossils and clay minerals in approximately equal percentages and trace amounts of coarser terrigenous material.

Several layers, as much as 10 cm thick, of medium- to fine-grained sandstone, are present. The layers have normal size grading, parallel and ripple-oblique laminae, and resemble Bouma T_{a-e}, T_{b-e}, and T_{c-e} sequences (e.g., Samples 103-638B-33R-4, 80-95 cm, 103-638B-34R-3, 35-50 cm, and 103-638B-34R-3, 57-62 cm). These are similar in composition to those in Subunit IIIB; they are described in detail in the following text.

Subunit IIIB (329.9-547.2 m; Samples 103-638B-35R-4, 55 cm, through 103-638B-45R, CC, 25 cm, and Samples 103-638C-1R-1, 0 cm, through 103-638C-14, CC, 30 cm)

Subunit IIIB was encountered in Hole 638B at a sub-bottom depth of from 329.9 to 431.1 m, and in Hole 638C, at a sub-bottom depth of from 411.9 to 547.2 m.

The upper boundary of Subunit IIIB, described previously, corresponds to the lithologic change from dominantly mudstone (above) to sandstone (below). At Site 638, 217.3 m of Subunit IIIB were cored, but the lower boundary was not reached. Core recovery was poor (<20%; Table 1). The recovered sediments are dominantly medium- to coarse-grained sandstone, interbedded with minor siltstone/claystone and marlstone turbidites.

The sandstone is medium to coarse grained, becoming very coarse grained to granule sized in Cores 103-638B-43R through 103-638B-45R and in the lowermost cores of Hole 638C. The sandstone is poorly sorted, and the grains are mostly angular. The composition is arkosic (quartz, 30%-40%; feldspar [microcline, orthoclase, and plagioclase], 15%-30%; and micas [including biotite and chlorite], 5%-15%). Chlorite typically occurs as an alteration product of biotite. Rock fragments, generally present in amounts of as much as 15%, are from felsic plutonic and metamorphic rocks (granite, quartzite, sericite-schist, biotite-chlorite-schist, and slightly metamorphosed sandstones). Micritic carbonate grains and micritized fragments of shallow-water fossils also occur in trace amounts. Accessory minerals include apatite, Fe-oxides, opaques, and other heavy minerals (zircon and rare epidote). Plant material comprises 3%-5% of the coarse-grained sandstone beds but increases to as much as 20% in the fine-grained sandstone and in the siltstone.

The sandstones are cemented by a crystalline mosaic of sparry carbonate, generally present in amounts ranging from 15%

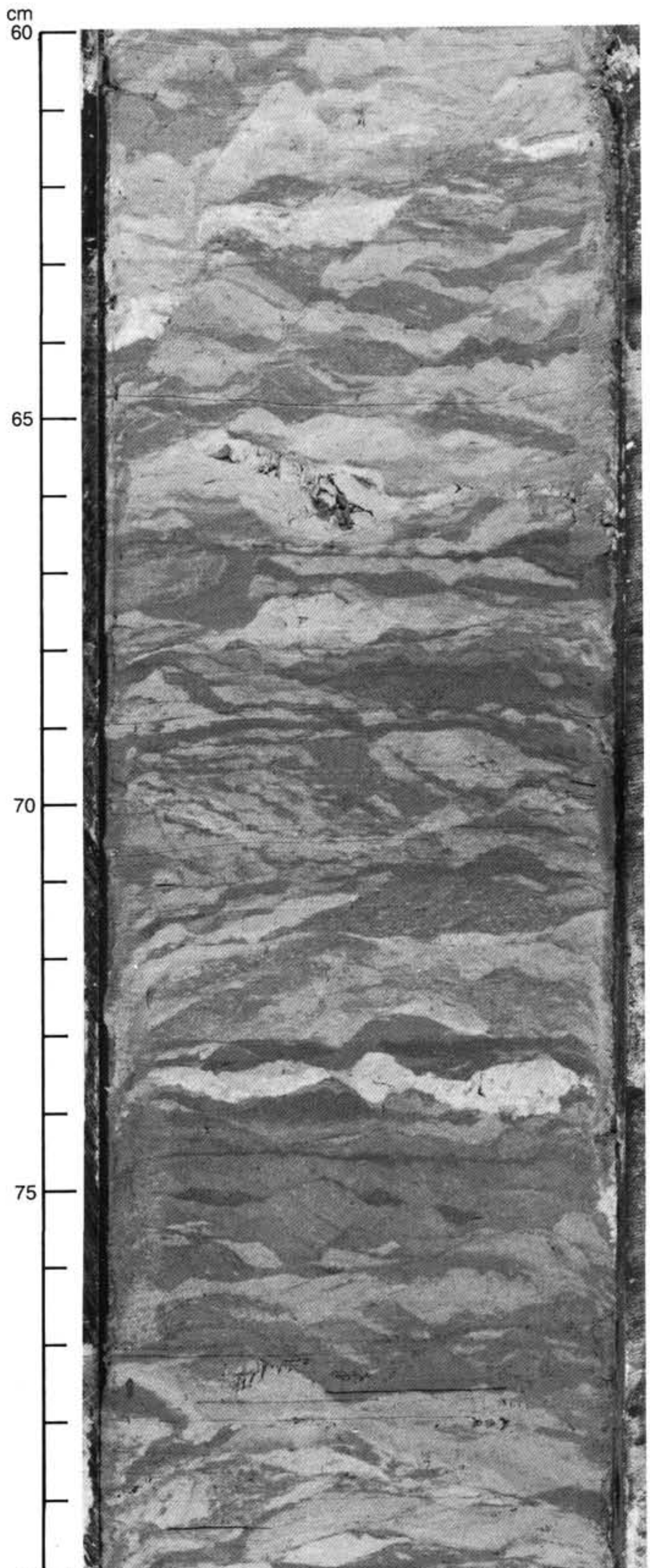

Figure 8. Alternating centimeter-thick layers of dark-gray to gray claystone and silty claystone and light greenish and olive-gray nannofossil marlstone of Subunit IIIA, disrupted and deformed (Sample 103-638B-33R-1, 60-80 cm).

to 25%. Based on microscopic examination of stained thin sections and on preliminary x-ray diffraction analyses, the carbonate is tentatively interpreted to be ferroan calcite, ferroan dolomite, dolomite, possibly siderite, and minor calcite. Displacive precipitation is observed; biotite grains are ruptured by carbonate crystallization along cleavage planes, and quartz and feldspar grains, where fractured, are displaced by carbonate cement (Fig. 9). Both feldspar and quartz grains are replaced to varying degrees along grain boundaries by ferroan sparry calcite (Fig. 10), indicating that Subunit IIIB sandstones have attained the locomorphic stage in their diagenetic evolution (Dapples, 1962).

Most of the sandstone beds, interpreted as being the coarse part of turbidites, range from 30 to 50 cm in thickness and are normally graded. In Cores 103-638C-1R through 103-638C-9R, the sandstone beds are evenly spaced and occur at a frequency of one to three per section. They are commonly massive at the base and/or parallel laminated (divisions T_a and T_b of the Bouma sequence). Thinner layers of fine sandstone, typically 4–7 cm

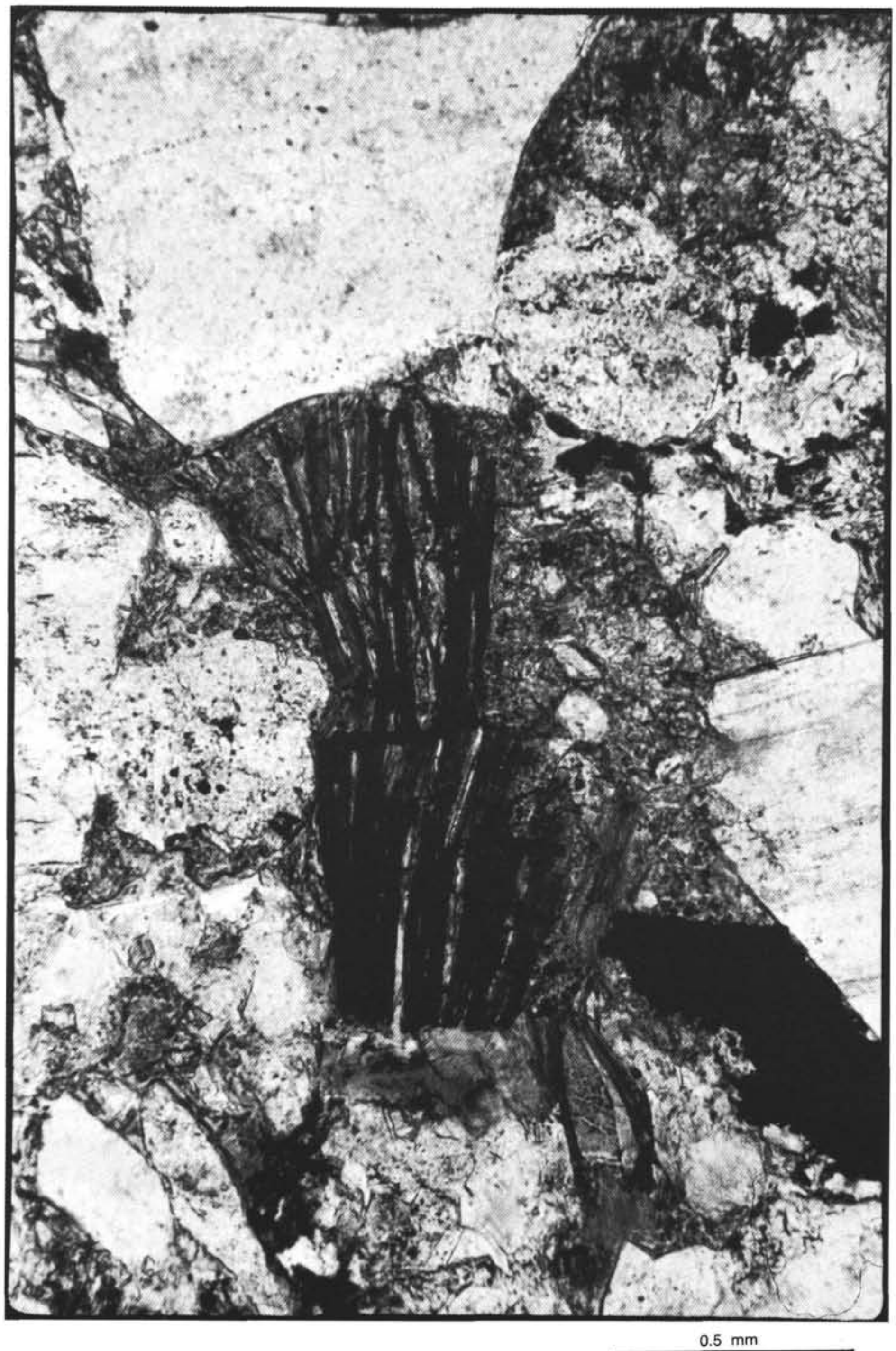

Figure 9. Detrital biotite split along cleavages by growth of calcite (Sample 103-638B-39R-1, 14–23 cm). Bar scale, 0.5 mm. Plane light.

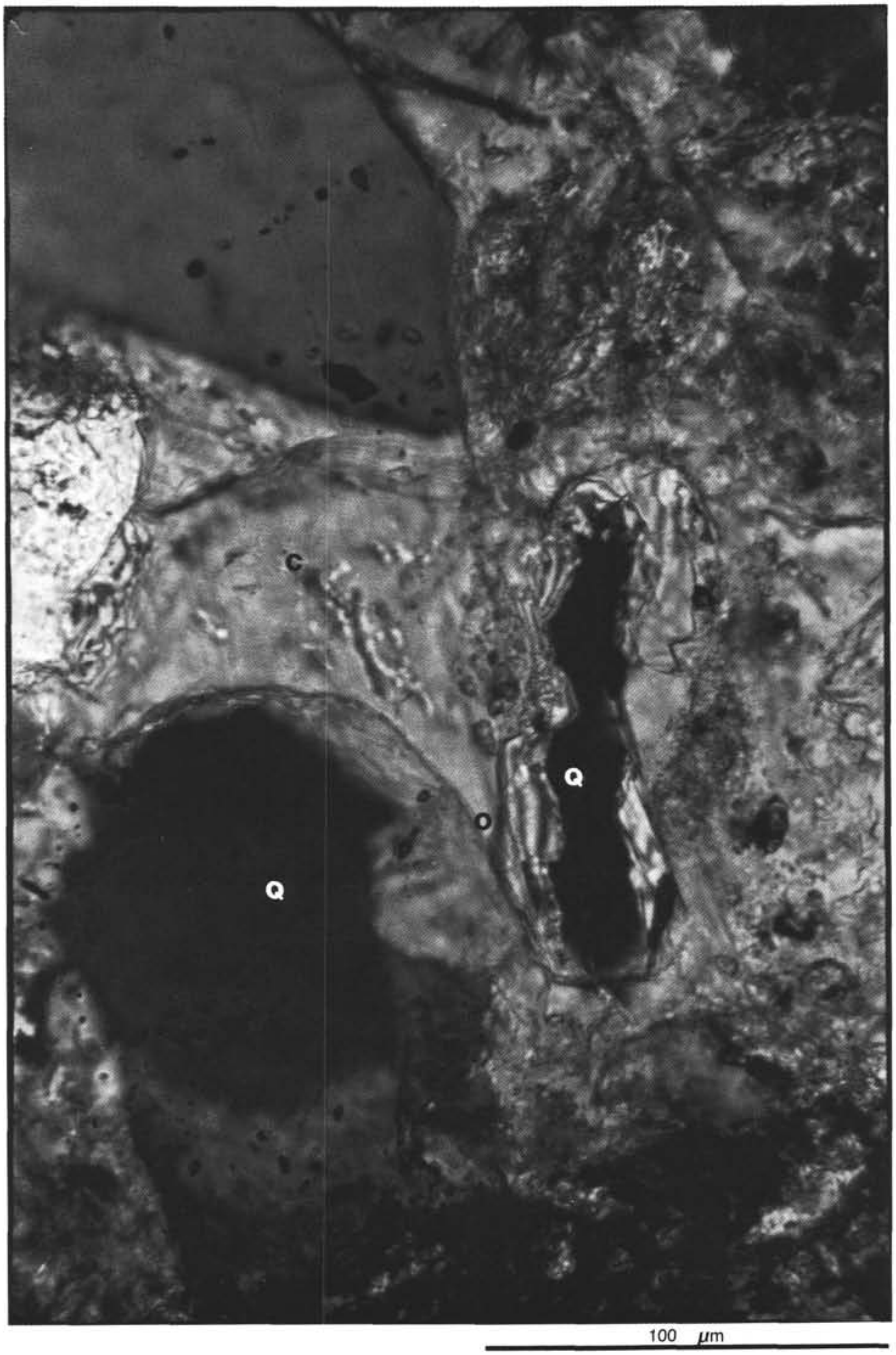

Figure 10. Carbonate replacement (C) of detrital quartz (Q). The outline of original quartz grains (O) suggests significant replacement (Sample 103-639B-41R, CC, 10–13 cm). Bar scale, 100 μm. Crossed nicols.

thick, display ripple-oblique and convolute laminated bedding (Bouma division T_c; Fig. 11). Dewatering structures ("dish" structures and water-escape pipes) are observed in Samples 103-638C-3R-2, 95 cm, and 103-638C-9R-2, 116–117 cm (Fig. 12). Some sandstone beds enclose rip-up clasts either in the massive sandstone of the Bouma T_a sequence (e.g., Sample 103-638B-41R-2, 40–45 cm) or at the boundary between T_a and the ripple-laminated T_c division (Sample 103-638C-8R-2, 11–22 cm; Fig. 13). At several levels (e.g., Section 103-638C-10R-1) thin, sharply bounded, ripple-laminated 1- to 2-cm-thick sandstone layers occur. They may be related to the action of bottom currents or, more likely, to the tails of the turbidity currents. High-angle, oblique laminae in coarse-grained sands, seen in Sample 103-638C-3R-1, 130–140 cm, might be related to the same processes.

Owing to <20% recovery in cores from this subunit, we suspect that finer grained, uncemented parts of turbidite beds were largely lost during drilling. Another explanation is that the coarsest parts of the sandstone beds are poorly cemented and thus

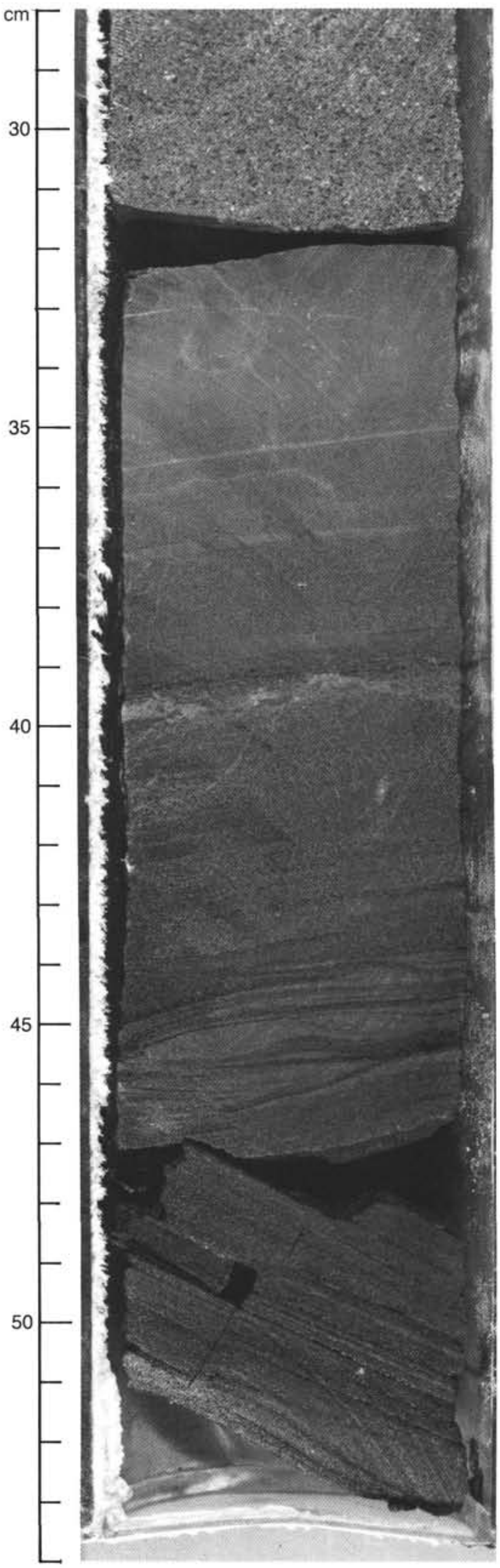

Figure 11. Fine-grained sandstone to claystone turbidite bed. Note the rippled T_c interval between the parallel-laminated T_b and T_d divisions and the massive claystone T_e at the top (Sample 103-638B-40R-1, 28-54 cm).

were not recovered. Little can be inferred about the vertical organization of the subunit.

Gray (5Y 5/1) mudstone, rich in plant debris, and dark-gray (5GY 4/1) claystone, alternating at a centimeter scale with light greenish gray (5Y 5/2) laminated nannofossil marlstone, are interbedded with the sandstone beds (Fig. 14). The claystone layers are typically less than 10 cm thick; in places they reach thicknesses of 20-30 cm (Core 103-638C-10R). They are silty at the base, faintly parallel laminated or massive, and resemble T_d and T_e of the Bouma sequence. Bioturbation, light to moderate throughout, is restricted to the upper part of some claystone units and is absent from others.

The marlstone occurs at the top of the claystone layers, in laminae or thin beds up to as thick as 1 cm. The boundary with the underlying claystone varies from sharp to gradational. Overall, marlstone makes up from 5% to 20% of the section in Cores 103-638C-1R through 103-638C-10R.

The claystone layers are interpreted as being turbidites and the marlstone as being the background pelagic deposit. This lithofacies is well developed in Cores 103-638B-42R, 103-638B-45R, and 103-638C-1R through 103-638C-10R.

Syn-sedimentary deformation (microfaults and slump structures) occurs in Samples 103-638C-4R-1, 120-130 cm, and 103-638C-8R-1, 50-130 cm (Fig. 15). In one place (Sample 103-638C-9R-3, 28-40 cm), calcite-filled veins are associated with faults (Fig. 16).

Diagenesis of Lower Cretaceous Carbonates at Site 638

The marl and calcareous clay of Subunit IIIB also contain other authigenic carbonates, including siderite, dolomite, and probably ferroan calcite and ankerite. Many of these crystals show a dark nucleus and zoned growth patterns. From Section 103-638C-7R-1 downward, siderite-rich carbonate occurs as discrete yellowish or brownish gray wavy laminae (Sample 103-638C-7R-2, 96 cm), thin beds less than 1 cm thick, or nodules. Siderite is generally localized between relatively clayey layers rich in coaly plant debris and pyrite, similar to those found near Vigo Seamount (Site 398, Basov et al., 1979). Siderite is a diagenetic mineral, diagnostic of highly reducing conditions, high partial pressure of CO_2, and a low carbonate content (Basov et al., 1979). Detrital, siderite-rich carbonate is also concentrated in the lower part of the dark-gray claystone layers (e.g., Samples 103-638C-1R-1, 56-60 cm, 103-638C-3R-1, 26-29 cm, and 103-638C-4R-1, 48-52 cm).

Preliminary Interpretation of the Mesozoic Succession

In summary, the Lower Cretaceous succession at Site 638 records the following sequence of events:

1. Deposition of terrigenous turbidite sand and mud during the late Valanginian-Hauterivian (Unit III).
2. Accumulation in the Hauterivian and perhaps the early Barremian (Subunit IIB) of a cyclically alternating sequence of pelagic marlstone and calcareous claystone, deformed in places by slumping and mass sliding.
3. Deposition of calcareous claystone turbidites in the late Barremian (Subunit IIA). These sediments are only 29 m thick and are truncated at the top by an unconformity.

The Valanginian(?)-Hauterivian sandstone contains abundant feldspar. Sand composition indicates derivation from a granitic or granodioritic terrain having minor amounts of schist and perhaps low-grade metamorphosed sandstone. The angular shape of the grains suggests little reworking and a relatively nearby source. The precise sources of the sand cannot be established, although the material ultimately could have been derived from the granites of the northern Spanish Meseta. Thick sequences of marginal-marine sediments of similar composition are known from wells drilled into the Lower Cretaceous offshore from Portugal (L. Jansa, pers. comm., 1985).

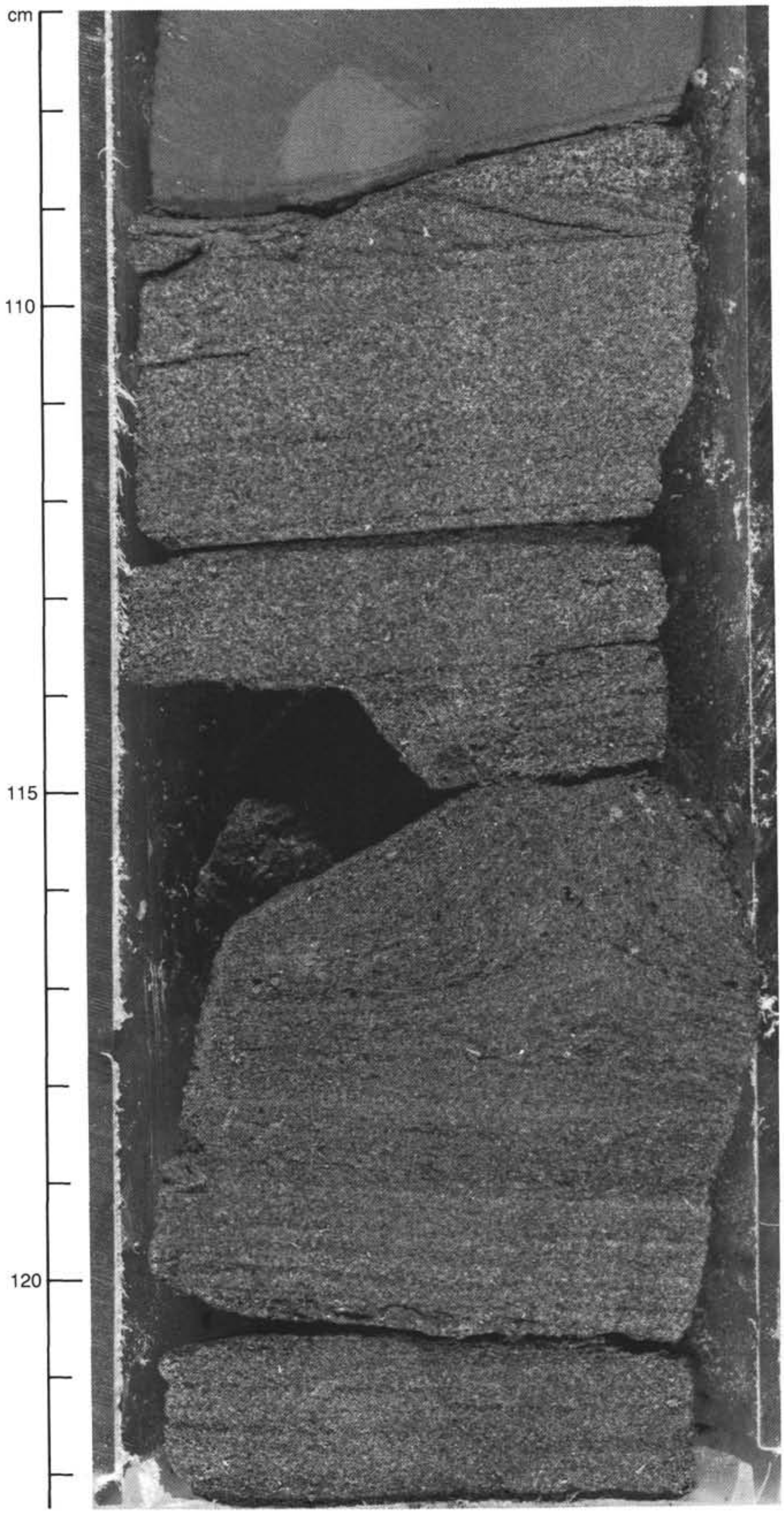

Figure 12. Water-escape pipe (at 116–117 cm) in $T_{b\text{-}c}$ turbidite bed (Sample 103-638C-9R-2, 107–122 cm).

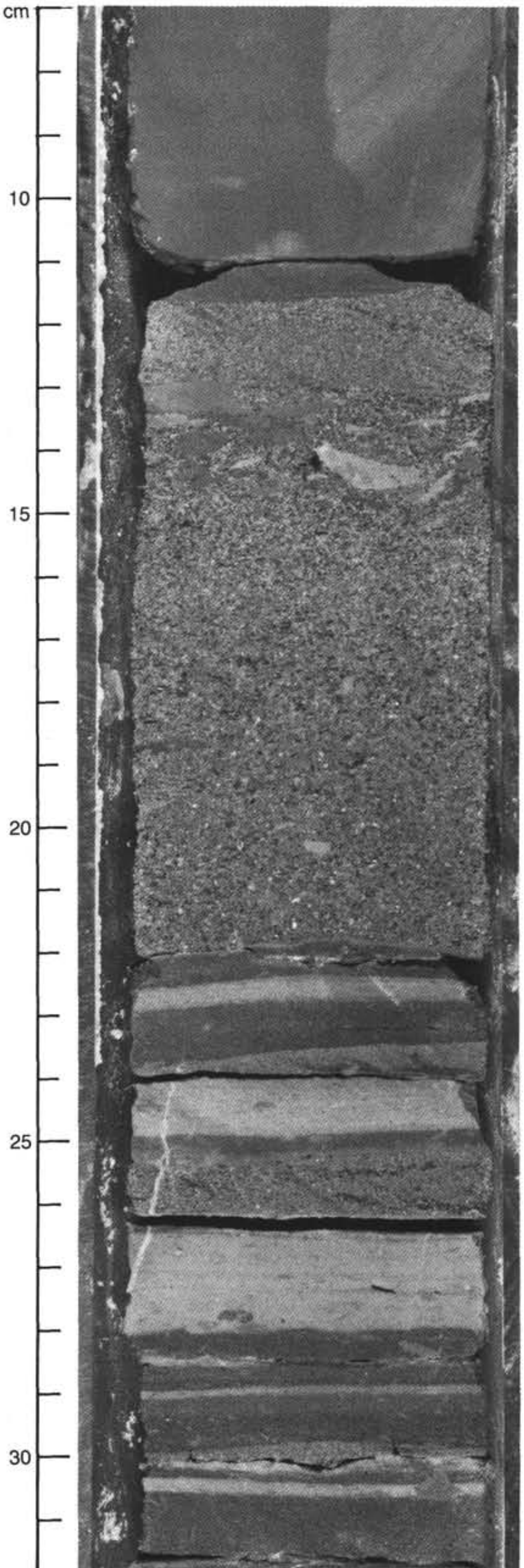

Figure 13. Turbidite bed (T_{a-d}; at 12–22 cm) showing a shale-clast-rich layer (at 13–18 cm) at the boundary between massive sandstone division T_a and ripple-laminated division T_c of the Bouma sequence (Sample 103-638C-8R-2, 7–32 cm).

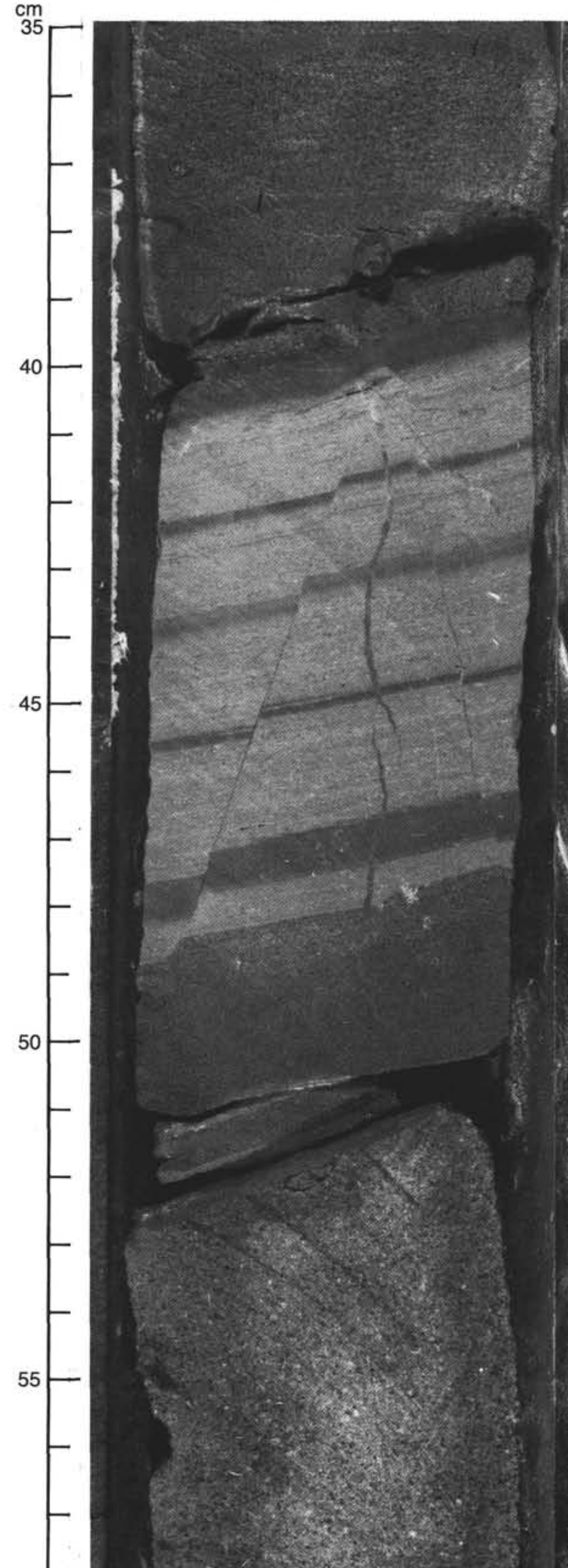

Figure 14. Millimeter-thick, dark claystone siltstone turbidites (40.5–51 cm), interbedded with light-colored, pelagic nannofossil marlstone and enclosed between two massive sandstone turbidites. Note normal fault and vertical, calcite-filled fracture (Sample 103-638B-42R-1, 35–58 cm).

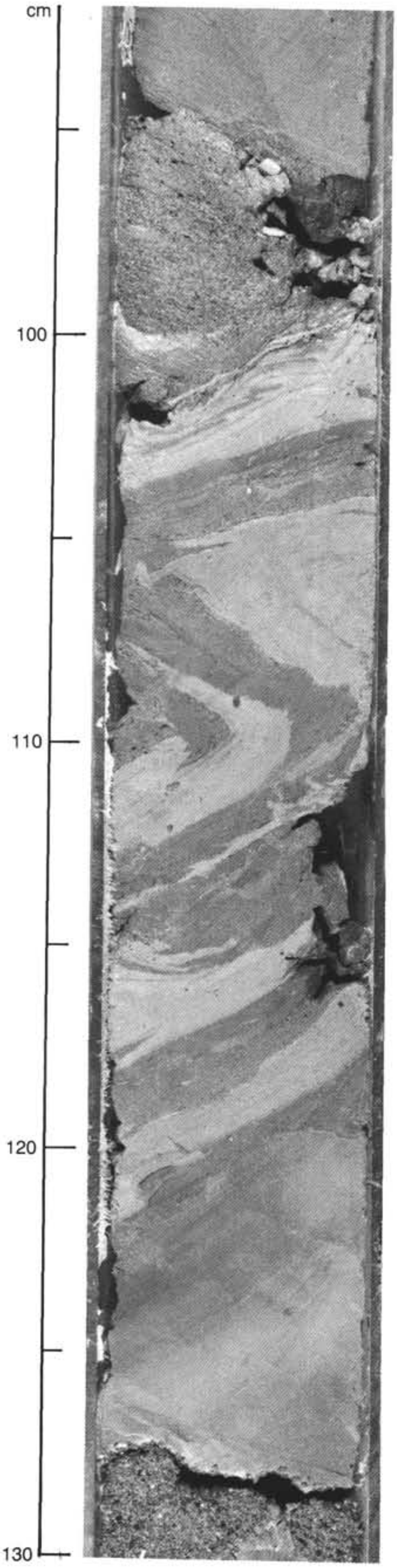

Figure 15. Syn-sedimentary slump-fold in claystone/marlstone of Subunit IIIB (Sample 103-638C-8R-1, 92–130 cm).

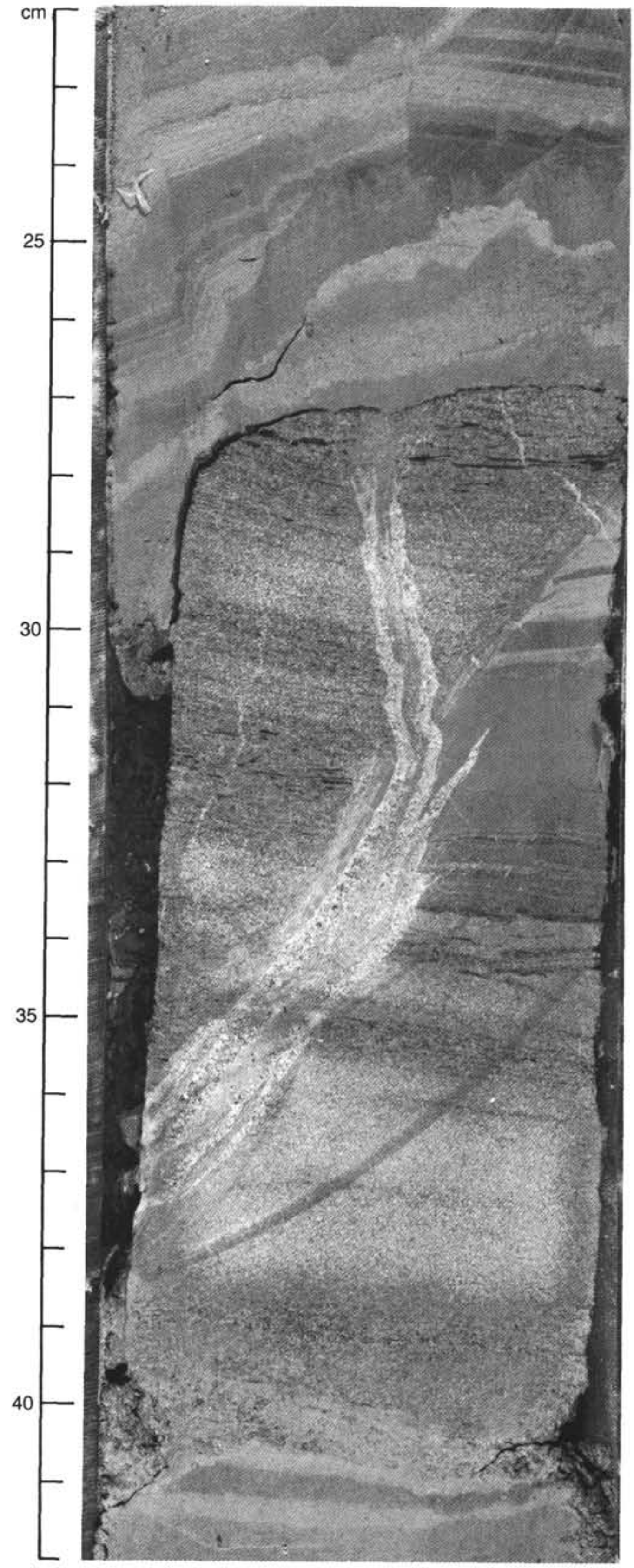

Figure 16. Microfault in sandstone of Subunit IIIB, sutured by calcite cement and cut by calcite-filled veins (Sample 103-638C-9R-3, 22–42 cm).

Terrigenous shelf deposits were widespread during the Early Cretaceous in most of Europe, along the eastern side of the Atlantic Ocean (i.e., northeastern Spain, Lusitanian Basin, Cantabrian Trough, Aquitaine Basin, and Wealden of southeast England; Anderton et al., 1979; von Rad and Arthur, 1979; Emery and Uchupi, 1984), as well as in the western Atlantic margin (eastern U.S. and Canada; Jansa and Wiedmann, 1982). Turbidites related to this period have been identified in the deep Atlantic Basin (Fuerteventura and northwest African turbidite basins; von Rad and Arthur, 1979; Robertson and Bernoulli, 1982), Moroccan Basin (Lancelot, Winterer, et al., 1980), and offshore New Jersey (Site 603; Sarti and von Rad, in press). The turbidites of Unit III clearly indicate that Site 638 is yet another locus of Early Cretaceous sand accumulation.

The turbidite sandstone beds of lithologic Unit III become finer grained and thinner upward, and the sequence gradually passes into a carbonate-rich pelagic marlstone unit (Subunit IIB). The change from terrigenous clastic sedimentation in Unit III to pelagic carbonates in Subunit IIB might be related to (1) a Hauterivian phase of tectonism and block tilting, which temporarily isolated the site from turbidity currents, or (2) a reduced clastic supply, either owing to reduced uplift and erosion or to trapping of sediments onshore because of a transgression.

Turbidite sedimentation resumed in late Barremian time and is characterized by very thin-bedded layers interbedded with pelagic deposits that are similar to those of the previous unit (Subunit IIB). The extent of late Barremian resedimentation cannot be established at Site 638, as Subunit IIA is largely eroded.

Subunit IIA is tentatively correlated with the carbonate-poor Subunit 4C of DSDP Site 398, in the Vigo Seamount area, which contains a wide variety of turbidite beds and debris-flow deposits (Sibuet, Ryan, et al., 1979). Subunit IIB may correlate with the carbonate-rich, cyclic Unit 5 at the same site.

BIOSTRATIGRAPHY

Foraminifers, nannofossils, and radiolarians were examined from core catchers and core-section intervals to provide a biostratigraphic framework for the sediments recovered from the three holes drilled at Site 638.

Hole 638A, drilled as a jet-in test for reentry operations (see "Operations" section, this chapter), provided a sample dated as early Pleistocene from nannofossil evidence. A single-bit pilot Hole 638B was drilled to a depth of 431.1 m. An upper sequence of calcareous ooze in this hole (0–184 m sub-bottom) is assigned a Neogene–Quaternary age based on both a well-preserved planktonic foraminiferal fauna and a similarly preserved nannofossil flora. The oldest Cenozoic sediments recovered from Hole 638B are late Miocene in age. Radiolarians are absent from the Cenozoic sequence of Hole 638B.

Unconformably underlying the Neogene–Quaternary sequence of Hole 638B are marly and sandy sediments of Early Cretaceous age. On the basis of foraminifer, nannofossil, and radiolarian content, these sediments are of Barremian to Valanginian age. Foraminifers are poorly to moderately well preserved and are of rare occurrence or absent from many samples, making some age assignments uncertain. Despite this, sediments of late Barremian age are indicated in Samples 103-638B-20R, CC, to 103-638B-24R, CC, by the presence of diagnostic planktonic forms. Nannofossil preservation and abundance is variable throughout Hole 638B and is lithology-dependent, though nannofossils are consistently more abundant than are foraminifers. Nannofossil assemblages allow determination of late Barremian to late Valanginian ages for the recovered sediments. Radiolarian assemblages occur throughout the Mesozoic sequence of Hole 638B but are generally poorly preserved. Pyrite replacements and overgrowths are common. Barremian-, Hauterivian-, and Valanginian-type radiolarian assemblages are observed.

A multiple reentry hole (Hole 638C) was drilled to 547.2 m at Site 638 to recover sediments as old as pre-rift and basement-rock age. Unfortunately, drilling problems forced abandonment of the hole while still in sediments of Valanginian age. Foraminifers, nannofossils, and radiolarians all indicate that the oldest sediments recovered at the bottom of Hole 638C are of the same age as the oldest sediments of Hole 638B, indicating very high sediment-accumulation rates during Valanginian time (see "Age-vs.-Depth-Curve" section, this chapter).

Foraminifers

Cenozoic

A 184-m-thick sequence of Neogene–Quaternary calcareous ooze was continuously cored in Hole 638B. Twenty-four samples (mostly core catchers) were examined for foraminiferal content to determine a biostratigraphic scheme. Planktonic foraminiferal assemblages recovered are generally well preserved, abundant, and moderately diverse. Samples from three levels (Samples 103-638B-10R-2, 149–150 cm, and 103-638B-14R, CC, and Core 103-638B-18R) contain a rare and very poorly preserved microfauna. The relative proportion of benthic foraminifers in these samples is greater than that in the others and may be a result of stronger dissolution of planktonic tests concomitant with several glacial events in the North Atlantic realm (Moullade, in press). Foraminifers at several levels indicate a trend toward a warmer-water-type assemblage, though most of the samples contain dominantly cold-water forms and lack most of the common tropical markers. Figure 17 summarizes the main observations and interpretations based on the planktonic foraminifers.

An earliest Pleistocene age is assigned to the uppermost 3 m of Core 103-638B-1R and is based on the simultaneous occurrence of *Globorotalia truncatulinoides, G. tosaensis,* and *Globigerinoides obliquus*. As at Site 637, Hole 638B appears to lack the latest Pleistocene.

The interval comprising the lower part of Core 103-638B-1R and Cores 103-638B-2R and 103-638B-3R is assigned a late Pliocene age (Zones PL4 to PL6) on the basis of the occurrence of *Globorotalia tosaensis, G. inflata, G. hirsuta,* and *Sphaeroidinella dehiscens* and the absence of *G. truncatulinoides*. The lack of such tropical markers as *G. miocenica* and *Globoquadrina altispira* precludes precise determination of Pliocene Zones PL4, PL5, and PL6.

Cores 103-638B-4R to 103-638B-9R, approximately of middle Pliocene age, proved difficult to interpret, partly because of the lack of recovery in Core 103-638B-5R. In addition, Sample 103-638B-4R-1, 149–150 cm, reveals a simultaneous highest occurrence of *Globorotalia praehirsuta* (known to range up to the PL4 Zone), *G. puncticulata* (which became extinct at the PL2/3 boundary; Moullade, in press; Ma'alouleh and Moullade, in press), and *G. margaritae* (the last occurrence of which is used to determine the PL2/3 boundary; Berggren, 1977). These abnormally simultaneous highest occurrences may be explained by a small amount of reworking or a hiatus that eliminates Zone PL3 and perhaps part of PL4. The lowermost part of the interval (Core 103-638B-9R) is thought to be no younger than Zone PL1c. This inference is based on the presence of *G. crassaformis*, the first occurrence of which defines the lower limit of this zone. Core 103-638B-10R is assigned to Zone PL1b owing to the occurrence of *G. puncticulata* and the absence of *G. crassaformis*. Sample 103-638B-11R, CC, is assigned an earliest Pliocene age (PL1a) as indicated by the presence of *G. margaritae* and *G. gr. cibaoensis-juanai* together with *G. plesiotumida* and *G. conoidea* (both of which straddle the Miocene/Pliocene boundary; Berggren et al., 1983) and the absence of distinctive Miocene markers. The Miocene/Pliocene boundary, therefore, is placed between Cores 103-638B-11R and 103-638B-12R.

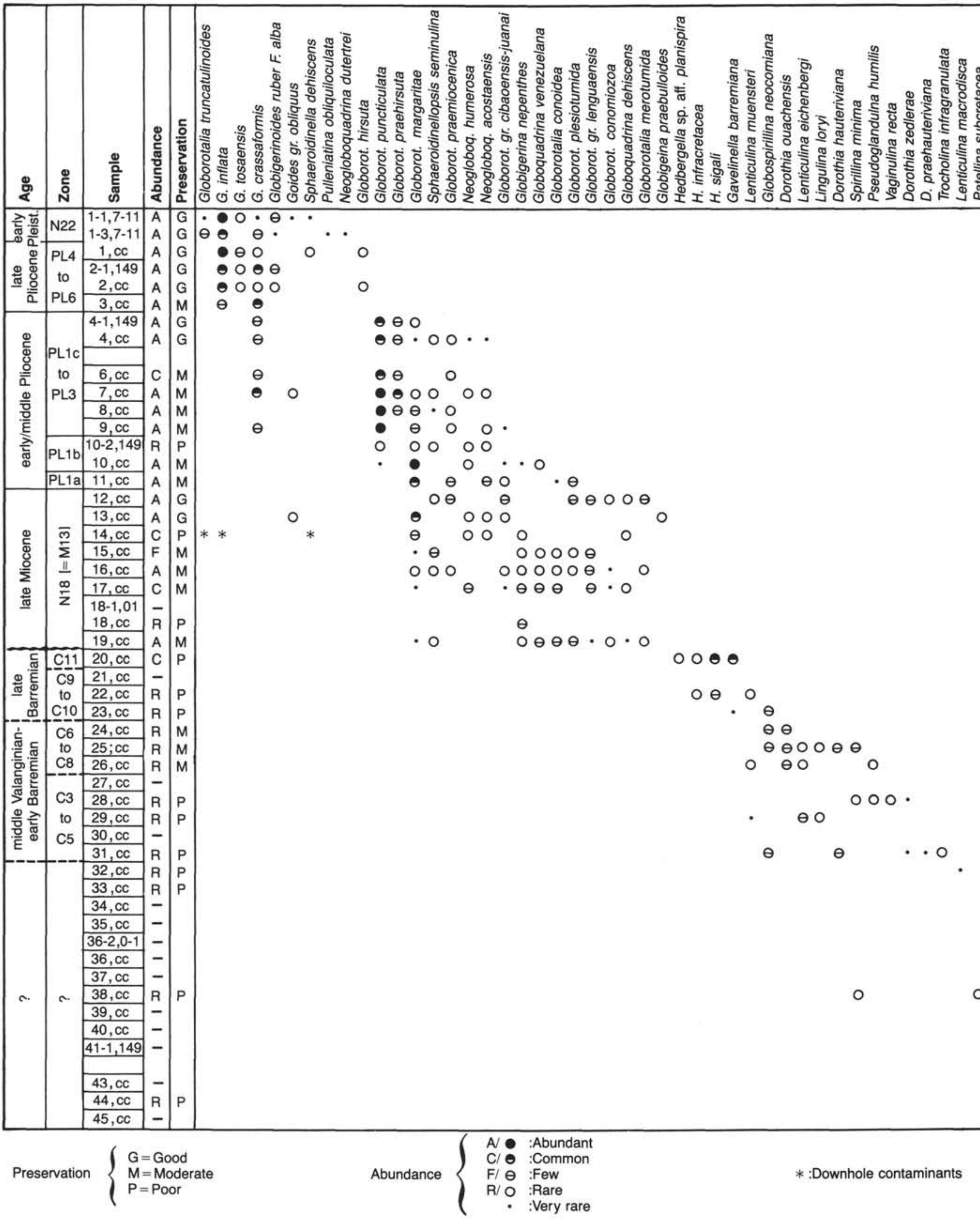

Figure 17. Vertical distribution of selected Cenozoic planktonic and Mesozoic benthic and planktonic foraminifers in Hole 638B.

The underlying Neogene interval, including Cores 103-638B-12R to 103-638B-19R and the first 3 m of Core 103-638B-20R is assigned a latest Miocene age (late Messinian), based on the consistent co-occurrence of *G. margaritae, G. conomiozoa, G. merotumida, Globoquadrina dehiscens*, and *G. lenguaensis-paralenguaensis*. The species *Neogloboquadrina humerosa* and *G. gr. cibaoensis* are restricted to the upper part of this interval. The co-occurrence of *G. margaritae* and *Globoquadrina dehiscens* has been shown to define Zone M13 (uppermost Miocene = late Messinian; Berggren et al., 1983) and is equivalent to Zone 18 described by Blow (1969).

Many Neogene samples in Hole 683B contain small amounts of reworked planktonic foraminifers of middle Cretaceous, Late Cretaceous, and Paleocene–Eocene age. This indicates that strata of these ages were eroded during the Miocene, Pliocene, and early Quaternary. A few errant occurrences of late Pliocene–Pleistocene forms in the middle Pliocene (Sample 103-638B-6R, CC) and the Miocene (Samples 103-638B-14R, CC, and 103-638B-16R, CC) are thought to be the result of downhole contamination.

Mesozoic

Hole 638B

Some 247 m of marly and sandy deposits of Early Cretaceous age, recovered from Hole 638B, unconformably underlie sediments of Neogene age. Core-catcher samples examined for foraminiferal content reveal rare, very small and poorly preserved specimens. A few planktonic species accompanied by a minor benthic component occur in the uppermost part of the Cretaceous section (i.e., Cores 103-638B-20R to 103-638B-22R). From Core 103-638B-23R down to Core 103-638B-44R, however, only benthic foraminifers were recovered.

Foraminiferal zonation schemes developed by Moullade (1966, 1974, 1983) and Magniez-Jannin et al. (1984) (mainly established in the Tethyan realm) were used to interpret these Early Cretaceous assemblages. The vertical distribution of planktonic and selected benthic species in Hole 638B is shown in Figure 17.

Lithologic Subunit IIA (see "Sediment Lithology" section, this chapter), comprising the lowermost part of Core 103-638B-20R, Cores 103-638B-21R, and 103-638B-22R, and the upper part of Core 103-638B-23R, is tentatively assigned a late Barremian (Zones C9–12) age on the basis of the following criteria:

1. The occurrence of rare specimens of *Hedbergella* sp. aff. *planispira* (sensu Moullade, 1966; non *similis* Longoria) in Samples 103-638B-20R, 13–17 cm, and 103-638B-20R, CC. This taxon is known to occur first in the latest Barremian.
2. The occurrence of *Gavelinella barremiana* in Samples 103-638B-20R, CC (as common) and 103-638B-23R, CC (as a single specimen only). This taxon first appears in the Tethyan domain at the early/late Barremian boundary.

On the other hand, both of these two markers are known to range up into the early Aptian. The presence of *H. sigali* and *H. infracretacea*, which are found to be relatively common in Samples 103-638B-20R, CC, and 103-638B-22R, CC, do not help solve this problem because they are both long-ranging species. Both taxa first appeared in the late Hauterivian and became extinct either in the earliest Gargasian (*sigali*) or in the middle Albian (*infracretacea*). That the sediments involved are Barremian age is indicated by the presence of one orbitolinid specimen attributed to *Paleodictyoconus barremianus* (a shallow-water early–middle Barremian species). This neritic form was identified in a thin section made from Sample 103-638B-22R-3, 126–128 cm, for which the paleoenvironmental interpretation indicates contemporaneous redeposition rather than reworking from older horizons.

Dating of lithologic Subunit IIB (Sections 103-638B-23R-3 to 103-638B-32R-2) on the basis of its foraminiferal content is more difficult, owing to the sporadic occurrence of assemblages of low diversity composed of small, mostly bathyal calcareous specimens. Furthermore, ample sedimentologic evidence ("Sediment Lithology" section, this chapter) indicates that most if not all these microfaunas (sometimes enriched by rare shallow-water components) were transported to greater depths by turbidity currents and quickly buried to depths where they were well protected from dissolution below the CCD. As a result, it is practically impossible to discern whether the lowest and highest foraminiferal occurrences observed in Hole 638B truly represent first and last appearances as used in the current zonal schemes. Therefore, Subunit IIB can be only tentatively assigned a middle Valanginian to early Barremian(?) age. The following is evidence for this:

1. Specimens of *Dorothia ouachensis*, a species that first occurred in the middle Hauterivian, were recovered from Samples 103-638B-24R, CC, 103-638B-25R, CC, and 103-638B-26R, CC.
2. Specimens of *D. hauteriviana* and *D. zedlerae*, taxa that first occurred in the middle Valanginian and whose last occurrences are recorded at the Hauterivian/Barremian boundary, were recovered in Samples 103-638B-25R, CC, 103-638B-29R, CC, and 103-638B-31R, CC.
3. Very rare specimens of *D. praehauteriviana*, a middle Valanginian marker, occur in Sample 103-638B-31R, CC.

From the late Barremian age of Subunit IIA and the age of Sample 103-638B-25R, CC, which cannot be younger than the Hauterivian/Barremian boundary, it appears that only Core 103-638B-24R and part of Core 103-638B-25R might belong to the early Barremian (i.e., in Hole 638B, this substage is either condensed or missing). Cores 103-638B-25R and 103-638B-26R are definitely Hauterivian according to their foraminiferal content. A late Valanginian age is not fully demonstrated for the lower part of Subunit IIB.

Lithologic Unit III cannot be dated using foraminifers, owing to the recovery of only extremely rare and non-age diagnostic forms such as small nodosariids, *Ammodiscus-Spirillina*-like pyritized tests, and primitive tiny agglutinated forms from below Core 103-638B-32R. The general paucity of foraminifers in this unit is due either to an extreme dilution of the specimens with rapidly sedimented terrigenous deposits and/or a depositional environment near or below the CCD.

Hole 638C

The 135-m-thick silty clay and sandstone sequence cored in Hole 638C is almost completely devoid of foraminifers. Only extremely rare, relatively well-preserved benthic species (mostly lenticulinids) were found in Samples 103-638C-1R, CC, 103-638C-4R, CC, 103-638C-9R, CC, and 103-638C-14,CC. Almost all these lenticulines (*Lenticulina macrodisca, L. subangulata, L. subalata, L. crassa,* and *L. roemeri*) are long-ranging species, encountered mainly in sediments deposited in outer-shelf and bathyal (upper- to mid-slope) environments from the Lower Cretaceous in the Tethyan realm (Bartenstein and Bettenstaedt, 1962; Moullade, 1966; Neagu, 1972, 1975; Guerin, 1981). A rare occurrence of *Lenticulina nodosa*, the acme of which defines the early Valanginian (Zone C2) (Moullade, 1979, 1984, in press), occurs in Sample 103-638C-4R, CC, though the few specimens are not sufficient to determine a precise age.

The lenticulinid microfauna occurs only rarely in Hole 638C and perhaps represents elements of an autochthonous foraminiferal benthos.

Samples 103-638C-1R, CC, and 103-638C-4R, CC, also reveal very rare, small, and poorly preserved trocholinas (*Trocholina paucigranulata* and *T. infragranulata*). These shallow-water specimens were probably displaced from the inner shelf and redeposited by turbidites.

A few aptychi (Ammonites operculae) are also common in the washed residues that contain foraminifers. One belemnite specimen (*Pseudobelus bipartitus*, determ. J. Wiedmann) was observed in Sample 103-638C-4R-2, 65 cm. The occurrence of such macrofossils is consistent with our interpretation of deposition of Hole 638C sediments in an outer-shelf or upper- to mid-slope environment.

Nannofossils

Cenozoic

Hole 638B

Late Miocene through early Pleistocene nannofossil assemblages were recovered from 184 m of nannofossil and clayey nannofossil oozes at this site. Late Miocene assemblages indicative of the *Discoaster neohamatus* Zone (CN-8) unconformably overlie Cretaceous strata in Section 103-638B-20R-3. Nannofossils are abundant throughout the Cenozoic section; preservation is moderate to good in Pliocene/Pleistocene assemblages, but poor to moderate in late Miocene assemblages. Core recoveries, although low in many cores, were better than those at Site 637. However, a large percentage of the section was highly disturbed by drilling. The absence of *Discoaster berggrenii* and *D. quinqueramus* and the genus *Ceratolithus* (except for isolated specimens in two samples) greatly reduce biostratigraphic resolution in upper Miocene and lower Pliocene sediments.

Two hiatuses were recognized in the Cenozoic section at this site. The first occurs between Samples 103-638B-2R-1, 34-35 cm, and 103-638B-2R-1, 125-126 cm, where a large part of the upper Pliocene and possibly part of the early Pleistocene are absent. Core 103-638B-1R and the top part of Section 103-638B-2R-1 contain *Gephyrocapsa oceanica, Helicosphaera sellii,* and *Calcidiscus macintyrei. G. oceanica* first occurs at the base of the *Helicosphaera sellii* Zone at Site 637, suggesting that the lowermost Pleistocene *Calcidiscus macintyrei* Zone is absent at this site. Samples 103-638B-2R-1, 125-126 cm, through 103-638B-4R-7, 11-12 cm, contain *Discoaster tamalis, D. surculus, D. pentaradiatus, D. assymmetricus,* and *D. brouweri* and are assigned to the *Discoaster tamalis* Subzone (CN-12A) of early-late Pliocene age. A second hiatus is recognized below this. Sample 103-638B-4R, CC, contains *Amaurolithus delicatus, A. primus,* and *Reticulofenestra pseudoumbilica* and is dated in the early Pliocene *Amaurolithus tricorniculatus* Zone (CN-10).

Division of the *Amaurolithus tricorniculatus* Zone (CN-10) into subzones and subsequent determination of the Miocene/Pliocene boundary is based on species of the genus *Ceratolithus*. Isolated specimens of *Ceratolithus rugosus* in Samples 103-638B-8R-7, 45-46 cm, and 103-638B-8R-5, 76-77 cm, were the only ceratoliths observed in this section and indicate an early Pliocene age (*Ceratolithus rugosus* Subzone CN-10C) or younger for the bottom of Core 103-638B-8R. The presence of *Discoaster tamalis* and *D. asymmetricus* in Sections 103-638B-8R-5 and 103-638B-8R-6, respectively, confirms an early Pliocene age for this core. These two species, for which first occurrences are generally reported above the extinction level of the genus *Amaurolithus* in the *Reticulofenestra pseudoumbilica* Zone (CN-11), overlap in occurrence with the amauroliths at both Sites 637 and 638.

The next reliable datum downcore is the lowest occurrence of the genus *Amaurolithus* in Sample 103-638B-17R-1, 20-21 cm, which defines the base of the late Miocene *Amaurolithus primus* Subzone (CN-9B). Thus, Cores 103-638B-9R through 638B-17R-1 cannot be precisely zoned and are considered undifferentiated upper Miocene to lower Pliocene. The highest consistent occurrence of *Triquetrorhabdulus rugosus* in Sample 103-638B-11R-3, 25-26 cm, is weak evidence of Miocene below that sample, although the last occurrence of this species has been used to approximate the Miocene/Pliocene boundary. The rare and sporadic occurrences of this species further uphole and in lower Pliocene sediments at Site 637 and other deep-sea sections is reason for caution. Samples 103-638B-17R, CC, through 103-638B-18R-5, 67-68 cm, contain *Discoaster surculus* but no amauroliths, and the late Miocene *Discoaster berggrenii* Subzone (CN-9A) is determined for that interval. Both *D. loeblichii* and *Minylitha convallis* have their highest occurrences in Sample 103-638B-18R-3, 57-58 cm. The former species has a reported first occurrence at the base of the *Discoaster neohamatus* Zone (CN-8) (Perch-Nielsen, 1985). Its presence in samples without *D. surculus* below Sample 103-638-18R-5, 67-68 cm, dates the base of the Cenozoic section at this site in the *Discoaster neohamatus* Zone (CN-8).

Mesozoic

Hole 638B

Late-Barremian- through late-Valanginian-age nannofossil assemblages are present in Section 103-638B-20R-3 through Core 103-638B-45R (lithologic Units II and III; see "Sediment Lithology" section, this chapter). An unconformity is recognized between lithologic Subunits IIA and IIB in Section 103-638B-23R-3, 27 cm; the lower Barremian and part of the upper Hauterivian are missing. Below this unconformity and down to the bottom of the hole, the section appears continuous and contains nannofossil assemblages of late Valanginian to late Hauterivian age. Age determinations for the Mesozoic section in Hole 638B are based on Thierstein (1971, 1973, 1976), Sissingh (1977), Perch-Nielsen (1979), and Roth (1983).

Nannofossils are generally common to abundant in both claystone and marlstone from Unit II and Subunit IIIA. Assemblages are moderately well preserved in the claystone and poor to moderately preserved in the marlstone. The limestones restricted to Subunit IIA contain few to common, poorly preserved nannofossils. Abundance and preservation quality of assemblages decrease in Subunit IIIB compared with younger strata. The decrease in abundance may be due to dilution by terrigenous material.

Lithologic Subunit IIA (103-638B-20R-3, 3 cm, to 103-638B-23R-3, 27 cm) is assigned to the *M. hoschulzii* Zone (CC-6), late Barremian in age (Sissingth, 1977). The absence of *Rucinolithus irregularis*, which has its first occurrence at the Barremian/Aptian boundary (Thierstein, 1973; Perch-Nielsen, 1979), and the occurrence of *Chiastozygus tenuis* and *Haysites radiatus* are evidence of an age no younger than late Barremian for Subunit IIA. The boundary between Subunit IIA and Subunit IIB (Sample 103-638B-23R-3, 27 cm) marks the highest occurrence of both *Lithraphidites bollii* and *Calcicalathina oblongata.* These two species became extinct in the early Barremian, and the last occurrence of *Calciclathina oblongata* is often utilized as a datum for the top of the lower Barremian (Thierstein, 1976; Sissingh, 1977; Perch-Nielsen, 1979). *Speetonia colligata*, a species having its last-occurrence datum in the late Hauterivian, occurs in this hole one core section below the top of Subunit IIB in Sample 103-638B-23R-4, 55-56 cm. Thus, the interval from the highest *Speetonia colligata* to the highest *Calcicalathina oblongata* (late Hauterivian to early Barremian) is represented by only one core section (103-638B-23R-3); evidently, part of the upper Hauterivian and all of the lower Barremian are missing at the lithologic boundary between Subunits IIA and IIB.

Samples 103-638B-23R-4, 55-56 cm, through 103-638B-24R, CC, contain *Lithraphidites bollii* and *Speetonia colligata* but not *Cruciellipsis cuvillieri.* A late Hauterivian age is assigned to this interval. Samples 103-638B-25R-1, 86-87 cm, through 103-638B-29R, CC, contain both *Cruciellipsis cuvillieri* and *Lithraphidites bollii* and are dated as early to late Hauterivian. The interval including Samples 103-638B-23R-3, 27 cm, through 103-

638B-29R, CC, is assigned to the *Cretarhabdus loriei* Zone (CC-4b; Sissingh, 1977).

A relationship exists between lithology and species composition in Unit II. Above Section 103-638B-26R-1, nannoconids are abundant in both marlstone and limestone, whereas few are found in the claystone. The only exception to this is a single sample of claystone in Subunit IIA that contains abundant nannoconids; a microthin layer of calcareous-rich material was possibly included in this sample. Below Section 103-638B-26R-1, nannoconids are not abundant in any lithology. Conversely, *Tubodiscus verenae* and *Diadorhombus rectus* occur preferentially in claystone. Both species are found much higher in the section than expected. Their presence may be due to reworking, though other species that normally occur with them in Valanginian sediments at other localities do not appear in the younger horizons together with (or above) these species.

The placement of the Hauterivian/Valanginian boundary in the interval from Cores 103-638B-30R through 103-638B-45R, CC, is difficult for several reasons. *Tubodiscus verenae* and *Diadorhombus rectus*, which are thought to be restricted to the Valanginian and are used by some (Thierstein, 1973; Roth, 1983) to delineate the Valanginian/Hauterivian boundary, occur in many samples from this interval. *Tubodiscus verenae* occurs consistently up to Sample 103-638B-24R-4, 55–56 cm (above the first-occurrence datum of *Lithraphidites bollii*), and *Diadorhombus rectus* occurs sporadically up to the top of the Lower Cretaceous part of the section. The first occurrence of *Cretarhabdus loriei*, which is used by Sissingh (1977) to delineate this stage boundary, resembles older forms and is difficult to use. The first occurrence of *Nannocous bucheri* cannot be used because of the absence of nannoconids in the sand turbidite sequence. The lowest occurrence of *Chiastozygus striatus*, used by Perch-Nielsen (1979) to delineate this boundary, is also difficult to use because of its rare occurrence downhole and its close resemblance to a smaller form described at Site 397 (Wind and Cepek, 1979) as *Eiffellithus* sp. Transitional forms between the two are observed in Cores 103-638B-31R-1 through 103-638B-44R-1. This smaller species has also been observed in Valanginian-age sediments from the Angles section in France. The lowest occurrence of *Chiastozygus striatus* (sensu stricto) is placed in Sample 103-638B-33R-1, 135–136 cm, whereas the lowest occurrence of *Eiffellithus* sp. is in Sample 103-638B-44R-1, 38–39 cm. Whether or not this smaller form is an ecologic variant of *C. striatus* is unclear. For these reasons, we do not now attempt to place a Hauterivian/Valanginian boundary.

The occurrence of *Parhabdolithus infinitus* and *Calcicalathina oblongata* to the bottom of the hole is evidence of an age no older than late Valanginian. The interval between Samples 103-638B-30R-1 to 103-638B-45R, CC, is placed in the *Calcicalathina oblongata/Cretarhabdus loriei* Zones (CC3/CC4a) of a late Valanginian to early Hauterivian age (Thierstein, 1971; Sissingh, 1977).

Hole 638C

Nannofossils are rare to common in fine-grained sediment recovered from Hole 638C. Because of dilution by terrigenous material, nannofossils are rare or absent in siltstone and sandstone. Assemblages in the layers of light-colored, fine-grained sediment are moderately well preserved. The persistent occurrence of *Speetonia colligata* and *Cruciellipsis cuvillieri* in the absence of *Lithraphidites bollii*, a species that occurs higher uphole in Hole 638B, indicates an age no younger than early Hauterivian for sediments recovered from Hole 638C. The occurrence of *Parhabdolithus infinitus* in all samples examined from Hole 638C is evidence of an age no older than late Valanginian (Thierstein, 1976; Wind and Cepek, 1979; Roth, 1983). The absence of *Rucinolithus wisei* (late Berriasian to early Valanginian) is also noted. *Diadorhombus rectus, Tubodiscus verenae*, and *Calcicalathina oblongata* are present in almost all samples. These three species are known to have their earliest occurrences near the base of the Valanginian. The entire section recovered from Hole 638C is assigned to the *Calcicalathina oblongata/Cretarhabdus loriei* Zones (CC3/CC4a), late Valanginian to early Hauterivian in age.

Radiolarians

Cenozoic

Radiolarian preparations were made for all core-catcher samples from the Cenozoic section recovered from Hole 638B and for an additional 60 samples from Cores 103-638B-1R to 103-638R-20R. The noncalcareous fraction (>62 μm) is dominated by small amounts of detrital mineral grains, mainly mica and quartz, and rare lithic grains. Samples 103-638B-7R, CC, to 103-638B-18R, CC, contain pyrite.

Radiolarians and other siliceous microfossils are absent in Samples 103-638B-1R-2 to 103-638B-20R, CC, although spherical aggregates of pyrite in Samples 103-638B-12R, CC, 103-638B-16R, CC, and 103-638B-17R, CC, may be the remains of radiolarians.

Mesozoic

All core-catcher samples together with an additional 150 samples from Cores 103-638B-20R to 103-638B-45R (except 103-638B-45R, where the core catcher contained only massive sandstone) were examined for radiolarians.

Well-preserved radiolarians were obtained from Core 103-638B-21R-1 down to Core 103-638B-25R, CC. Radiolarians recovered from marly or limestone intervals are preserved in silica, whereas radiolarians recovered from the clayey and organic-rich intervals are preserved in pyrite. Additional, poorly preserved radiolarian assemblages (usually pyritized) are scattered throughout the sequence cored at this site (Fig. 18).

Radiolarian occurrences and mode of preservation permit recognition of two intervals within the Cretaceous sedimentary section of Hole 638B.

1. In Cores 103-638B-20R to 103-638B-31R (lithologic Unit II), radiolarians are common both in the bioturbated marlstone as well as in the silty detrital layers enriched in terrestrial plant material and mica. The preservation of the taxa is not uniform. In Samples 103-638B-21R-1, 4–6 cm and 103-638B-22R-1, 94–96 cm, the radiolarians are replaced by calcite (Fig. 19A); only a small amount of the specimens remain preserved in silica as quartz recrystallized from biogenic opal (Fig. 19B). The ratio between spumellarians and nassellarians is approximately 1:1. Sample 103-638B-21R, CC, also contains siliceous radiolarians, but here spumellarians dominate strongly over nassellarians, and taxa belonging to the Hagiastridae and Patulibracchidae form the largest part of the preserved fauna. All specimens show extensive dissolution patterns on the surface of the tests (Fig. 19C).

Sample 103-638B-25R, CC, where radiolarians are also common and well preserved, represents the third type of preservation observed in this interval. The original tests were replaced by pyrite without destruction of the fine patterns of the skeletons (Fig. 19D).

In some samples, internal molds of zeolites and framboidal pyrite occur (Sample 103-638B-22R, CC; Figs. 19E and 19F).

2. In Cores 103-638B-32R to 103-638B-45R (lithologic Unit III), radiolarians are confined to silty-sandy layers and are scarce (except for Samples 103-638B-35R-1, 148–150 cm, 103-638B-43R-1, 148–150 cm, and 103-638B-45R-1, 146–150 cm, where radiolarians are common but mainly recrystallized). Many internal molds of pyrite (with or without the original skeleton) are also observed (Fig. 19G). This recrystallization, together with

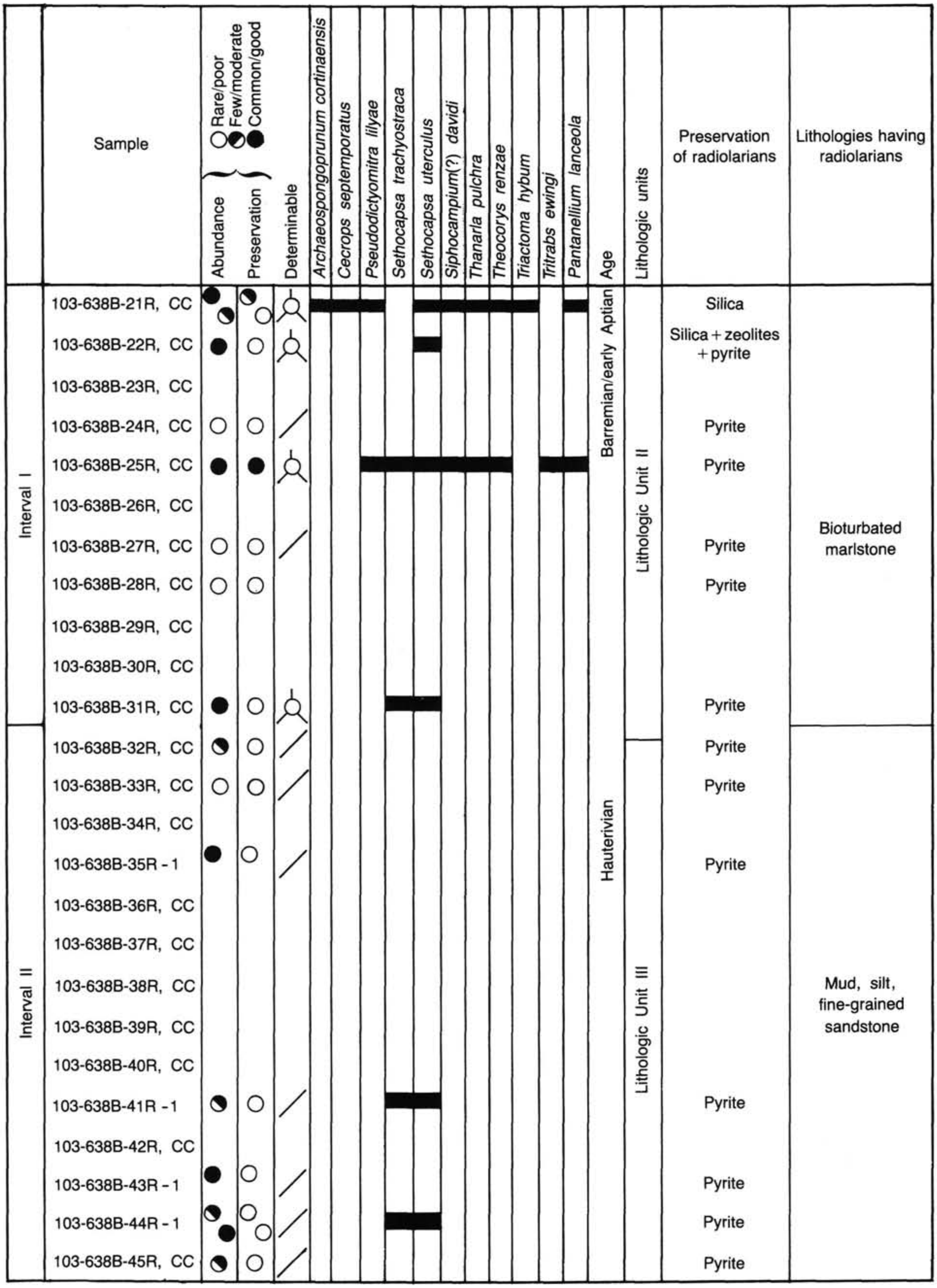

Figure 18. Radiolarian distribution, Hole 638B.

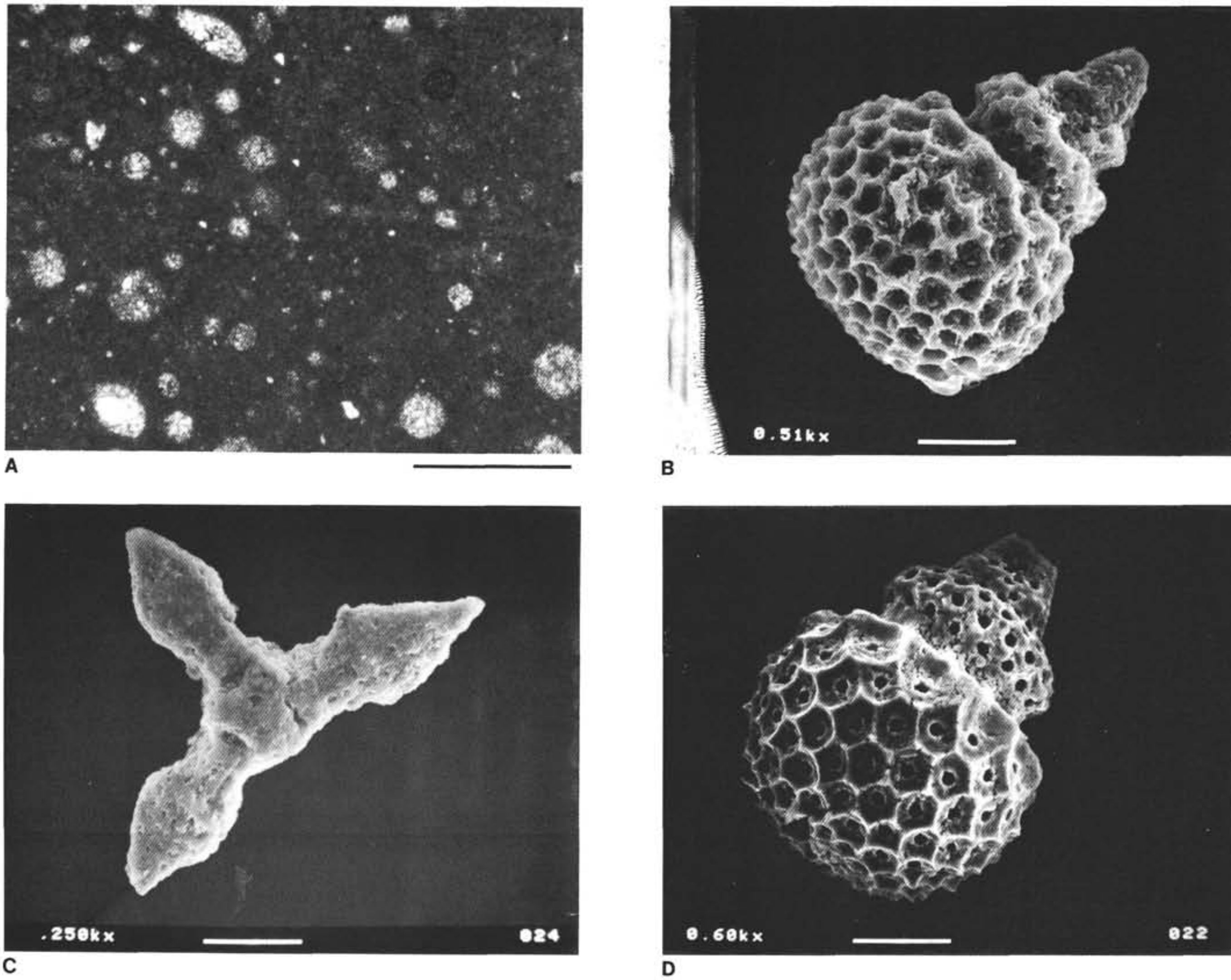

Figure 19. Preservation of radiolarians from the Hauterivian–Barremian interval of Hole 638B. A. Bioturbated marlstone with calcite-replaced radiolarians. (Thin-section of Sample 103-638B-22R-1, 94–96 cm.) Scale bar, 500 μm. B. Quartz recrystallization of radiolarian test (*Sethocapsa uterculus*). Scale bar, 40 μm. (Sample 638B-21R-1, 4–6 cm.) C. Dissolution pattern of radiolarian test recrystallized in quartz. Scale bar is 80 μm. (Sample 103-638B-21R, CC.) D. Pyrite recrystallization of radiolarian test. Scale bar, 35 μm. (Sample 103-638B-25R, CC.) E. Mold of radiclarian test (*Pseudodictyomitra* sp.) Scale bar, 45 μm. (Sample 638B-22R, CC.) F. Close up of E, with zeolite crystals. Scale bar, 10 μm. G. Pyrite mold of radiolarians with pyrite overgrowth. Scale bar, 50 μm. (Sample 103-638B-31R, CC.) H. Pyrite crystals growing from radiolarian test that is recrystallized in pyrite (*Archaeodictyomitra*). Scale bar, 40 μm. (Sample 103-638B-31R, CC.)

crystal overgrowth by pyrite, masks specimens and does not allow the determination of significant taxa (Fig. 19H).

The zonation established by Schaaf (1984) for the Lower Cretaceous could not be used owing to the lack of the marker species in Hole 638B. However, use of his range chart and the detailed description of characteristic short-ranging taxa enabled the time interval drilled to be fixed. Results correspond to the data for nannofossils and foraminifera (Fig. 18). All samples with well-preserved radiolarians contain some elements in common, although not all the distinctive species are present in all the samples. The rich assemblage in Sample 103-638B-21R-1, 4–6 cm, contains numerous taxa that indicate a Hauterivian/Barremian age. More precisely, the co-occurrence of *Siphocampium*(?) *davidi, Theocorys renzae, Cecrops septemporatus, Sethocapsa uterculus*, and *Pseudodictyomitra lilyae* indicates a middle Hauterivian to middle Barremian age. A few specimens of *Archaeospongoprunum cortinaensis* and *Triactoma hybum*, known to have their lowest occurrence at the base of the Barremian, suggests early to middle Barremian age. Sample 103-638B-21R-5, 52–54 cm (dissolved limestone), contains *Grolanium pythiae*, the marker species for late Barremian/early Aptian, and restricts Core 103-638B-21R to this age. The equally rich fauna in Sample 103-638B-25R, CC, contains almost the same assemblage, except that the occurrence of *Tritrabs ewingi* and taxa similar to *Sethocapsa trachyostraca* restrict the age to Hauterivian–earliest Barremian. The poor preservation in Samples 103-638B-31R, CC, 103-638B-41R-1, 148–150 cm, and 103-638B-44R, CC, prevents a precise age assignment, although the occurrence of *Sethocapsa uterculus* and *Sethocapsa* cf. *trachyostraca* makes a Hauterivian age reasonable. Moreover, this is supported by Sample 103-638B-31R-2, 34–38 cm, which contains *Dibolachras tytthopora*(?), *Sethocapsa leiostraca*, and *S. tracyostraca*. The co-occurrence of these forms indicate an Hauterivian age for this sample.

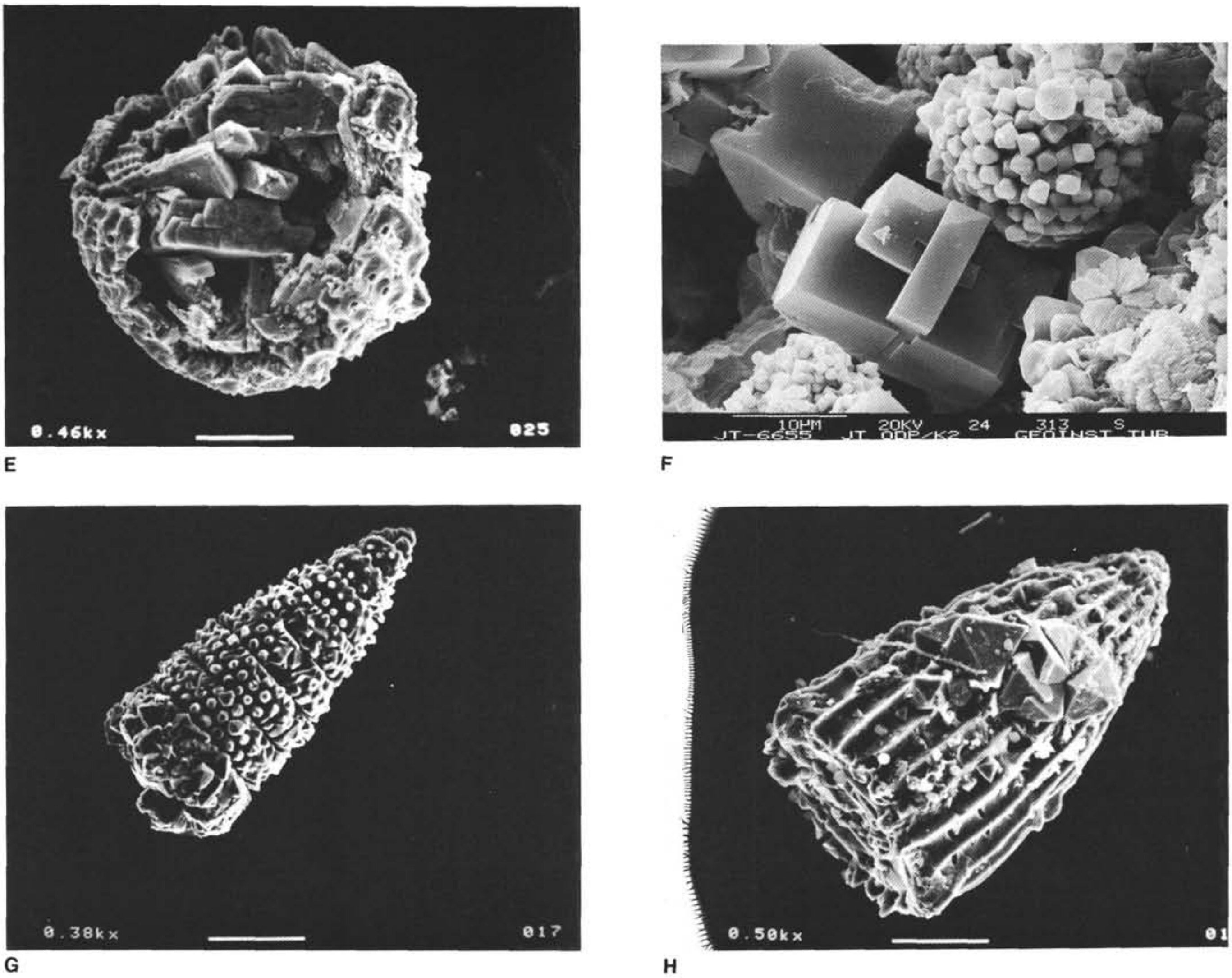

Figure 19 (continued).

Hole 638C

Radiolarians are generally common in Hole 638C. All faunas are recrystallized in pyrite having strong crystal overgrowth. Except in only a few specimens, pyrite molds are preserved.

Sample 103-638C-5R, CC, contains *Podocapsa* cf. *amphitreptera*, a taxon having its latest occurrence in the middle Berriasian of the Tethys region (Baumgarter, 1984) and in the middle Valanginian of the Pacific Ocean (Schaaf, 1984). The co-occurrence of the nannofossil *Calcicalathina oblongata* supports a middle Valanginian age for this sample.

Summary

1. Site 638, drilled on the Iberian margin, recovered sediments ranging in age from Valanginian to Quaternary.
2. Foraminifers and nannofossils are generally well preserved and abundant in the Neogene–Quaternary sequence of calcareous ooze.
3. The oldest Neogene sediments recovered are late Miocene in age.
4. The upper Miocene is unconformably underlain by Lower Cretaceous sediments of late Barremian age.
5. Foraminifers are rare or absent in all Lower Cretaceous sediments of Hole 638B and 638C. Nannofossils are generally more abundant and better preserved. Radiolarians are present but generally poorly preserved and mainly pyritized.
6. Foraminiferal, nannofossil, and radiolarian evidence indicates the presence of upper Barremian, Hauterivian, and Valanginian sediments.

Figure 20 summarizes the biostratigraphic conclusions derived through examination of foraminifers, nannofossils, and radiolarians present in sediment recovered from Hole 638B.

PALEOMAGNETICS

The shipboard paleomagnetics program at Site 638 consisted entirely of sampling for magnetostratigraphy after it became apparent that rust-flake contamination rendered whole-round rotary-core analysis useless (as explained in the "Explanatory Notes" chapter, this volume). None of the discrete samples were analyzed aboard ship, owing to their weak intensities (generally only slightly above the background noise related to the roll of the ship) and the lack of thermal-demagnetization equipment.

Forty-one oriented cubes (6 cm^3) were collected from the Neogene nannofossil ooze of Cores 103-638B-7R through 103-638B-20R, and 202 oriented minicores and cubes were taken from the Lower Cretaceous limestone and turbidites of Cores 103-638B-20R through 103-638B-45R and Cores 103-638C-1R through 103-638C-14R. Intervals in the Lower Cretaceous that are unaf-

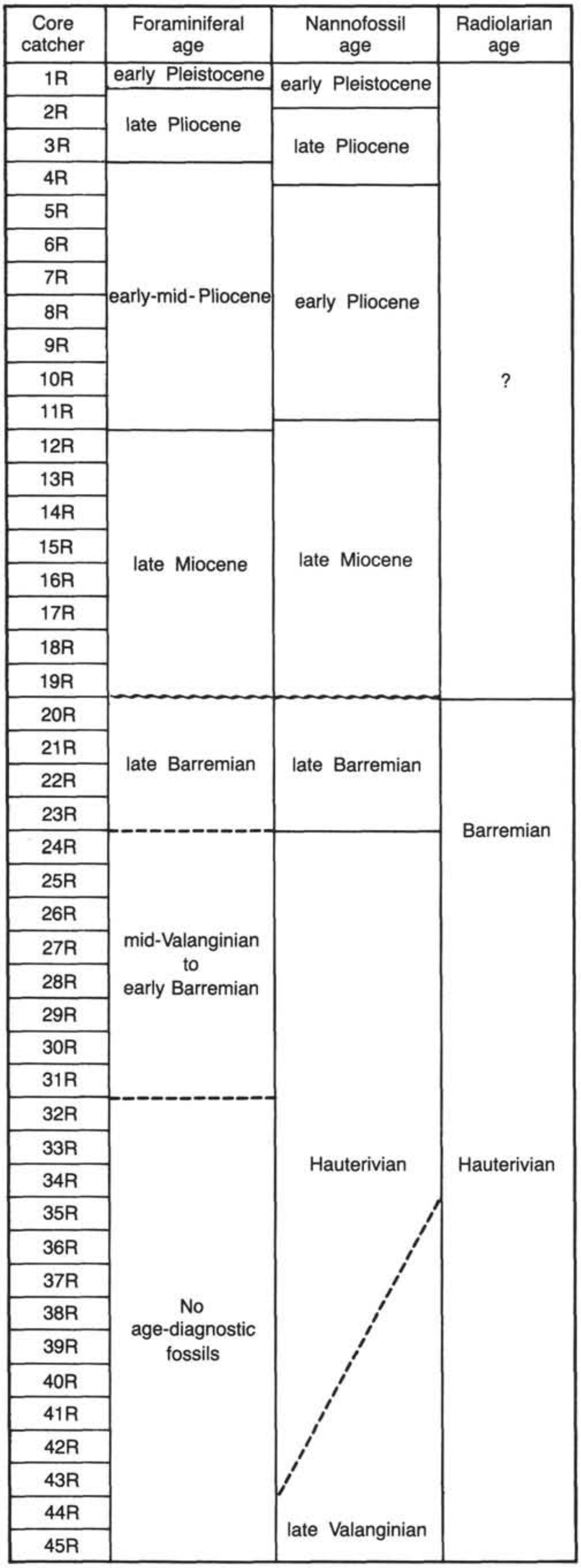

Figure 20. Biostratigraphic summary of Hole 638B.

fected by slumping have an apparent dip of 19° to 23° in Hole 638B and 10° to 15° in Hole 638C (the difference is thought to be caused by the greater deviation from vertical of Hole 638B). The relative declination of the paleomagnetic samples with respect to this dip direction was recorded for use in declination control during later analysis. Pelagic sediment (bioturbated limestone/chalk or laminated marlstone) was sampled preferentially, though several samples were taken in the finer grained clastic turbidites of Hauterivian–Valanginian age.

Shore-Based Analysis Procedure

A detailed description of the paleomagnetic sample measurement and data analysis procedures is given by Ogg (in press) and in the paleomagnetics chapters that will be published in the Leg 103 Part B volume. These procedures are summarized as follows:

The samples were analyzed with a two-axis cryogenic magnetometer at the paleomagnetics laboratory of the University of Wyoming. Progressive thermal demagnetization was the main technique for determining the characteristic magnetization, but alternating field (AF) demagnetization was applied to those samples contained in plastic cubes (the Neogene-ooze suite and 40 cubes from the Lower Cretaceous of Hole 638B). Magnetic polarity was determined from the plots of the magnetic vectors during demagnetization. Least-squares line fit of the removed vectors (Kirschvink, 1980) yielded the characteristic direction of magnetization for samples having straight-forward demagnetization behavior. Samples that (1) displayed unstable endpoints, (2) became magnetically viscous upon demagnetization, or (3) gave unusual directions were assigned indeterminant or uncertain polarity.

Neogene Ooze (Middle Pliocene–Late Miocene; Cores 103-638B-7R through 103-638B-20R)

Recovery of the Neogene sediment was generally less than 50%, and much of this recovered material was heavily disturbed; as a result, the samples taken of undisturbed intervals are too sparse for deriving a magnetostratigraphic pattern (Fig. 21). The tentative assignments of standard polarity chrons are based entirely on the foraminiferal ages of the polarity zones and the biostratigraphy-magnetic polarity time scale of Berggren et al. (in press). These assignments are not considered to be reliable.

Lower Cretaceous Limestone and Turbidites (Barremian–Late Valanginian; Cores 103-638B-20R to 103-638B-45R and 103-638C-1R to 103-638C-14R)

The intensity of magnetization of Lower Cretaceous limestones at Site 638 and other sites are generally weak, commonly less than 5×10^{-8} emu/cm^3 (= 5×10^{-5} A/m). Nearly two-thirds of the samples yielded reliable polarity determinations.

The correlation of magnetic polarity chrons to biostratigraphy is not yet known in precise detail. The Early Cretaceous magnetic polarity time scale compiled by Ogg (in press) is based primarily on magnetostratigraphy, dinoflagellate zonations, and nannofossil datums from DSDP sites in the western Central Atlantic. The dinoflagellate biostratigraphy of the Leg 103 sites was not yet complete at the time of this writing; therefore, the nannofossil datums were used to assign tentative polarity chrons to the observed magnetic polarity zones. Several of the nannofossil datums occur in a slightly different sequence than at other sites, and the occurrence of different species enabled the use of a Boreal zonation rather than the central Atlantic zonation. A more accurate assignment of polarity chrons will be possible when the dinoflagellate biostratigraphy is available. The polarity pattern by itself is too vague or too distorted by variations in sedimentation rate to enable direct matching of magnetostratig-

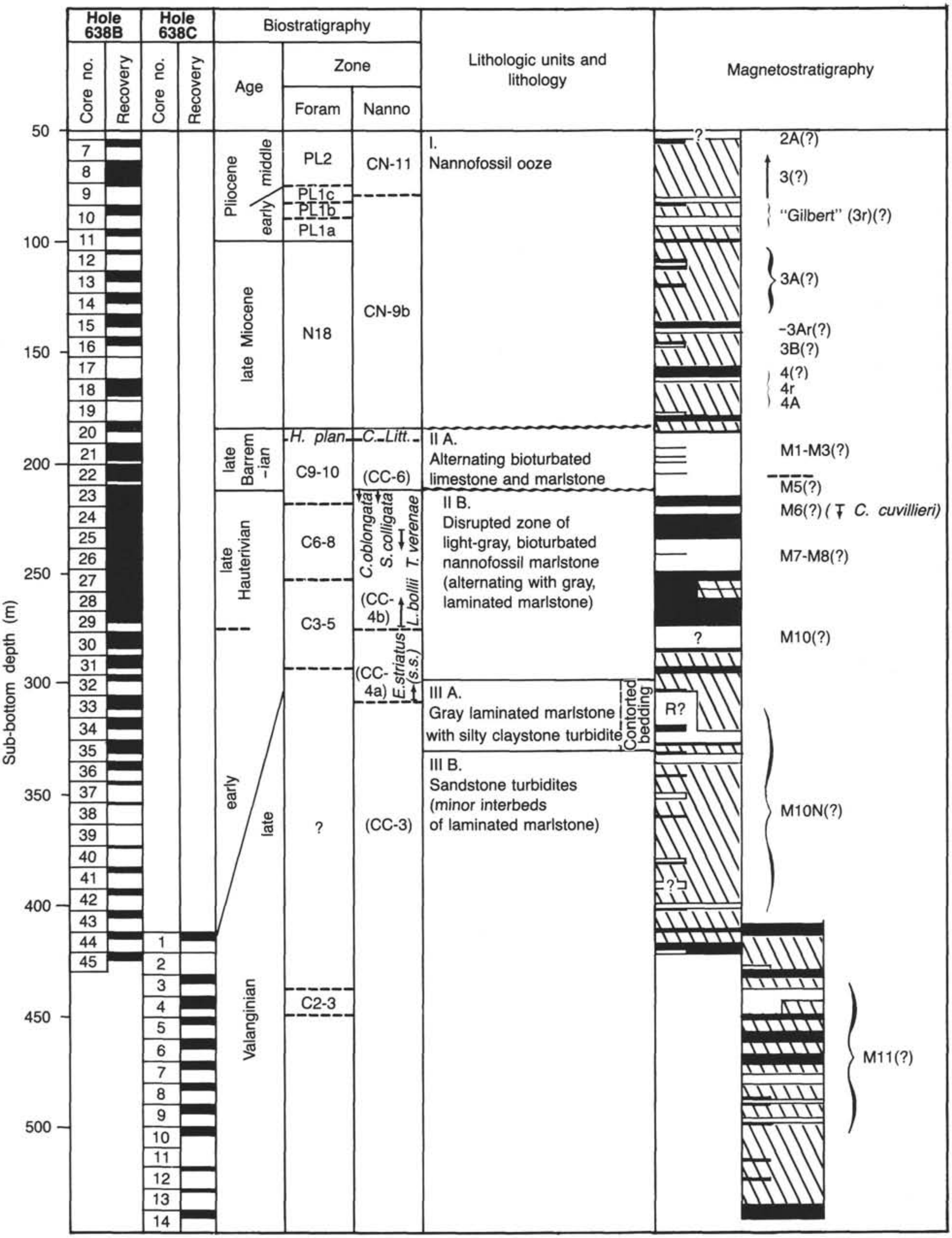

Figure 21. Magnetostratigraphy with tentative assignment of polarity chrons of Holes 638B and 638C. Black shading is normal polarity zones, and white is reversed polarity. Diagonal pattern indicates gaps in recovery or intervals of indeterminant or unreliable polarity. A half bar represents a single sample having a polarity interpretation opposite the adjacent samples or indicates that only one sample was available for the core. Assignment of magnetic polarity chrons is the best current guess based upon the biostratigraphy given in this site chapter and upon published magnetic polarity time scales. Complete tables of the paleomagnetic data and polarity interpretations will be given in the Leg 103 Part B volume.

raphy to the magnetic polarity time scale without accurate biostratigraphic age control.

The middle–late Barremian (*M. hoschulzii* nannofossil zone, basal Core 103-638B-20R to middle of Core 103-638B-23R) yielded predominantly reversed polarity; this zone may correspond to polarity chrons M1 and/or upper M3 of similar age. The early Barremian and latest Hauterivian is not present at this site.

The underlying disrupted (slumped?) limestone of late Hauterivian age (lithologic Subunit IIB) has the last occurrence of *C. cuvillieri* just below a narrow reversed polarity zone in Core 103-638B-24R; this nannofossil datum occurs below polarity chron M6 in the western central Atlantic. The last occurrence of *T. verenae* is not a useful datum, and the first occurrence of *L. bollii* has not been previously correlated to magnetic polarity chrons because it does not occur in the western central Atlantic. According to the shipboard age determinations, the other reversed polarity zones in this unit may represent M9 through M5, but exact assignment is not possible at this time. Overturned strata may be within this disrupted unit (and the underlying contorted bedding of lithologic Subunit IIIA), which cause misleading polarity identifications.

The late Valanginian–earliest Hauterivian is dominated by clastic turbidites. Core recovery was generally poor, but the rapid rate of sedimentation enables recognition of at least three normal polarity zones within a predominantly reversed polarity interval. The first occurrence of *C. striatus* (sensu stricto) was noted in Core 103-638B-33R, which was used as a marker for the Valanginian/Hauterivian boundary. If this proves to correspond to the Valanginian/Hauterivian boundary, as defined by dinoflagellate biostratigraphy, then the reversed polarity dominating Cores 103-638B-33R to 103-638B-43R includes polarity chron M10N. Polarity chron M11 could be present in Hole 638C. No early Valanginian was penetrated; therefore, the oldest possible polarity chron present is M12. We hope that a correction for turbidite expansion and a dinoflagellate-age control will improve these tentative guesses of polarity chrons.

ORGANIC GEOCHEMISTRY

Organic Carbon Analysis

Seventy-seven sediment samples were taken at Site 638 for organic carbon and nitrogen determination, using the Perkin-Elmer elemental analyzer. Results of the organic carbon percentage on a dry-sediment weight basis and percentage carbonate are plotted vs. depth in Figure 22. Because of technical problems, reliable determination of elemental nitrogen was impossible. Since

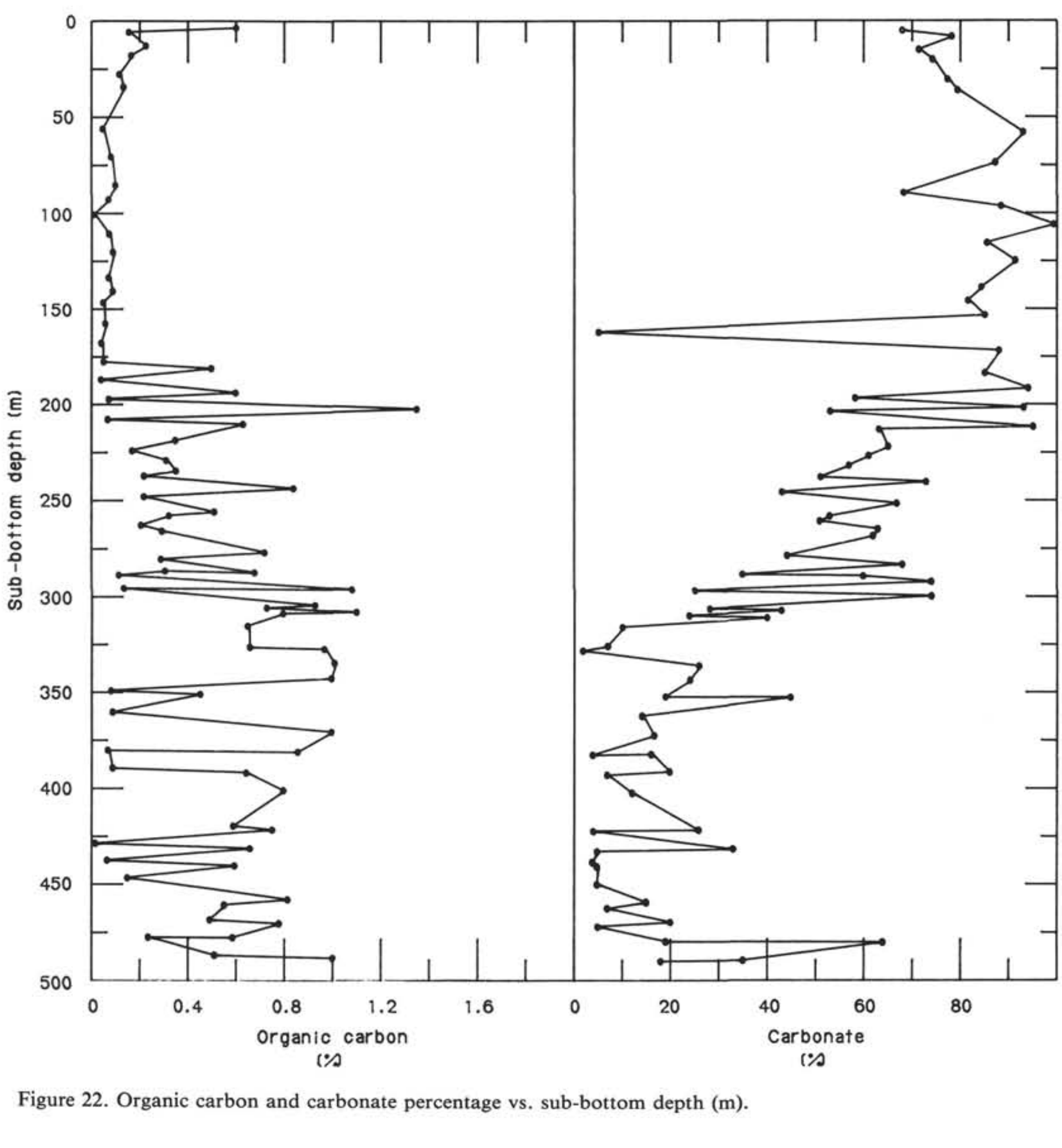

Figure 22. Organic carbon and carbonate percentage vs. sub-bottom depth (m).

atomic carbon-to-nitrogen ratios were not available, the type of organic matter (marine vs. terrestrial) was based solely on Rock-Eval interpretation.

The amount of organic matter preserved in deep-ocean sediments is a small fraction of the material originally available from continental runoff and marine productivity. Microbial and oxidative processes degrade sinking organic matter, losses being greatest during the early stages of burial. High sedimentation rates decrease the sediment/water interface time and tend to enhance preservation. Still higher sedimentation rates, however, act to dilute organic matter. In general, preservation of organic matter at Site 638 is closely related to lithology and depositional setting.

From 0 to 180 m sub-bottom depth, preservation of organic matter is poor, averaging 0.11%, which is below the 0.3% average for ancient deep-ocean sediments (McIver, 1975). This 180 m of organic-lean sediment corresponds to lithologic Unit I (see "Sediment Lithology" section, this chapter). Below 180 m sub-bottom depth, organic carbon concentrations become cyclic, exhibiting alternating organic-carbon-rich and -lean layers. Within lithologic Subunit IIA, organic-carbon-lean layers are bioturbated limestones, whereas organic-carbon-rich layers are marlstones. Organic matter is moderately well preserved from 213 to 298 m sub-bottom (Subunit IIB), averaging 0.40%.

In Subunit IIIA organic matter is well preserved, averaging 0.86%. In Subunit IIIB, from 330 m sub-bottom to the total depth of Hole 638C (547 m), organic carbon concentrations vary with the three major lithologies. Organic-rich layers (about 1.0%) are associated with the claystone, moderate organic-rich layers (about 0.6%) with marlstone, and organic-carbon-lean layers (about 0.1%) with sandstone. Preservation of organic carbon within Subunit IIIB is directly related to grain size: clay-size particles show very good preservation, silt moderate preservation, and sand poor preservation.

Rock-Eval Analysis

Ten samples representing all the various sediment types recovered at Site 638 were analyzed using the Rock-Eval. Results are shown in Figure 23, using a modified van Krevelen diagram. The organic matter at Site 638 is composed mostly of terrigenous (Type III) kerogen. The hydrogen index (HI) and oxygen index (OI) average 158 and 295, respectively. High OI values such as these may indicate highly oxidized reworked organic matter. Such high oxidation or reworking may obscure the original character of the organic matter by diagenetic alterations. The temperature of the S2 peak maximum (T_{max}) is an indicator of the maturation of the organic matter (Espitalie et al., 1977); T_{max} values for the ten samples average 409°C. This low value indicates a low thermal history for the preserved kerogen.

Organic Carbon Isotope Analyses

Organic carbon isotope values are listed in Table 3. Isotope interpretation will be discussed in the Leg 103 Part B volume.

Summary

The preservation of organic matter in lithologic Unit I is poor and indicates normal degradation of deep-ocean organic matter. The layers rich in terrestrial organic matter in lithologic Units II and III must have originally been deposited in a shallow-water nearshore environment. In such a location, preservation is enhanced by higher sedimentation rates and shorter water-column residence times.

INORGANIC GEOCHEMISTRY

Interstitial-Water Chemistry

Eighteen whole-round sediment samples were taken from the rotary-drilled cores recovered at Site 638. The sampling strategy

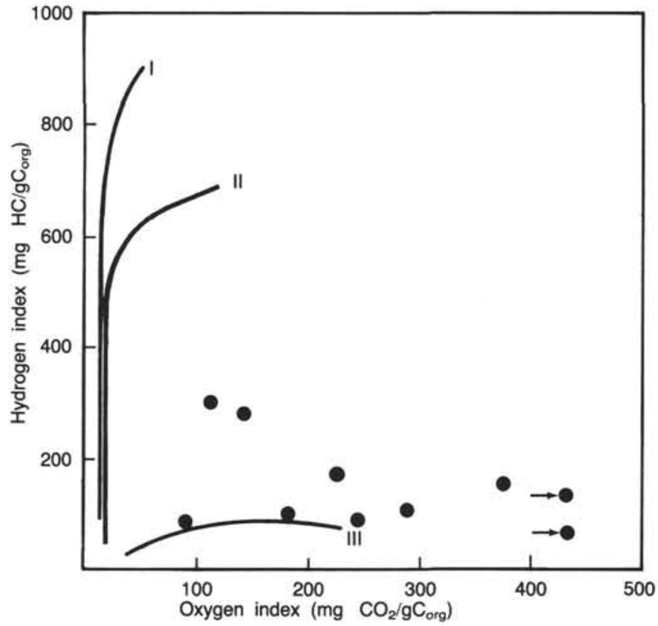

Figure 23. Modified van Krevelen plot of Rock-Eval results from Site 638. Arrows beside samples indicate oxygen index values greater than 400.

was to obtain one sample from each of the cores in the upper 50 m of the sediment column and two samples from the subsequent 40 m of cored sediment. Below 90 m sub-bottom depth, a sediment sample was taken every third core for interstitial-water analysis. This strategy was followed where sufficient sediment (i.e., at least 1.5 m) was recovered in the designated core. These samples were squeezed aboard ship to obtain the interstitial waters from the sediment. The water samples were analyzed for pH, alkalinity, chlorinity, salinity, calcium, and magnesium. The same methods used at Site 637 were employed for the samples recovered at Site 638. Once again, the primary standard used for calibration of the water analysis is IAPSO standard seawater, and a surface-seawater sample retrieved by a bucket overboard was used for comparison with the interstitial waters.

The results, listed in Table 4 and graphed in Figure 24, show some variation in the parameters with increasing depth. Alkalinity increases to a weak maximum in the upper 168 m of the sediment column, except for an abrupt decrease in one sample at 126 m sub-bottom depth (Sample 103-638B-14R-2, 140–150 cm). This trend toward increasing alkalinity values occurs in lithologic Unit I, which is composed primarily of nannofossil ooze.

The abrupt drop in alkalinity at 126 m may be attributed to drilling contamination by surface seawater having a much lower alkalinity value of 2.07 meq/kg. Discussion with Lamar Hayes, ODP Operations Superintendent, supports this theory because, if contamination were to occur, it would be with seawater from 20 ft below sea level, which is pumped down the hole as a circulating fluid. The sample taken at 126 m sub-bottom depth may have been contaminated with this surface seawater during drilling, as indicated by the soupy nature and slurry of sediment revealed in the split core (Fig. 25).

Below Sample 103-638B-18R-4, 140–150 cm, at 168 m sub-bottom depth, alkalinity progressively decreases to Sample 103-638B-29R-2, 140–150 cm, at 270 m sub-bottom depth. The beginning of this decrease in alkalinity roughly corresponds to the lithologic change from late Miocene nannofossil ooze (Unit I) to Barremian marlstone and limestone (Unit II); it continues through most of lithologic Unit II. This progressive decrease in alkalinity is not interpreted as being the result of surface-seawa-

Table 3. Organic carbon isotope values, Site 638. HI = hydrogen index; OI = oxygen index.

Sample (interval in cm)	Sub-bottom depth (m)	Age	Organic carbon (%)	$CaCO_3$ (%)	$\delta^{13}C$	HI	OI
103-638B 20R-2, 143-147	183.53	Barremian	0.05	88	−24.7	260	640
103-638B 20R-3, 4-9	183.64	Barremian	0.91	49	−26.2	60	46
103-638B 21R-2, 94-100	192.54	Barremian	0.37	76	−26.2	27	48
103-638B 21R-3, 78-84	193.88	Barremian	2.0	32	−28.3	216	35
103-638B 21R-6, 67-73	198.27	Barremian	1.63	41	−27.7	221	47
103-638B 23R-2, 19-25	210.99	Barremian	2.03	30	−26.7	158	46
103-638B 23R-2, 139-145	212.19	Barremian	0.16	79	−26.7	81	93
103-638B 23R-3, 20-26	212.50	Barremian	2.39	28	−26.8	111	47
103-638B 25R-2, 20-24	230.10	Hauterivian	1.44	33	−29.4	3	0
103-638B-25R-2, 28-35	230.18	Hauterivian	0.18	57	−26.6	138	333
103-638B 26R-1, 14-19	238.24	Hauterivian	1.46	41	−26.5	80	43
103-638B 35R-4, 86-91	330.26	Hauterivian	3.0	5	−25.8	18	11
103-638B 41R-1, 19-21	383.99	Hauterivian	0.85	7	−25.3	87	36
103-638B-41R-1, 37-43	384.17	Hauterivian	0.71	26	−25.1	47	19
103-638C 1R-2, 94-96	412.84	Valanginian	[a]na	na	−24.9	na	na
103-638C 3R-2, 118-120	433.88	Valanginian	0.66	5	−26.4	na	na
103-638C 5R-1, 98-100	451.48	Valanginian	0.15	5	−28.5	na	na
103-638C 9R-1, 120-122	490.40	Valanginian	na	na	−25.7	na	na
103-638C 9R-2, 77-79	491.47	Valanginian	1.0	18	−27.3	na	na

[a] na = not available.

Table 4. Shipboard interstitial-water analyses, Site 638.

Sample (interval in cm)	Sub-bottom depth (m)	pH	Alkalinity meq/kg	Salinity ‰	Chlorinity ‰	Ca^{++} mmol/L	Mg^{++} mmol/L
103-638B-1R-2, 140-150	2.9-3.0	7.62	3.25	33.8	18.67	10.51	50.96
103-638B-2R-4, 140-150	12.3-12.4	7.50	3.40	34.5	19.57	10.86	51.89
103-638B-3R-1, 140-150	17.4-17.5	7.25	3.31	35.3	19.87	10.83	51.04
103-638B-4R-4, 140-150	31.4-31.5	7.33	3.77	35.0	19.68	10.89	50.19
103-638B-7R-1, 140-150	55.8-55.9	7.28	4.02	36.3	19.87	11.19	51.08
103-638B-11R-2, 140-150	96.6-96.7	7.32	4.40	34.7	19.77	12.47	48.05
103-638B-14R-2, 140-150	125.8-125.9	7.62	3.28	35.0	19.40	12.06	48.62
103-638B-18R-4, 140-150	167.4-168.5	7.55	4.55	34.3	18.92	14.03	44.50
103-638B-21R-3, 140-150	194.5-194.6	7.43	3.78	34.1	17.41	13.61	47.47
103-638B-24R-5, 140-150	226.2-226.3	7.52	3.13	34.3	18.75	13.65	45.59
103-638B-26R-5, 140-150	245.5-245.6	7.50	2.77	36.0	19.41	13.12	44.93
103-638B-29R-2, 140-150	269.9-270.0	7.48	2.25	34.1	17.13	12.83	46.10
103-638B-32R-1, 140-150	297.4-297.5	7.73	2.43	35.0	19.60	13.42	46.42
103-638B-35R-3, 140-150	329.3-329.4	7.50	2.61	34.9	18.57	14.52	45.44
103-638B-45R-2, 140-150	424.4-424.5	7.53	3.87	34.7	17.93	17.34	43.82
103-638C-4R-2, 140-150	443.8-443.9	7.63	4.99	35.2	20.12	17.23	45.00
103-638C-7R-2, 140-150	472.8-472.9	7.43	3.77	35.3	20.17	18.53	43.86
103-638C-10R-1, 140-150	500.3-500.4	7.53	3.42	35.5	20.19	18.06	45.18

ter contamination because a progressive increase in drilling disturbance from Core 103-638B-18R through Core 103-638B-29R is not apparent and the difference in the degree of drilling disturbance in Core 103-638B-29R from that in Core 103-638B-28R or Core 103-638B-30R, both of which have higher alkalinity values, is not significant.

Near the base of Unit II, (Sample 103-638B-32R-1, 140-150 cm; 297 m sub-bottom depth), the alkalinity values begin to rise and continue gradually to increase to the bottom of Hole 638B (Sample 103-638B-45R-2, 140-150 cm, at 424 m sub-bottom depth). The alkalinity values continue to increase at deeper sub-bottom depths (443.8-500.3 m sub-bottom depth) in Unit III from Hole 638C. The gradual increase in alkalinity may be a result of high sedimentation rates and high organic carbon contents associated with the terrigenous turbidites in Unit III.

Total dissolved solids were measured using a Goldberg refractometer and are listed under salinity in Table 4 (as has been the convention with previous DSDP and ODP interstitial-water data). In Hole 638B, "salinity" and chlorinity values show no significant downhole trends of a progressive increase or decrease. A consistent and distinct shift is in both the chlorinity and salinity values in lithologic Unit II, specifically in Subunit IIB, which may relate to the lithologies generated from slumping and downslope sediment creep. In Hole 638C, salinity and chlorinity values are greater than those of interstitial waters from all the Hole 638B samples (Table 4). These samples from Unit III of Hole 638C are from deeper sub-bottom depths (443.8-500.3 m sub-bottom depth) than are the samples from Unit III from Hole 638B. This trend of higher values in Hole 638C is real and not due to differences in the operator's titration technique because the IAPSO seawater standard was re-run for calibration between samples from Hole 638B and 638C. Additionally, the difference between 17.93‰ chlorinity (Sample 103-638B-45R-2, 140-150 cm; 424.4 m sub-bottom depth) and 20.12‰ chlorinity (Sample 103-638C-4R-2, 140-150 cm; 443.8 m sub-bottom depth) is significantly greater than the common margin of error for these chlorinity titrations. The same operator can achieve accuracies better than 0.5% (Gieskes and Peretsman, 1986). The increase in the salinity and especially the chlorinity values may be interpreted in several ways. They may be the result of a small, nearby occurrence of gypsum rather than the dissolution of a large-scale deposit of evaporites because the diffusional gradi-

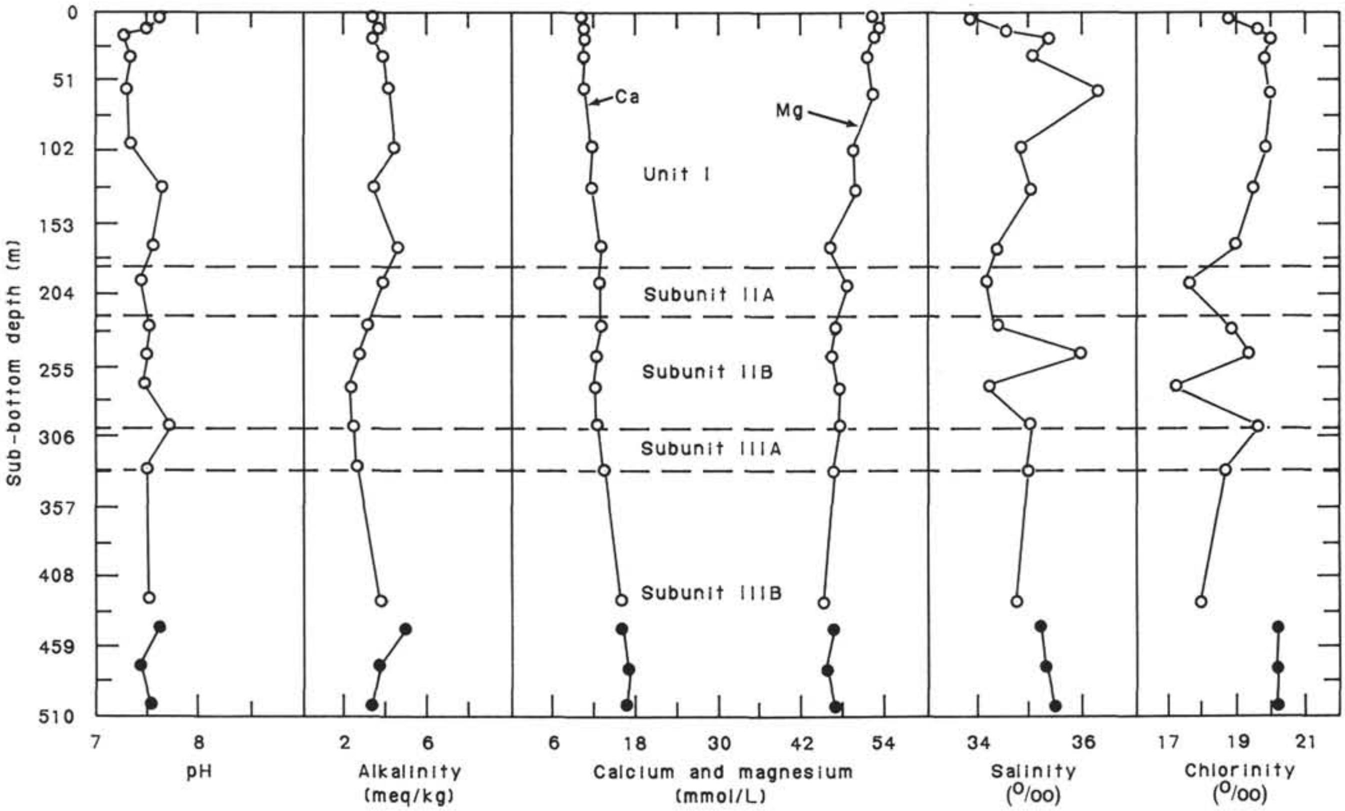

Figure 24. Summary of interstitial-water data from Site 638 and depth boundaries of the lithologic units. Data are given in Table 4. Data from Hole 638B are plotted as open symbols, whereas data from Hole 638C are plotted as solid symbols.

ent should be much higher. Another interpretation is that a highly porous nearby bed may be acting as an open system, owing to a seafloor outcrop and coincident contact and mixing with seawater at a location distant from Site 638.

The calcium and magnesium concentrations in the interstitial waters at Site 638 show distinct trends downhole. The calcium values gradually increase, whereas the magnesium values decrease with increasing sub-bottom depth (Fig. 26). A one-to-one relationship does not exist because the decrease in the magnesium concentration is not equal to the increase in the calcium concentration. The changes in the calcium values may be related to calcium carbonate dissolution or to release of calcium during dissolution of some silicates and reprecipitation as calcite cements or as zeolites. The decrease in magnesium downhole may be due to uptake in the detrital clay minerals such as chlorite. Much of the biotite in lithologic Unit III has been chloritized.

Calcium Carbonate

Approximately 150 dried sediment samples were analyzed for percentage carbonate, and the results are listed in Table 5 and graphed with respect to depth in Figure 27. These results yield a representative picture of the various lithologies recovered. Several distinct patterns appear in Figure 27, superimposed on the overall decrease in percentage carbonate from the top of the sedimentary column to the lowermost sample. Lithologic Unit I consists of nannofossil ooze having high carbonate contents (62%–99%). The single sample that is low in carbonate at 161.8 m sub-bottom depth was collected from an anomalous red-brown claystone in Section 103-638B-18R-1. Subunit IIA consists of bioturbated limestone, marlstone, and claystone/marlstone couplets. The overall high carbonate content (44%–95%) and the variation of the marlstone and limestone can be readily seen in Figure 27. Subunit IIB consists of light-gray, bioturbated nannofossil marlstone with cyclic clay-rich layers. The cyclicity of the increase in clays (or decrease in carbonate) is easily seen in Figure 27 by the rapid oscillations in carbonate content. Subunit IIIA appears on Figure 27 as a transition from Subunit IIB to Subunit IIIB and shows decreasing but still cyclic carbonate values. Subunit IIIA consists of turbidite claystone/marlstone couplets. The carbonate contents of samples from lithologic Subunit IIIB are typically much lower (2%–43%) than in the overlying strata because of the low percentage of carbonate in the coarse-grained turbidite sandstones in that subunit.

PHYSICAL PROPERTIES

Physical property measurements were made on sediments and sedimentary rocks from Cores 103-638B-1R through 103-638B-45R and Cores 103-638C-1R through 103-638C-14R. As at the previous site, unsplit cores were analyzed on the shipboard Gamma Ray Attenuation Porosity Evaluator (GRAPE), allowed to warm to room temperature for 4 hr, measured for thermal conductivity, and then split. After being split, sediments from the upper part of Hole 638B (Cores 103-638B-1R through 103-638B-18R) were analyzed on the vane-shear-strength apparatus; sediments and sedimentary rocks from throughout Holes 638B and 638C were measured for compressional seismic velocity on the Hamilton Frame velocimeter. Index properties (bulk and grain density, water content, and porosity) as calculated on the basis of weights obtained from a triple-beam balance and volumes obtained using the shipboard Penta-Pycnometer were performed on the same samples measured for seismic velocity. Index-property samples were also analyzed for carbonate content using the carbonate-bomb method (Müller and Gastner, 1971). Two-minute GRAPE wet-bulk density measurements were also made on the same sediment and sedimentary rock samples

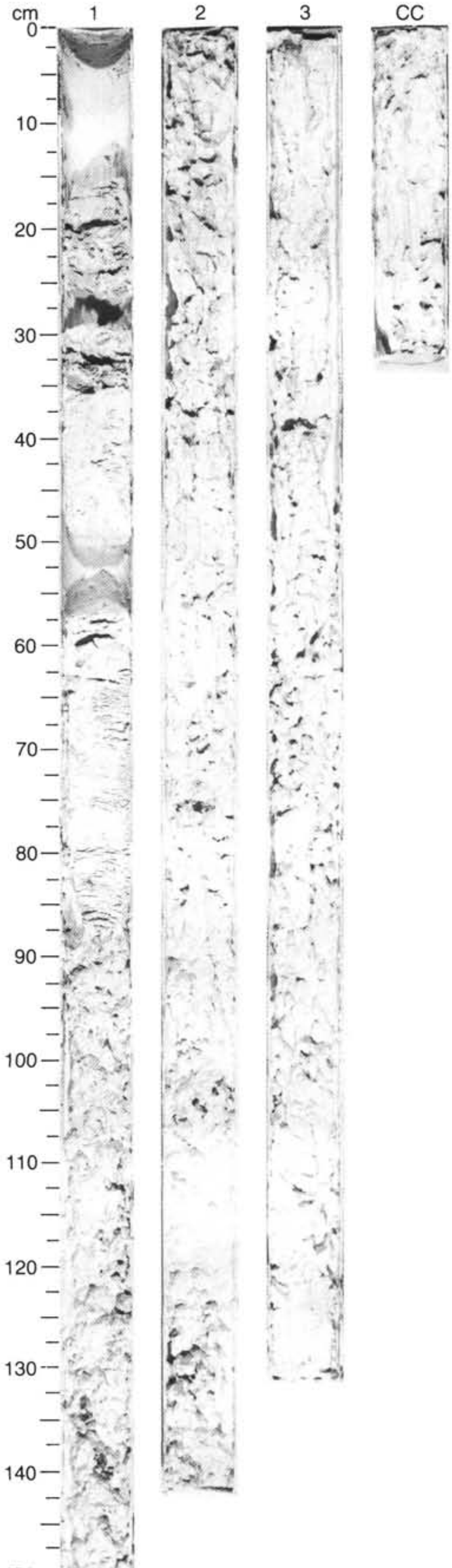

Figure 25. Core 103-638B-14R.

from Cores 103-638C-1R through 103-638C-13R as were used for Hamilton Frame velocimetry and index-property measurement.

Thermal Conductivity

Thermal-conductivity measurements were made on unlithified sediment from Cores 103-638B-1R through 103-638B-45R (0-431 m sub-bottom; Fig. 28A). Values increase slightly but steadily with increasing sub-bottom depth from about 2.4 to about 3.7×10^{-3} cal $\times$ $°C^{-1}$ $\times$ cm^{-1} $\times$ s^{-1} (calories/degree Celsius-centimeter-second). Thermal conductivity is fairly constant with depth only in the nannofossil marl of lithologic Subunit IIB (Cores 103-638B-23R through 103-638B-32R; 213-298 m sub-bottom; see "Sediment Lithology" section, this chapter); values in Subunit IIB range from about 2.9 to 3.5×10^{-3} cal $\times$ $°C^{-1}$ $\times$ cm^{-1} $\times$ s^{-1}.

We continued to measure thermal conductivity in Hole 638C from Core 103-638C-3R through 103-638C-14R (431-547 m sub-bottom). Values increase with depth from slightly less than the values obtained from greatest depths in Hole 638B; starting around 3.4×10^{-3} cal $\times$ $°C^{-1}$ $\times$ cm^{-1} $\times$ s^{-1} in Core 103-638C-3R (431-441 m sub-bottom), thermal conductivity increases to around 4.3×10^{-3} cal $\times$ $°C^{-1}$ $\times$ cm^{-1} $\times$ s^{-1} in Cores 103-638C-10R through 103-638C-13R (499-538 m sub-bottom) and decreases to 3.5×10^{-3} cal $\times$ $°C^{-1}$ $\times$ cm^{-1} $\times$ s^{-1} in Core 103-638C-14R (538-547 m sub-bottom).

Vane Shear

Vane-shear-strength measurements were made only on sediments from lithologic Unit I (see "Sediment Lithology" section, this chapter). Nannofossil ooze from Cores 103-638B-1R through 103-638B-17R (0-161.5 m sub-bottom) shows undrained shear-strength values ranging from 2 to 28 kPa (kiloPascals; Fig. 28B). Drilling disturbance is moderate to soupy in these cores, and measured shear strength is probably only a conservative indicator of *in-situ* shear strength.

In Section 103-638B-18R-1 (161.5-163.0 m sub-bottom), measured shear strength increases abruptly to 72 kPa in a stiff brown mud that occurs in this section. Although the rest of Core 103-638B-18R contains nannofossil ooze that has been disrupted to a soupy state by drilling, the shear strength is still high (as much as 46 kPa in Sample 103-638B-18R-5, 99 cm; 168.49 m sub-bottom). Rather than damage the blades of the vane, we ceased measuring undrained shear strength at this depth in Hole 638B.

Compressional Seismic Velocities

Seismic velocities were measured on sediments and sedimentary rocks over the entire depth of Holes 638B and 638C (Fig. 28C). The upper six cores of Hole 638B (0-54 m sub-bottom) show velocities averaging about 1.25 km/s. Such low values probably reflect the great degree of drilling disturbance at the top of Hole 638B, and have a precision of ± 0.04 km/s; velocity values below this interval have a precision of ± 0.02 km/s. Below about 54 m and excluding the soupy sediment of Core 103-638B-18R, velocities measured in the nannofossil ooze range from about 1.60 to about 1.75 km/s; average velocity for this lithologic unit below the most drilling-disturbed upper cores is about 1.65 km/s.

The base of lithologic Unit I in Core 103-638B-20R (184 m sub-bottom; see "Sediment Lithology" section, this chapter) corresponds well to a change in the nature of measured velocities that begins below Core 103-638B-20R and continues through Core 103-638B-23R (190-219 m sub-bottom). This interval is roughly that ascribed to Subunit IIA (see "Sediment Lithology" section, this chapter) and is distinguished here by the higher velocities measured in the limestone beds of the unit. Although the velocities in nannofossil marl are about the same as those

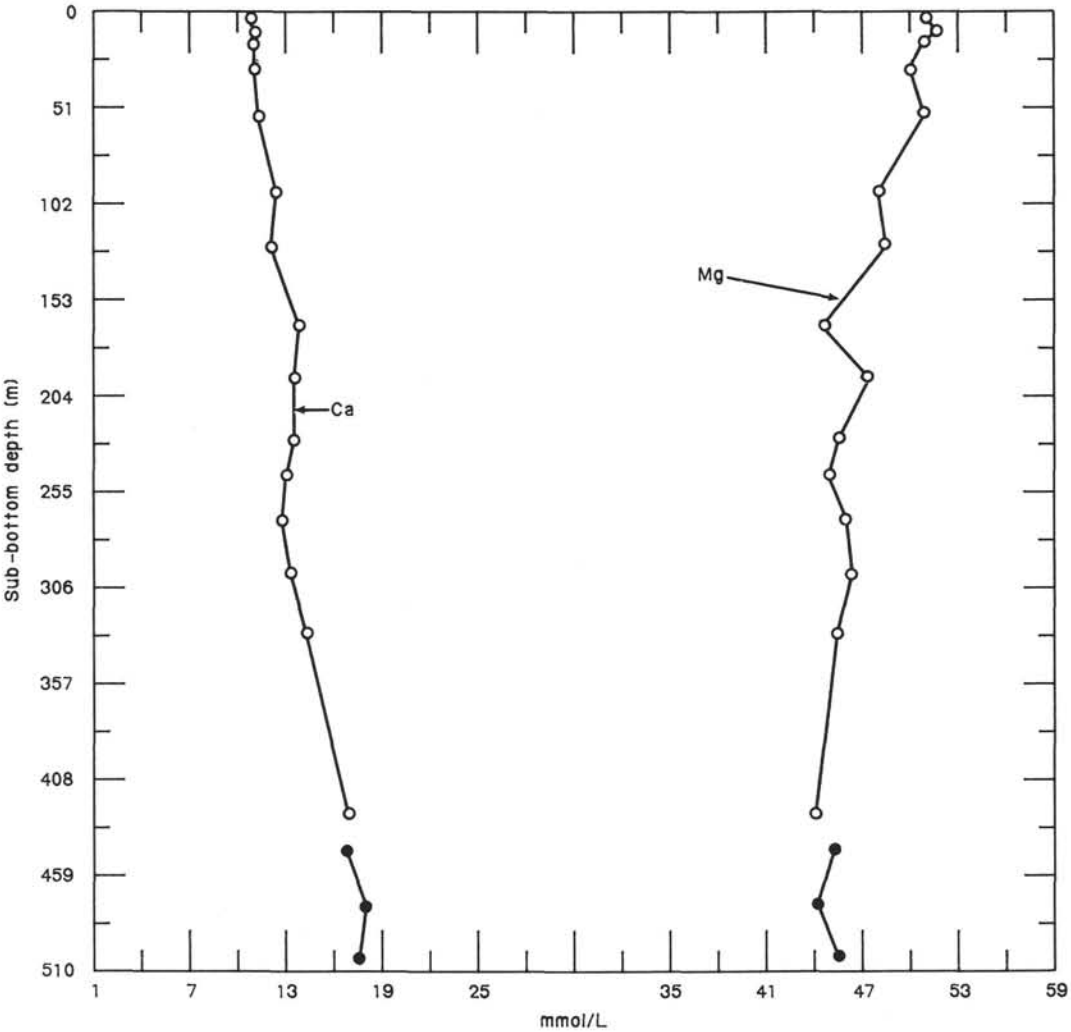

Figure 26. Calcium and magnesium cation concentrations in interstitial-water samples from Site 638. Data are given in Table 4. Data from Hole 638B are plotted as open symbols, whereas data from Hole 638C are plotted as solid symbols.

measured on the nannofossil ooze of Unit I, the limestone layers have seismic velocities of 3.0 to 3.7 km/s. We used the shipboard visual core-description forms to tabulate the thickness of limestone layers; by attributing a marl composition and velocity to the unrecovered part of the cores, we calculated an average seismic velocity on a core-by-core basis (Fig. 29). The average of mean velocities so obtained for the three cores of lithologic Subunit IIA is 1.76 km/s.

From about 219 to 344 m sub-bottom (Cores 103-638B-24R through 103-638B-36R), the seismic velocity of the marl remains fairly constant, averaging about 1.69 km/s. A few limestone layers (measured in Cores 103-638B-26R, 103-638B-29R, and 103-638B-32R) have seismic velocities of about 3.0 to 3.6 km/s. The boundary between Subunits IIIA and IIIB at 330 m sub-bottom (Core 103-638B-35R) is defined by the first appearance of a cemented sandstone layer more than 20 cm thick (see "Sediment Lithology" section, this chapter), but this boundary is not marked by a great change in seismic velocity. Cemented sandstone layers first occur in Core 103-638B-34R.

A velocity contrast is observed at the top of Core 103-638B-37R (344 m sub-bottom). Below this depth, some 15% of the section is composed of mostly well-cemented sandstone beds (estimated by tabulation of visual core-description occurrences as described in previous text) with velocities ranging from 3.2 to 5.3 km/s and averaging about 4.2 km/s. Unlithified marl in this unit yields a seismic velocity range of 1.65–21.3 km/s and an average velocity of 1.77 km/s. A core-by-core average seismic velocity of this unit was calculated by tabulating lithologies from the visual core descriptions as described previously, assuming all unrecovered material consists of marl having a velocity of 1.77 km/s; results are illustrated in Figure 29A. Averaging the core-by-core velocities so obtained yields a mean velocity below 344 m sub-bottom in Hole 638B of about 1.92 km/s.

The average velocity measured in the marl of Cores 103-638C-1R through 103-638C-14R (412–547 m sub-bottom) is 1.83 km/s. This velocity shows a slight increase with depth. Sandstone velocities range from 3.1 to 5.1 km/s; coarser grained, less completely cemented sandstone velocities fall in the lower part of the range. Although we made velocity measurements on water-saturated samples as a matter of standard procedure, the importance of this practice became apparent when we measured the same coarse-grained sandstone saturated with seawater and again when it was dry; compressional seismic velocity of the dry sample was 1–1.5 km/s greater than the same sample when water saturated.

Less sandstone was recovered in the cores of Hole 638C (412–547 m sub-bottom) than in the basal parts of lithologic Subunit IIIB recovered from Hole 638B (330–432 m sub-bot-

Table 5. Carbonate-bomb data, Site 638.

Sample (interval in cm)	Sub-bottom depth (m)	Carbonate (%)	Lithology[a]
103-638B-1R-2, 120	2.7	68	Clayey nannofossil ooze
103-638B-1R-4, 70	5.2	78	Clayey nannofossil ooze
103-638B-2R-1, 100	7.4	79	Foraminiferal-bearing clayey nannofossil ooze
103-638B-2R-2, 100	8.9	72	Foraminiferal-bearing clayey nannofossil ooze
103-638B-2R-4, 100	11.9	71	Clayey nannofossil ooze
103-638B-2R-5, 100	13.4	71	Clayey nannofossil ooze
103-638B-3R-1, 30-32	16.3	76	Foraminiferal clayey nannofossil ooze
103-638B-3R-2, 10-12	17.6	74	Foraminiferal clayey nannofossil ooze
103-638B-4R-2, 10-12	27.1	77	Clayey nannofossil ooze
103-638B-4R-4, 10-12	30.1	75	Clayey nannofossil ooze
103-638B-4R-6, 45-47	33.45	79	Foraminiferal-bearing clayey nannofossil ooze
103-638B-7R-1, 100-102	55.4	82	Clayey nannofossil ooze
103-638B-7R-2, 30-32	56.2	93	Foraminifer nannofossil ooze
103-638B-7R-2, 61-63	56.51	70	Foraminiferal-bearing clayey nannofossil ooze
103-638B-7R-2, 100-102	58.4	85	Foraminiferal-bearing clayey nannofossil ooze
103-638B-8R-5, 87-89	70.97	87	Foraminiferal-bearing clayey nannofossil ooze
103-638B-8R-6, 110-112	72.7	83	Foraminiferal-rich clayey nannofossil ooze
103-638B-10R-1, 95-97	85.05	79	Foraminiferal-bearing clayey nannofossil ooze
103-638B-10R-2, 130-132	86.9	68	Foraminiferal-bearing clayey nannofossil ooze
103-638B-10R-3, 30-32	87.4	77	Foraminiferal-bearing clayey nannofossil ooze
103-638B-11R-1, 130-132	95.0	88	Foraminiferal-rich clayey nannofossil ooze
103-638B-11R-2, 130-132	96.5	89	Foraminiferal-rich clayey nannofossil ooze
103-638B-12R-1, 106-108	104.46	99	Foraminiferal-bearing nannofossil ooze
103-638B-13R-1, 79-81	113.89	85	Clayey nannofossil ooze
103-638B-14R-1, 39-41	123.29	91	Foraminiferal-rich nannofossil ooze
103-638B-15R-4, 80-82	137.9	84	Clayey nannofossil ooze
103-638B-16R-2, 81-83	144.51	81	Clayey nannofossil ooze
103-638B-17R-1, 20-22	152.0	85	Clayey nannofossil ooze
103-638B-18R-1, 30-32	161.8	5	Red-brown claystone
103-638B-18R-1, 120-122	162.7	83	Clayey nannofossil ooze
103-638B-18R-2, 120-122	164.2	88	Clayey nannofossil ooze
103-638B-18R-3, 120-122	165.7	84	Clayey nannofossil ooze
103-638B-18R-4, 120-122	167.2	87	Foraminiferal-rich clayey nannofossil ooze
103-638B-18R-5, 120-122	168.7	84	Foraminiferal-rich clayey nannofossil ooze
103-638B-19R-1, 12-14	171.22	88	Clayey nannofossil chalk
103-638B-20R-1, 55-56	181.15	85	Clayey nannofossil chalk
103-638B-20R-2, 108-110	183.18	88	Clayey nannofossil chalk
103-638B-20R-3, 38-40	183.22	62	Marl
103-638B-21R-1, 84-86	190.94	94	Micritic limestone
103-638B-21R-3, 118-120	194.28	44	Marlstone
103-638B-21R-4, 53-55	195.13	91	Micritic limestone
103-638B-21R-4, 115-117	195.75	58	Marlstone
103-638B-22R-1, 112-114	200.82	93	Radiolarian micritic limestone
103-638B-22R-3, 56-58	203.26	53	Marlstone
103-638B-22R-3, 134-136	204.04	93	Radiolarian micritic limestone
103-638B-23R-2, 52-54	211.32	95	Radiolarian micritic limestone
103-638B-23R-2, 92-98	211.72	63	Marlstone
103-638B-24R-2, 69-71	220.99	65	Marlstone
103-638B-24R-4, 105-107	224.35	62	Marlstone
103-638B-24R-6, 33-35	226.63	61	Marlstone
103-638B-25R-2, 111-113	231.01	57	Nannofossil marlstone
103-638B-25R-4, 95-97	233.85	64	Nannofossil marlstone
103-638B-25R-6, 83-85	236.73	51	Nannofossil marlstone
103-638B-26R-1, 100-102	239.10	73	Nannofossil marlstone
103-638B-26R-2, 106-108	240.66	49	Nannofossil marlstone
103-638B-26R-3, 97-99	242.07	40	Nannofossil marlstone
103-638B-26R-4, 100-102	243.6	52	Nannofossil marlstone
103-638B-26R-5, 100-102	245.1	43	Nannofossil marlstone
103-638B-26R-6, 50-52	246.1	57	Nannofossil marlstone
103-638B-27R-2, 98-100	250.18	67	Nannofossil marlstone
103-638B-27R-4, 98-100	253.18	49	Nannofossil marlstone
103-638B-28R-1, 131-135	258.61	44	Nannofossil marlstone
103-638B-28R-2, 131-135	260.11	51	Nannofossil marlstone
103-638B-28R-3, 140-142	261.7	49	Nannofossil marlstone
103-638B-28R-4, 140-142	263.2	58	Nannofossil marlstone
103-638B-28R-5, 140-142	264.7	63	Nannofossil marlstone
103-638B-29R-1, 42-44	267.42	62	Nannofossil marlstone
103-639B-29R-2, 106	269.56	76	Clayey limestone
103-639B-30R-2, 67-69	278.87	44	Nannofossil marlstone
103-638B-30R-4, 31-33	281.57	48	Nannofossil marlstone
103-638B-30R-4, 144	282.64	68	Nannofossil marlstone
103-638B-31R-2, 42-44	288.22	35	Nannofossil marlstone
103-638B-31R-2, 122-124	289.02	60	Nannofossil marlstone
103-638B-31R-3, 47-49	289.77	65	Nannofossil marlstone
103-638B-31R-4, 94-96	291.74	74	Clayey limestone

Table 5 (continued).

Sample (interval in cm)	Sub-bottom depth (m)	Carbonate (%)	Lithology[a]
103-638B-32R-1, 77–79	296.77	25	Calcareous clay
103-638B-32R-2, 77–79	298.27	74	Clayey limestone
103-638B-33R-1, 90–92	306.5	28	Calcareous clay
103-638B-33R-2, 90–92	308.0	43	Marl
103-638B-33R-3, 90–92	309.5	24	Calcareous clay
103-638B-33R-4, 125–127	311.35	40	Marl
103-638B-34R-1, 114–117	316.44	11	Calcareous claystone
103-638B-34R-2, 46–48	317.26	10	Silty claystone
103-638B-34R-2, 145–147	318.25	24	Carbonate-cemented sandstone
103-638B-35R-1, 128–130	326.18	4	Silty claystone
103-638B-35R-2, 123–124	327.63	7	Silty claystone
103-638B-35R-4, 57–58	329.97	2	Claystone
103-638B-36R-1, 98–99	335.48	6	Silty claystone
103-638B-36R-2, 110–112	337.1	26	Calcareous claystone
103-638B-37R-1, 22–24	344.42	24	Carbonate-cemented sandstone
103-638B-38R-1, 29–31	354.09	19	Carbonate-cemented sandstone
103-638B-38R-1, 32–34	354.12	45	Marlstone
103-638B-39R-1, 34–36	363.84	14	Carbonate-cemented sandstone
103-638B-40R-1, 52–54	373.62	17	Carbonate-cemented sandstone
103-638B-41R-1, 70–72	383.5	19	Carbonate-cemented sandstone
103-638B-41R-1, 134	384.14	4	Claystone
103-638B-41R-2, 4–6	384.34	16	Carbonate-cemented silty sandstone
103-638B-41R-2, 27–30	384.57	24	Carbonate-cemented coarse sandstone
103-638B-42R-1, 62–64	393.12	20	Carbonate-cemented coarse sandstone
103-638B-42R-2, 26–28	394.26	7	Claystone
103-638B-43R-1, 130–132	403.5	12	Calcareous claystone
103-638B-44R-1, 110–112	413.0	7	Carbonate-cemented sandstone
103-638B-45R-1, 115–117	422.65	26	Calcareous claystone
103-638B-45R-2, 74–76	423.75	4	Claystone
103-638C-1R-1, 37–39	412.27	43	Nannofossil marlstone
103-638C-1R-1, 68–70	412.58	26	Coarse-grained sandstone
103-638C-1R-1, 92–94	412.82	17	Silty claystone
103-638C-1R-2, 53–55	413.93	5	Silty claystone
103-638C-1R-2, 94–96	414.34	25	Coarse-grained sandstone
103-638C-3R-1, 98–100	432.18	7	Silty claystone
103-638C-3R-1, 118–120	433.38	33	Medium-grained sandstone
103-639C-3R-2, 97–99	433.67	29	Medium-grained sandstone
103-638C-3R-2, 118–120	433.88	5	Silty claystone
103-638C-4R-1, 10–12	441.0	25	Medium-grained sandstone
103-638C-4R-1, 68–70	441.58	7	Silty claystone
103-638C-4R-2, 77–79	443.17	5	Silty claystone
103-638C-4R-3, 46–48	444.36	25	Medium-grained sandstone
103-638C-5R-1, 54–56	451.04	5	Silty claystone
103-638C-5R-1, 98–100	451.48	28	Coarse-grained sandstone
103-638C-5R-2, 50–52	452.50	31	Calcareous clay
103-638C-5R-2, 75–77	452.75	21	Coarse-grained sandstone
103-638C-6R-1, 44–46	460.64	33	Medium-grained sandstone
103-638C-6R-1, 82–84	461.02	15	Nannofossil claystone
103-638C-6R-2, 3–4	461.73	20	Coarse-grained sandstone
103-638C-6R-2, 133–135	463.03	5	Clay
103-638C-6R-3, 66	463.86	7	Clay
103-638C-7R-1, 127–128	471.17	20	Nannofossil claystone
103-638C-7R-2, 125–127	472.65	5	Medium-grained sandstone
103-638C-7R-3, 9–11	472.99	5	Claystone
103-638C-7R-CC, 6–8	473.35	22	Medium- to fine-grained sandstone
103-638C-8R-1, 141–142	480.91	19	Claystone
103-638C-8R-2, 26–28	481.26	64	Nannofossil marlstone
103-638C-8R-CC, 8–10	482.04	16	Granule conglomerate
103-638C-9R-1, 35–36	489.55	10	Silty claystone
103-638C-9R-1, 120–122	490.4	31	Medium-grained sandstone
103-638C-9R-1, 133–135	490.53	35	Fine-grained sandstone
103-638C-9R-2, 73–75	491.43	22	Nannofossil marlstone
103-638C-9R-2, 77–79	491.47	18	Calcareous claystone
103-638C-10R-1, 129–131	500.19	11	Calcareous claystone
103-638C-10R-2, 117–119	501.57	5	Claystone
103-638C-12R-1, 90–92	519.1	11	Silty clay
103-638C-13R-1, 35–38	528.25	5	Clay
103-638C-14R-1, 118–120	538.68	10	Claystone
103-638C-14R-2, 4–6	539.04	28	Medium-grained sandstone
103-638C-14R-2, 47–49	539.47	5	Claystone

[a] Lithologic names are those used on the barrel sheets.

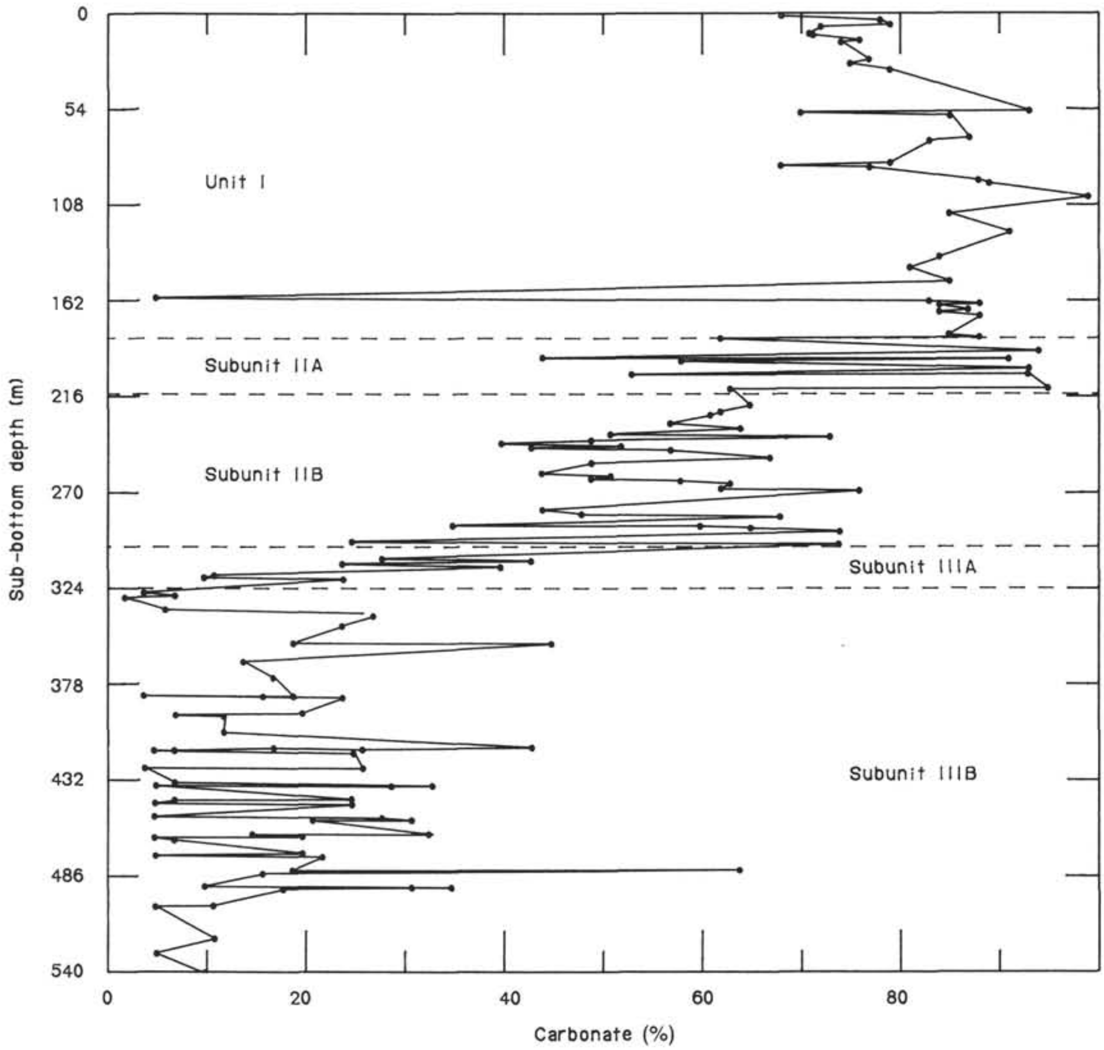

Figure 27. Percentage carbonate in dried-sediment samples from Site 638. Boundaries of the lithologic units are superimposed. Data are given in Table 5.

tom). Tabulation of sandstone occurrences documented in the visual core descriptions, assuming the unrecovered material consists of marl having a velocity of 1.83 km/s, results in a calculated average velocity of 2.0 km/s for Hole 638C. Figure 29B illustrates average core-by-core velocity plotted against depth in Hole 638C. We observed that hard, coarse-grained sandstone that was slow to cut under the saws of the core laboratory, nevertheless, tended to crumble at the edges more severely than did fine sandstone. That the broken bits of sandstone were washed away during drilling may account for low sediment recovery. If this is true, then the velocity averages of Figure 29 must be considered to be highly conservative estimates.

In general, laboratory-based measurements of compressional velocity yield lower velocities than expected and lower velocities than those measured *in situ* during logging of the Cenozoic (see "Logging Results" section, this chapter). One reason for this may be a phenomenon described by Hamilton (1976) as "porosity rebound." The term refers to the expansion of compressible sediments upon release of confining pressure, resulting in an increase in sediment porosity when the sediment is removed from overburden pressures. Although the effect is less pronounced in calcareous sediments, empirical curves for fine-grained terrigenous sediment show an increase in porosity of from 0% to 8% after removal of 0 to 500 m overburden; for terrigenous sediment, the relationship is nearly linear. Other empirical relationships discussed by Hamilton (1974) relate porosity or density to seismic velocity. For turbidites, his equation is

$$V_p = 1669.1 - 1.85(P); \; s = 19.2\%$$

where V_p is compressional seismic velocity, P is porosity, and s is the standard deviation. Factoring in the effect of porosity rebound and applying the resulting porosity value to this linear relationship results in higher *in-situ* velocities proportional to the amount of overburden. At Site 638, the expected velocity correction is 0% at the sediment/water interface and is about 9% at 530 m sub-bottom. However, even after increasing laboratory velocities linearly with depth from 0% at the sediment surface to about 9% at the bottom of Hole 638C, the porosity rebound corrections are still not great enough to reconcile the 0.2–0.4 km/s discrepancy between laboratory-measured velocities and logging velocities in the upper 200 m of Hole 638B; porosity rebound correction for 0–200 m sub-bottom is only 0–3.5% (Hamilton, 1976). The discrepancy may be resolved through a further correction for the release of overburden pressure in the water column as well as in the sedimentary column.

In a series of seismic-velocity measurements on calcareous sediments from the Rio Grande Rise, Carlson and Christensen

(1983) showed a velocity increase from 2.7 to 2.9 km/s on sediments subjected to 600 bars pressure (6000 m depth equivalent) and observed some 7%–14% increase in velocity. In similar experiments monitoring density and velocity changes under a pressure of 500 bars, Carlson and Christensen (1983) found an increase in velocity of 0.2–0.3 km/s over a density range of from 1.8 to 2.3 g/cm^3, which falls within that of sediments of Site 638. The velocity-lowering effect of pore pressure may counter the consequent velocity increase of high confining pressure (Wyllie et al., 1958).

Changes in sediment volume and porosity with release of overburden pressure may be especially evident in unlithified sediments; the correspondence of core diameter to lithology may yield some indication of the volume expansion that occurs in unlithified sediment. Owing to vibration of the coring bit, cores are slightly reduced in diameter as they pass through the throat of the bit. Lithified sediment and hard-rock cores are generally about 58 mm in diameter; by contrast, unlithified sediment completely fills the core liner to its inner diameter of 64 mm. Assuming that the unlithified sediment also entered the core liner at a diameter of 58 mm, a volumetric expansion of about 20% resulting from overburden pressure release is implied. Depending on the depth interval sampled, this is two to four times greater than the porosity or volumetric difference predicted by Hamilton (1976) and may account for the low laboratory-measured velocities. Alternatively, because of the up and down heave of the tool string, much of the unlithified sediment was compressed into drilling "biscuits" or "cakes," which fill the core liner to 64 mm. The weight on the bit is commonly 10,000–20,000 lb, and if all this weight is applied to the core surface, such localized compression might damage the sediment fabric, creating a lower velocity. However, the velocity of "biscuited" sediment is generally not less than expected in these intervals. The unusually low velocities occur closer to the sediment/water interface and may also be attributed to drilling disturbance and biogenic gas expansion as discussed in the summary of this section.

Note that the synthetic seismogram constructed for Hole 638C used laboratory velocity and density values that are uncorrected for porosity rebound from sediment overburden or hydrostatic pressure.

Index Properties

Figures 28D and 28E illustrate the values obtained for bulk density and porosity plotted against depth in Holes 638B and 638C. Bulk-density values increase steadily from about 1.6 g/cm^3 in the soupy, drilling-disturbed nannofossil ooze at the top of lithologic Unit I to about 2.0 g/cm^3 at the base of Unit I (Section 103-638B-20R-3; 184 m sub-bottom), hold steady at about 2.0 g/cm^3 throughout the mud and marl of lithologic Unit II and the upper part of Unit III (i.e., down to the base of Core 103-638B-36R; 344 m sub-bottom), and increase to a steady value of about 2.1 g/cm^3 in the marl below (Cores 103-638B-37R through 103-638B-45R; 344–431 m sub-bottom). Limestone layers in lithologic Subunit IIA yield bulk-density values of from 2.38 to 2.76 g/cm^3, averaging 2.56 g/cm^3; well-cemented sandstone layers of lithologic Unit III yield values of 2.62–2.75 g/cm^3, averaging 2.68 g/cm^3.

Two-minute GRAPE wet-bulk-density values are comparable to those acquired by gravimetric technique. Generally, the difference in values obtained on the same sample is less than 5%.

Porosity values predictably mirror the trends observed in bulk density, steadily decreasing from a high value of 71% in the nannofossil ooze of Core 103-638B-1R at the top of lithologic Unit I to about 59% in Core 103-638B-8R (74 m sub-bottom). Drilling disturbance may account for the scatter of porosity values observed in Core 103-638B-10R (84–94 m sub-bottom; 34%–74%). Below Core 103-638B-10R, porosity resumes its steady decrease with depth to a value of about 50% at the base of lithologic Unit I (Section 103-638B-20R-3; 184 m sub-bottom). Marl, mud, and clay of lithologic Units II and III vary within a range of about 27%–57%; values cluster between 45% and 50% in Hole 638B and between 35% and 40% in Hole 638C. As expected, the porosity of limestone layers in lithologic Subunit IIA is low (21%–27%). Low porosity values (3%–15%) in sandstone layers in lithologic Unit III indicate extensive cementation.

Grain-density values are consistent with those expected of sediment composed predominantly of felsic silicates and carbonates. Most measured values fall within a range of 2.65–2.80 g/cm^3.

Figure 30 illustrates the positive correlation between bulk density and compressional velocity as a function of decreasing porosity downhole. The set of data points within area A corresponds to unlithified sediments, which show a slight increase in seismic velocity and bulk density with greater burial depth. The set of points in area B corresponds to cemented sandstone and limestone.

Acoustic Impedances and Predicted Reflectors

At several depths in Hole 638B, the average density and velocity of the recovered material changes over a small interval. We calculated the reflectivity of these interfaces to help interpret the seismic profiles available from earlier site surveys (see "Seismic Stratigraphy" section, this chapter). Figure 28F shows acoustic impedance (the product of compressional velocity and bulk density) plotted against sub-bottom depth. As annotated in the figure, three depths occur at which average impedance of an interval changes significantly. Such contrasts in acoustic impedance could generate a seismic reflection. We calculated the reflectivity R between adjacent layers 1 and 2 at these sub-bottom depths by using the equation:

$$\frac{V_{p1}\rho_{b1} - V_{p2}\rho_{b2}}{V_{p1}\rho_{b1} + V_{p2}\rho_{b2}}$$

where V_p = compressional seismic velocity (km/s) and ρ_b = bulk density (g/cm^3).

The first depth at which we expect a reflector is about 190 m sub-bottom between the Cenozoic lithologic Unit I and the late Barremian lithologic Subunit IIA; a second possible reflector may occur at about 212 m sub-bottom between lithologic Subunits IIA and IIB (Hauterivian to possible late Valanginian); the third reflector may exist at about 344 m sub-bottom, where sandstone beds occur in significant thickness at the top of Core 103-638B-37R (still in the Hauterivian to possible late Valanginian; see "Biostratigraphy" section, this chapter). Table 6 shows the average velocities and bulk densities for each of the lithologic units used to calculate impedances and reflectivities at Hole 638B. The resulting reflection coefficients (R) are conservative estimates made assuming that Subunit IIA contains only 10% limestone and Subunit IIIB contains only 15% sandstone.

Coring data support the existence of two of the possible reflectors. In Figure 31, core number and sub-bottom depth are plotted against the length of time necessary to drill the core. Abrupt breaks both in drilling time and in trend of change in drilling time with depth occur at the depths of the two deeper reflectors conjectured to occur at about 212 and 344 m sub-bottom. Caution must be used in interpreting these data because changes in the drilling time may reflect changes in the weight applied to the drill bit, in the number of revolutions per minute (RPM) of the bit, and in the pressures and volumes of water pumped through the bit, rather than changes in lithology. Although the possible reflector at 212 m sub-bottom is suggested

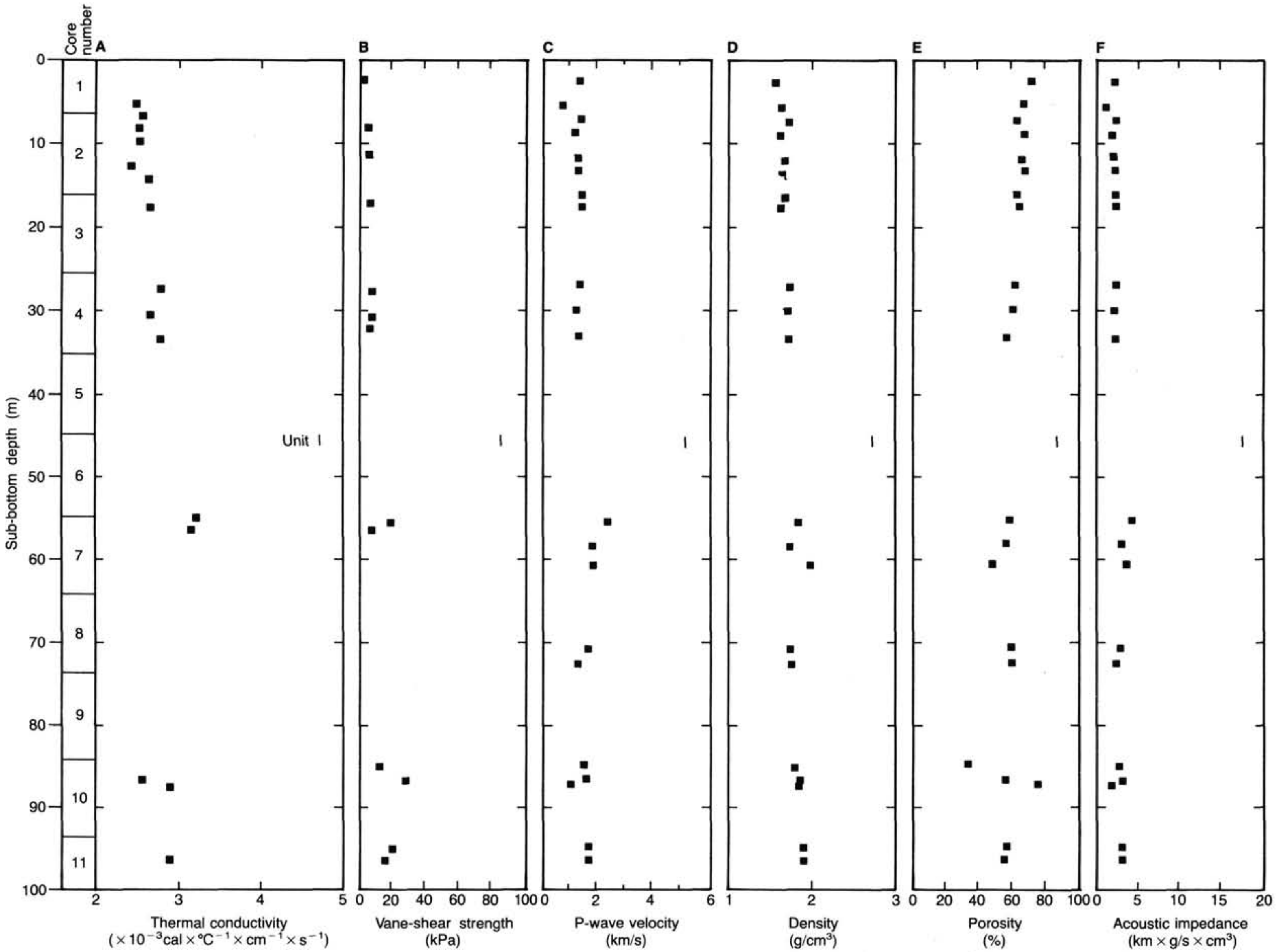
Core number
A
B
C
D
E
F
Sub-bottom depth (m)
Unit I
Thermal conductivity
(× 10⁻³cal × °C⁻¹ × cm⁻¹ × s⁻¹)
Vane-shear strength
(kPa)
P-wave velocity
(km/s)
Density
(g/cm³)
Porosity
(%)
Acoustic impedance
(km × g/s × cm³)

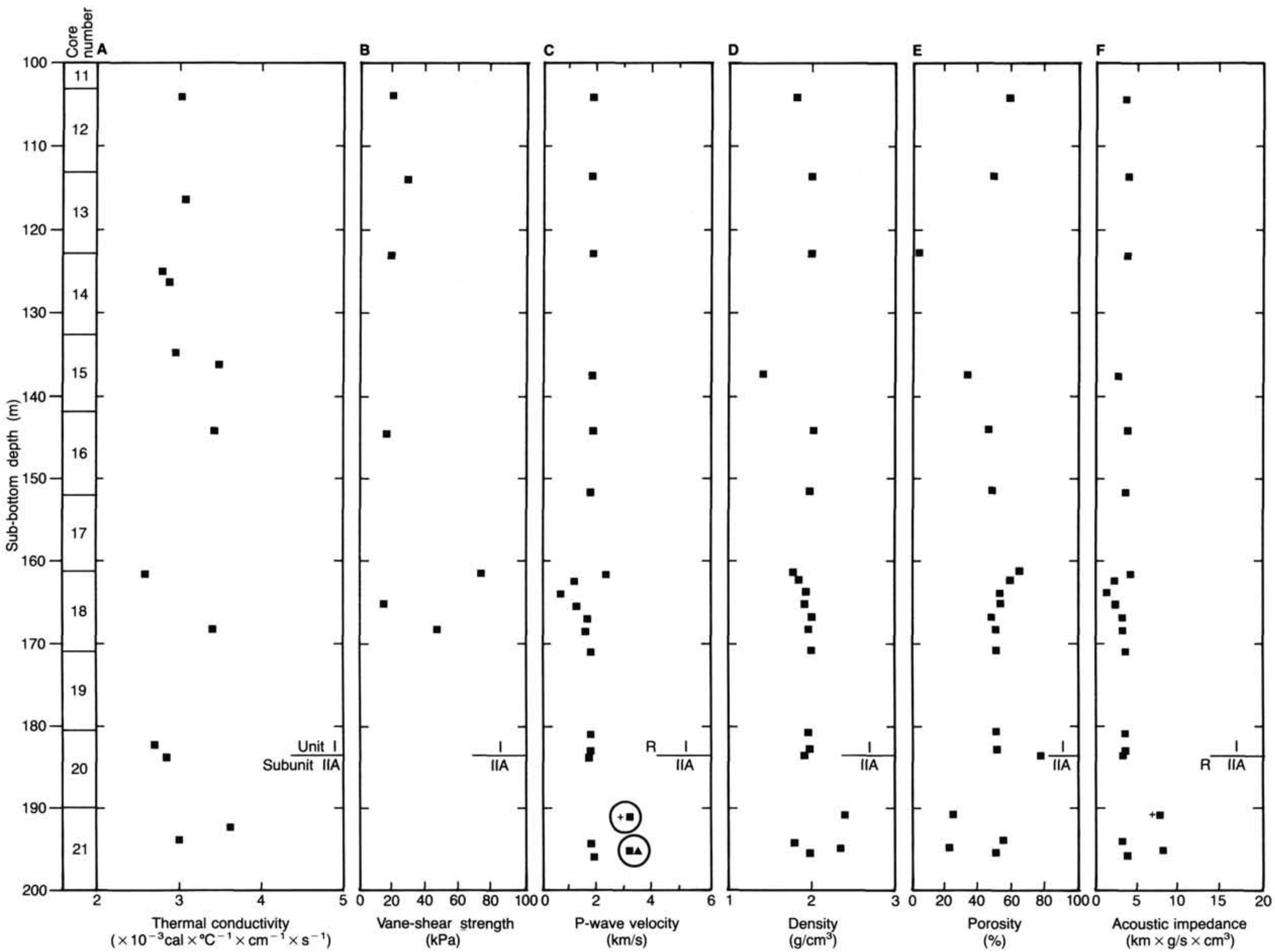

Figure 28. Physical-property measurements on sediments and sedimentary rocks from Holes 638B and 638C plotted against sub-bottom depth. Lithologic units as described in the "Sediment Lithology" section (this chapter) are indicated on the right side of the columns. A. Thermal-conductivity values ($\times 10^{-3}$ cal $\times$ °C^{-1} $\times$ cm^{-1} $\times$ s^{-1}). B. Vane-shear strength (kiloPascals). C. Compressional seismic velocity (kilometers per second). Square data points indicate velocities measured in the plane of the core diameter and parallel to the cut face of the core (c-direction), triangular data points indicate velocities measured in the plane of the core diameter and parallel to the cut face of the core (b-direction), and crosses indicate velocities measured perpendicular to the plane of the core diameter (a-direction). Cemented-rock data points (limestone and sandstone) are encircled. D. Bulk density (grams per cubic centimeter). E. Porosity (percent). F. Acoustic impedance (compressional velocity $\times$ bulk density, km $\times$ g/s $\times$ cm^3).

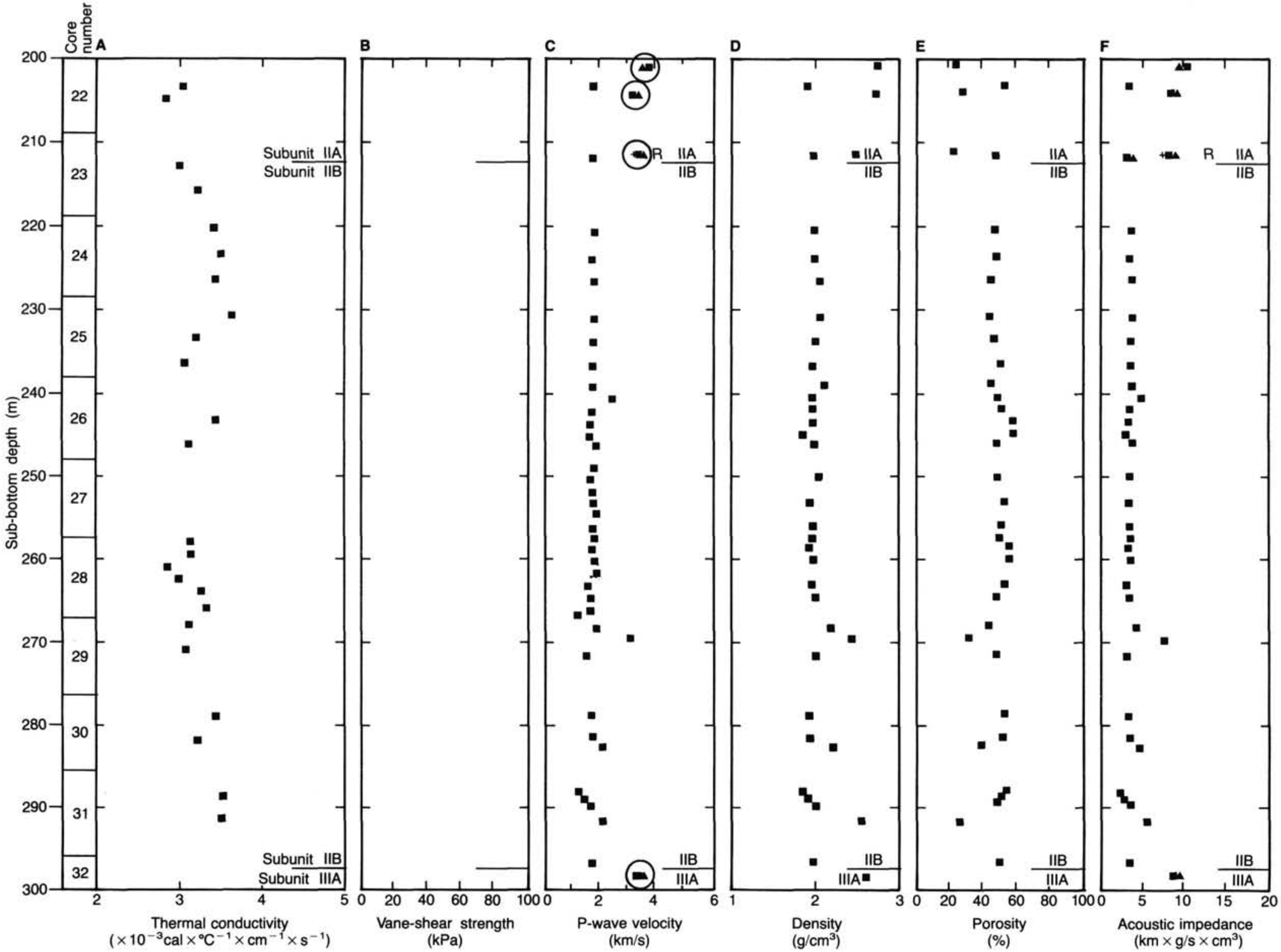
Core number
A
B
C
D
E
F
Sub-bottom depth (m)
22
23
24
25
26
27
28
29
30
31
32
Subunit IIA
Subunit IIB
Subunit IIB
Subunit IIIA
R
IIA
IIB
IIIA
Thermal conductivity
(×10⁻³cal × °C⁻¹ × cm⁻¹ × s⁻¹)
Vane-shear strength
(kPa)
P-wave velocity
(km/s)
Density
(g/cm³)
Porosity
(%)
Acoustic impedance
(km × g/s × cm³)

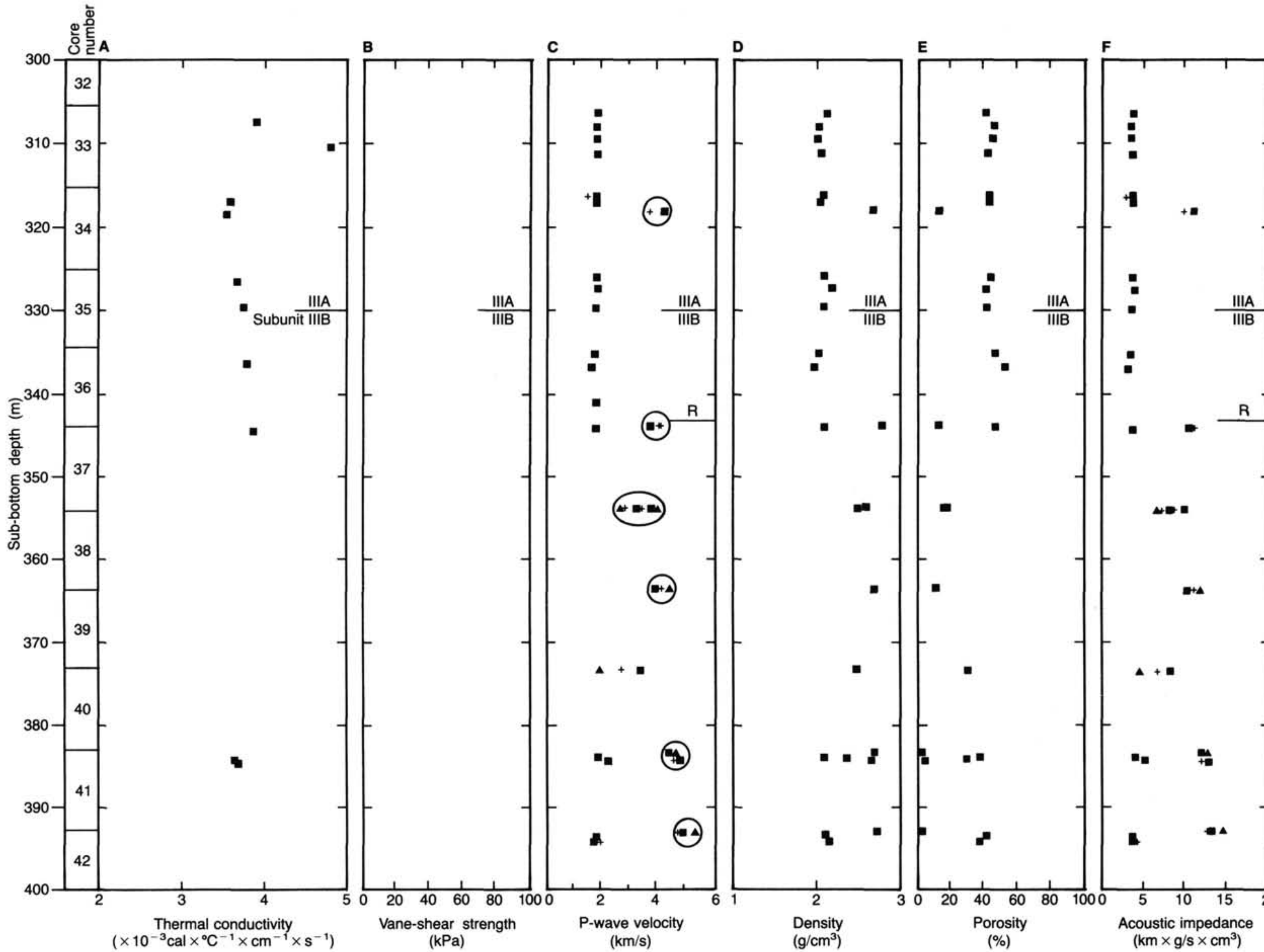

Figure 28 (continued).

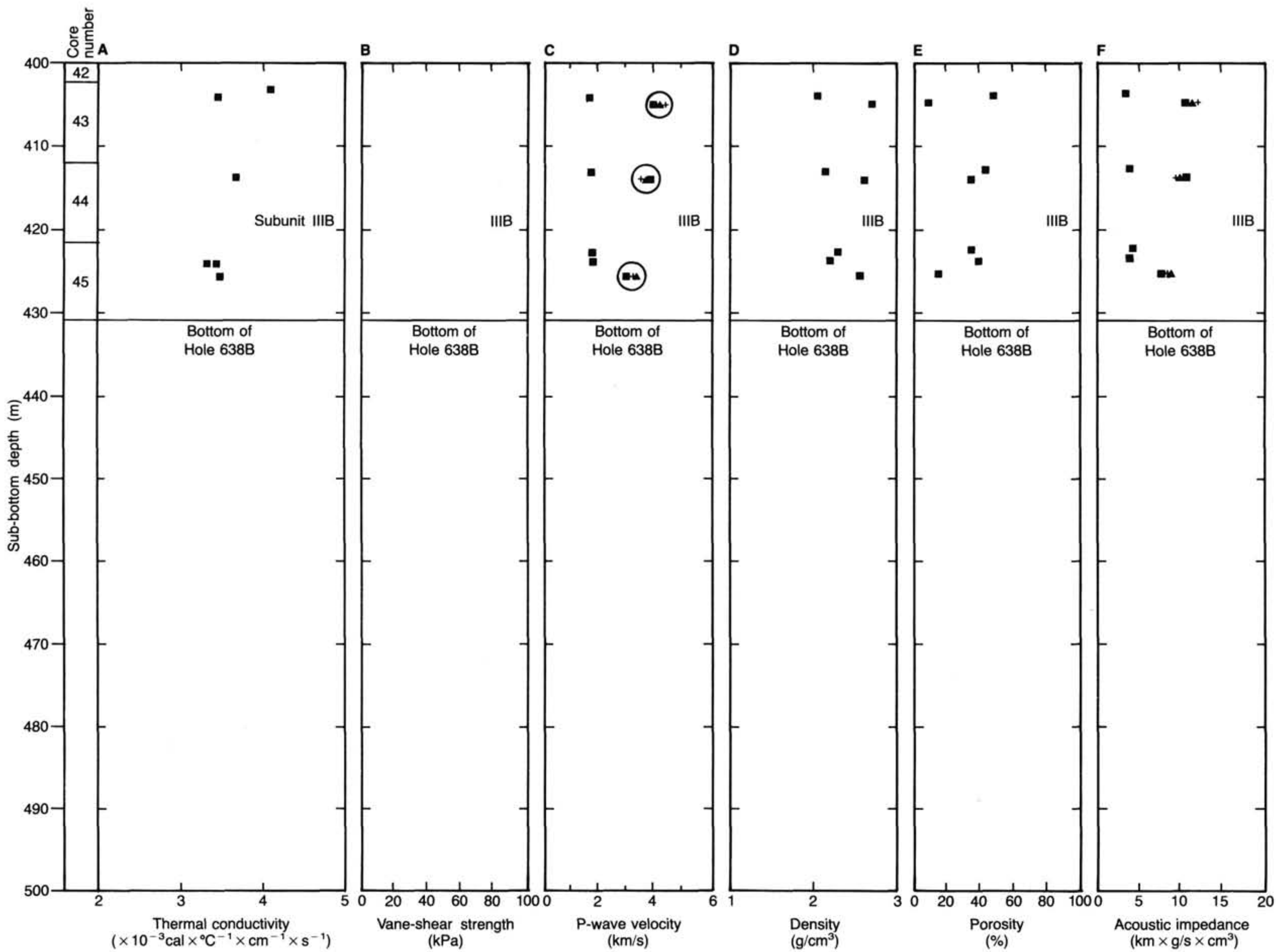
Core number
A
B
C
D
E
F
42
43
44
45
Subunit IIIB
IIIB
Bottom of Hole 638B
Sub-bottom depth (m)
Thermal conductivity (×10⁻³cal×°C⁻¹×cm⁻¹×s⁻¹)
Vane-shear strength (kPa)
P-wave velocity (km/s)
Density (g/cm³)
Porosity (%)
Acoustic impedance (km×g/s×cm³)

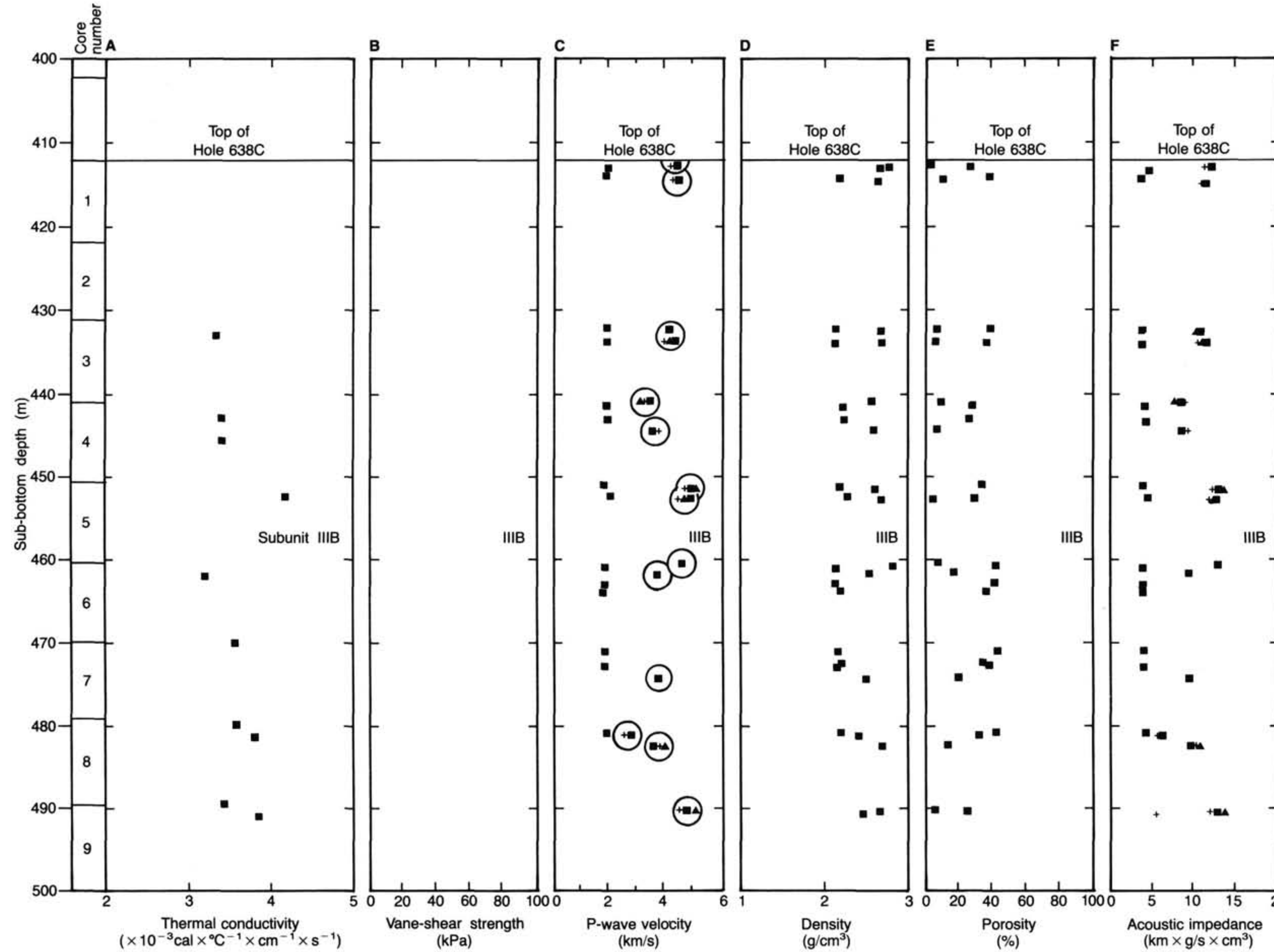

Figure 28 (continued).

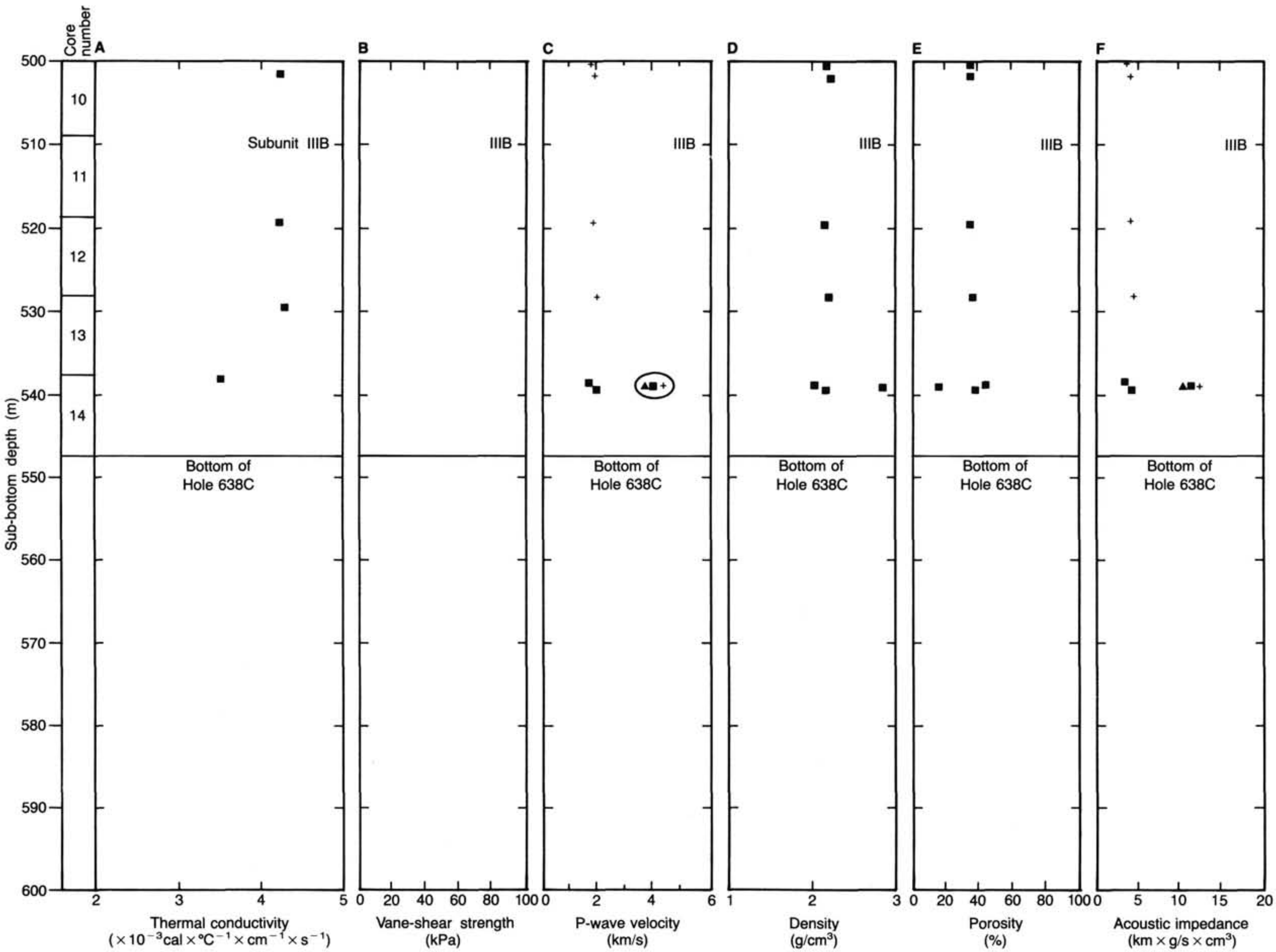

Figure 28 (continued).

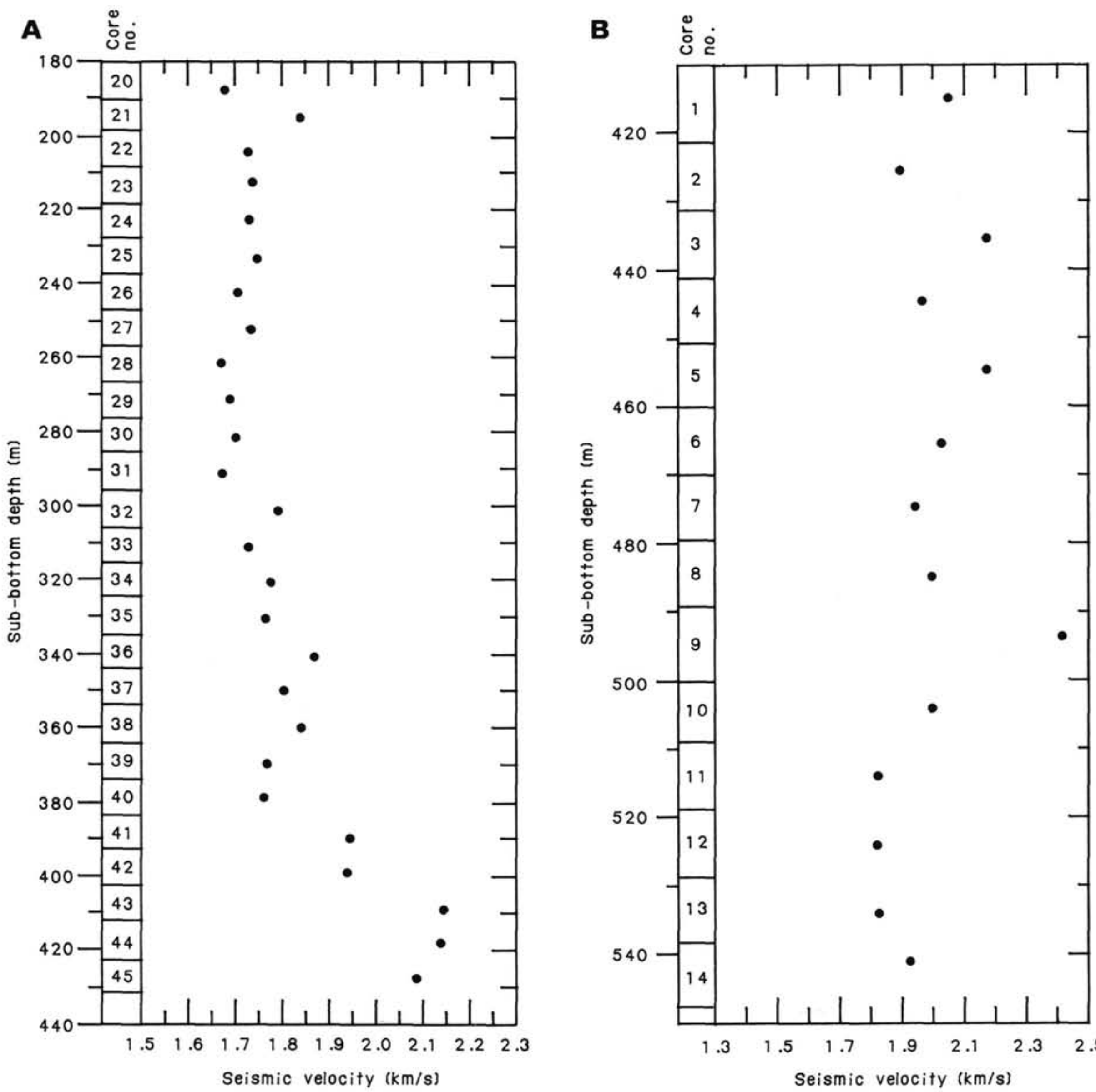

Figure 29. A. Calculated average seismic velocity of cores from the Mesozoic section of Hole 638B (lithologic Units II and III; Cores 103-638B-20R through 103-638B-45R, 181–431 m sub-bottom) plotted against sub-bottom depth. B. Calculated average seismic velocity of cores from Hole 638C.

not only by changes in lithology and physical properties but also by a drilling time decrease, between Core 103-638B-22R (199.7–209.3 m sub-bottom) and Core 103-638B-23R (209.3–218.8 m sub-bottom) the hydraulic pump accelerated from 35 to 60 RPM, and hydraulic pressure was increased from 350 to 500 pounds per square inch (psi). The shift in drill rate at this interval is, thus, of ambiguous origin and may not support the existence of a reflector here.

In drilling the cores spanning the depth of the conjectured reflector at 344 m sub-bottom (Core 103-638B-36R from 334.5 to 344.2 m sub-bottom and Core 103-638B-37R from 344.2 to 353.8 m sub-bottom), the same drilling parameters were maintained, and the observed decrease in drilling rate is, therefore, less ambiguously attributable to lithologic changes. The drilling-time decrease at 344 m sub-bottom correlates with the beginning of sandstone occurrences in a large proportion of recovered material. Although sandstone is harder than the surrounding cohesive marl beds, its rigidity may make it more easily drilled.

The computer-generated synthetic seismogram (see "Logging Results" section, this chapter) and some of the physical-properties data presented in this section places a reflector near this lower reflector at about 300 m sub-bottom. At about 300 m, the first sandstone sample was measured for seismic velocity and bulk density. The several measurements of sandstone velocity and index properties between 300 and 344 m sub-bottom may give a false impression of the proportion of sandstone recovered in the cores; sandstone does not appear in significant proportion in the cores until about 344 m sub-bottom.

Summary

Thermal conductivity of unlithified sediments from Holes 638B and 638C generally increases with depth from about 2.4 to about 4.3 cal $\times$ °C^{-1} $\times$ cm^{-1} $\times$ s^{-1}. The increase with depth

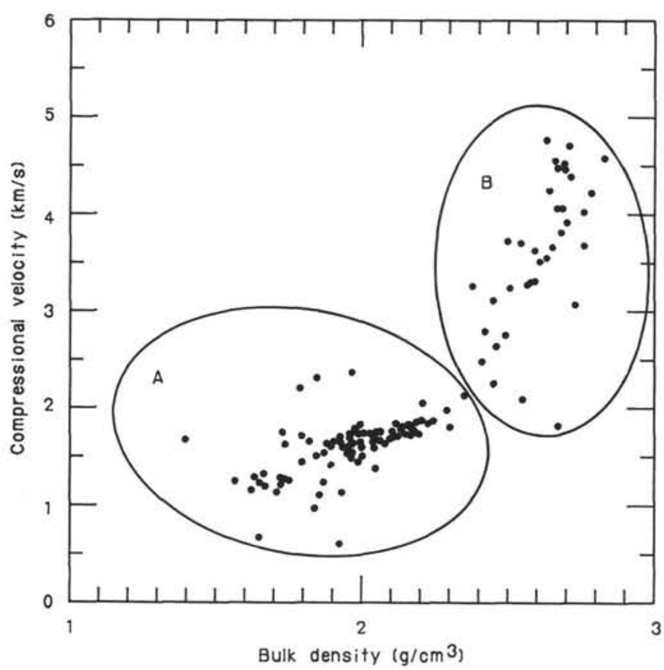

Figure 30. Bulk density plotted against compressional seismic velocity of Holes 638B and 638C. The set of data points within area A corresponds to unlithified sediments that show a slight increase in seismic velocity with increasing bulk density. The set of data points in area B corresponds to cemented sandstone and limestone.

Table 6. Average compressional seismic velocities (V_p) and bulk densities (ρ_b) used to calculate acoustic impedance ($V_p\rho_b$) and reflectivity (R) between lithologic units.

	V_p (km/s)	ρ_b (g/cm^3)	$V_p\rho_b$	R
Unit I	1.65	2.00	3.30	
Subunit IIA	1.76	2.06	3.62	0.046 (I/IIA)
Subunits IIB + IIIA	1.69	2.00	3.38	0.034 (IIA/IIB + IIIA)
Subunit IIIB	1.92	2.19	4.20	0.108 (IIB + IIIA/IIIB)

is fairly constant except over the interval ascribed to lithologic Subunit IIB (213–298 m sub-bottom, Cores 103-638B-23R to 103-638B-32R). Thermal conductivity over this interval falls within a narrower range of 2.6–3.5 cal × °C^{-1} × cm^{-1} × s^{-1}. The change of thermal conductivity with depth is probably linked most closely with the downhole decrease in porosity and consequent increased transmission efficiency of lattice vibration.

Vane-shear-strength measurements on sediment from lithologic Unit I in Cores 103-638B-1R through 103-638B-18R show a gradual increase with depth of undrained shear strength. This somewhat reflects the greater degree of drilling disturbance in the upper part of Hole 638B. Note that the exponential increase of shear strength with sub-bottom depth is not accompanied by a similarly dramatic increase in other physical properties, such as seismic velocity or bulk density; remote-sensing techniques such a seismic profiling or logging cannot be used to predict sediment cohesiveness.

Compressional seismic velocities in sediments and sedimentary rocks of Hole 638B generally increase with depth. In the nannofossil ooze of the Neogene lithologic Unit I, velocities increase from about 1.25 km/s in the upper six cores to about 1.75 km/s at the base of the unit; the mean velocity measured below the drilling-disturbed upper 54 m is about 1.65 km/s. The very low velocities measured in the upper six cores are puzzling. We are not certain whether the low values reflect (1) a greater admixture of air from core handling after the material had been brought aboard ship, (2) the expansion of gas generated in the biologically more active upper 50 m or so of sediment when ambient pressure is reduced to 1 atmosphere, or (3) the inability of the Hamilton Frame velocimeter to measure accurately the seismic velocity of sediment having high water content.

The upper boundary of lithologic Unit II is distinguishable not by a shift in nannofossil-ooze or -marl velocity but by the presence of several layers of chalk and limestone, which raise the average velocity in Subunit IIA to 1.76 km/s. Seismic velocities in lithologic Subunit IIB (212–298 m sub-bottom; Cores 103-638B-23R to 103-638B-32R) are remarkably uniform and indistinguishable from those measured in lithologic Subunit IIIA (298–330 m sub-bottom; Cores 103-638B-32R through 103-638B-35R), except for the occurrence of a few higher velocity sandstone layers in the latter; average seismic velocity for both units, based on visual core description tabulation, is 1.74 km/s. At about 344 m sub-bottom the average seismic velocity of the interval increases because of both an increase in the number of sandstone layers (with a seismic velocity average of about 4.2 km/s) and an increase in velocity of unlithified marl and clay in Subunit IIIB below about 344 m sub-bottom.

The core-by-core average seismic velocities presented in Figure 29 were calculated assuming that any unrecovered sediment consisted of unlithified marl. Had we assumed that the unrecovered material consisted of unlithified sand, the outcome would not be greatly altered because seismic velocities in uncemented sand range from 1.7 to 1.85 km/s (Bryant et al., 1981), and the velocities we used for marl generally fell within this range.

Bulk-density and porosity values predictably reflect the decreasing water content with depth. Despite drilling disturbance in the upper seven cores of Hole 638B, the velocity-to-bulk density ratio over the length of these cores (about 0.8) is roughly the same as that maintained through the length of the section at Holes 638B and 638C. The lack of change in these properties throughout Subunits IIB and IIIA suggests that these materials are at a consolidation limit, which may reflect an earlier, greater amount of overburden subsequently removed by erosion; the presence of chalk and limestone layers in Subunit IIA supports this suggestion (Hamilton, 1976). Biostratigraphic evidence, adding further support, indicates unconformities between Neogene nannofossil ooze in Unit I and late Barremian-early Aptian(?) limestone, marl, and marlstone in Subunit IIA, and between Subunit IIA and lower-middle Valanginian–Hauterivian nannofossil marl and marlstone in Subunit IIB.

Empirical diagrams of depth vs. porosity by Hamilton (1976) imply that an overburden of about 400 m is necessary to attain a porosity of about 45%, and an overburden of some 800 m is required to achieve a porosity of 35% in fine-grained terrigenous sediment. By this simplistic relationship, the porosities of 45%–50% measured at the top of lithologic Unit II at a sub-bottom depth of around 190 m indicate that about 200 m of overburden has been removed, whereas the porosities clustering around 35% at sub-bottom depths greater than about 450 m indicate about 350 m removal of overburden. Porosity–depth studies are limited in general application; variation of the sediment composition (grain size, carbonate content) and the rate of sediment accumulation can greatly affect the shape of the curve. Comparison of other sections with an empirical curve derived for a specific section are most useful when the two regions have a similar sedimentation history and sediment composition. Cautious application of Hamilton's (1976) porosity–depth curve for fine-grained terrigenous sediment to the porosity values of Cretaceous sediments at Site 638 results in an estimated removal of 200 m of overburden from the present section at the level of the unconformity.

The changes in average bulk density and average seismic velocity across lithologic unit boundaries between Units I and IIA, IIA and IIB, and IIIA and IIIB may have expression in

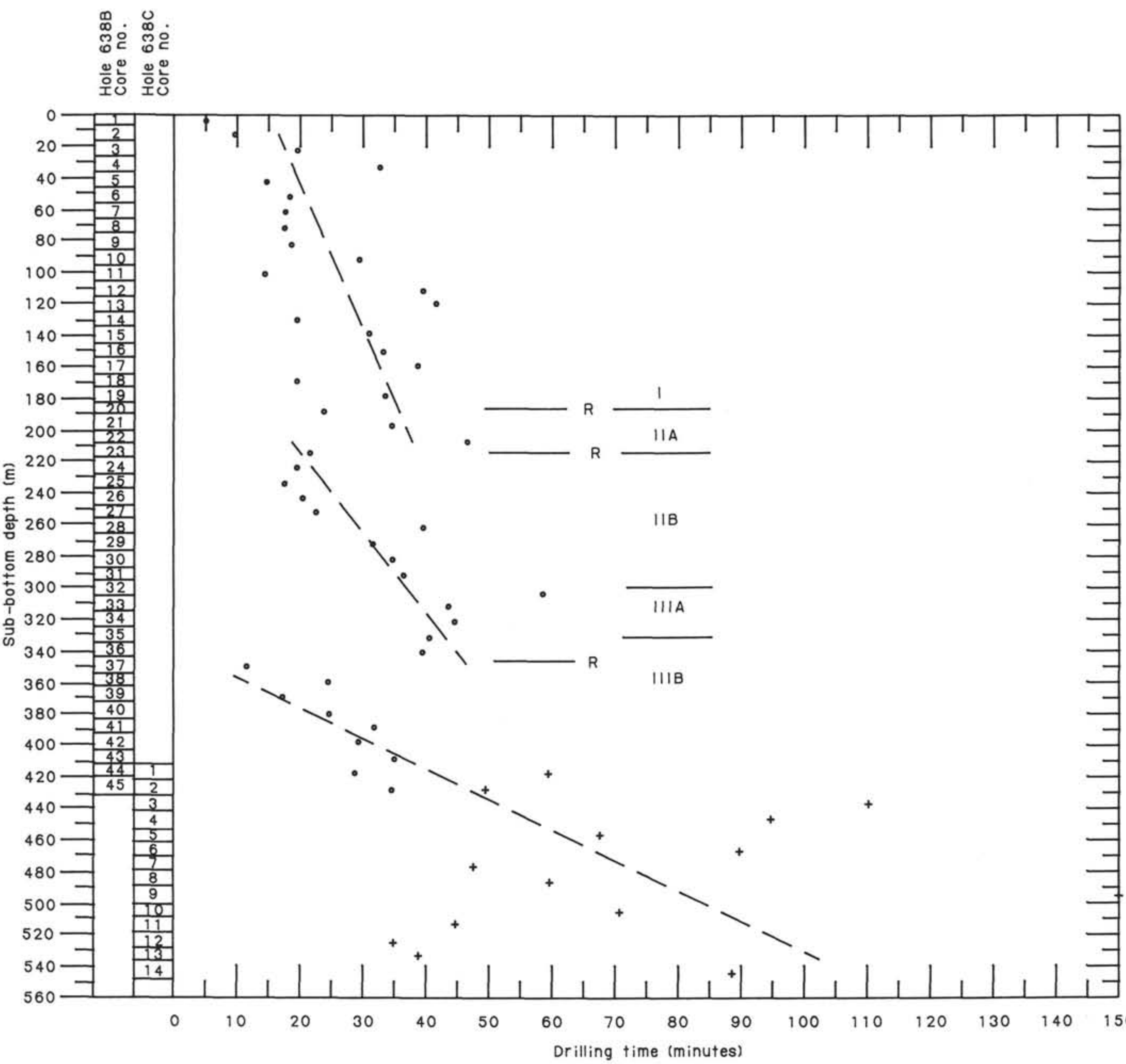

Figure 31. Drilling time plotted against sub-bottom depth. Solid circles are data from Hole 638B and crosses are Hole 638C data. Lithologic units (Roman numerals) and possible reflectors (R) are indicated.

seismic reflectors; calculated reflectivity coefficients at these boundaries are rather low. Because the velocities and bulk densities used are averages based on extrapolation of values measured in cores having poor recovery, our reflection coefficients are probably conservative. The major uncertainty in defining the strongest reflector at about 344 m sub-bottom depth is the occurrence of sandstone beds; a strong reflector may not exist if the increase in the proportion of section occupied by sandstone is gradational.

One clue in the identification of reflectors may be extracted from coring data: at two of the conjectured reflectors (between lithologic Units IIA and IIB and at 344 m sub-bottom in lithologic Unit IIIB), the amount of time necessary to drill the length of a core shifts abruptly.

AGE-VS.-DEPTH CURVE

The age-vs.-depth curve for Holes 638B and 638C is shown in Figure 32, along with calculated values of sedimentation and accumulation rates.

In the Neogene, a discrepancy exists between foraminiferal- and nannofossil-age determinations; consequently, two curves are shown for the interval from about 50 to 183 mbsf. The differences are small and make virtually no difference in the calculated rates. The calculated rates are high for the late Miocene (about 20 g/cm^2/1000 yr) and for the middle Pliocene (about the same value) but much slower for the early Pliocene and the late Pliocene. Most of the Pleistocene is missing or perhaps was not cored (see "Operations" section, this chapter).

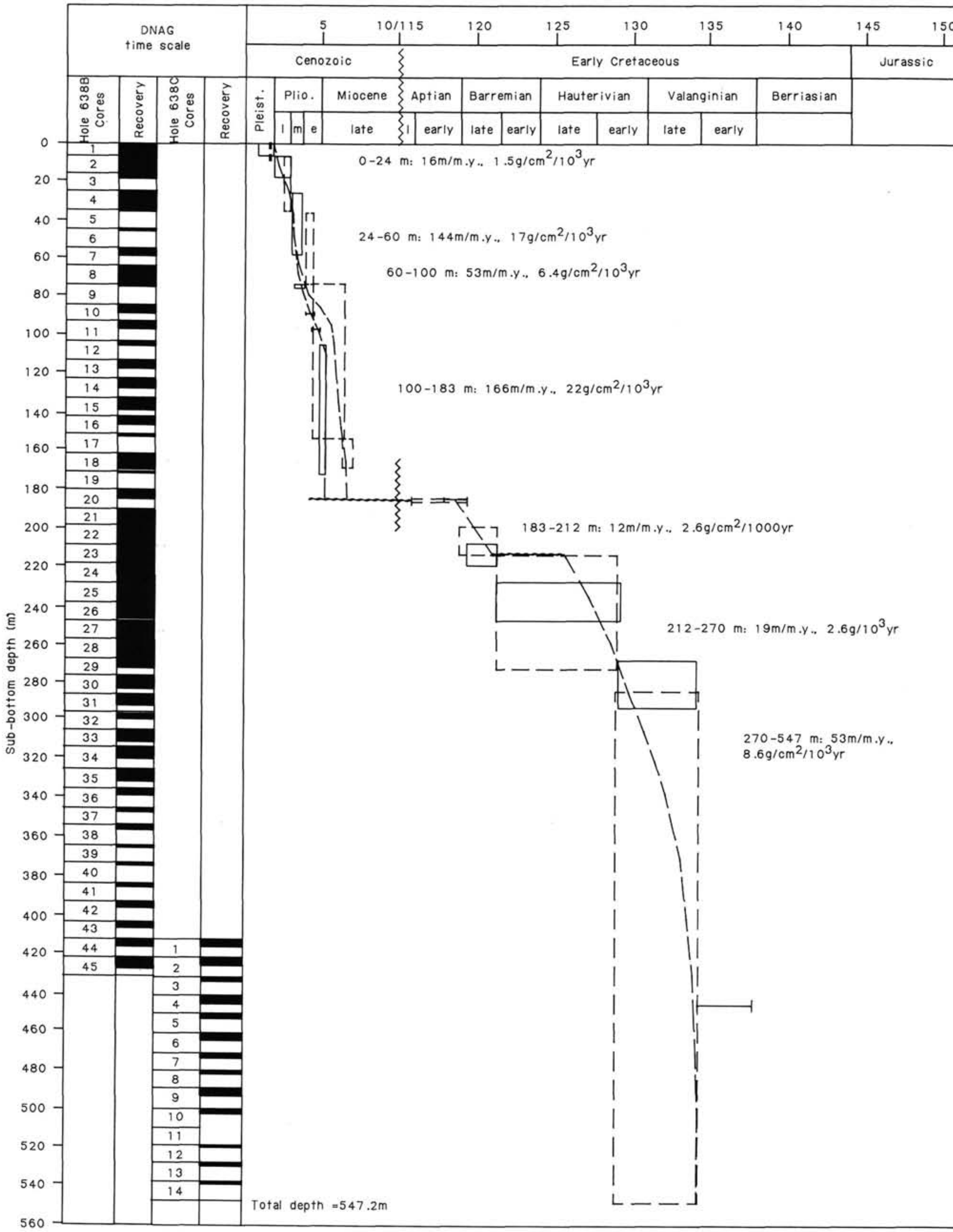

Figure 32. Age of biostratigraphically dated intervals in Holes 638B and 638C, expressed in millions of years, plotted against depths of the samples in the holes. The range of uncertainty in age assignments is indicated by the width of the age-range bars and boxes. Note that a gap of 105 m.y. appears in the diagram, indicated by a zig-zag vertical line. The figures to the right of the curve indicate, for each more-or-less straight-line segment, the rate of sedimentation in m/m.y. and the rate of accumulation, in g/cm^2/1000 yr, adjusted for porosity and grain density of sediments from each interval and made using the values measured in the laboratory.

During the Early Cretaceous, rates were moderately high (about 10 g/cm^2/1000 yr) in the Valanginian and slowed to about one-fourth this value during the Hauterivian and Barremian, reflecting the change from sandy turbidite to clay and marl deposition.

LOGGING RESULTS

Introduction

Geophysical logs were obtained at Site 638 in the pilot hole (638B) and the reentry hole (638C). The total depth of Hole 638B was 431.1 mbsf. Schlumberger long-spaced sonic, dual-induction, gamma-ray, and caliper tools were first run in Hole 638B from 100 to 278 mbsf. After a wiper trip was made in an attempt to get deeper into the hole, the L-DGO multichannel sonic (MCS) tool was run in the interval 100–164 mbsf. Neither run successfully reached total depth as a result of impassable bridges at 278 and 164 mbsf, respectively.

The total depth of reentry Hole 638C was 547.2 mbsf. The same suite of Schlumberger tools used in Hole 638B was used to log the deeper sedimentary interval but was again stopped by a bridge at 287 mbsf. A second suite, including lithodensity, neutron, and natural gamma-ray spectrometry tools, was employed from 105 to 250 mbsf, where a shallower constriction limited logging operations.

Both holes were drilled with a 9.875-in. bit and filled with 9.7 lb/gal fresh gel mud. The 5-in. (outer diameter) drill pipe and 8.25-in. (outer diameter) drill collars were pulled up to 100 mbsf before logging. The logs were recorded as the tools were pulled uphole at approximately 1000 ft/hr.

Log Analysis

Three characteristic log-lithologic units are determined from the tool responses over the logged interval. These units are identified by distinct changes in the logs, shown in Figures 33 through 35. The ranges of the log values are summarized in Tables 7 (Hole 638B) and 8 (Hole 638C). Borehole rugosity and washout prevent reliable log data in several intervals in log-lithologic Units B and C in both holes. These intervals are apparent in the logs by low values of induction (ILD and SFLU) and density (RHOB and PEF) and high values of sonic slowness (DT), porosity (NPHI), and caliper (CAL) logs. Some improvement of the hole condition in Hole 638C resulted in a reliable sonic log where "cycle skipping" occurred in the log from Hole 638B. Other logs show no significant differences between Holes 638B and 638C attributable to changes in the hole condition.

Log-lithologic Unit A has relatively homogeneous log character; gamma-ray readings are about 25 API units, sonic velocities between 1.96 and 2.3 km/s, and resistivity values about 1.3 ohmm (Figs. 33A and 33B). Bulk density and neutron porosity logs in Hole 638C vary between 1.7 to 2.0 g/cm^3 and 42% to 54%, respectively. Compressional velocities obtained from the multichannel sonic log in Hole 638B range between 2 and 2.25 km/s from 100 to 164 mbsf. In the interval between 154 and 164 mbsf, gamma-ray values increase with depth to 45 API units, sonic velocity decreases to 1.6 km/s, and resistivity measurements vary inversely with the caliper changes, which range between 10.75 and 12.25 in. These rapid variations may be due to washed-out clay, which blocked the MCS tool at 164 mbsf.

Log-lithologic Unit B has a heterogeneous log profile with sharp boundaries and variations in borehole diameter between 9.75 and 12.25 in. (Figs. 34A and 34B). Gamma-ray, resistivity, density, and neutron porosity values fluctuate, and there are several intervals where "cycle-skipping" occurs in the sonic log. Despite cycle-skipping on sonic logs, reliable values range between 90 and 180 μs/ft, caused by the alternation of clay and limestone in 1- to 4-m thick layers. The top and bottom of this unit in Hole 638C is located 3 m higher and 17 m lower than in Hole 638B. Therefore, Unit B is 20 m thicker in Hole 638C.

In log-lithologic Unit C, the variations of gamma-ray and resistivity values again suggest relative changes in clay content (Figs. 35A and 35B). Clay-poor intervals have both low resistivity (0.4 ohmm) and velocity (1.6 km/s) values relative to clay-rich intervals. Variations in borehole diameter in this unit severely affect the log measurements in both holes.

Lithostratigraphic Correlation

The three log-lithologic units correspond reasonably well with the lithostratigraphic units described from the recovered cores (see "Sediment Lithology" section, this chapter). This correlation is summarized in Table 9. In log-lithologic Unit A, low gamma-ray values generally correspond to the nannofossil ooze and chalk of lithologic Unit I. High gamma-ray values correspond to the stiff, reddish brown clay in Core 103-638B-17R and Section 103-638B-18R-1. This clay interval is absent in Hole 638C.

The Cenozoic/Mesozoic boundary between lithologic Units I and II correlates with sharp changes in log responses. Log-lithologic Unit B is heterogeneous, consistent with the three different lithologies identified in lithologic Subunit IIA (see "Sediment Lithology" section, this chapter). A correlation exists between (1) low gamma-ray and high resistivity values and bioturbated limestone and (2) high gamma-ray and low resistivity values and calcareous clay.

In Unit C, high gamma-ray and resistivity values probably correspond to alternating layers of nannofossil and clay-rich marls in lithologic Subunit IIB. Low gamma-ray and resistivity readings may relate to slumped intervals in Section 103-638B-23R-3 and Core 103-638B-26R.

Preliminary Seismic Correlation

A synthetic seismogram was calculated from a simplified physical-properties model of the sedimentary sequence at Site 638. In the logged section, bulk-density and sonic-velocity values were averaged in intervals determined from log analysis; elsewhere, selected laboratory measurements were used. Corrections for rebound porosity of the laboratory samples were ignored, and poor core recovery increased the depth uncertainty of the laboratory data. As a result, the composite log/lab model in Table 10 is only a possible interpretation of the data. Slight modifications of this model, however, do not significantly change the major results.

The depths in Table 10 correspond to the top of each interval, and the compressional velocity is constant below. A zero-phase wavelet, band limited between 10 and 60 Hz, was used to approximate the source function for the synthetic computation. The effects of internally reflected energy are included, although mode conversions and spherical divergence are ignored. The resulting synthetic seismogram at Site 638 is shown in Figure 36 with the nearby underway seismic record. Relative seismic amplitude is plotted vs. two-way traveltime. Prominent high-amplitude reflections in the synthetic seismogram at about 6240, 6290, 6380, and 6480 ms correspond to impedance contrasts in the sediments at approximately 58, 105, 185, and 298 mbsf, respectively, as indicated in Figure 36. These depths are identified by sharp changes in the velocity and density values in Table 10. Note, however, that these seismic phases are influenced by changes in the model and assumptions about the source signature. We advise caution, therefore, in making interpretations using this correlation.

SEISMIC STRATIGRAPHY

Interpretation of the Seismic Line Recorded on *JOIDES Resolution*

During the transit of the drill ship from Sites 637 to 638, we generated a seismic-reflection profile, part of which is shown in Figure 37. Comparison of the seismic stratigraphy of the sedimentary basin west of Site 638 with that seen on seismic profiles near DSDP Site 398 (about 200 km southeast of Site 638), which were calibrated by drilling (Sibuet, Ryan, et al., 1979), suggests that the oldest strata shown on the *JOIDES Resolution* profile are black shale beds of Albian to middle Cenomanian age (seismic sequence 3 on Fig. 37). Layers older than sequence 3, such as the syn-rift and pre-rift units seen on multichannel seismic lines, cannot be identified on the unprocessed profile.

Near Site 638, the profile is more difficult to interpret. The drill site is in a valley having side slopes that create side echoes in the form of hyperbolic traces, and the unprocessed profile has a large vertical exaggeration (about 19×). Even so, two seismic reflectors, labeled R1 and R2 on Figure 37, are plainly seen east of the valley. The acoustically transparent unit between the two reflectors we identify as seismic sequence 3, the black shale, seen on the processed multichannel line GP-101 (Fig. 38C). Reflector R1, thus, is probably middle Cenomanian in age, and R2 is near the Albian/Aptian boundary and marks the regional "break-up" unconformity between syn- and post-rift sedimentary sequences. Another display of the *JOIDES Resolution* profile, processed to reduce the vertical exaggeration and to emphasize strong-amplitude reflections, is shown in Figure 38A.

Correlations Between Drilling Data and Seismic Profiles

Although Site 638 is about 1 km north of multichannel seismic line GP-101 (Figs. 5 and 38), the seismic profile recorded from *JOIDES Resolution* during the approach to the site (Fig. 37) is similar to line GP-101. In particular, the seismic stratigraphy at the point where we dropped the acoustic beacon resembles that at shotpoint 3085. The two places are at about the same position relative to the axis of the submarine valley and have nearly the same water depth; reflectors R1, R2, and R3 intersect the seafloor at about the same relative positions along the valley and dip eastward at about the same angle. For these reasons, we shall use both line GP-101 at shotpoint 3085 and the seismic section at Site 638 in relating the drilled sequence to the seismic stratigraphy.

To make reliable correlations between the seismic and physical stratigraphy, data on density and velocity from downhole logging and from laboratory measurements are required. Logging data on sonic velocity and density exist for only the interval from about 105 to 272 mbsf for velocity and 105 to 243 mbsf for density and thus provide only weak support for correlations. The log velocity data are, furthermore, at odds with the data from direct laboratory measurements on core samples and require us to assume a velocity change of about 15% from effects of pressure release on the samples to bring the log and laboratory results into harmony (see "Physical Properties" section, this chapter).

Figure 39 shows a synthetic seismogram, constructed by combining both logging and *uncorrected* laboratory data on velocity and density and then convolving the resultant impedance curve with an artificial source signal in a frequency band similar to that used in processing multichannel seismic line GP-101 (see "Logging Results" section, this chapter). Because of assumptions made in the model, the relative amplitude of reflections in the synthetic seismogram may be distorted.

The correspondence between major reflectors on the GP-101 seismic profile (Fig. 40) and lithologic changes recorded by the cores and log data from Site 638 are discussed as follows, from youngest to oldest:

1. At Site 638, the 184-m-thick Neogene ooze and chalk sequence rests unconformably on Cretaceous strata. This sequence correlates with the valley-fill unit seen on the seismic profiles (Figs. 38B and 38C). The strong peak in seismic amplitude on the synthetic seismogram at the level of the unconformity has a calculated two-way traveltime of approximately 220 ms; the actual seismic profile has a strong reflector at 220 ms.

2. The outcrop of reflector R1, believed to be near the Cenomanian, is on the lower slopes of the hill east of Site 638; the reflector was, therefore, not intersected during drilling. Likewise, reflector R2, which correlates with the regional break-up unconformity near the Aptian/Albian boundary, has its subcrop beneath the Neogene valley fill slightly east of the drill site; hence, no Albian or Cenomanian black shale underlies Site 638.

3. The interval from 184 to 212 m consists of upper Barremian claystone, marlstone, and limestone, assigned to lithologic Subunit IIA (Table 2, this chapter), which is separated from the underlying Subunit IIB by an unconformity. This unconformity is associated with one of the weak reflectors above R3, within the wedge of syn-rift sediments that thickens eastward into the half graben (Fig. 40).

4. Before drilling at Site 638, we had thought that reflector R3 marked the top of the Jurassic/Lower Cretaceous carbonate platform. One of the most important findings of the drilling is that R3 is instead a reflector within the Lower Cretaceous clastic syn-rift sequence.

R3 is visible both on the GP-101 (Figs. 38B and 40) and on the *JOIDES Resolution* seismic lines (Fig. 38A). At the position corresponding to Hole 638B, the reflector is at 315–320 ms bsf on both lines, i.e., at about 300 mbsf on the synthetic seismogram. Within the syn-rift sequence drilled at Site 638, there is one major change in lithology at 298 mbsf, between turbidite sandstone of lithologic Unit III and the overlying claystone and marlstone of Unit II. On the synthetic seismogram, a large spike in seismic amplitude at 298 mbsf (315 ms) (Fig. 39) corresponds to the highest sample of high-velocity sandstone of Unit III within a series of samples of alternating lower velocity claystone and high-velocity sandstone. Thus, all data are coherent, and we conclude that reflector R3 marks the boundary between lithological Units II and III (Fig. 40).

Close study of the seismic records shows that the stratigraphy within the syn-rift sequence is highly complex and includes many lenses and local unconformities. Reflector R3 is clear at the position of Hole 638, but as it is traced eastward on line GP-101, continuity is uncertain, owing to a divergent pattern of reflectors that branch away from R3. R3 has the appearance of an unconformity on line GP-101; reflectors near the base of the overlying wedge overlap R3; R3, in turn, seems to truncate reflectors of the underlying sequence.

5. The deepest reflector R4, at about 530 ms below the seafloor at Site 638, is very strong and implies a large impedance contrast. Because shallow-water limestone was dredged from the west-facing escarpment where this strong reflector crops out, about 6 km north of Site 638 (see "Background and Objectives," this chapter), we thought after drilling Site 638 that this reflector marks the top of Mesozoic carbonate-platform rocks; this was confirmed by drilling at Site 639 (see Site 639 chapter, this volume). If we use an average (weighted) velocity of 3.4 km/s, from the combined log and lab data (Table 10), for the interval from 298 m to the total depth of 547 mbsf and simply extrapolate to the reflector R4 at 530 ms, which is the reflector marking the top of the carbonate platform, we obtain a depth of 667 mbsf.

We can improve this estimate by using data from Hole 639A. The highest strata in the Mesozoic in Hole 639A (see Site 639

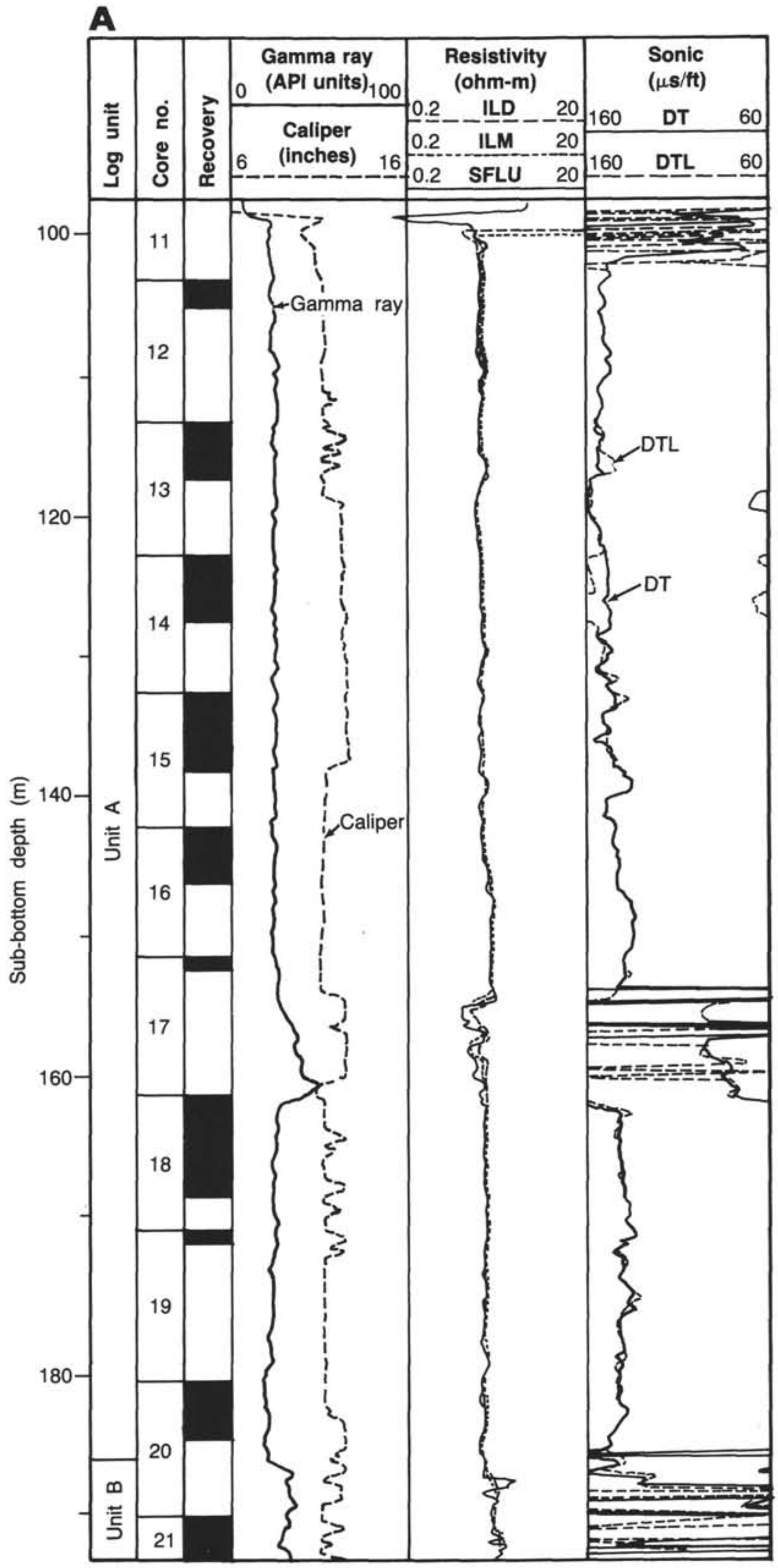

Figure 33. A. Composite log and core recovery in log-lithologic Unit A (Hole 638B). See text for description of logs. B. Composite log in log-lithologic Unit A (Hole 638C). See text for description of logs.

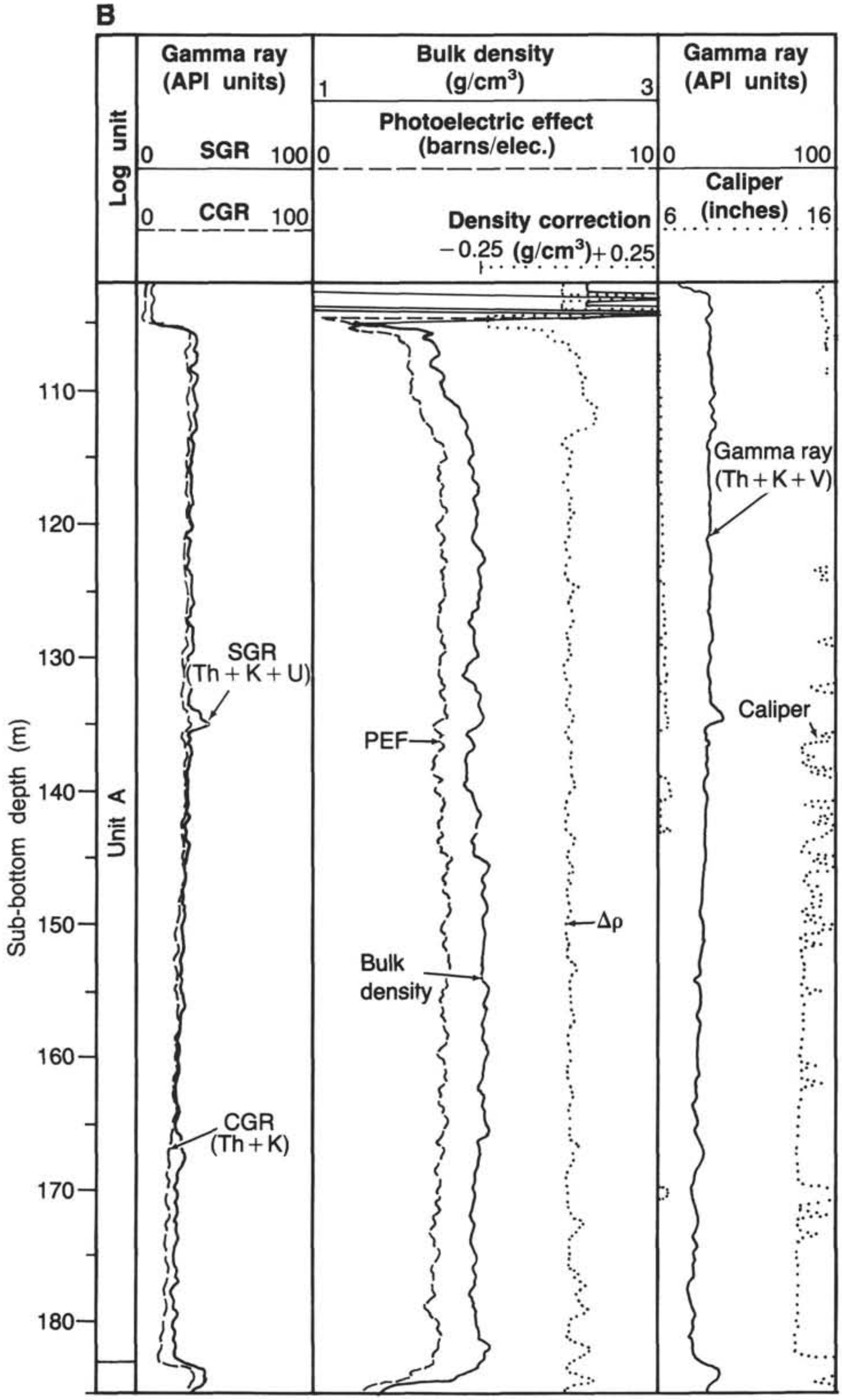

Figure 33 (continued).

chapter, this volume) are beds of Valanginian sandstone, similar to those near the bottom of Hole 638C but underlain by some 30-40 m of marl and marlstone having a velocity of only about 2.0 km/s and lying directly on the carbonate platform rocks. Taking into account these strata and the seismic velocities, we estimate the thickness at Site 638 of Cretaceous strata between 298 m and the top of the carbonate platform to be as follows: (1) Hauterivian-Valanginian sandstone turbidites (lithologic Unit III) are 300 m thick (based on an assumed velocity of 3.43 km/s and a seismic thickness of 175 ms), and (2) Valanginian marl and marlstone are 40 m thick (based on an assumed seismic velocity of 2.0 km/s and a seismic thickness of 40 ms).

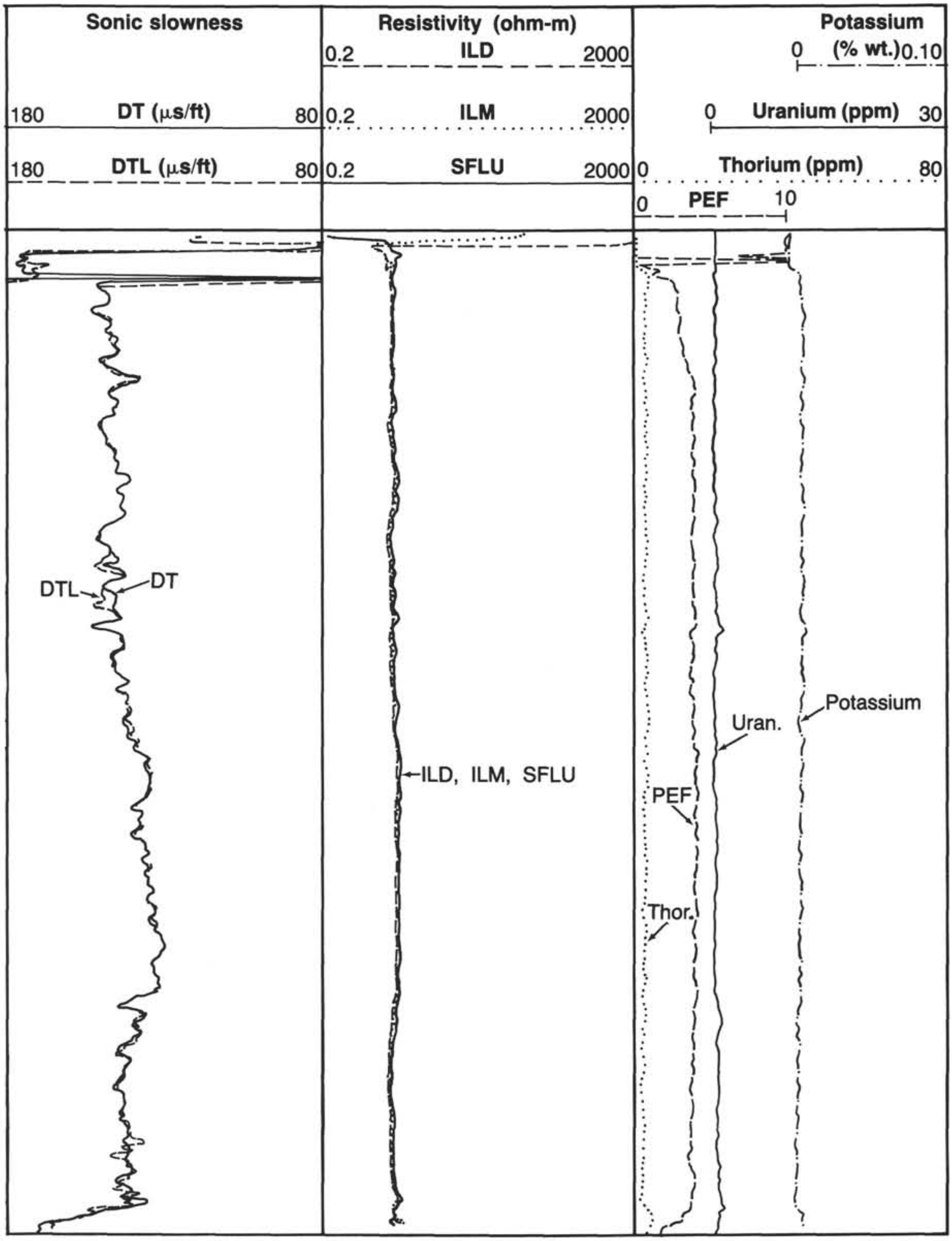

Figure 33 (continued).

The estimated depth at Site 638 to the top of the carbonate platform is thus 638 m, or about 91 m below the total depth reached. This estimate implies that about 50 m of turbidite sandstone lies between the bottom of Hole 638C and the top of Hole 639A.

SUMMARY AND CONCLUSIONS

Site 638 is about midway across a tilted fault block that is typical of the succession of such blocks forming a staircase descending the outer part of west Galicia margin. Such tilted blocks are common and even characteristic of many passive margins. To understand their origin and history has been one of the major aims of scientific ocean drilling since the inception of the JOIDES program nearly two decades ago. The site was chosen because exploration of the entire pre-rift sequence there appeared possible, albeit time consuming. The JOIDES Planning Committee, therefore, allotted about 5 to 6 weeks for completion of the drilling and logging at the site. The scientific staff included many specialists in carbonate petrology and in micropaleontology of Lower Cretaceous and Jurassic strata. Site 638 drilling was to be a major undertaking.

The particular goal of drilling at Site 638 was to core through the Cretaceous syn-rift sediments that we believed formed a relatively thin cover over a pre-rift shallow-water carbonate platform and then to continue on through the platform rocks into crystalline basement rock. The drilling plan was based on the conventional model of the seismic stratigraphy of the Galicia margin. We thought that the strong reflector R4 (Fig. 40), which forms acoustic basement, was the top of the Hercynian basement complex known at outcrop on the Iberian mainland and from a dredge haul only a few kilometers north of Site 638 (Mougenot et al., 1985). The conspicuous reflector R3, about 0.3 s above acoustic basement, we identified as being the top of the carbonate platform. We expected the presence of, above the carbonate platform, only a thin wedge of syn-rift sediments, covered by Neogene sediments in the submarine valley in which the site is located. We estimated the thickness of sediments above basement to be about 1000 to 1200 m.

Although we did not reach the basement at this site, we were rewarded by finding a stratigraphic succession different from the one predicted. The interval between acoustic basement and the conspicuous reflector 0.3 s above it is occupied not by platform carbonates but by syn-rift strata, comprising sandstone turbidites, mainly of Valanginian age, overlain by Hauterivian and Barremian marlstone and claystone. We estimate the thickness of syn-rift sediments at the drill site to be about 500 m, but the thickness increases to several times this value only a few kilometers farther east, in the half graben (Fig. 41).

The details of the stratigraphic section drilled at Site 638 are shown in Figure 42, and the salient features are described below.

Stratigraphy of the Syn-Rift Cretaceous Rocks at Site 638

The sediments of the syn-rift sequence at Site 638 consist of about 250 m of sandstone turbidites interbedded with claystone and minor marlstone, overlain by about 100 m of alternating marlstone and claystone, much disturbed by slumping and creep structures. The sandstone is mainly Valanginian, and the overlying claystone and marlstone is Hauterivian and upper Barremian. The graded sandstone beds typically begin with massive, Bouma T_a lithology at the base, and few beds include the ripple cross-lamination of Bouma T_c. Granules occur at the base of some beds, especially in the lowest part of the sequence cored, and even a few small pebbles occur in one bed. Redeposited plant debris from the land is ubiquitous and forms almost lignitic concentrations at a few places. The claystone beds contain about 1% organic carbon, the marlstone beds about 0.6%, and the sandstone layers about 0.1%.

Clearly, we are dealing here with relatively proximal turbidites, as confirmed by inspection of the seismic-profiler records, which show a confused pattern of lenticular units and local unconformities, caused perhaps by deposition of the turbidites in lobes or channels. The relatively poor recovery rate for cores in the sandstone unit precludes our identifying upward-fining or -coarsening sequences; on the other hand, the proportion of claystone and marlstone beds shows a broad tendency to increase upward, and the upper 20 m of sandstone are gradational into the overlying claystone and marlstone unit. No reliable *in-situ* indicators of the environments of deposition are present in the microfaunal and nannofloral assemblages since most of the microfossils are probably resedimented. Yet, a whole range of depth environments, from neritic to infrabathyal is represented in the transported foraminiferal assemblages, along with ammonite aptychi, denoting depths below the dissolution levels for aragonite. Modern marine turbidites generally do not accumulate in depths of less than 500–1000 m, and the coarse texture of the sandstone turbidites at Hole 638C imply high-energy currents, requiring substantial submarine relief for steep canyons to funnel the sands toward the basins.

The contact with the overlying unit, which is at about 300 mbsf, is marked by a prominent seismic reflector about 315 ms below the seafloor, according to the synthetic seismogram constructed by combining laboratory and logging data on sound velocity and density (Fig. 39); indeed a prominent reflector appears in that position on the seismic profile recorded from *JOIDES Resolution* across the site (Fig. 38A).

Of what lies below 547 m, we have no completely satisfactory way to estimate the thickness of sediments between the deepest level reached in Hole 638C and the top of the prominent seismic reflector that marks the top of the shallow-water carbonate rocks sampled at Site 639. We estimate, from logs and laboratory data, the sound velocity of any turbidite sandstone/claystone lithology in this interval to be about 3.4 km/s. We also have laboratory data from the 40 m of lower Valanginian marlstone just above the carbonate rocks drilled at Hole 639A (see Site 639 chapter, this volume) that show velocities of about 2 km/s. Using these interval velocities, we estimate a thickness of about 90 m left to drill below the bottom of Hole 638C to reach the carbonate platform. Of this amount, some 40 m were penetrated and sampled at Hole 639A, leaving about 50 m of unsampled sandstone below the total depth of Hole 638C.

Above the turbidite sandstone, an interval about 190 m thick of claystone and marlstone begins in the upper Valanginian or lower Hauterivian and extends to the upper Barremian; an unconformity omits the lower Barremian. The claystone and marlstone alternate at scales of a few centimeters to a meter or so. The claystone probably largely represents distal turbidites, and indeed some layers have a silty base and show grading. Small bits of terrestrial plant debris are common in some layers, and the average content of organic carbon is about 0.4%. The marlstone occurs both as the upper member of claystone/marlstone couplets, where it probably represents the finest material in turbidity currents of turbid flows, and as separate layers, commonly more bioturbated than the claystone. Both marlstone and claystone commonly show microslumping structures, and larger slump masses occur, some measuring several meters thick. The thickest of these is just beneath the Hauterivian–upper Barremian unconformity. The upper Barremian interval, which is only about 30 m thick, is different from the beds below because it includes interbeds of bioturbated clayey limestone between the intervals of claystone/marlstone couplets.

The organic matter in the Cretaceous rocks at Site 638 is mostly composed of terrigenous Type III kerogen, according to analyses using the Rock-Eval, and is highly oxidized and detrital. The organic matter has not had enough thermal intensity to bring it near maturity.

Interstitial waters from the Cretaceous at Site 638 show a downward increase in calcium, suggesting calcium dissolution at depth, and a concomitant decrease in magnesium, perhaps owing to formation of diagenetic clay. A marked increase in salinity occurs in one sample of Hauterivian claystone, possibly resulting from lateral advection of seawater along a permeable (slumped?) layer of an outcrop at the seafloor.

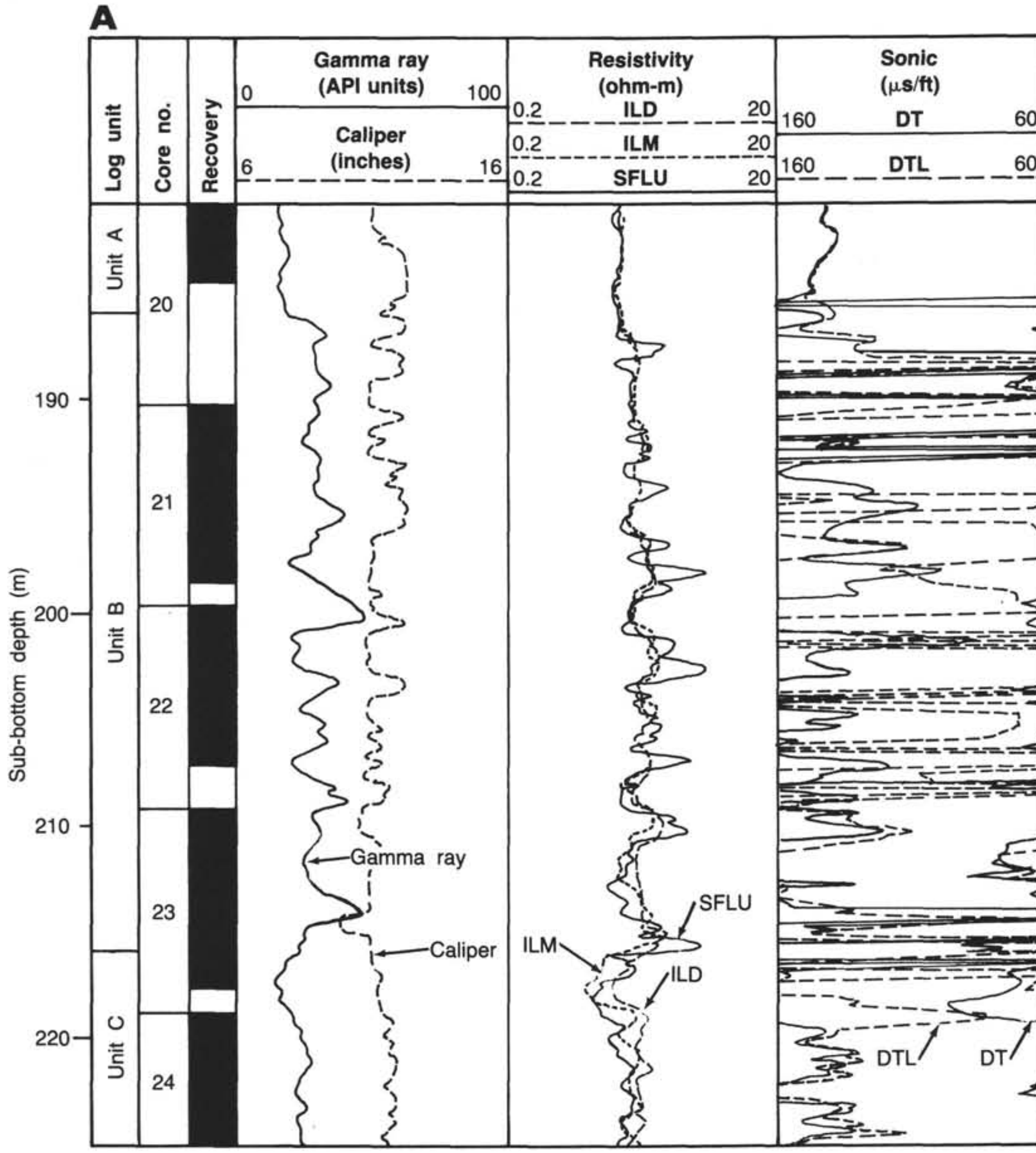

Figure 34. A. Composite log and core recovery in log-lithologic Unit B (Hole 638B). See text for description of logs. B. Composite log in log-lithologic Unit B (Hole 638C). See text for description of logs.

Neogene Valley Fill

As seen on the seismic profiles (Figs. 38A and 38B) and on the location map (Fig. 4), Site 638 is on the floor of a valley that runs parallel to and east of the submarine cuesta formed by the resistant carbonate beds at the western edge of the tilted fault block. The valley heads on the southwest edge of Galicia Bank, some 40 km to the north, and after crossing Site 638 turns southwest across the broad, gentle turbidite slope that leads down to the Iberian Abyssal Plain. Site 638 is slightly east of the present-day thalweg of the valley (Fig. 4) but is nearly over the deepest part of the now back-filled erosional valley defined by the angular unconformity between the Neogene and the underlying Cretaceous strata (Fig. 38). As shown on the seismic profile, the valley was first carved deeply into the Cretaceous strata, perhaps migrating eastward down a bedding surface in the Cretaceous sequence, most likely along the limestone beds in the upper Barremian.

Deposition in the valley began during the late Miocene and has mainly been by pelagic processes or by gentle traction currents, rather than by turbidity currents. No clearly graded beds were seen in the cores in the Neogene, although reworked older fossils are present at many levels. In one interval, about 152 mbsf, pebbles of Cretaceous black shale suggest a possible debris flow interstratified in the sequence, but the pebbles may be cavings from the seafloor. The lowest part of the Neogene section is white nannofossil chalk, having a calcium carbonate content of about 90%; this passes gradually upward into nannofossil ooze, whereas the calcium carbonate values decrease to only about 70% in the uppermost part of the sequence. In several cores, generally badly disturbed Pleistocene brownish ooze and a few pebbles occur, leading us to suspect cavings. Since the topmost core material recovered at the site is lower Pleistocene gray ooze, we further suspect that a few meters of even younger brownish ooze lies just beneath the seafloor but was not sampled. That the depth to the seafloor and to the skirt of the reen-

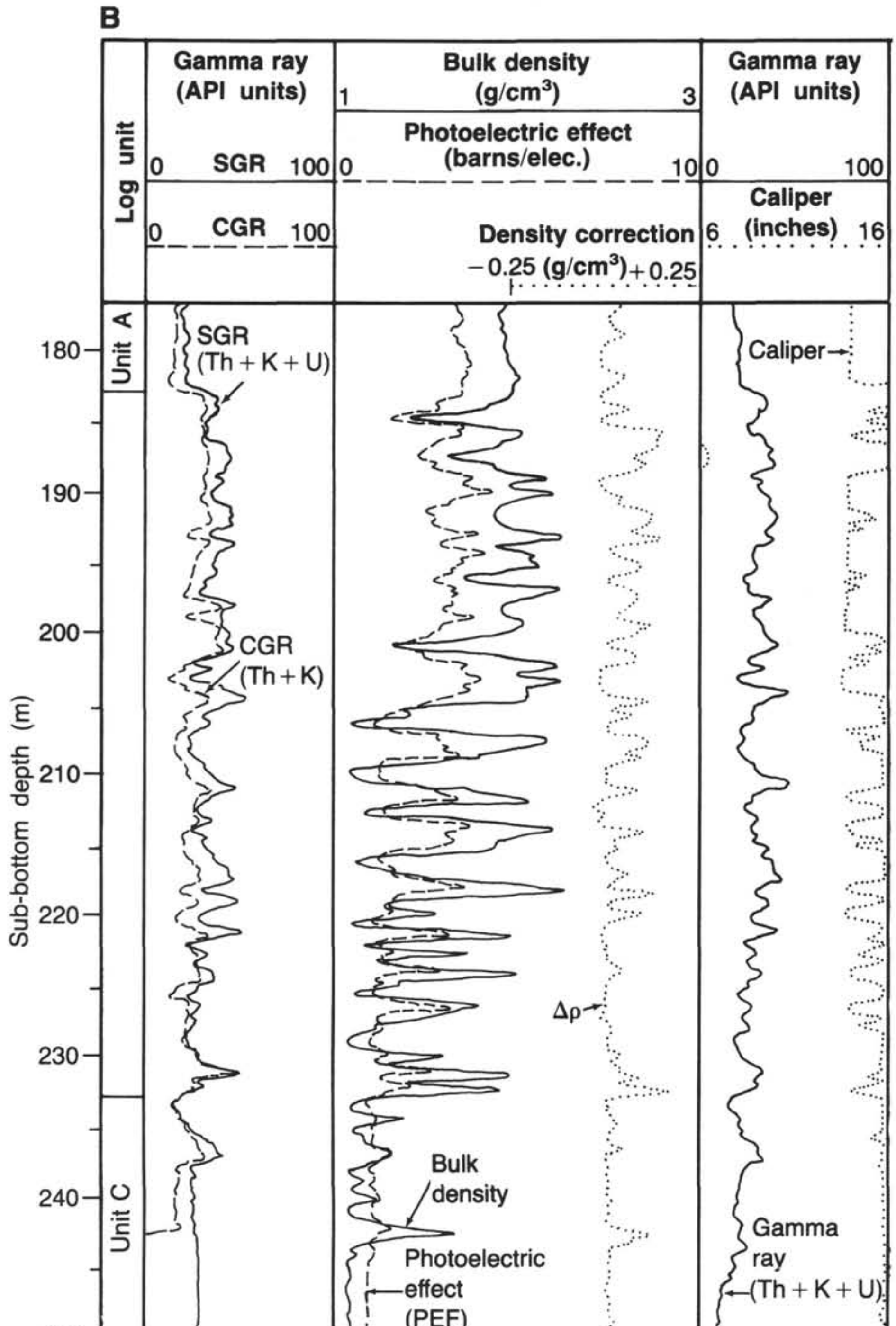

Figure 34 (continued).

try cone seen by the sonar search tool used during reentry at Hole 638C was several meters shallower than the depth at which we took the first core strengthens this possibility.

Regional Implications of the Cretaceous Syn-rift Strata at Site 638

The discovery of syn-rift rather than pre-rift strata between the two reflectors R3 and R4 (Fig. 38) has important implications for interpretations of seismic profiles elsewhere in the region. The general scheme previously accepted by most workers for correlating seismic profiles and physical stratigraphy is now shown to be incorrect on a fundamental point, and a reinterpretation of the stratigraphy beneath the regional break-up unconformity is necessary.

Two examples illustrate the reinterpretation required. At DSDP Site 398, about 90 km southeast of Site 638, the seismic profiles have generally been interpreted (Bouguigny and Willm, 1979; Groupe Galice, 1979; Sibuet and Ryan, 1979) as showing that the reflector identified as "acoustic basement" is the base of the syn-rift sequence, which from the drilling results at Site 398 would be somewhere in the Hauterivian. As pointed out by Sibuet and Ryan (1979), strata beneath this "acoustic basement"

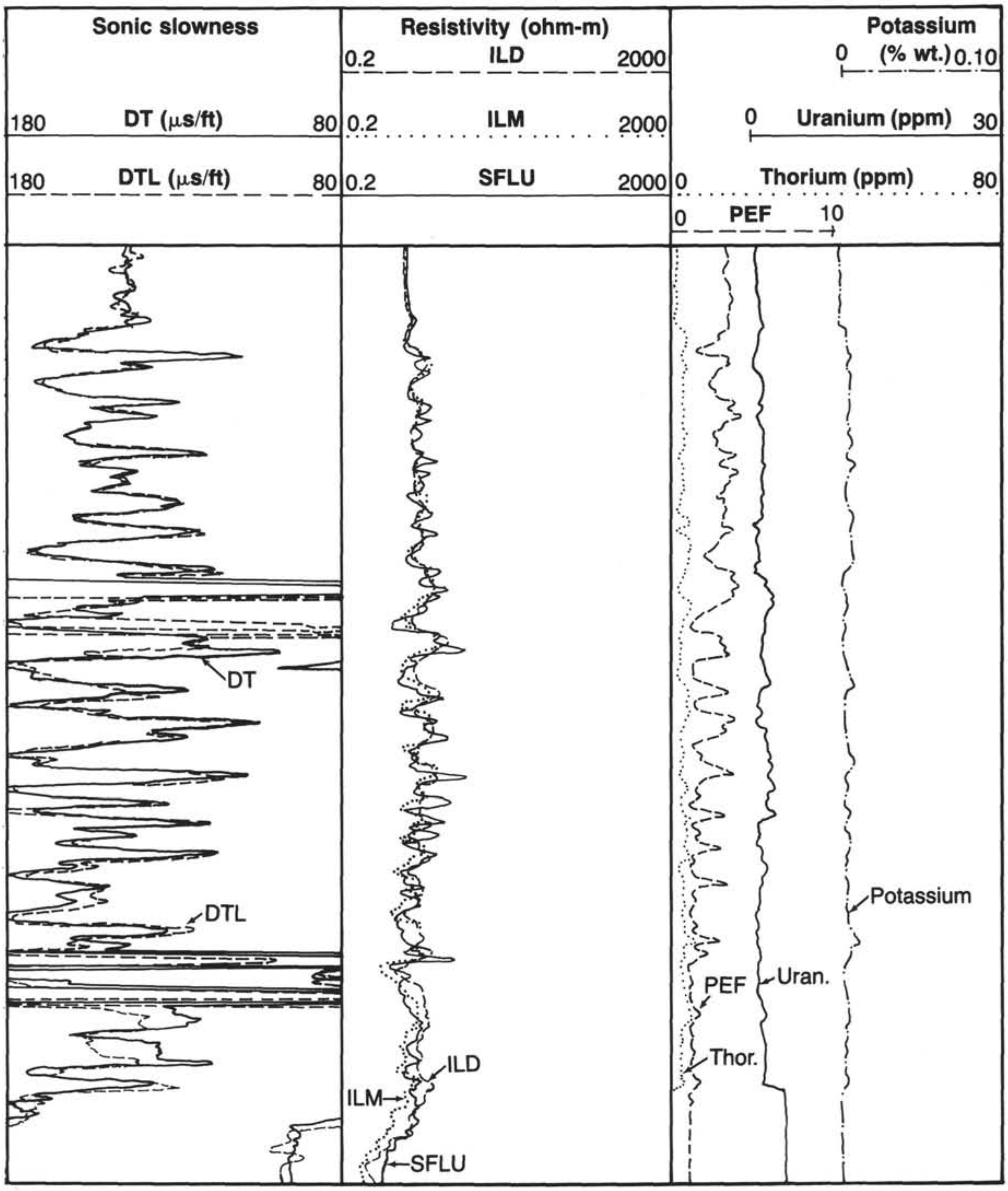

Figure 34 (continued).

are clearly sedimentary near Site 398 and, on the basis of drilling results at Site 638, we think also include important thicknesses of pre-Hauterivian syn-rift sediments. The second example is more remote, on the Armorican margin facing the Bay of Biscay. A typical seismic profile across a tilted fault block deep in that margin is shown by Montadert et al. (1979) (Fig. 43). The base of seismic formation 3, basal Albian in age, is identified as the break-up unconformity, and only formation 4 is regarded as syn-rift; the next underlying "acoustic basement" formation is recognized as sedimentary by Montadert et al. (1979), but assigned to pre-rift, Jurassic time. The similarity in geometry and reflection character between the "acoustic basement" formation on the Biscay margin and the Lower Cretaceous syn-rift sequence in the half graben drilled at Site 638 suggests that they may be correlatives.

Beyond the major recalibration of seismic profiles is the more fundamental question of the timing of rifting on Galicia Bank. The results from Site 638 clearly demonstrate that rifting began at least as long ago as early as the Valanginian, about 25 m.y. before the onset of seafloor spreading at the end of the Aptian. This early inception of rifting predates by nearly 15 m.y. the reported beginning of rifting on the Armorican margin, even

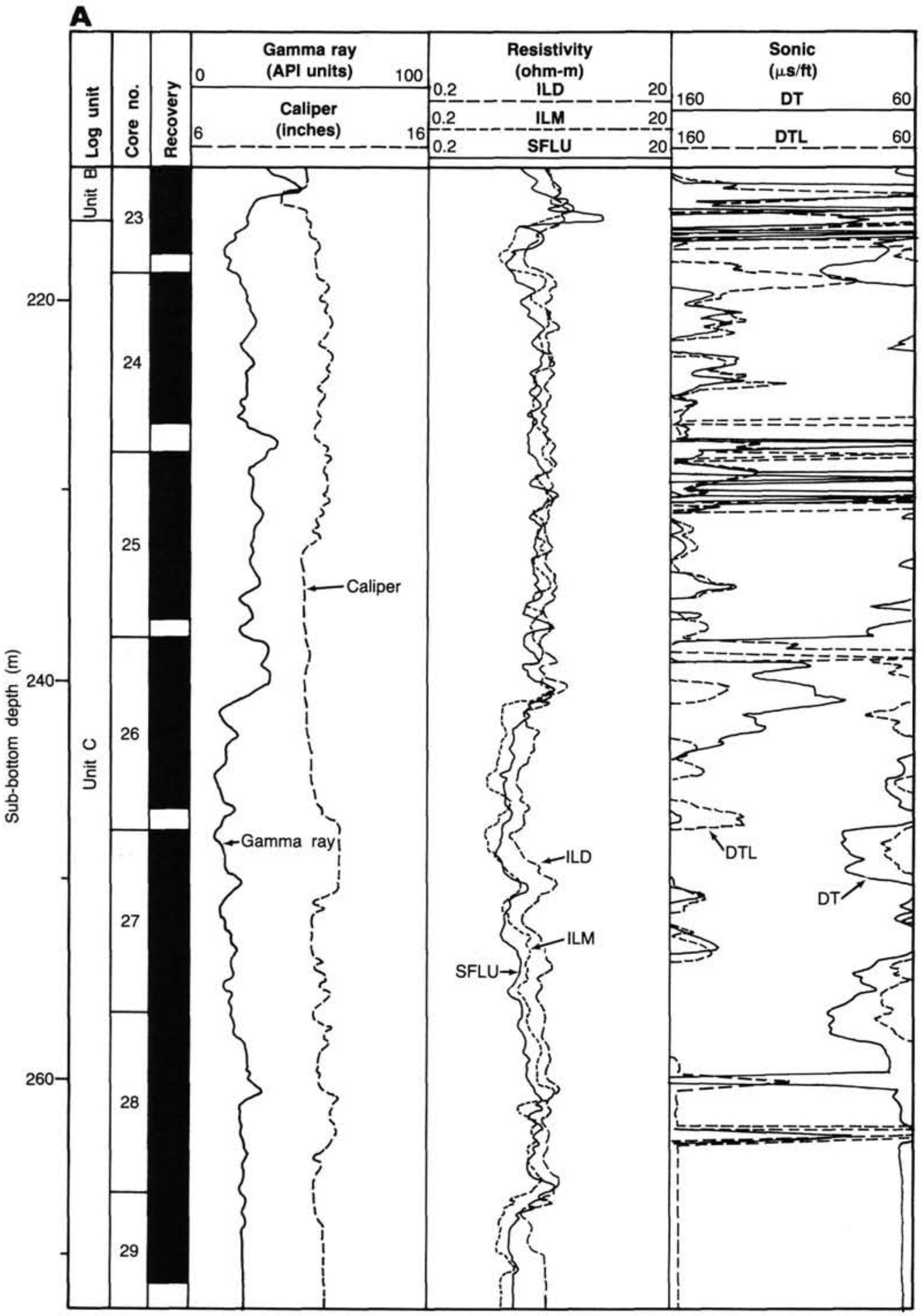

Figure 35. A. Composite log and core recovery in log-lithologic Unit C (Hole 638B). See text for description of logs. B. Composite log in log-lithologic Unit C (Hole 638C). See text for description of logs.

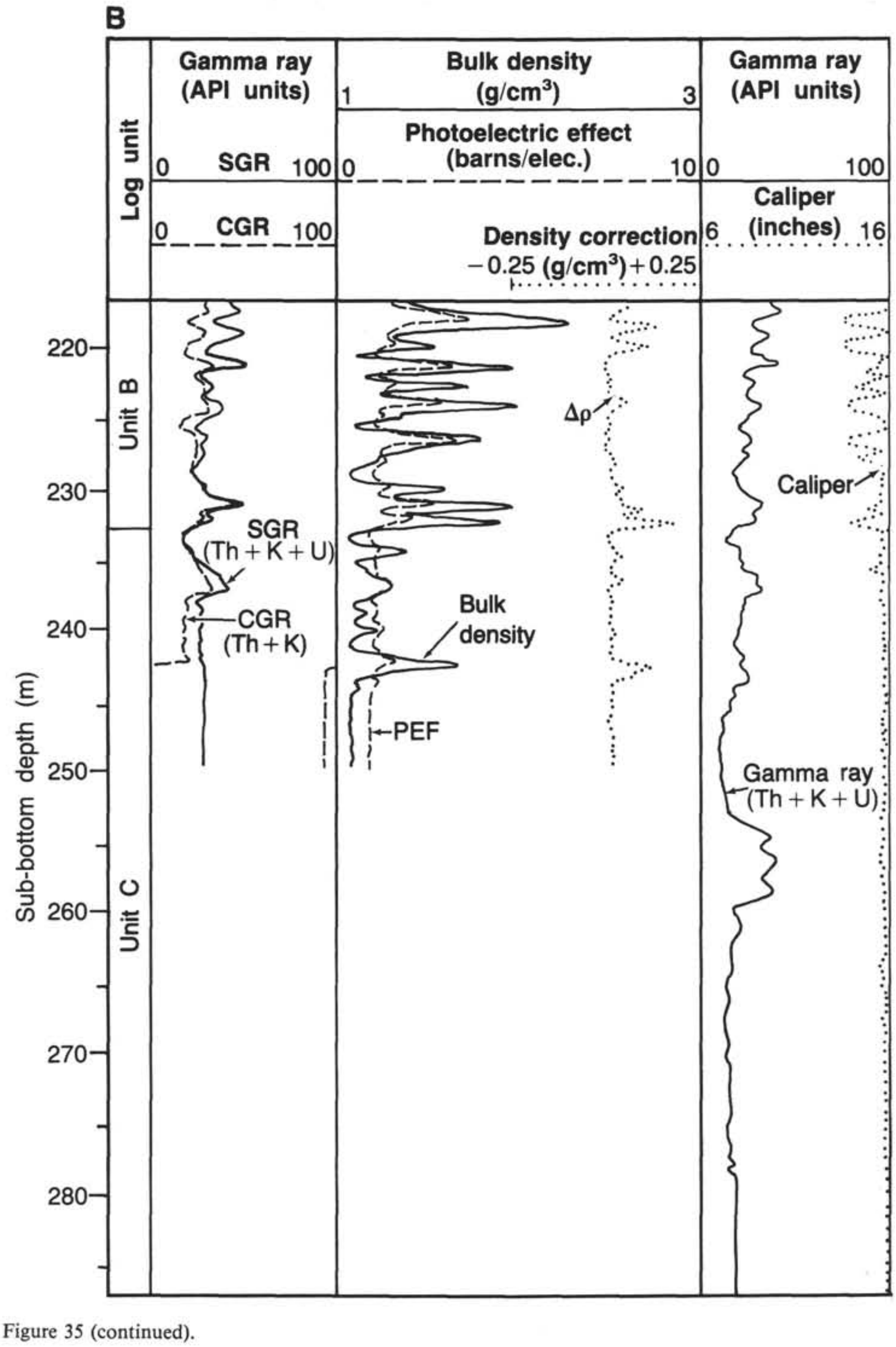

Figure 35 (continued).

though the break-up unconformity lies between lowest Albian and upper Aptian beds on both the Galicia and Amorican margins (Sibuet, Ryan, et al., 1979; de Graciansky, Poag, et al., 1985). As suggested in the foregoing discussion on recalibration of seismic formations on the Armorican margin, our correlations suggest that rifting began on the Biscay margin studied by Montadert et al. (1979) much earlier in the Cretaceous than formerly believed.

The time during which the syn-rift sediments accumulated on the Galicia margin corresponds roughly to the emplacement time of the vast clastic deposits collectively lumped under the term "Wealdan," after the formation in the south of England. Wealden deltas were built out onto the continental margin at many places on both sides of central and North Atlantic (Castelain, 1965; Jansa and Wade, 1975; von Rad and Arthur, 1979; von Rad and Sarti, in press), and thick turbidites accumulated in deep water on both sides of central North Atlantic, off Morocco (Lancelot and Winterer, 1980), and off New Jersey (Sarti and von Rad, in press). The plate-tectonic events that led to rifting on the margins of Galicia and its conjugate, Newfoundland, were felt widely, both on the Afro-Iberian plate (these had been joined since sometime in the Late Jurassic), and on the North American plate. The great influx of clastic sediment, revealed mostly by the textural and mineralogical immaturity of the sand-

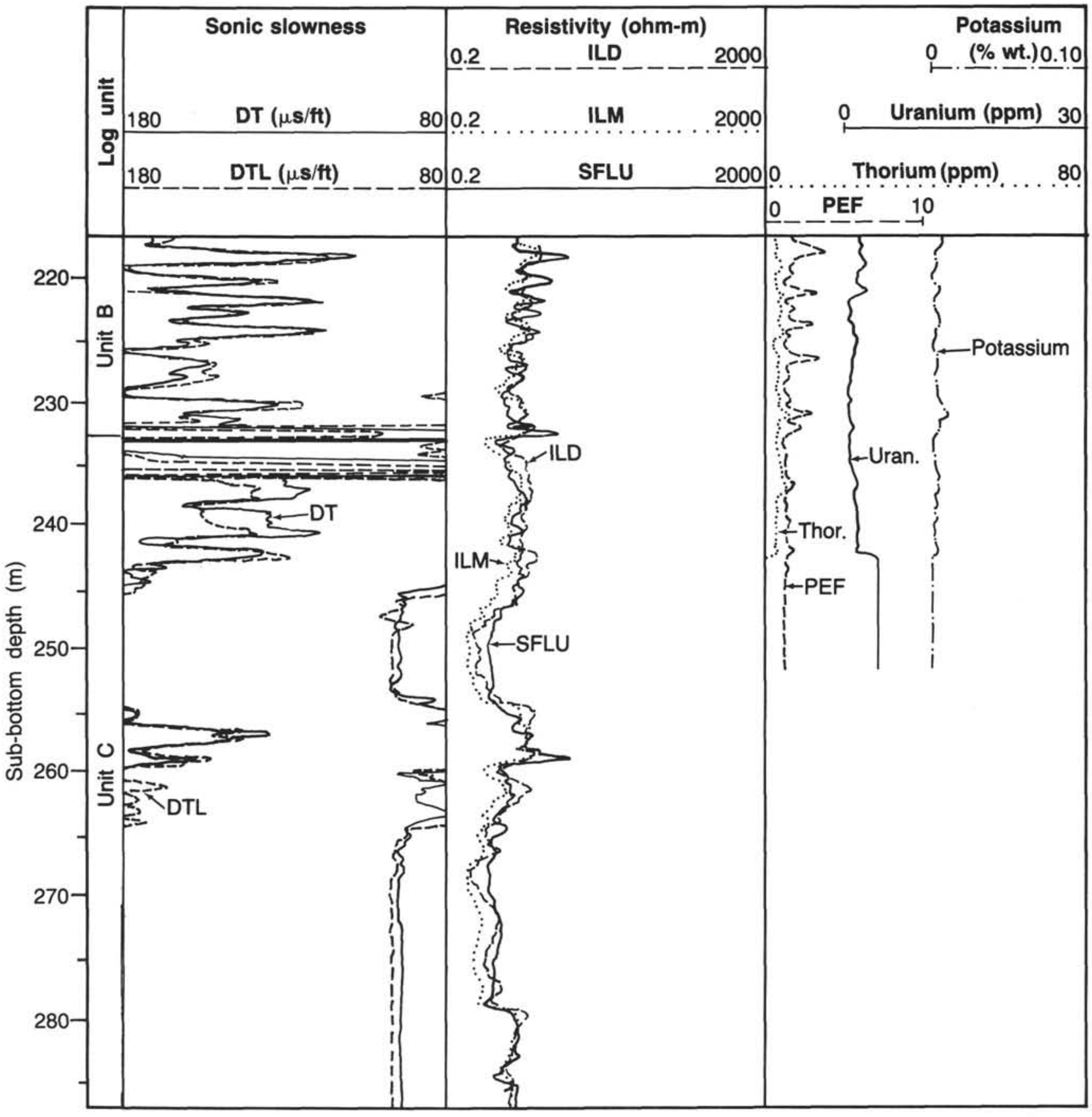

Figure 35 (continued).

stone characteristics of first-cycle derivation from crystalline basement, implies uplift of crystalline basement rocks on the land, perhaps accompanied by climatic changes that resulted in higher sediment loads in streams feeding the North Atlantic.

REFERENCES

Anderton, R., Bridges, P. H., Leeder, M. R., and Sellwood, B. H., 1979. *A Dynamic Stratigraphy of the British Isles: A Study in Crustal Evolution*: London (George Allen and Unwin).

Bartenstein, H., and Bettenstaedt, F., 1962. Marine Unterkreide (Boreal und Tethys). *Leitfossilien der Mikropalaeontologie*, 7:225–297.

Basov, V. A., Gramberg, I. S., Danjushevskaya, A. I., Kaban'kov, V. Y., Lazurkin, V. M., and Patrunov, D. K., 1979. Lower Cretaceous lithostratigraphy near Galicia Bank. *In* Sibuet, J. C., Ryan, W. B. F., et al., *Init. Repts. DSDP*, 47, Pt. 2: Washington (U.S. Govt. Printing Office), 638–717.

Baumgartner, P. O., 1984. A middle Jurassic–Early Cretaceous low-latitude radiolarian zonation based on unitary associations and age of Tethyan radiolarites. *Eclogae Geol. Helv.*, 77/3:729–837.

Berggren, W. A., 1977. Late Neogene planktonic foraminiferal biostratigraphy of the Rio Grande Rise (South Atlantic). *Mar. Micropaleontol.*, 2:265–313.

Berggren, W. A., Aubry, M. P., and Hamilton, N., 1983. Neogene magnetobiostratigraphy of Deep Sea Drilling Project Site 516 (Rio Grande Rise, South Atlantic). *In* Barker, P. F., Carlson, R. L., Johnson, D. A., et al., *Init. Repts. DSDP*, 72: Washington (U.S. Govt. Printing Office), 675–713.

Berggren, W. A., Kent, D. V., and Van Couvering, J. A., in press. Neogene geochronology and chronostratigraphy. *In* Snelling, N. J. (Ed.), *Geochronology and the Geologic Record. Geol. Soc. of London Spec. Pap.*

Blow, W. H., 1969. Late Middle Eocene to Recent planktonic foraminiferal biostratigraphy. *In* Broenniman, P., and Renz, H. H. (Eds.), *Proc. First Int. Conf. Plankt. Microfossils*: Leiden (E. J. Brill), 1: 199-422.

Bouguigny, R., and Willm, C., 1979. Tentative calibration of Site 398 and special processing of parts of lines GP-19 and GP-23. *In* Sibuet, J. C., Ryan, W. B. F., et al., *Init. Repts. DSDP*, 47B: Washington (U.S. Govt. Printing Office), 623-630.

Bryant, W. R., Bennett, R. H., and Katherman, C. E., 1981. Shear strength, consolidation, porosity, and permeability of oceanic sediments. *In* Emiliani, C., (Ed.), *The Sea*. New York (John Wiley), 7: 1555-1616.

Carlson, R. L., and Christensen, N. I., 1983. Velocity anisotropy and physical properties of deep-sea sediments from the western South Atlantic, *In* Barker, P. F., Carlson, R. L., Johnson, D. A., et al., *Init. Repts. DSDP*, 72: Washington (U.S. Govt. Printing Office), 555-559.

Castelain, J., 1965. Aperçu stratigraphique et micropaléontologique du bassin du Senegal. Historique de la découverte paléontologique. *Bur. Rech. Geol. Min., Mem.*, 32:135-159.

Dapples, E. C., 1962. Stages of diagenesis in the development of sandstones. *Geol. Soc. Am. Bull.*, 73:913-933.

de Graciansky, P. C., Poag, C. W., et al., 1985. *Init. Repts. DSDP*, 80: Washington (U.S. Govt. Printing Office).

Emery, K. O., and Uchupi, E., 1984. *The Geology of the Atlantic Ocean:* New York (Springer-Verlag).

Espitalie, J., Madec, M., and Tissot, B., 1977. Source rock characterization method for petroleum exploration. *Ninth Annual Offshore Technology Conference Proceedings*, 399-404.

Gieskes, J. M., and Peretsman, G., 1986. *Water-Chemistry Procedures Aboard the JOIDES Resolution—Some Comments, ODP, Technical Note No. 5.*

Groupe Galice, 1979. The continental margin off Galicia and Portugal: acoustical stratigraphy, dredge stratigraphy, and structural evolution. *In* Sibuet, J. C., and Ryan, W. B. F., et al., *Init. Repts. DSDP*, 47 (Pt. 2): Washington (U.S. Govt. Printing Office), 633-662.

Guerin, S., 1981. Utilisation des formaniféres planctontiques et benthiques dans l'étude des paléoenvironnements océaniques au Crétacé moyen: application au material des forages D.S.D.P. de l'Atlantique Nord et Sud. Comparaison avec la Techys [Thesis]. Univ. of Nice, *Trav. Cent. Rech. Micropaleont. Jean Cuvillier*, 2.

Hamilton, E. L., 1974. Prediction of deep-sea sediment properties: state of the art. *In* Inderbitzen, A. L., (Ed.), *Deep-Sea Sediments: Physical and Mechanical Properties.* New York (Plenum), 1-43.

________, 1976. Variations of density and porosity with depth in deep-sea sediments. *J. Sed. Pet.*, 46:280-300.

Jansa, L. F., and Wade, J. A., 1975. Geology of the continental margin off Nova Scotia and Newfoundland. *In* van der Linden, W. J. M., and Wade, J. A., (Eds.), Offshore Geology of Eastern Canada: Regional Geology (Pt. 2): *Can. Geol. Surv. Pap.*, 74-30:51-106.

Jansa, L. F., and Wiedmann, J., 1982. Comparison of the northwest African and northeast American margins. *In* von Rad, U., et al. (Eds.), *Geology of the Northwest African Continental Margin:* Berlin (Springer-Verlag), 215-269.

Kirschvink, J. L., 1980. The least-squares line and plane and the analysis of paleomagnetic data. *Geophys. J. R. Astron. Soc.*, 62:699-718.

Lancelot, Y., and Winterer, E. L., et al., 1980. *Init. Repts. DSDP*, 50: Washington (U.S. Govt. Printing Office).

Ma'alouleh, K., and Moullade, M., in press. Biostratigraphic and paleoceanographic study of Neogene and Quaternary planktonic foraminifers from the Lower Continental Rise of the New Jersey margin (western North Atlantic), DSDP Leg 93 Site 603. *Init. Repts. DSDP*, 93: Washington (U.S. Govt. Printing Office).

McIver, R., 1975. Hydrocarbon occurrence from JOIDES Deep Sea Drilling Project. *Proceedings Ninth World Petroleum Congress*, 269-280.

Magniez-Jannin, F., Moullade, M., and Tronchetti, G., 1984. Crétacé inférieur, echelles biostratigraphiques. Foraminifères planctoniques et benthiques de bassin. *In* Debrand-Passard, S. (Ed.), *Synthèseè géologique du Sud-Est de la France. Mém. B.R.G.M.*, 125,1:297: 299.

Montadert, L., de Charpal, O., Roberts, D., Guenoc, P., and Sibuet, J. C., 1979. Northeast Atlantic passive continental margin: rifting and subsidence processes. *In* Talwani, M., Hay, W. W., and Ryan, W. B. F., (Eds.), *Deep Drilling Results in the Atlantic Ocean: Continental Margins and Paleoenvironment, Maurice Ewing Series:* Washington (Am. Geophys. Union), 3:154-186.

Mougenot, D., Capdevila, R., Palain, C., Depeuble, P. A., and Mauffret, A., 1985. Nouvelles données sur les sédiments anté-rift et le socle de la marge continentale de Galice. *Acad. Sci. Paris, C.R.*, 301(II): 323-328.

Moullade, M., 1966. Étude stratigraphique et micropaléontologique du Crétacé inférieur de la "fosse vacotienne." *Doc. Lab. Geol. Fac. Sci.*, Lyon, 15:369.

________, 1974. Zones de Foraminifères du Crétacé inférieur mesogeen. *Acad. Sci., Paris, C. R.*, D, 278:1813-1816.

________, 1979. Les Foraminifères du Valanginien hypostratotypiques. *In* Busnardo, R., Thieuloy, J. P., Moullade, M. (Eds.), *Hypostratotype Mesogeen de l'étage Valanginien*: Les Stratotypes Français, *C. N. R. S.*, 6:110-126.

________, 1983. Upper Neogene and Quaternary planktonic foraminifera from the Blake Outer Ridge and Blake Bahama Basin (western North Atlantic. *In* Sheridan, R. E., Gradstein, E. M., et al., *Init. Repts. DSDP*, 76: Washington (U.S. Govt. Printing Office), 511-535.

________, 1984. Intérêt des petits foraminifères benthique profonds pour le biostratigraphie et l'analyse des paléoenvironnements océaniques mésozoiques. *Benthos '83*: Second International Symposium Benthic Foraminifera, Pau, 429-464.

________, in press. Distribution of Neogene and Quaternary planktonic foraminifers from the upper continental rise of the New Jersey margin (western North Atlantic), DSDP Site 604: biostratigraphical analysis, sedimentary and paleoceanographic implications. *Init. Repts. DSDP*, 93: Washington (U.S. Govt. Printing Office).

Müller, G., and Gastner, M., 1971. The "Karbonaté-Bombe," a simple device for determination of the carbonate content in sediments, soils, and other materials. *Neues Jahrb. Mineral. Monatsh.*, 10:466-469.

Neagu, T., 1972. The Eo-Cretaceous foraminiferal fauna from the area between the Ialomitza and Prahova valleys (eastern Carpathians). *Rev. Esp. de Micropaleont.*, 4, 2:181-224.

________, 1975. Monographie de la faune des Foraminifères eocrétacés du couloir de Dimbovicioara, de Codlea et des monts Persani (Couches de Carhaga). *Institut Géologie Géophysique. Mem.*, 35.

Ogg, J. G., in press. Early Cretaceous magnetic polarity time scale and the magnetostratigraphy of DSDP Sites 603 and 534, western Central Atlantic. *In* Van Hinte, J., Wise, S., et al., *Init. Repts. DSDP*, 93: Washington (U.S. Govt. Printing Office).

Perch-Nielsen, K., 1979. Calcareous nannofossils from the Cretaceous between the North Sea and the Mediterranean. *In* Wiedmann, J. (Ed.), *Aspekte der Kreide Europas:* Int. Union Geol. Sci. Ser. A, 6 Stuttgart (Schweizerbart), 223-272.

________, 1985. Cenozoic calcareous nannofossils. *In* Saunders, J. B., Bolli, H., and Perch-Nielsen, K. (Eds.), *Plankton Stratigraphy.* Cambridge (Cambridge University Press), 427-554.

Roth, P. H., 1983. Jurassic and Lower Cretaceous calcareous nannofossils in the western North Atlantic (Site 534). Biostratigraphy, preservation, and some observations on biogeography and paleoceanography. *In* Sheridan, R. E., Gradstein, F. M., et al., *Init. Repts. DSDP*, 76: Washington (U.S. Govt. Printing Office), 587-621.

Sarti, M., and von Rad, U., in press. Early Cretaceous turbidite sedimentation at DSDP Site 603, off Cape Hatteras (USA) (DSDP/IPOD Leg 93). *In* Van Hinte, J. E., and Wise, S., et al. (Eds.), *Init. Repts. DSDP*, 93: Washington (U.S. Govt. Printing Office).

Schaaf, A., 1984. Les radiolaires du Crétacé inférieur et moyen: biologie, systematique, biochronologie et paléoenvironment [Thèse]. University of Strasbourg.

Sibuet, J. C., and Ryan, W. B. F., 1979. Site 398: evolution of the West Iberian passive continental margin in the framework of the early North Atlantic Ocean. *In* Sibuet, J. C., Ryan, W. B. F., et al., *Init. Repts. DSDP*, 47, Pt. 2: Washington (U.S. Govt. Printing Office), 761-776.

Sibuet, J. C., Ryan, W. B. F., et al., 1979. *Init. Repts. DSDP*, 47, Pt. 2: Washington (U.S. Govt. Printing Office).

Sissingh, W., 1977. Biostratigraphy of Cretaceous calcareous nannoplankton. *Geol. Mijnbouw,* 56:37-65.

Thierstein, H. R., 1971. Tentative Lower Cretaceous calcareous nannoplankton zonation. *Eclog. Geol. Helv.*, 64(3):459-488.

________, 1973. Lower Cretaceous calcareous nannoplankton biostratigraphy. *Abh. Geol. Bundesanst.*, Wien, 29.

———, 1976. Mesozoic calcareous nannoplankton biostratigraphy of marine sediments. *Mar. Micropaleontol.*, 1:325–362.

von Rad, U., and Arthur, M. A., 1979. Geodynamic, sedimentary and volcanic evolution of the Cape Bojador continental margin (NW Africa). *In* Talwani et al. (Eds.), *Deep Drilling Results in the Atlantic Ocean: Continental Margins and Paleoenvironments, Maurice Ewing Series:* Washington (Am. Geophys. Union), 3:187–203.

von Rad, U., and Sarti, M., in press. Early Cretaceous "events" in the evolution of the eastern and western North Atlantic continental margins. *Geol. Rundschau.*

Wind, F. H., and Čepek, P., 1979. Lower Cretaceous calcareous nannoplankton from DSDP Hole 397A (northwest African margin). *In* von Rad, U., Ryan, W. B. F., et al., *Init. Repts. DSDP*, 47, Pt. 1: Washington (U.S. Govt. Printing Office), 221–256.

Wyllie, M. R. J., Gregory, A. R., and Gardner, G. H. E., 1958. An experimental investigation of factors affecting elastic wave velocities in porous media. *Geophys.*, 23:459–493.

Table 7. Minimum/maximum values in log-lithologic units in Hole 638B. GR = gamma ray, ILD = deep induction, SFLU = spherical focused, DT = sonic slowness.

Log unit	Unit A	Unit B	Unit C
Depth (mbsf)	99–186	186–216	216–271
GR (API units)	20/45	20/47	10/34
ILD (ohmm)	1.1/1.3	1.5/3	1/2.1
SFLU (ohmm)	1/1.3	1.1/6	0.7/2
DT (μs/ft)	145/185	cycle skipping	cycle skipping

Table 8. Minimum/maximum values in log-lithologic units in Hole 638C. GR = gamma ray, DT = sonic slowness, ILD = deep induction log, SFLU = spherical focused log, RHOB = bulk density, PEF = photoelectric effect, POTA = potassium content, URAN = uranium content, THOR, = thorium content, NPHI = neutron porosity.

Log unit	Unit A	Unit B	Unit C
Depth (mbsf)	105–183	183–233	233–286
GR (API units)	20/41	20/52	7/38
DT (μs/ft)	132/155	90/180	112/195
ILD (ohmm)	1.1/1.5	1.1/4.1	0.4/2.5
SFLU (ohmm)	1.2/1.5	0.9/7	0.6/7
RHOB (g/cm^3)	1.7/2.0	1.05/2.3	1.05/1.65
PEF (barns/elect.)	3.5/4	1/4.2	1/1.5
POTA (% wt)	0.003/0.01	0.003/0.012	0.002/0.012
URAN (ppm)	0/1	0/2.3	0/1
THOR (ppm)	1/2	1/4	1/4
NPHI (%)	42/54	28/75	62/75

Table 9. Preliminary correlation between log-lithologic and lithologic units in Hole 638B.

Log unit	Lithologic unit	Cores	Lithology
Unit A	Unit I	103-638B-11R to 103-638B-20R	Nannofossil ooze
Unit B	Subunit IIA	103-638B-20R to 103-638B-23	Bioturbated limestone and marl; clay and marl couplets
Unit C	Subunit IIB	103-638B-23R to 103-638B-29R	Bioturbated nannofossil marl

Table 10. Average velocity and density values calculated in intervals determined by log analysis and using uncorrected laboratory data (see text). The values shown correspond to the interval below each depth.

Depth (mbsf)	Density (g/cm^3)	Velocity (km/s)
0	1.57	1.24
12	1.67	1.22
18	1.64	1.32
27	1.74	1.28
58	1.74	1.77
71	1.74	1.62
86	1.80	1.45
95	1.90	1.62
104	1.80	1.72
105	1.75	1.99
111	1.90	2.12
116	1.95	2.06
130	1.90	2.07
140	1.93	2.18
145	2.00	2.22
165	1.93	2.10
184	1.45	1.79
185	2.05	2.77
187	1.70	1.79
189	2.20	2.26
191	1.90	1.91
193	2.20	2.54
194	2.10	1.97
197	2.00	2.34
202	2.20	2.65
211	2.00	1.67
221	1.95	1.74
224	2.00	1.68
226	1.80	1.75
230	1.90	1.76
242	1.60	1.66
253	1.93	1.72
265	2.00	1.61
280	1.91	1.67
283	2.21	2.05
297	1.96	1.68
298	2.61	3.52
308	2.01	1.69
318	2.65	3.68
344	2.76	4.01
354	2.59	3.31
364	2.67	4.05
374	2.46	2.63
384	2.69	4.49
385	2.66	4.54
393	2.71	4.70
405	2.71	4.39
412	2.78	4.20
414	2.64	4.24
433	2.68	4.05
441	2.57	3.27
444	2.59	3.62
451	2.63	4.76
453	2.69	4.47
461	2.83	4.56
475	2.50	3.72
481	2.41	2.49
483	2.68	3.82
490	2.67	4.46
491	2.45	2.25
500	2.18	1.78
519	2.17	1.84
528	2.21	1.97
538	2.05	1.68
539	2.85	4.35
540	2.16	1.94

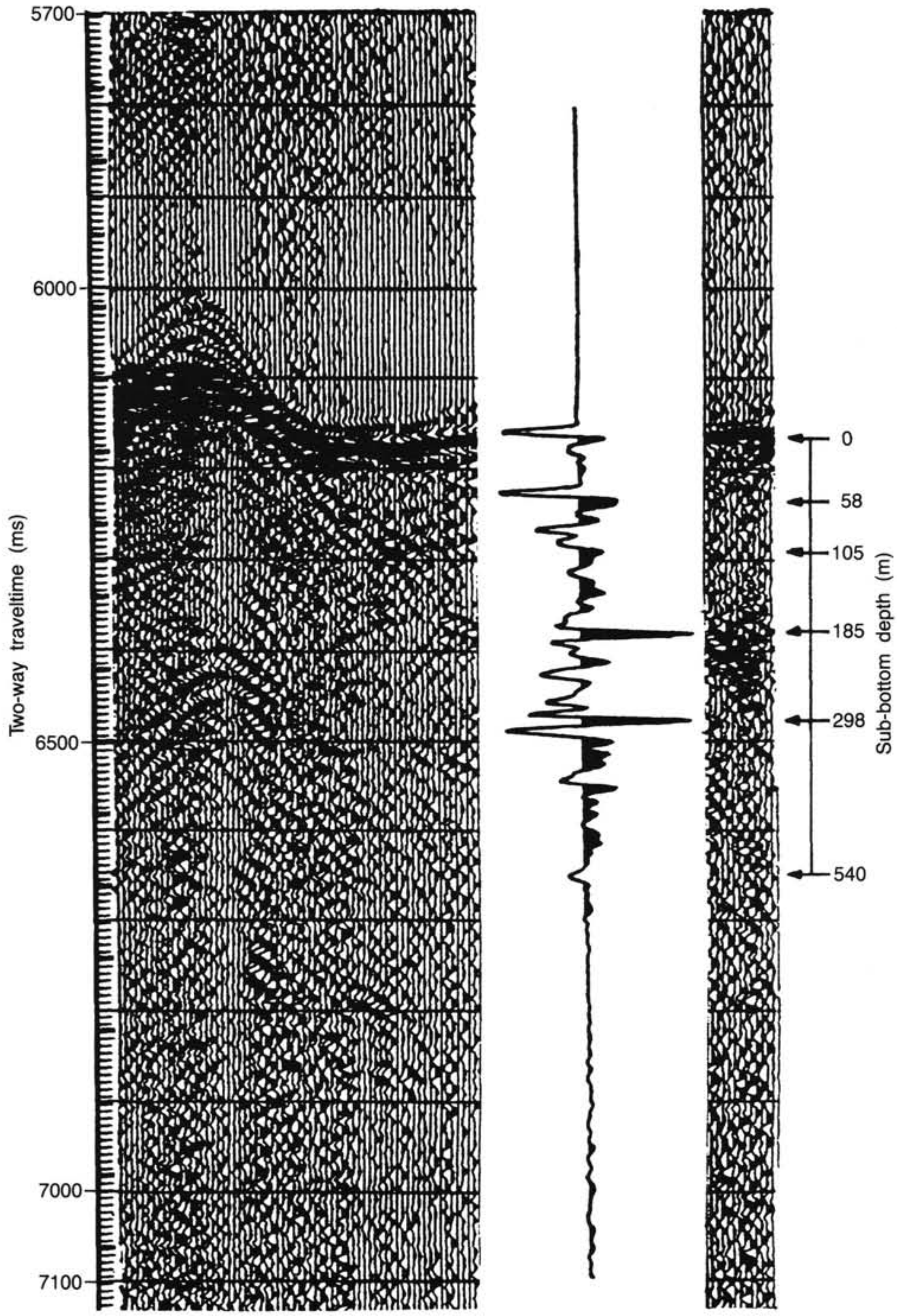

Figure 36. Preliminary seismic correlation. Synthetic seismogram calculated from 69-layer velocity/density model in Table 10. Source used is zero-phase and band-limited between 10 and 60 Hz (see text).

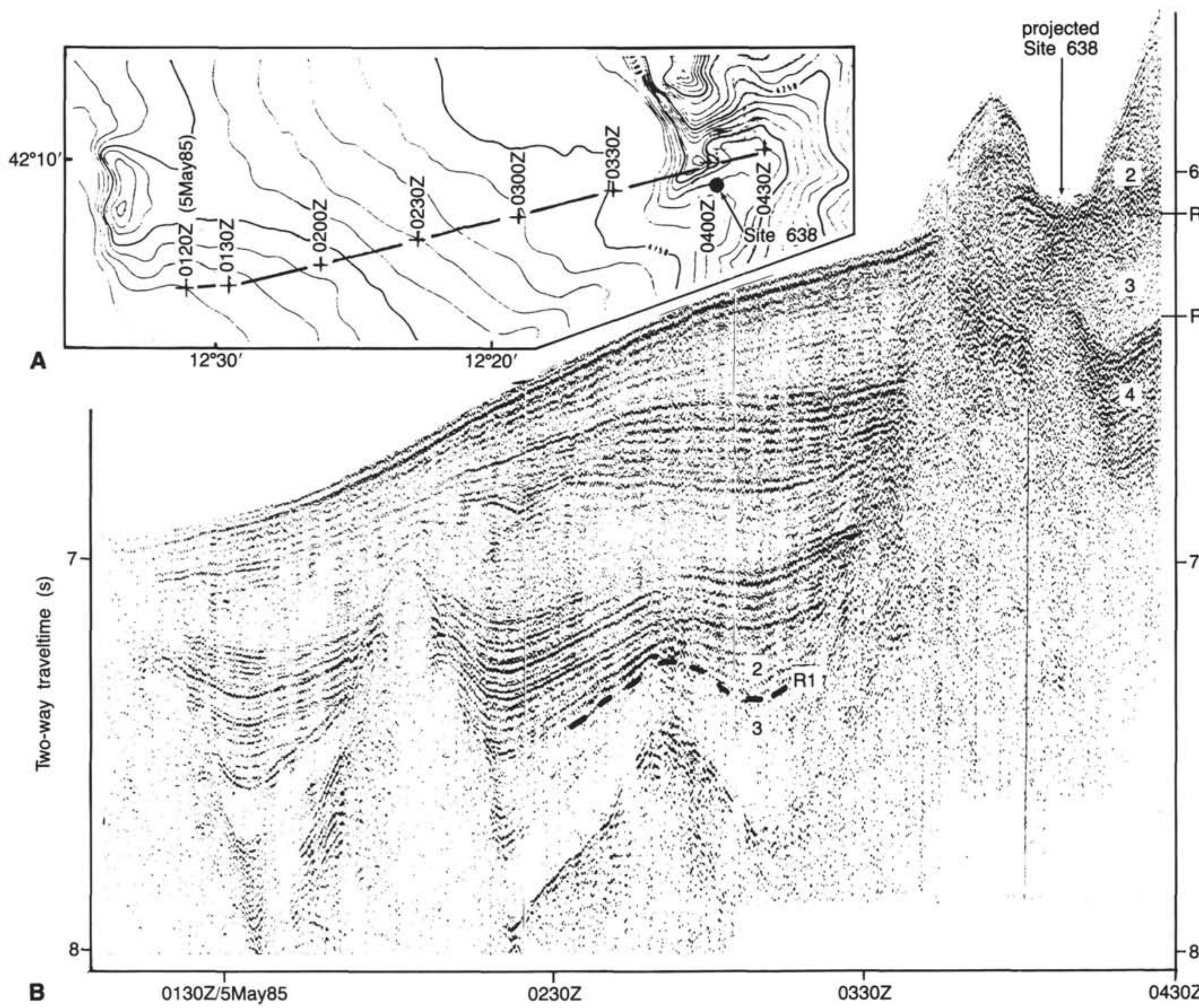

Figure 37. A. Part of Sea Beam map showing trackline of *JOIDES Resolution* seismic line from Site 637 to Site 638, and location of Site 638. B. Seismic line recorded from *JOIDES Resolution* while approaching Site 638. R1, reflector correlated with boundary between middle Cenomanian black shale (3) and Upper Cretaceous pelagic sediments (2); R2, reflector correlated with "break-up" unconformity between Albian black shale and Barremian–Aptian syn-rift sediments; (4) syn-rift (pre-Albian) strata.

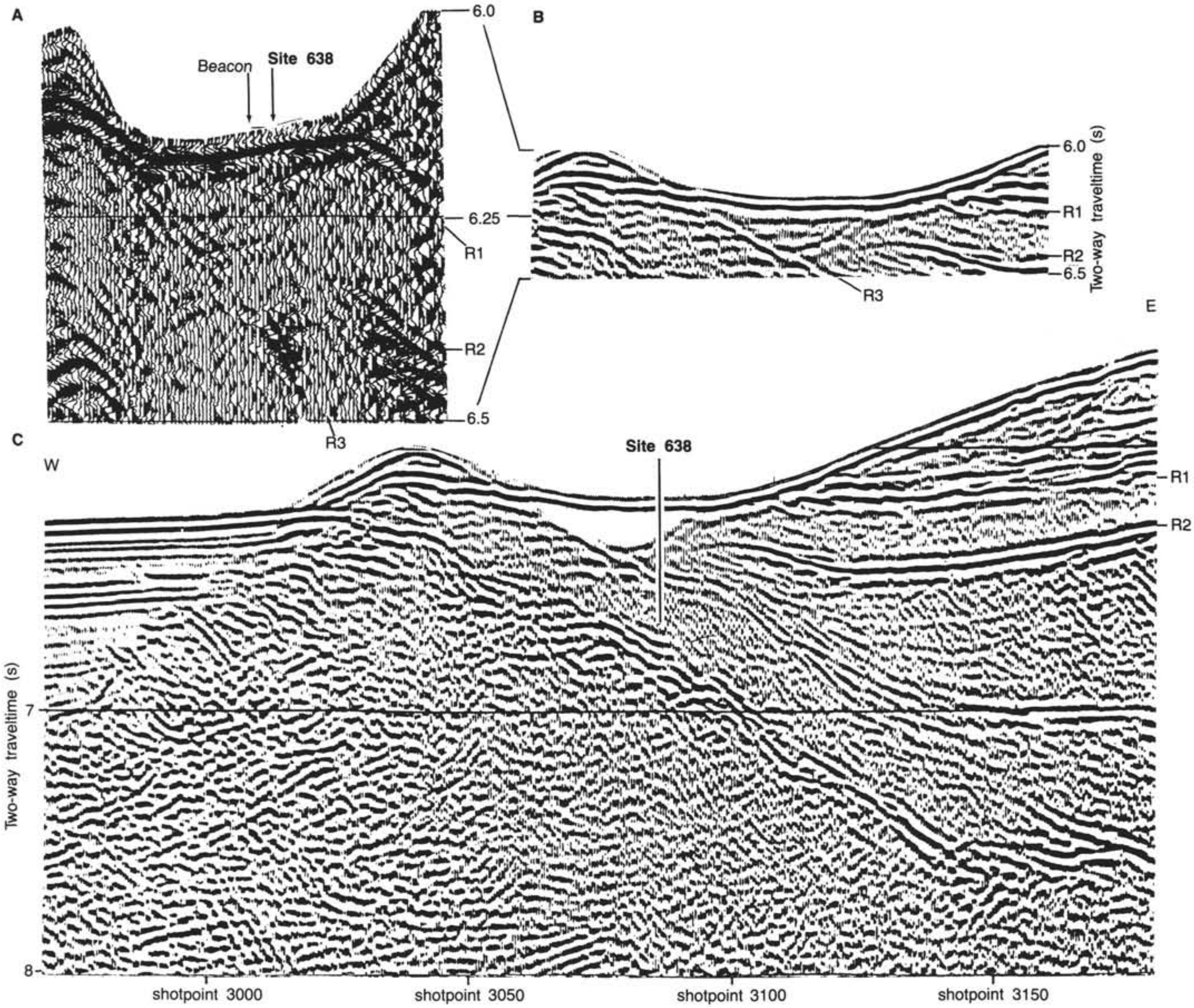

Figure 38. A. Location of the acoustic beacon and of Site 638 on processed seismic line taken from *JOIDES Resolution*. Reflectors R1, R2, and R3 are indicated by tick marks. B. Part of processed multichannel seismic line GP-101 near Site 638 (see Fig. 4 for location of line), showing reflectors R1, R2, and R3. C. A larger part of line GP-101, depicting the downward and lateral continuation of reflectors shown in Figure 38B. The Neogene valley fill near Site 638 has been left without shading.

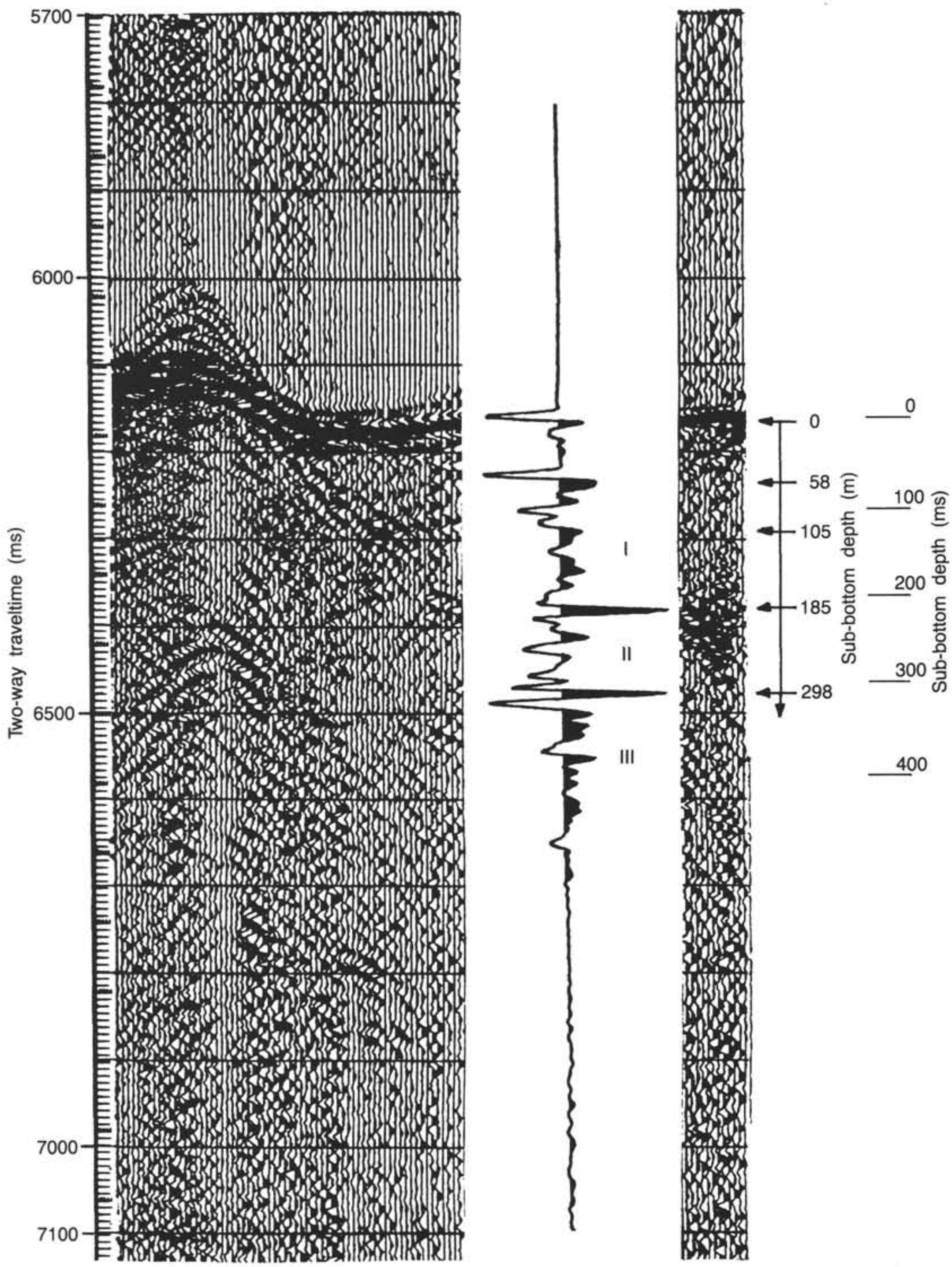

Figure 39. Seismic-reflection profile through Site 638, synthetic seismogram constructed using both downhole logs and laboratory data on velocity and density, and source signal used in processing multichannel line GP-101. The positions of lithologic Units I, II, and III are indicated with their depths.

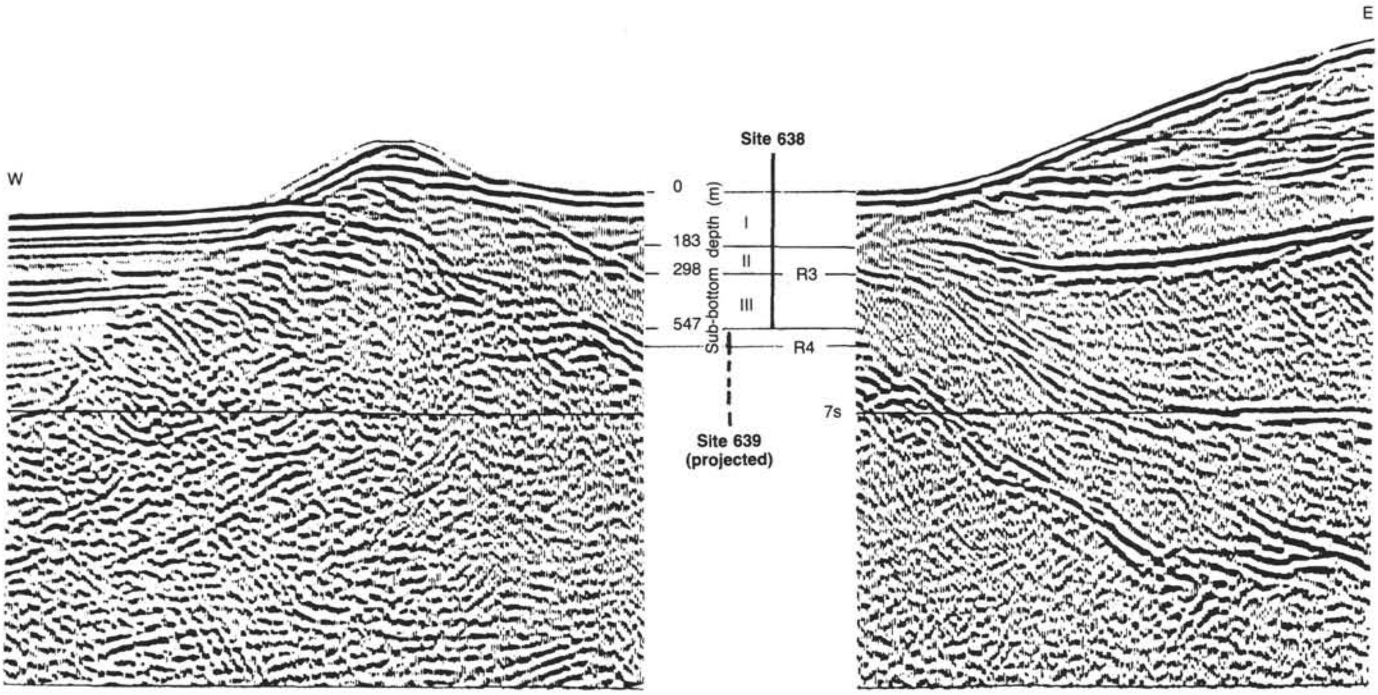

Figure 40. Correlation between the seismic line GP-101 and the drilled sequence at Sites 638 and 639 (projected). Location of seismic line shown in Figure 4.

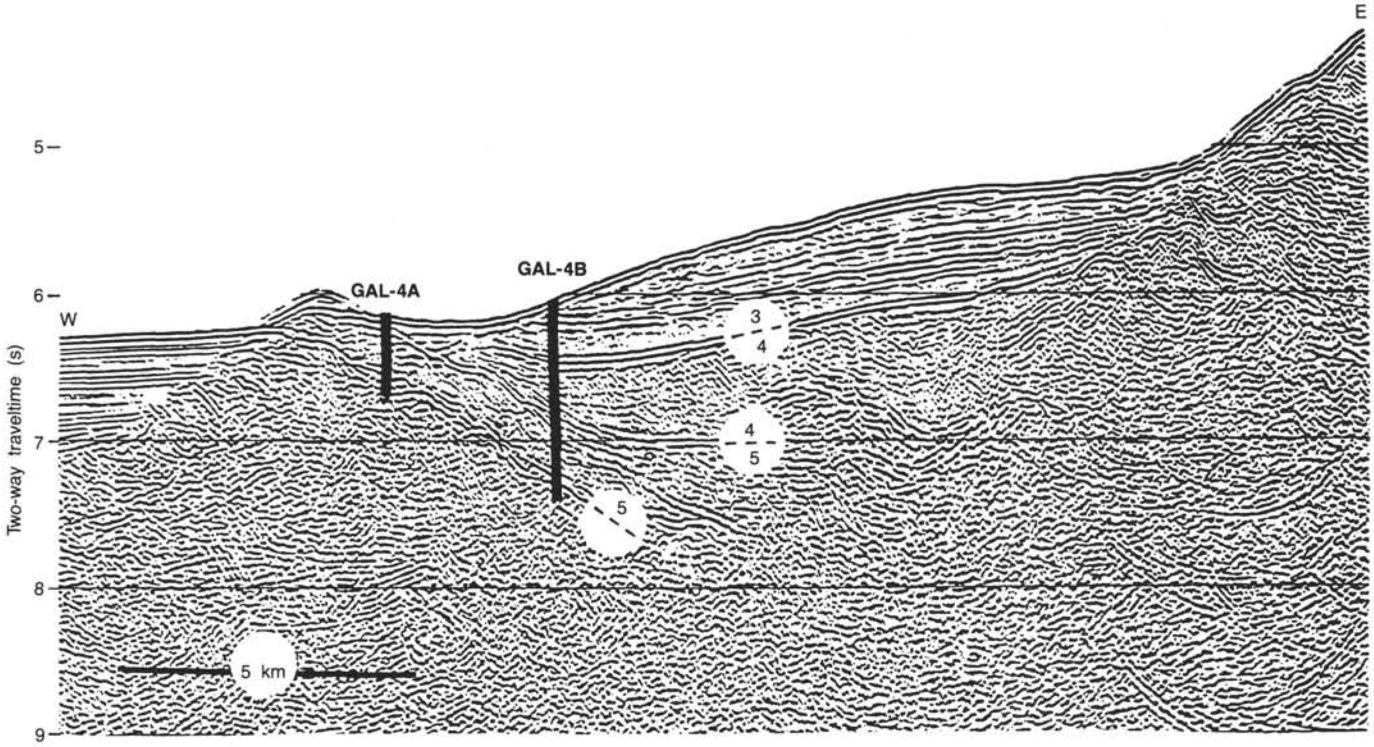

Figure 41. Multichannel seismic-reflection profile across the locations of target sites GAL-4A and GAL-4B, showing the seismic stratigraphic units recognized widely over most of the Galicia margin. The original caption on this figure, from the Scientific Prospectus for Leg 103 reads, "Note the pre-rift series (5) tilted with the basement block and the syn-rift series (4)." Site 638 is about 1 km east and 1 km north of target site GAL-4A.

Location: 42°09.2′N, 12°11.8′W Water depth: 4673 m below derrick floor (4663 mbsl)

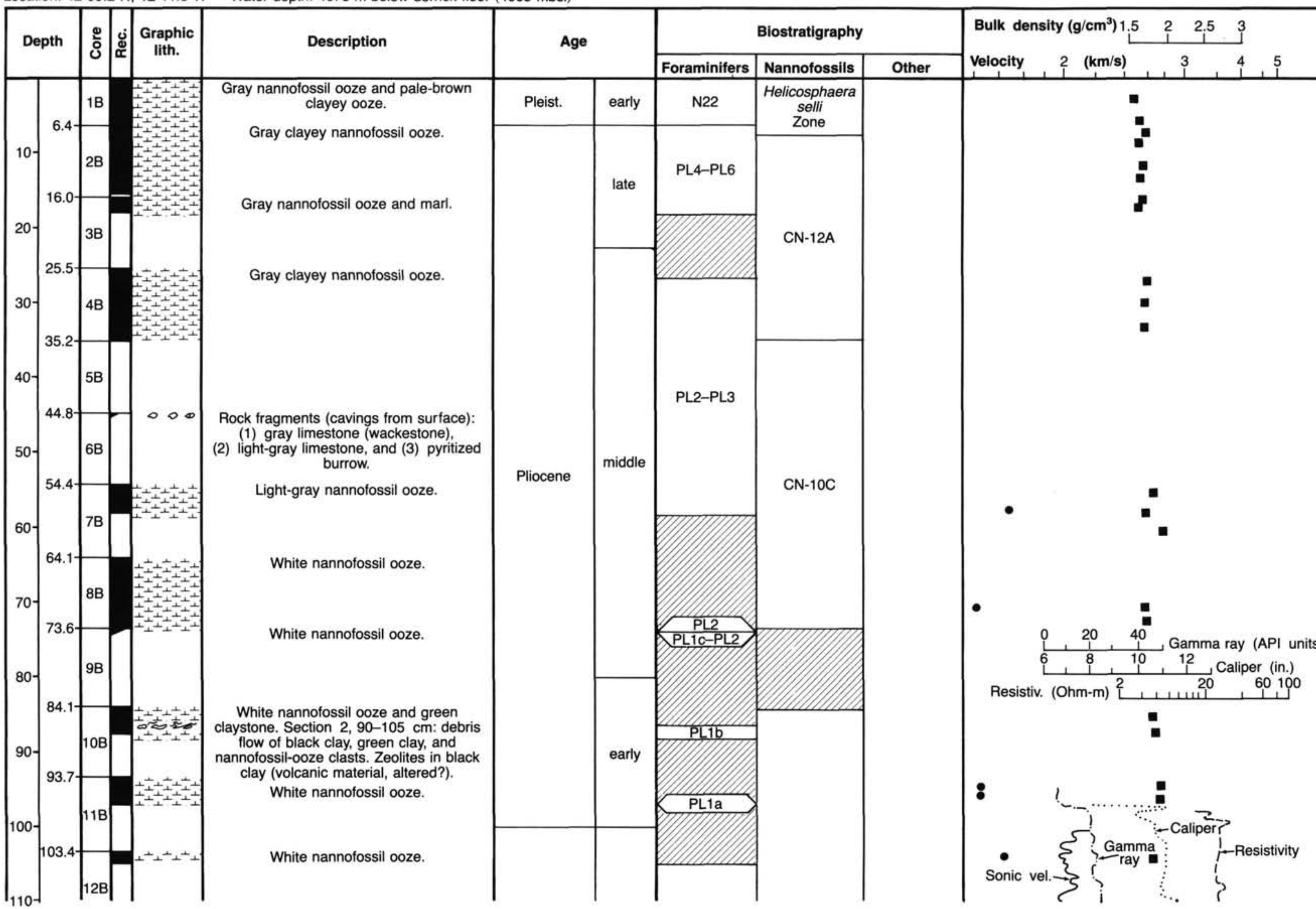

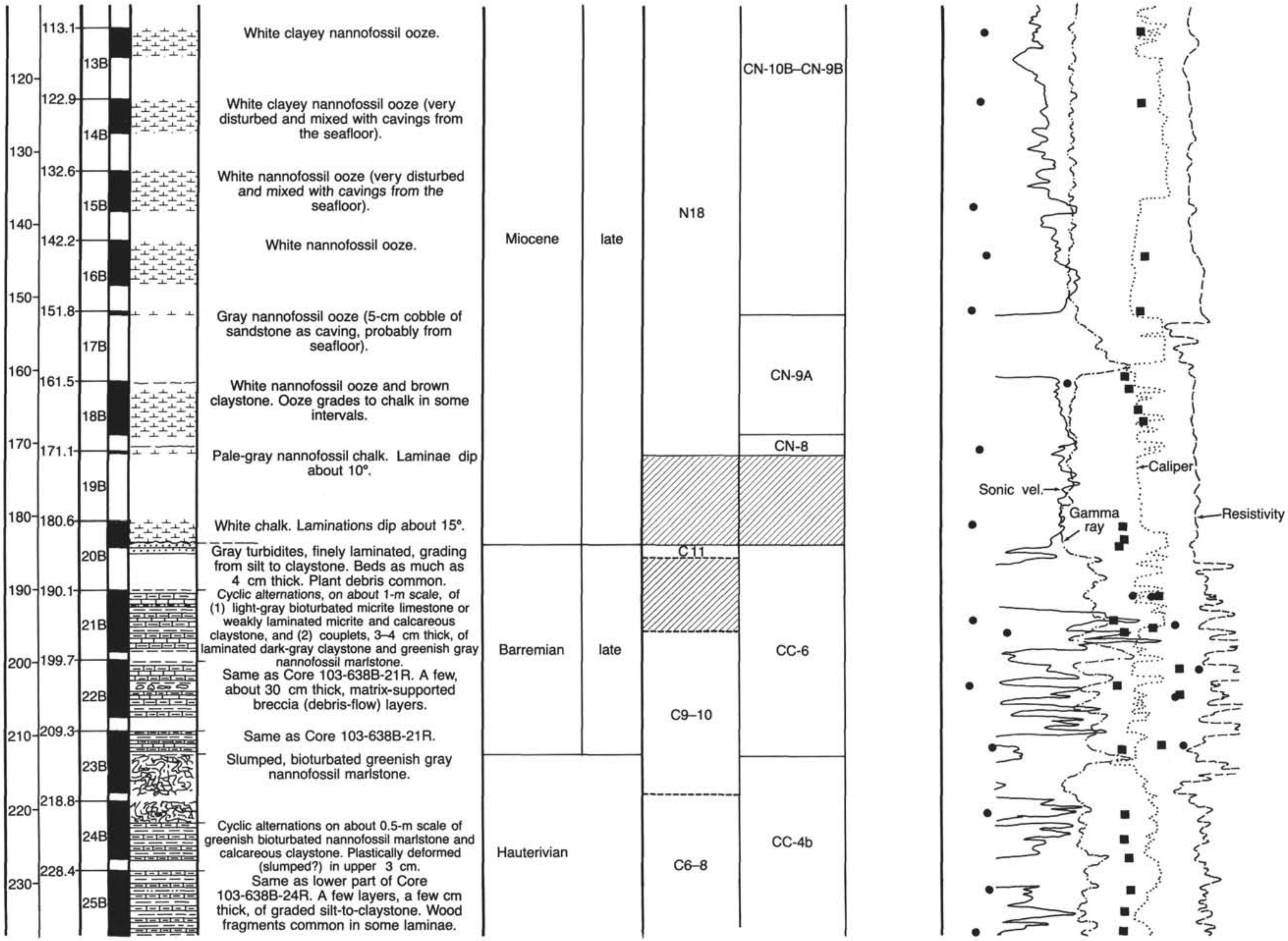

Figure 42. Site 638 summary logs. In right-hand columns, velocity data points are indicated by dot symbols; bulk-density data points are indicated by square symbols.

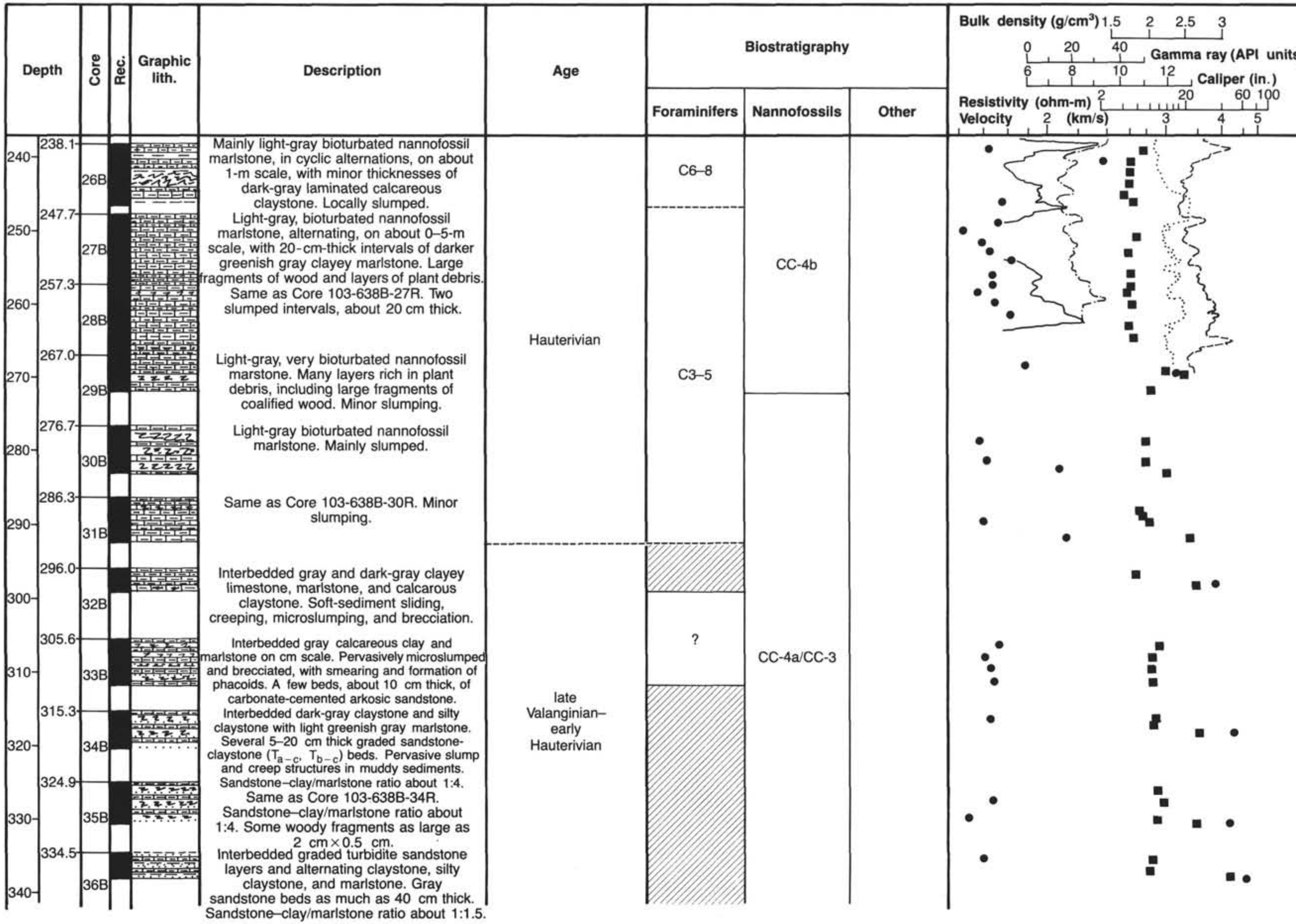

Depth
Core
Rec.
Graphic lith.
Description
Age
Biostratigraphy
Foraminifers
Nannofossils
Other
Bulk density (g/cm³) 1.5 2 2.5 3
Gamma ray (API units) 0 20 40
Caliper (in.) 6 8 10 12
Resistivity (ohm-m) 2 20 60 100
Velocity 2 (km/s) 3 4 5
240
250
260
270
280
290
300
310
320
330
340
238.1
247.7
257.3
267.0
276.7
286.3
296.0
305.6
315.3
324.9
334.5
26B
27B
28B
29B
30B
31B
32B
33B
34B
35B
36B
Mainly light-gray bioturbated nannofossil marlstone, in cyclic alternations, on about 1-m scale, with minor thicknesses of dark-gray laminated calcareous claystone. Locally slumped.
Light-gray, bioturbated nannofossil marlstone, alternating, on about 0–5-m scale, with 20-cm-thick intervals of darker greenish gray clayey marlstone. Large fragments of wood and layers of plant debris.
Same as Core 103-638B-27R. Two slumped intervals, about 20 cm thick.
Light-gray, very bioturbated nannofossil marstone. Many layers rich in plant debris, including large fragments of coalified wood. Minor slumping.
Light-gray bioturbated nannofossil marlstone. Mainly slumped.
Same as Core 103-638B-30R. Minor slumping.
Interbedded gray and dark-gray clayey limestone, marlstone, and calcarous claystone. Soft-sediment sliding, creeping, microslumping, and brecciation.
Interbedded gray calcareous clay and marlstone on cm scale. Pervasively microslumped and brecciated, with smearing and formation of phacoids. A few beds, about 10 cm thick, of carbonate-cemented arkosic sandstone.
Interbedded dark-gray claystone and silty claystone with light greenish gray marlstone. Several 5–20 cm thick graded sandstone-claystone (T_{a-c}, T_{b-c}) beds. Pervasive slump and creep structures in muddy sediments. Sandstone–clay/marlstone ratio about 1:4.
Same as Core 103-638B-34R. Sandstone–clay/marlstone ratio about 1:4. Some woody fragments as large as 2 cm × 0.5 cm.
Interbedded graded turbidite sandstone layers and alternating claystone, silty claystone, and marlstone. Gray sandstone beds as much as 40 cm thick. Sandstone–clay/marlstone ratio about 1:1.5.
Hauterivian
late Valanginian–early Hauterivian
C6–8
C3–5
?
CC-4b
CC-4a/CC-3

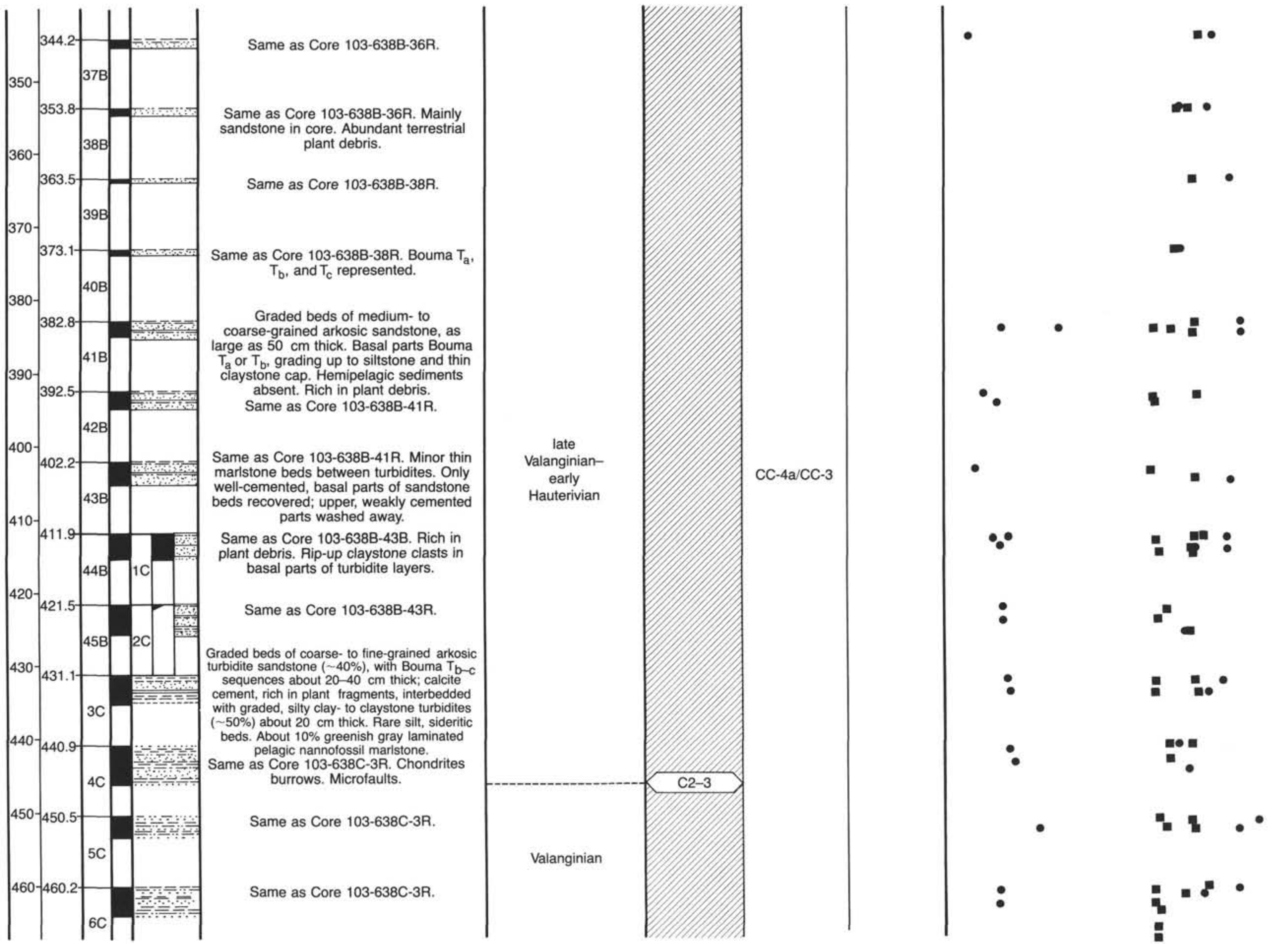

Figure 42 (continued).

Depth		Core	Rec.	Graphic lith.	Description	Age	Biostratigraphy: Foraminifers	Biostratigraphy: Nannofossils	Biostratigraphy: Other	Bulk density (g/cm³) 1.5 2 2.5 3 / Velocity 2 (km/s) 3 4 5
470	469.9	7C			Same as Core 103-638C-3R. A few uncemented or poorly cemented fine-grained sandstone beds about 20 cm thick. Marlstone about 20% of core.	Valanginian		CC-4a/CC-3		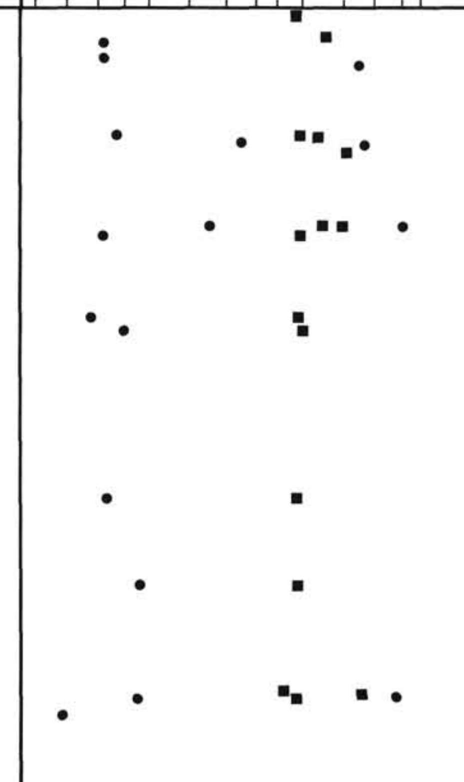
480	479.5	8C			Same as Core 103-638C-3R. Granule-bearing sandstone and rip-up claystone clasts. Marlstone about 5% of core.					
490	489.2	9C			Same as Core 103-638C-3R. Microfaults, cut by calcite veins, in some layers. Water-escape structure at one place. Marlstone about 5% of core.					
500	498.9	10C			Same as Core 103-638C-3R. Marlstone about 10% of core.					
510	508.5	11C			No recovery. This is most likely interval in which drill string stuck. Possibly loosely cemented sandstone.					
520	518.2	12C			Sandstone (a few layers, <5 cm thick), claystone, and marlstone. Plant debris constitutes about 20% of sandstone and claystone beds.					
530	527.9	13C			Claystone, silty claystone, and fine- to medium-grained sandstone, graded, in stringers and blebs. Siderite-rich clay layers 1–2 mm thick at a few places.	?				
540	537.5	14C			Same as Core 103-638C-3R. Marlstone about 10%. Sandstone, both well-cemented and poorly cemented.	?				
	547.2									

Total depth = 547.2 m

Figure 42 (continued).

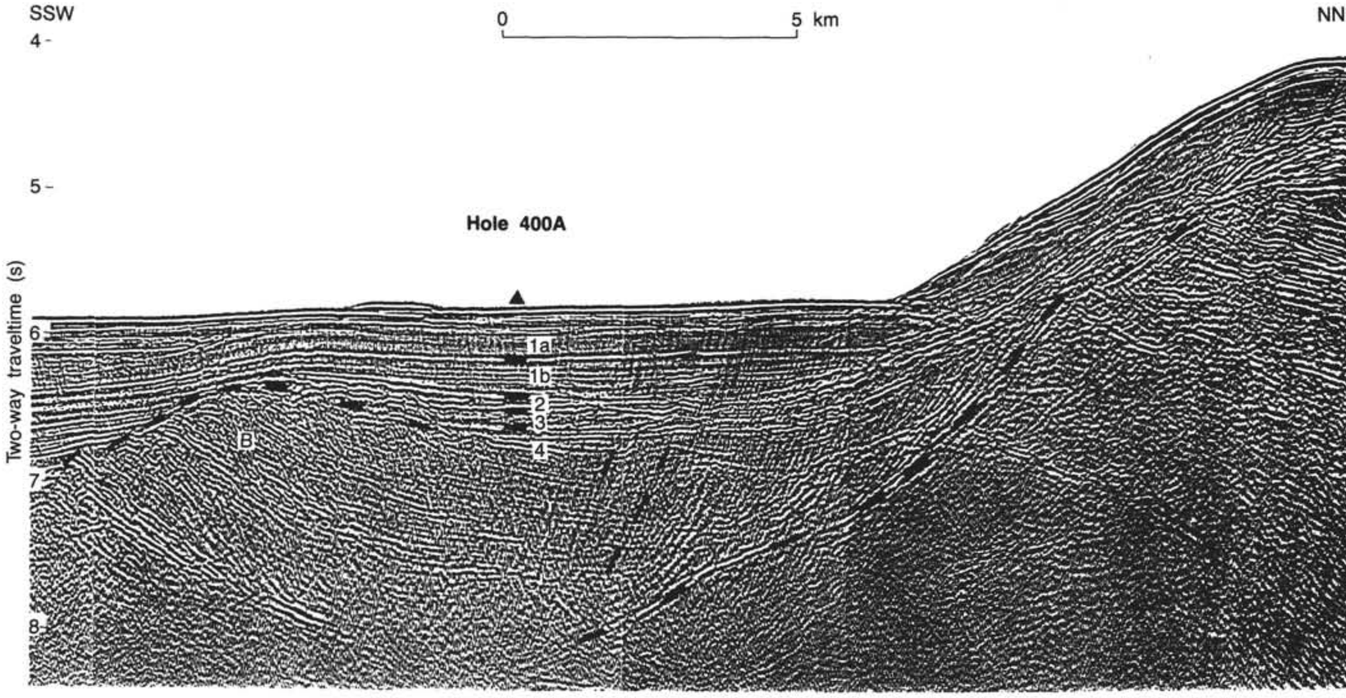

Figure 43. Seismic-reflection profile of part of the Armorican margin, near Hole 400A, drilled during DSDP Leg 48. The original caption includes the following: "Acoustical basement B consists in large part of layered sedimentary rocks of probable Jurassic and early Mesozoic age. These formerly continuous layers were faulted and tilted during the Early Cretaceous rifting phase." We interpret seismic formation B as being syn-rift Lower Cretaceous sediments, not as pre-rift Jurassic strata. The top of the carbonate platform is probably at about 7 s of two-way reflection time at the left side of the profile. From Montadert et al., 1979.

SITE 638 HOLE A CORE 1 R CORED INTERVAL 0.0–44.6 mbsf

TIME-ROCK UNIT | BIOSTRAT. ZONE/FOSSIL CHARACTER: FORAMINIFERS, NANNOFOSSILS, RADIOLARIANS, DIATOMS | PALEOMAGNETICS | PHYS. PROPERTIES | CHEMISTRY | SECTION | METERS | GRAPHIC LITHOLOGY | DRILLING DISTURB. | SED. STRUCTURES | SAMPLES | LITHOLOGIC DESCRIPTION

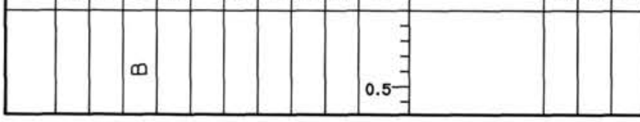

NANNOFOSSIL OOZE

This core consisted of a few centimeters of nannofossil ooze used by the paleontologists for dating.

SITE 638 HOLE B CORE 1 R CORED INTERVAL 4662.7-4669.1 mbsl; 0-6.4 mbsf

TIME-ROCK UNIT | BIOSTRAT. ZONE/FOSSIL CHARACTER: FORAMINIFERS, NANNOFOSSILS, RADIOLARIANS, DIATOMS | PALEOMAGNETICS | PHYS. PROPERTIES | CHEMISTRY | SECTION | METERS | GRAPHIC LITHOLOGY | DRILLING DISTURB. | SED. STRUCTURES | SAMPLES | LITHOLOGIC DESCRIPTION

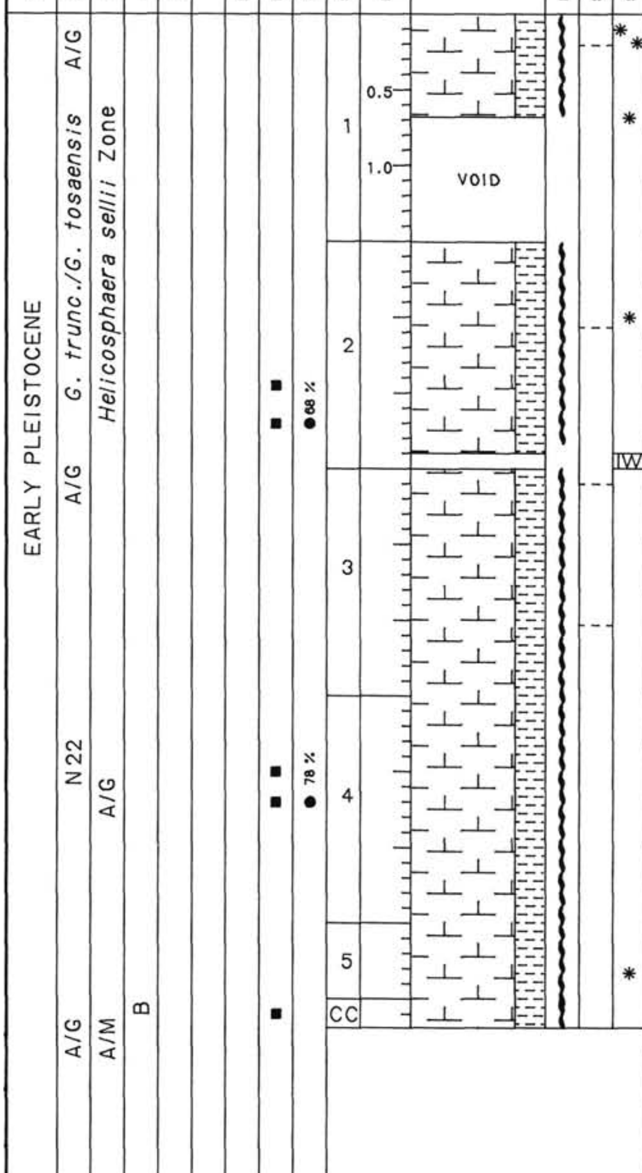

GRAY and PALE BROWN CLAYEY NANNOFOSSIL OOZE

This core consists of highly disturbed light gray (5Y7/1) and pale brown (10YR6/3) clayey nannofossil ooze. The two lithologies are badly mixed by drilling. More clayey layers are recognizable at Section 1, 23-68 cm; Section 2, 0-60 cm; and Section 3, 10-105 cm. Any internal structure has been destroyed by drilling. Pyrite concretions were found at Section 1, 9 cm, and Section 2, 60 cm. A round limestone pebble was found at Section 2, 80 cm.

SMEAR SLIDE SUMMARY (%):

	1,7 D	1,10 M	1,66 D	2,53 D	5,36 M
TEXTURE:					
Silt	5	12	10	3	3
Clay	95	88	90	97	97
COMPOSITION:					
Quartz	–	–	Tr	Tr	–
Feldspar	–	–	–	Tr	–
Mica	Tr	Tr	Tr	Tr	Tr
Clay	2	5	10	87	40
Accessory Minerals (Pyrite, Opaques)	Tr	10	1	Tr	–
Foraminifers	5	2	15	3	3
Nannofossils	93	83	74	10	57
Sponge Spicules	–	–	Tr	–	–

PHYSICAL PROPERTIES DATA:

	2,95	2,121	4,50	4,71	5,70
V_p (c)	–	1.24	–	–	–
ρ_b	–	1.57	–	–	1.65
γ	1.70	–	–	–	–
T_c	–	–	2.48	–	–

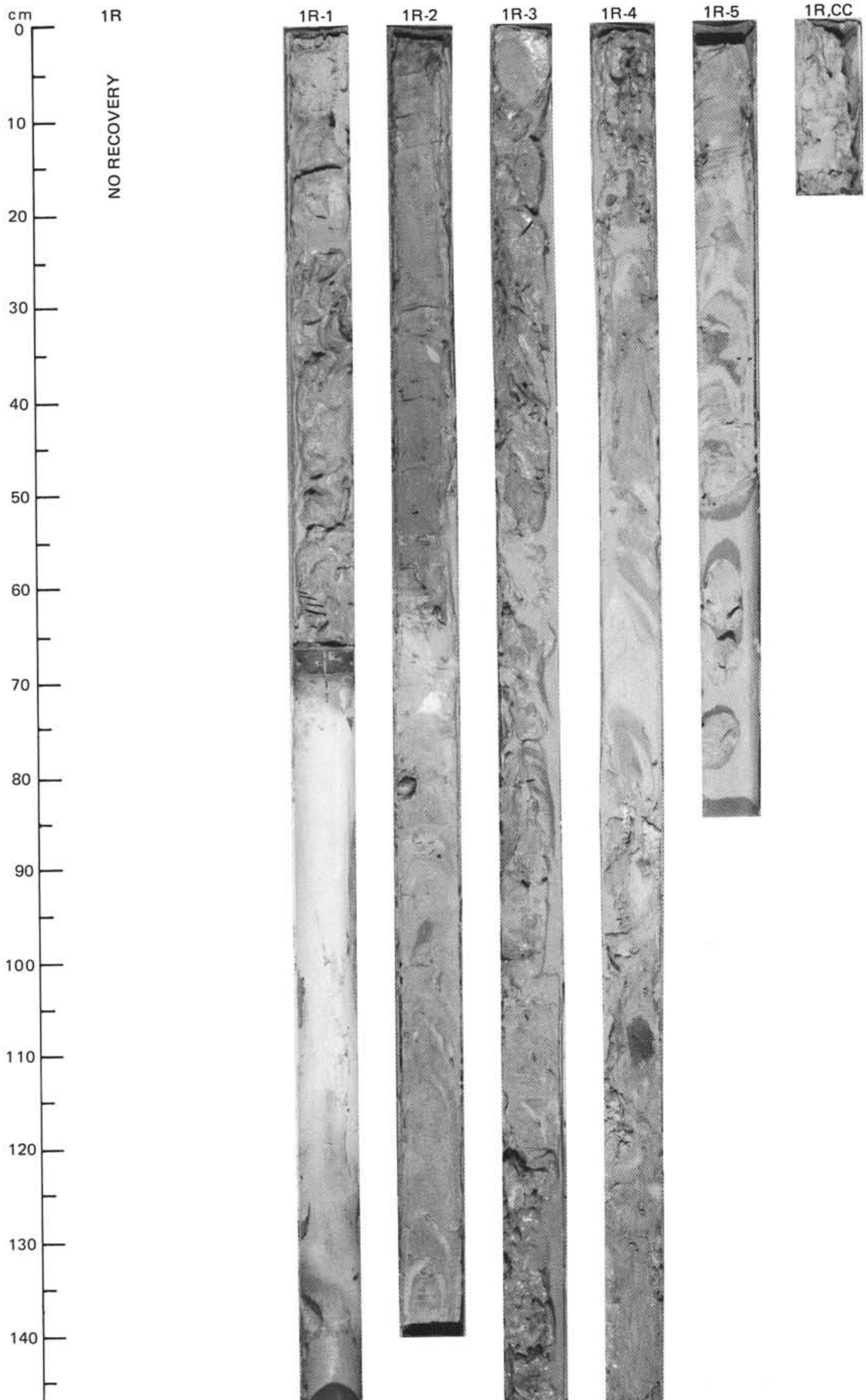
cm
0
10
20
30
40
50
60
70
80
90
100
110
120
130
140
150
1R
NO RECOVERY
1R-1
1R-2
1R-3
1R-4
1R-5
1R,CC

SITE 638 HOLE B CORE 2 R CORED INTERVAL 4669.1-4678.7 mbsl; 6.4-16.0 mbsf

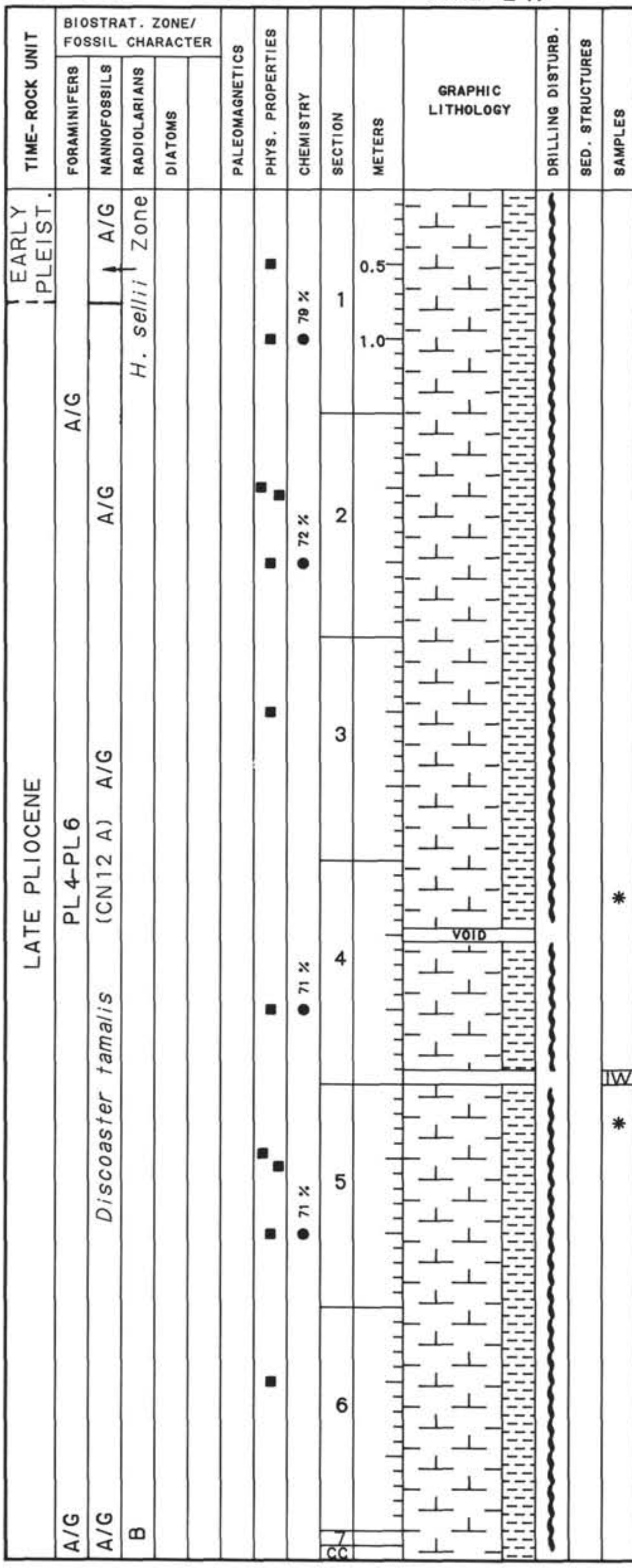

LITHOLOGIC DESCRIPTION

GRAY CLAYEY NANNOFOSSIL OOZE

This core consists of light gray (5Y6/1) clayey nannofossil ooze and foram-bearing clayey nannofossil ooze. The whole core has been badly disturbed by drilling. Some black specks of pyrite can be seen but otherwise the ooze has lost any internal structure.

SMEAR SLIDE SUMMARY (%):

	4,25 D	5,26 D
TEXTURE:		
Silt	Tr	–
Clay	100	100
COMPOSITION:		
Quartz	Tr	Tr
Mica	Tr	–
Clay	35	5
Accessory Minerals (Zircon?)	–	Tr
Foraminifers	5	–
Nannofossils	60	95
Sponge Spicules	Tr	–

PHYSICAL PROPERTIES DATA:

	1,50	1,101	2,50	2,55	2,101	3,50
V_p (c)	–	1.28	–	–	1.15	–
ρ_b	–	1.73	–	–	1.63	–
γ	–	–	–	4.98	–	–
T_c	2.57	–	2.53	–	–	2.53

	4,101	5,50	5,55	5,101	6,50
V_p (c)	1.22	–	–	1.24	–
ρ_b	1.67	–	–	1.66	–
γ	–	–	5.44	–	–
T_c	–	2.42	–	–	2.64

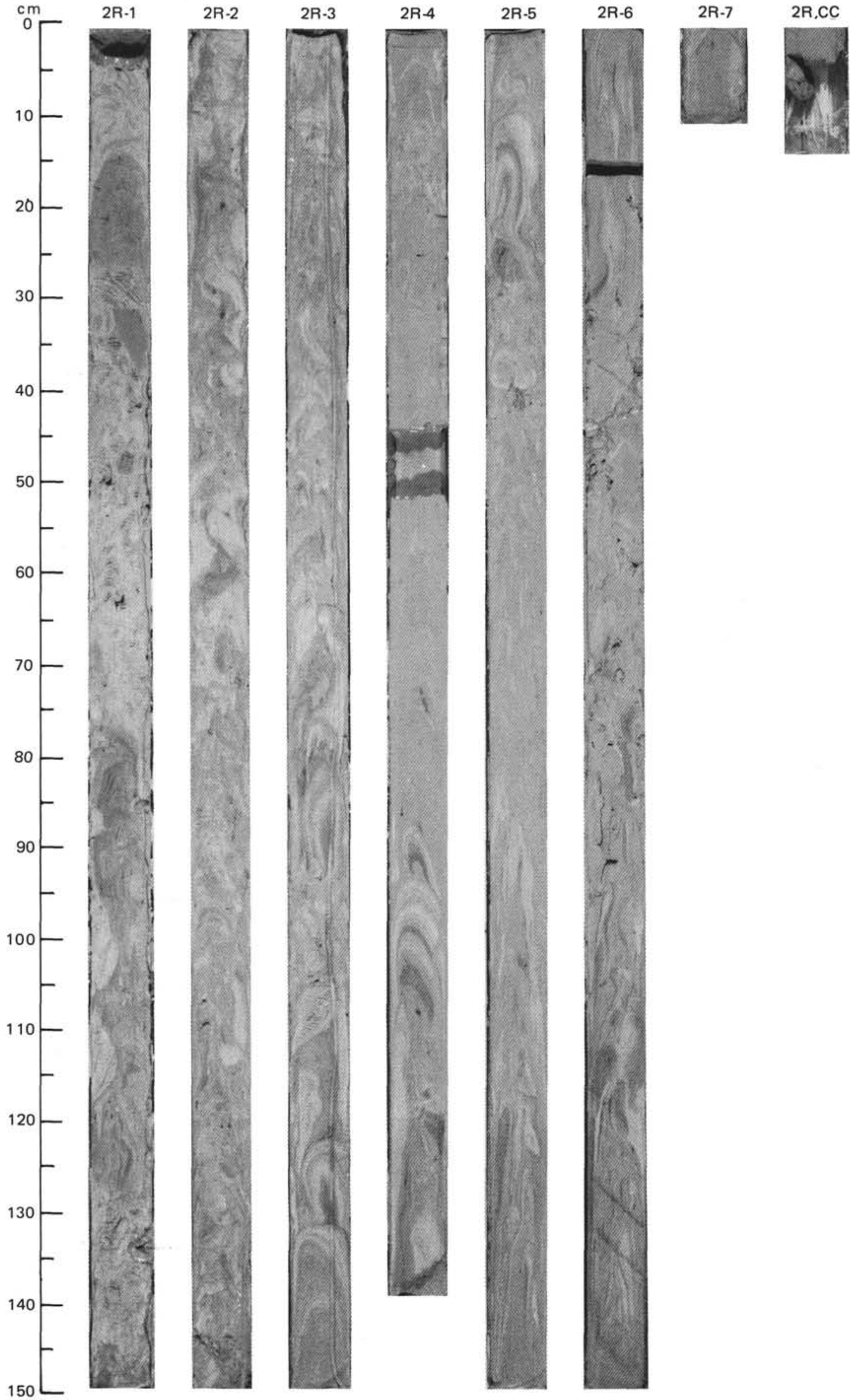
cm
0
10
20
30
40
50
60
70
80
90
100
110
120
130
140
150
2R-1
2R-2
2R-3
2R-4
2R-5
2R-6
2R-7
2R,CC

SITE 638 HOLE B CORE 3 R CORED INTERVAL 4678.7-4688.2 mbsl; 16.0-25.5 mbsf

TIME-ROCK UNIT	FORAMINIFERS	NANNOFOSSILS	RADIOLARIANS	DIATOMS	PALEOMAGNETICS	PHYS. PROPERTIES	CHEMISTRY	SECTION	METERS	GRAPHIC LITHOLOGY	DRILLING DISTURB.	SED. STRUCTURES	SAMPLES
LATE PLIOCENE	PL 4-PL 5 A/M	*Discoaster tamalis* (CN12 A) A/G	B			■ ■ ■■	● 76 % ● 74 %	1 2 CC	0.5 1.0	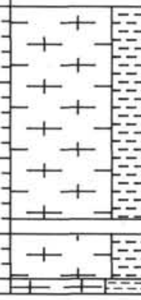			* * IW

LITHOLOGIC DESCRIPTION

GRAY CLAYEY FORAMINIFERAL NANNOFOSSIL OOZE and MARL

This core consists of soft white to light gray (5Y8/1) clayey nannofossil ooze with some brownish gray (2.5Y6/2) nannofossil marl patches. Whole core has been badly disturbed by drilling.

SMEAR SLIDE SUMMARY (%):

	1,30	1,102
	D	D
TEXTURE:		
Sand	–	5
Silt	65	25
Clay	35	70
COMPOSITION:		
Quartz	2	–
Clay	30	35
Calcite/Dolomite	–	3
Accessory Minerals (Opaques)	2	Tr
Foraminifers	20	15
Nannofossils	46	47
Fish Remains	Tr	–

PHYSICAL PROPERTIES DATA:

	1,31	1,130	2,11	2,20
V_p (c)	1.33	–	1.32	–
ρ_b	1.67	–	1.64	–
γ	–	6.46	–	–
T_c	–	–	–	2.66

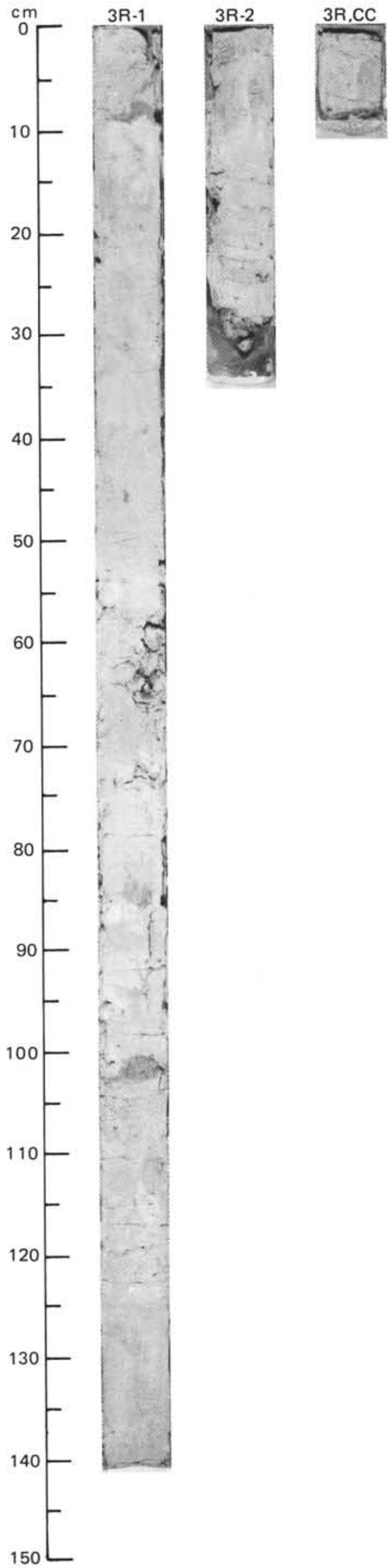
cm
0
10
20
30
40
50
60
70
80
90
100
110
120
130
140
150
3R-1
3R-2
3R,CC

SITE 638 HOLE B CORE 4 R CORED INTERVAL 4688.2-4697.9 mbsl; 25.5-35.2 mbsf

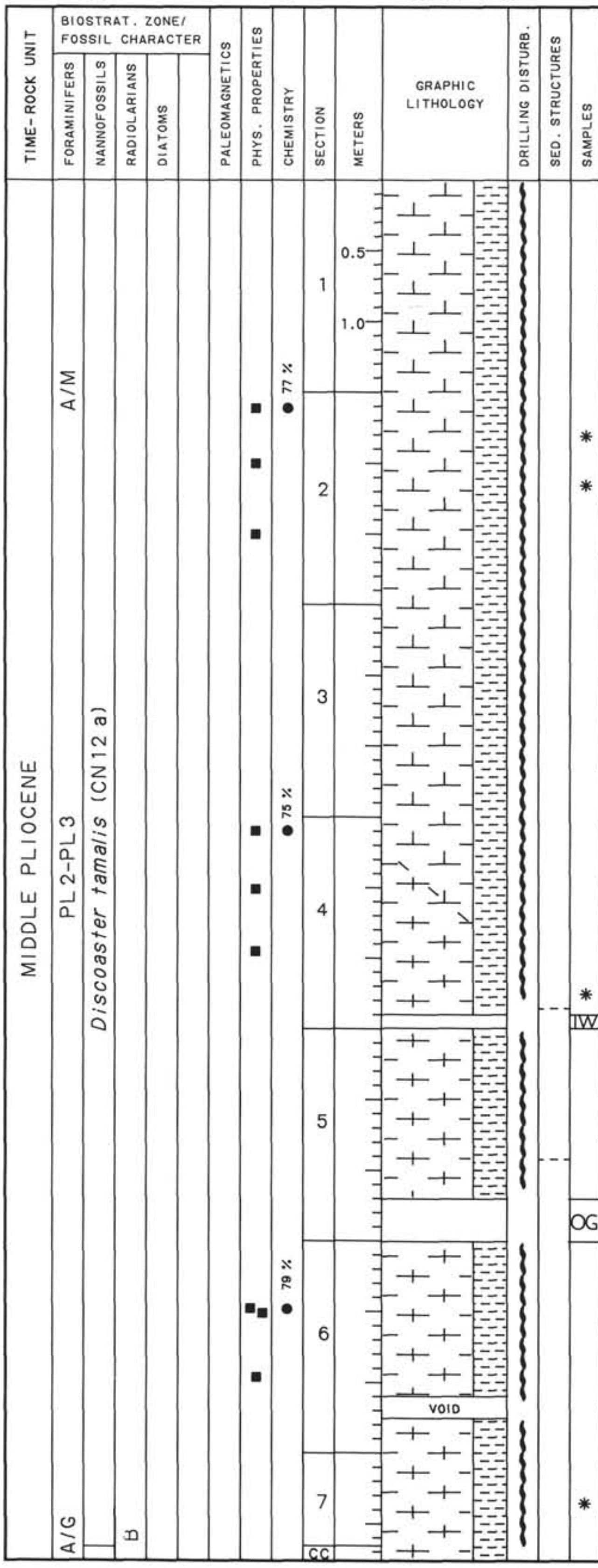

LITHOLOGIC DESCRIPTION

GRAY CLAYEY NANNOFOSSIL OOZE

This core consists of soft, white to light gray (5Y7/1) clayey nannofossil ooze grading down in Section 4 to foraminiferal nannofossil ooze. The sediment is badly disturbed and homogenized by drilling. There are some darker gray spots of local iron/manganese sulphide concentration in Sections 4 through 6. There is a pyritized burrow in Section 6, 100-102 cm.

SMEAR SLIDE SUMMARY (%):

	2,33	2,66	4,125	7,37
	D	D	D	D
TEXTURE:				
Sand	5	–	10	15
Silt	60	10	60	–
Clay	35	90	30	85
COMPOSITION:				
Quartz	1	Tr	1	Tr
Mica	–	Tr	Tr	–
Clay	20	15	20	15
Calcite/Dolomite	2	1	–	–
Accessory Minerals (Opaques)	1	Tr	Tr	–
Foraminifers	6	Tr	15	20
Nannofossils	70	84	64	65
Fish Remains	–	–	Tr	–

PHYSICAL PROPERTIES DATA:

	2,11	2,50	2,100	4,11	4,50
V_p (c)	1.28	–	–	1.16	–
ρ_b	1.74	–	–	1.72	–
γ	–	–	7.81	–	–
T_c	–	2.78	–	–	2.66

	4,100	6,46	6,50	6,93
V_p (c)	–	1.25	–	–
ρ_b	–	1.73	–	–
γ	7.47	–	–	6.68
T_c	–	–	2.79	–

CORE 5 R NO RECOVERY


cm
0
10
20
30
40
50
60
70
80
90
100
110
120
130
140
150
4R-1
4R-2
4R-3
4R-4
4R-5
4R-6
4R-7
5R
NO RECOVERY
4R,CC

SITE 638 HOLE B CORE 6 R CORED INTERVAL 4707.5–4717.1 mbsl; 44.8–54.4 mbsf

TIME-ROCK UNIT	BIOSTRAT. ZONE/ FOSSIL CHARACTER: FORAMINIFERS	NANNOFOSSILS	RADIOLARIANS	DIATOMS		PALEOMAGNETICS	PHYS. PROPERTIES	CHEMISTRY	SECTION	METERS	GRAPHIC LITHOLOGY	DRILLING DISTURB.	SED. STRUCTURES	SAMPLES	LITHOLOGIC DESCRIPTION
EARLY / MIDDLE PLIOCENE	C/M PL2-PL3	C/M CN10c	B						CC						LIMESTONE FRAGMENTS

LIMESTONE FRAGMENTS

This core consists only of three rock fragments found in the CC:

(1) Gray limestone (wackestone) with iron-manganese coating, burrowed, some burrows filled with calcite.

(2) Light gray limestone with minor borings.

(3) Pyritized burrow 4 cm long by 1 cm diameter.

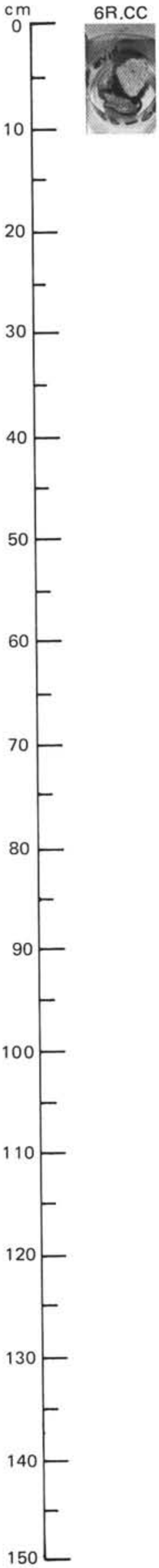
cm
6R,CC
0
10
20
30
40
50
60
70
80
90
100
110
120
130
140
150

SITE 638 HOLE B *CORE 7 R CORED INTERVAL 4717.1-4726.8 mbsl; 54.4-64.1 mbsf

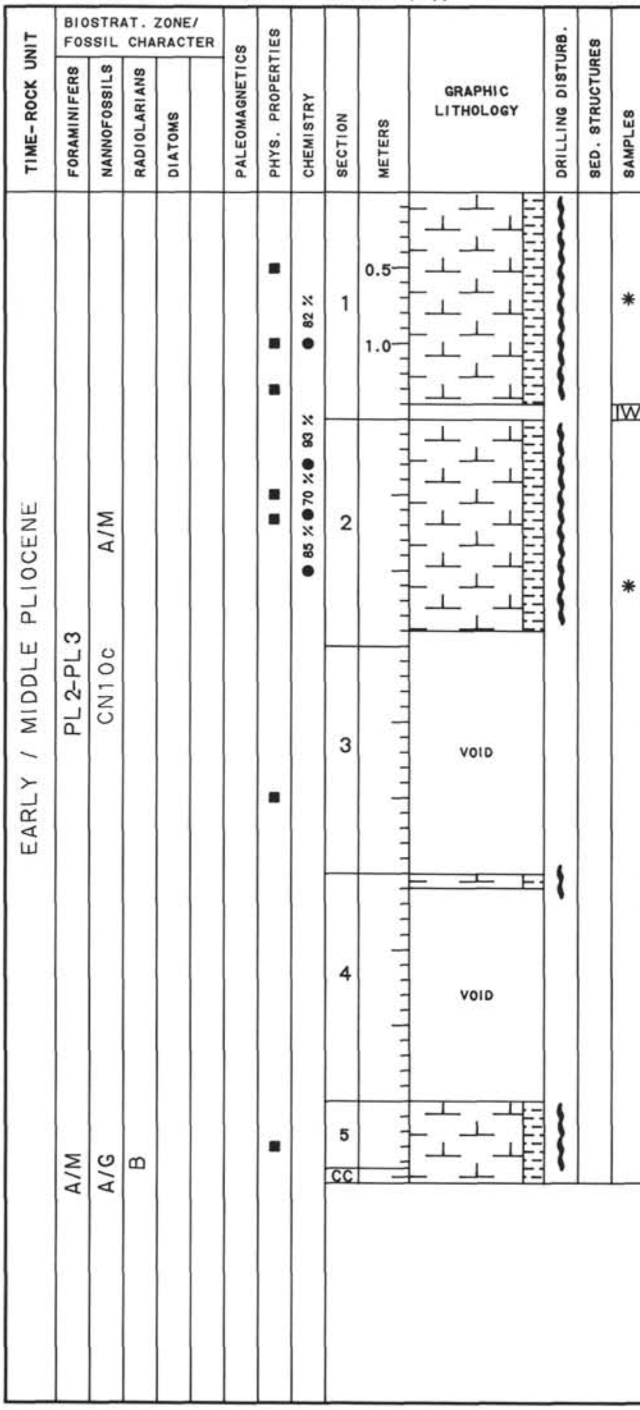

LITHOLOGIC DESCRIPTION

LIGHT GRAY CLAYEY NANNOFOSSIL OOZE

This core consists of white to light gray (5Y8/1 to 5Y7/1) nannofossil ooze to clayey nannofossil ooze. The core is highly disturbed by drilling but some faint lamination is discernible. Specks of pyrite are dispersed throughout the core, along with widely scattered quartz grains. A foraminiferal sand layer (probably the result of washing during drilling) is at Section 5, 7-9 cm.

SMEAR SLIDE SUMMARY (%):

	1,75	2,105
	D	M
TEXTURE:		
Silt	2	40
Clay	98	60
COMPOSITION:		
Quartz	Tr	–
Mica	Tr	–
Clay	10	50
Foraminifers	2	–
Nannofossils	88	50

PHYSICAL PROPERTIES DATA:

	1,50	1,101	1,127	2,50
V_p (c)	–	2.31	–	–
ρ_b	–	1.85	–	–
γ	–	–	19.25	–
T_c	3.22	–	–	3.16

	2,65	3,101	5,31
V_p (c)	–	1.77	1.76
ρ_b	–	1.74	1.98
γ	7.36	–	–

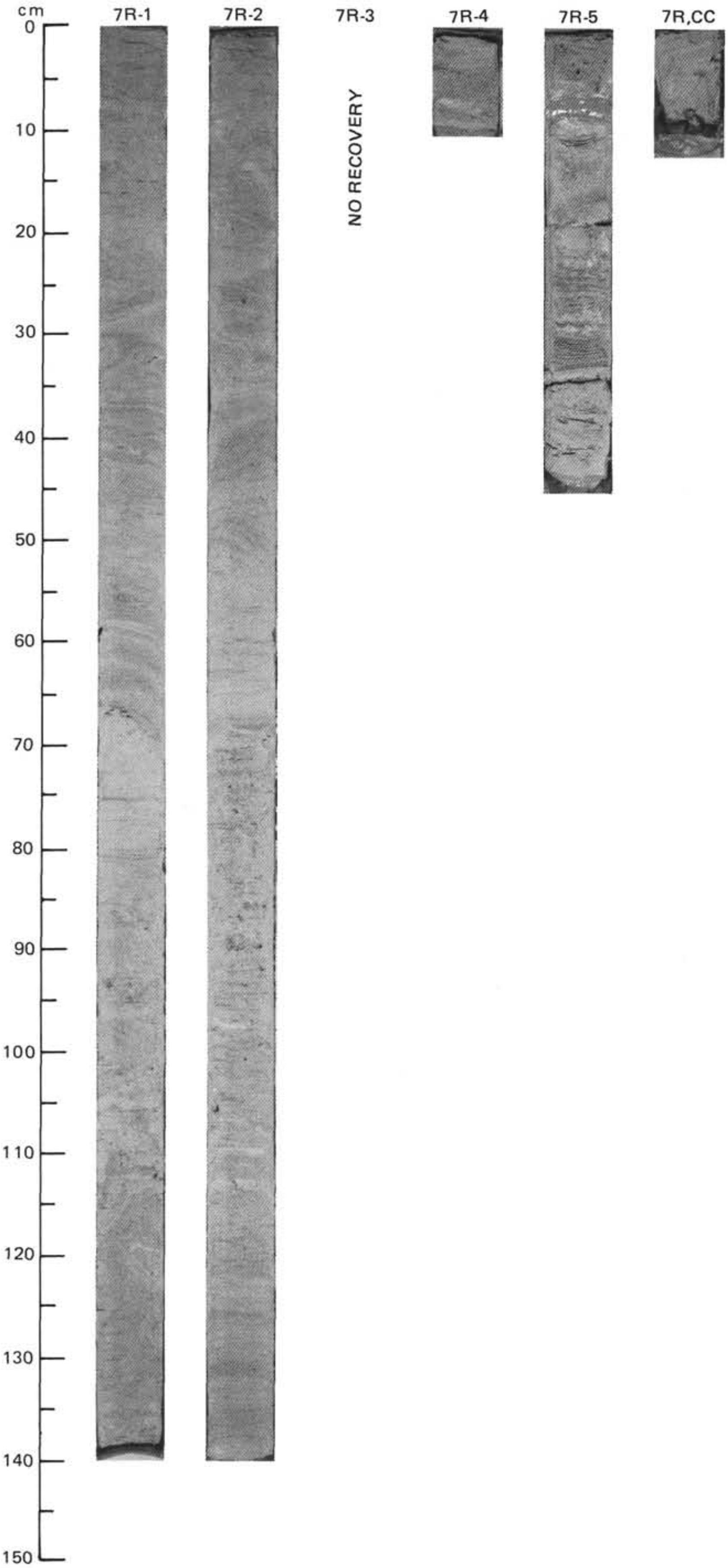
cm
0
10
20
30
40
50
60
70
80
90
100
110
120
130
140
150
7R-1
7R-2
7R-3
NO RECOVERY
7R-4
7R-5
7R,CC

SITE 638 HOLE B CORE 8 R CORED INTERVAL 4726.8-4736.3 mbsl; 64.1-73.6 mbsf

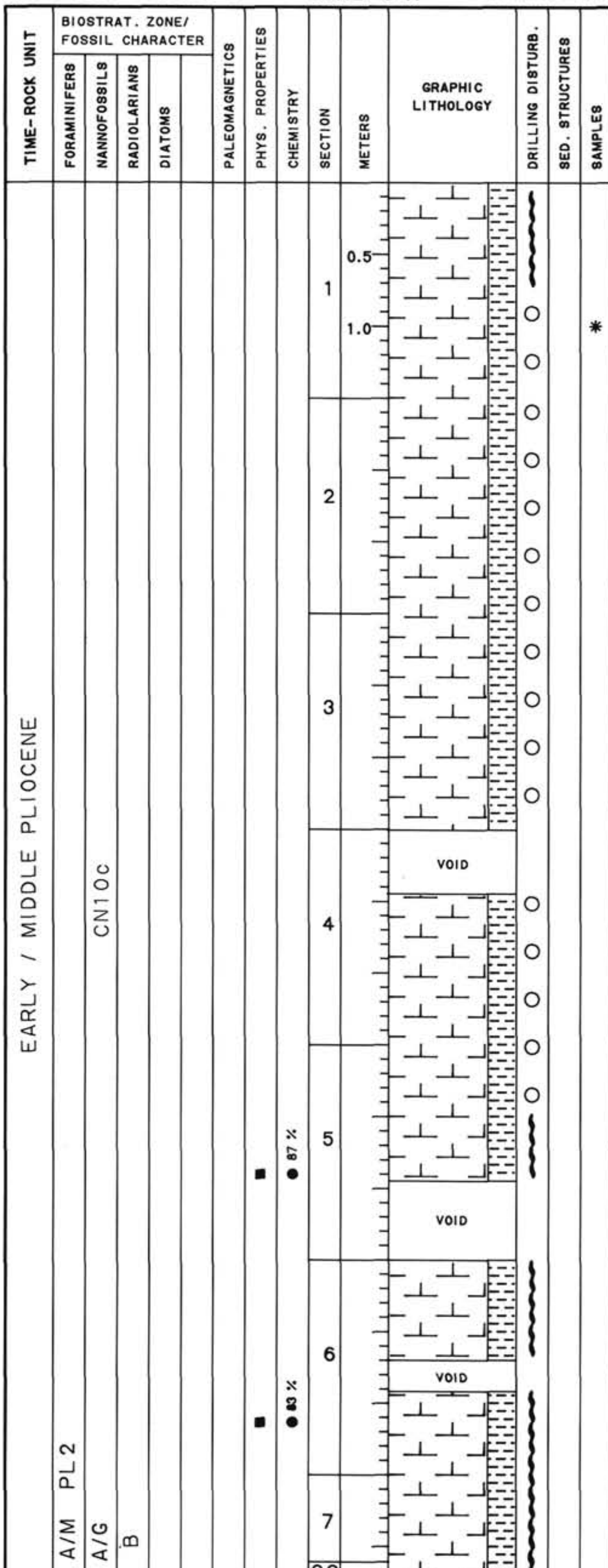

LITHOLOGIC DESCRIPTION

WHITE CLAYEY OOZE

This core consists of soupy white (5Y8/1) clayey nannofossil ooze. All internal structure has been destroyed by drilling.

SMEAR SLIDE SUMMARY (%):

	1,103
	D
TEXTURE:	
Silt	30
Clay	70
COMPOSITION:	
Clay	5
Foraminifers	10
Nannofossils	85

PHYSICAL PROPERTIES DATA:

	5,88	6,111
V_p (c)	1.62	1.27
ρ_b	1.74	1.75

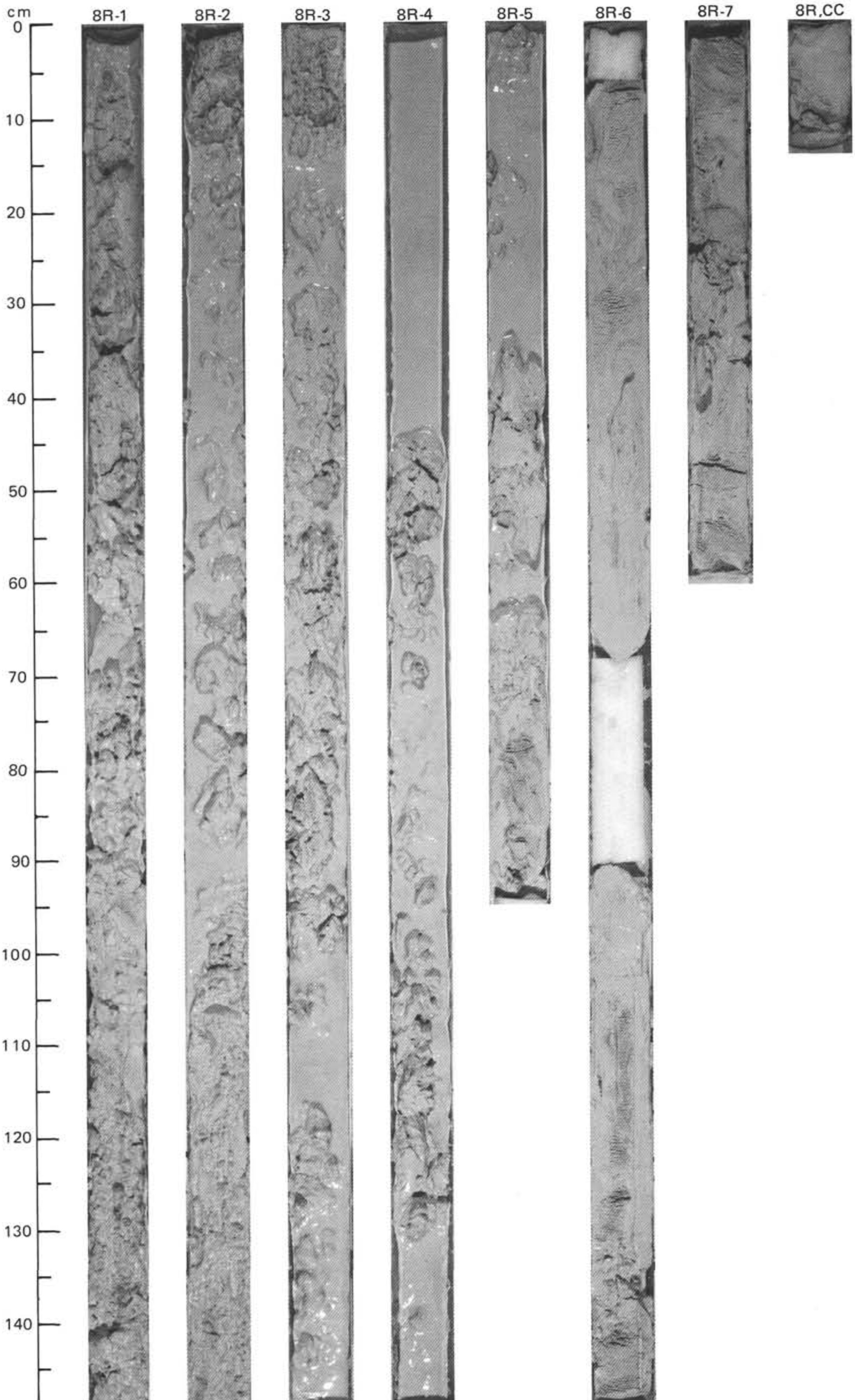
cm
0
10
20
30
40
50
60
70
80
90
100
110
120
130
140
150
8R-1
8R-2
8R-3
8R-4
8R-5
8R-6
8R-7
8R,CC

SITE 638 HOLE B CORE 9 R CORED INTERVAL 4736.3-4746.8 mbsl; 73.6-84.1 mbsf

TIME-ROCK UNIT	BIOSTRAT. ZONE/ FOSSIL CHARACTER: FORAMINIFERS	NANNOFOSSILS	RADIOLARIANS	DIATOMS	PALEOMAGNETICS	PHYS. PROPERTIES	CHEMISTRY	SECTION	METERS	GRAPHIC LITHOLOGY	DRILLING DISTURB.	SED. STRUCTURES	SAMPLES
EARLY/MIDDLE PLIOCENE	A/M PL1C-PL2	A/G CN10 B(?)	B					CC					*

LITHOLOGIC DESCRIPTION

WHITE CLAYEY NANNOFOSSIL OOZE

Only a CC sample was recovered. It consists of 15 cm of white (5Y8/1) nannofossil ooze with 3 pyritized burrows.

SMEAR SLIDE SUMMARY (%):

	CC M
TEXTURE:	
Clay	100
COMPOSITION:	
Quartz	Tr
Mica	Tr
Clay	30
Calcite/Dolomite	Tr
Accessory Minerals	Tr
Foraminifers	1
Nannofossils	40
Micrite	29

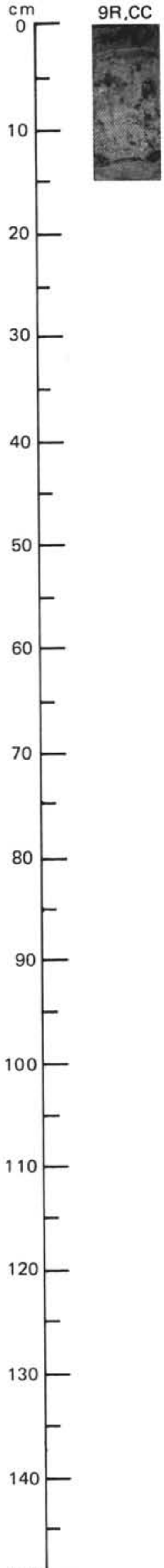
cm
9R,CC
0
10
20
30
40
50
60
70
80
90
100
110
120
130
140
150

SITE 638 HOLE B CORE 10 R CORED INTERVAL 4746.8-4756.4 mbsl; 84.1-93.7 mbsf

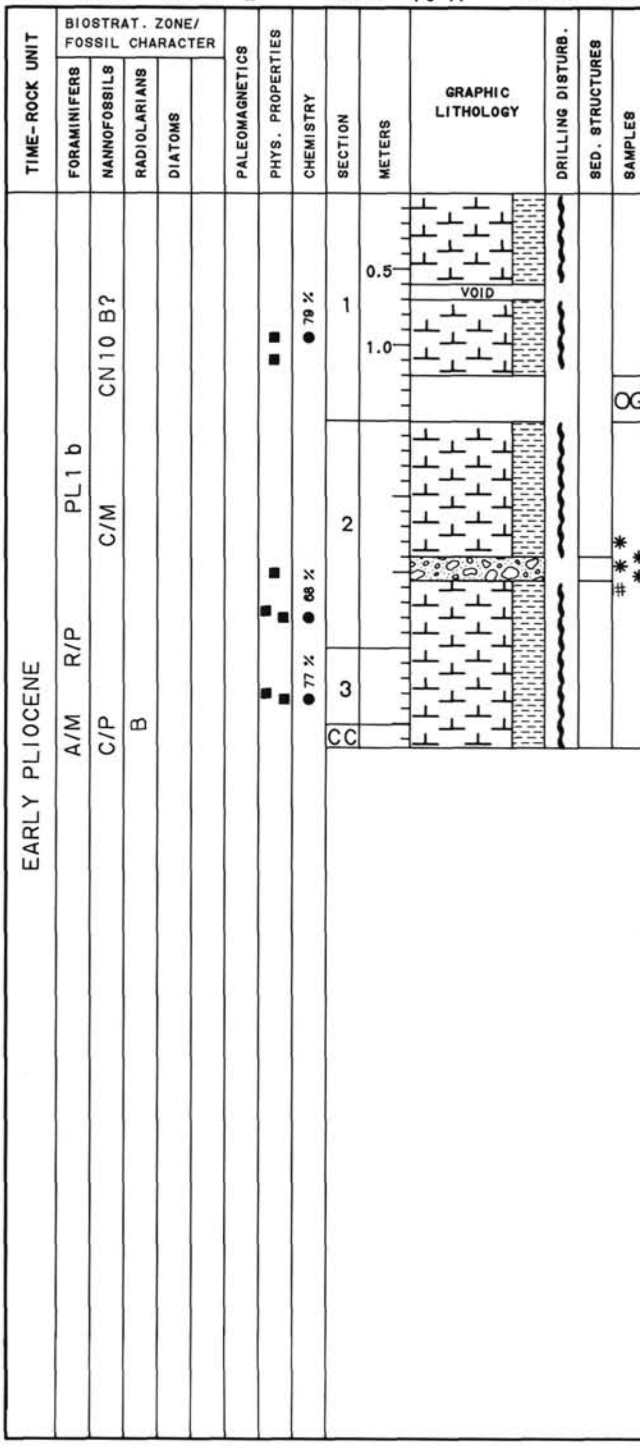

LITHOLOGIC DESCRIPTION

WHITE CLAYEY OOZE AND GREEN CLAYSTONE

This core consists dominantly of white (5Y8/1) clayey nannofossil ooze like the cores above. Section 2, 90-105 cm consists of green (10G4/2) claystone with black zeolitic clay laminae at the top and 1-2 cm clasts of black clay, nannofossil ooze and green clay from 97-105 cm. The unit appears to be a debris flow composed of clay and altered volcanic material.

SMEAR SLIDE AND THIN SECTION SUMMARY (%):

	2,83 D	2,91 M	2,93 M	2,98 D	2,119-123
TEXTURE:					
Sand	–	20	–	–	25
Silt	40	40	20	–	60
Clay	60	40	80	100	15
COMPOSITION:					
Feldspar	–	10	5	–	–
Clay	5	10	85	10	–
Volcanic Glass	–	20	–	–	–
Accessory Minerals:					
Opaque Minerals	–	20	10	–	–
Zeolites	–	10	–	–	–
Foraminifers	10	Tr	–	–	1
Nannofossils	85	30	–	90	–
Pellets	–	–	–	–	70
Bioclasts	–	–	–	–	1
Micrite	–	–	–	–	15
Microspar cement	–	–	–	–	13

PHYSICAL PROPERTIES DATA:

	1,96	1,105	2,100	1,125
$V\rho$ (c)	1.45	–	–	–
ρ_b	1.80	–	–	–
γ	–	11.89	–	27.75
T_c	–	–	2.56	–

	2,131	3,30	3,31
$V\rho$ (c)	1.52	–	–
ρ_b	1.85	–	1.84
T_c	–	2.89	–

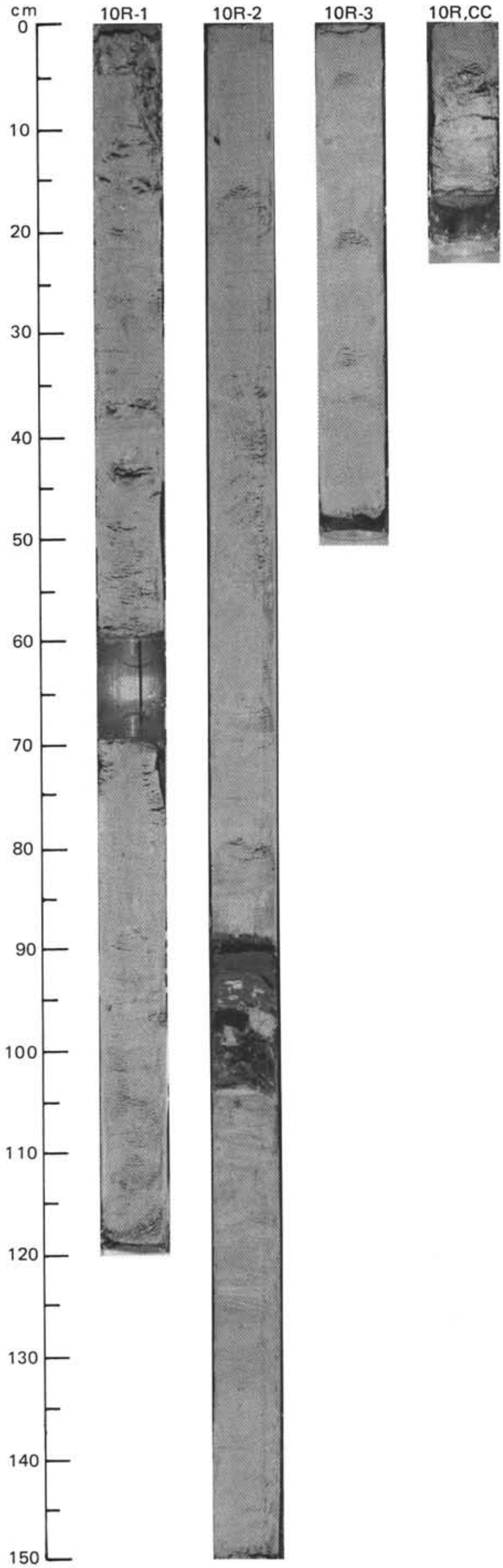
cm
0
10
20
30
40
50
60
70
80
90
100
110
120
130
140
150
10R-1
10R-2
10R-3
10R,CC

SITE 638 HOLE B CORE 11 R CORED INTERVAL 4756.4-4766.1 mbsl; 93.7-103.4 mbsf

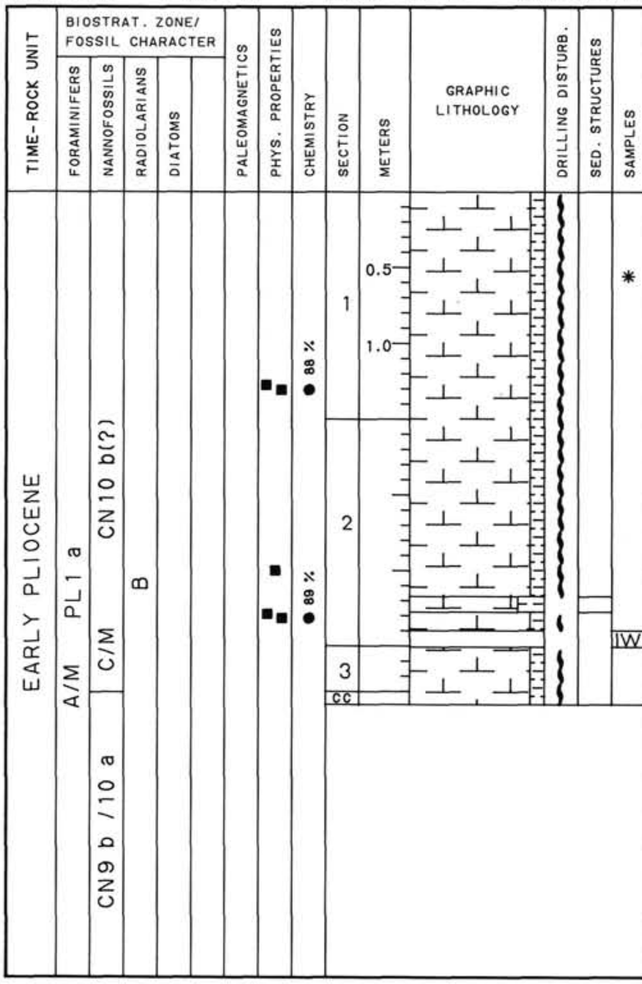

LITHOLOGIC DESCRIPTION

WHITE CLAYEY NANNOFOSSIL OOZE

This core consists of faintly laminated bluish white (N8 to 2.5Y8/0) clayey nannofossil ooze, slightly to moderately disturbed by drilling. Thin darker (2.5Y7/0) bands occur throughout. Subangular clasts (3-4 cm) of bioclastic packstone occur at Section 2, 118-123 cm.

SMEAR SLIDE SUMMARY (%):

	1,57
	D
TEXTURE:	
Silt	10
Clay	90
COMPOSITION:	
Foraminifers	10
Nannofossils	90

PHYSICAL PROPERTIES DATA:

	1,130	1,131	2,100	2,128	2,131
V_p (c)	–	1.62	–	–	1.62
ρ_b	–	1.90	–	–	1.90
γ	20.10	–	–	15.60	–
T_c	–	–	3.17	–	–

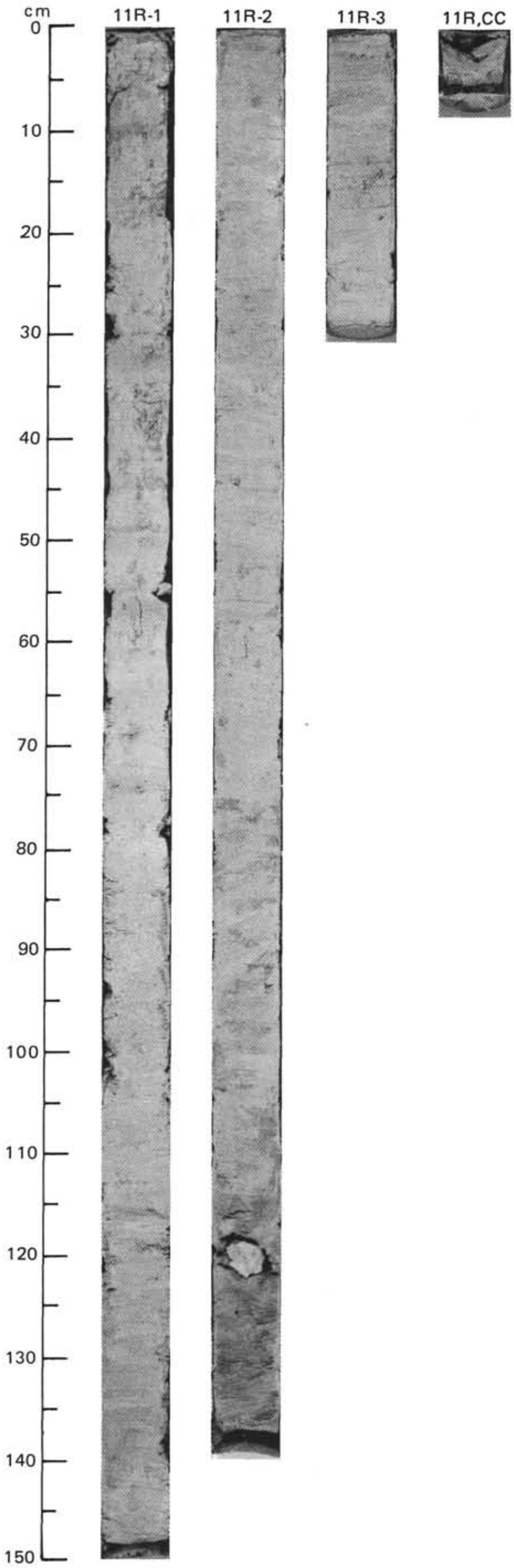
cm
0
10
20
30
40
50
60
70
80
90
100
110
120
130
140
150
11R-1
11R-2
11R-3
11R,CC

SITE 638 HOLE B CORE 12 R CORED INTERVAL 4766.1-4775.8 mbsl; 103.4-113.1 mbsf

TIME-ROCK UNIT	FORAMINIFERS	NANNOFOSSILS	RADIOLARIANS	DIATOMS	PALEOMAGNETICS	PHYS. PROPERTIES	CHEMISTRY	SECTION	METERS	GRAPHIC LITHOLOGY	DRILLING DISTURB.	SED. STRUCTURES	SAMPLES
LATE MIOCENE	N18 A/G	CN9 b/10 a C/M	B			■ ■■	● 99 %	1 CC	0.5 1.0	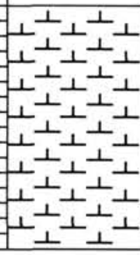			*

BIOSTRAT. ZONE/ FOSSIL CHARACTER

LITHOLOGIC DESCRIPTION

WHITE NANNOFOSSIL OOZE

This core consists of white (2.5Y8/1) to light gray (2.5Y7.5/1) foram-bearing nannofossil ooze. Purplish dark gray streaks (?manganese rich) occur throughout. The core is highly disturbed by drilling.

SMEAR SLIDE SUMMARY (%):

	1,94
	D
TEXTURE:	
Sand	15
Silt	5
Clay	80
COMPOSITION:	
Clay	15
Foraminifers	20
Nannofossils	65

PHYSICAL PROPERTIES DATA:

	1,95	1,105	1,107
V_p (c)	–	–	1.72
ρ_b	–	–	1.80
γ	–	17.60	–
T_c	3.03	–	–

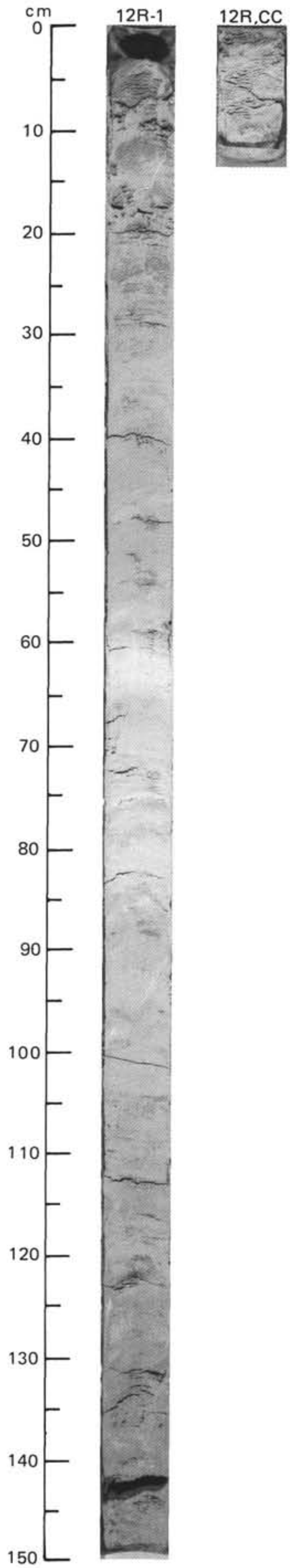
cm
12R-1
12R,CC
0
10
20
30
40
50
60
70
80
90
100
110
120
130
140
150

SITE 638 HOLE B CORE 13 R CORED INTERVAL 4775.8-4785.6 mbsl; 113.1-122.9 mbsf

TIME-ROCK UNIT	FORAMINIFERS	NANNOFOSSILS	RADIOLARIANS	DIATOMS	PALEOMAGNETICS	PHYS. PROPERTIES	CHEMISTRY	SECTION	METERS	GRAPHIC LITHOLOGY	DRILLING DISTURB.	SED. STRUCTURES	SAMPLES
LATE MIOCENE	N18	CN9 b/10 a				■ ■	● 85 %	1	0.5 1.0	VOID			*
								2					* OG
	A/G	C/M	B			■		3					
								CC					

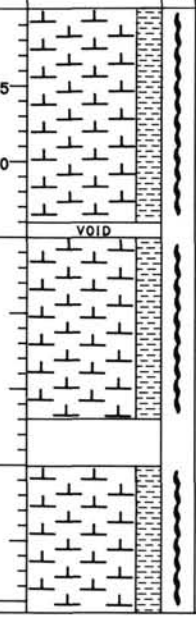

LITHOLOGIC DESCRIPTION

WHITE CLAYEY NANNOFOSSIL OOZE

This core consists of white (7.5YR8/0) clayey nannofossil ooze. Moderate to high drilling disturbance has obscured much of the structure; faint parallel lamination is discernible.

SMEAR SLIDE SUMMARY (%):

	1,83	2,90
	D	D
TEXTURE:		
Sand	5	5
Silt	2	2
Clay	93	93
COMPOSITION:		
Clay	15	10
Calcite/Dolomite	Tr	–
Foraminifers	7	7
Nannofossils	78	83

PHYSICAL PROPERTIES DATA:

	1,80	1,126	3,46
V_p (c)	1.73	–	–
ρ_b	1.99	–	–
γ	–	26.60	–
T_c	–	–	3.06

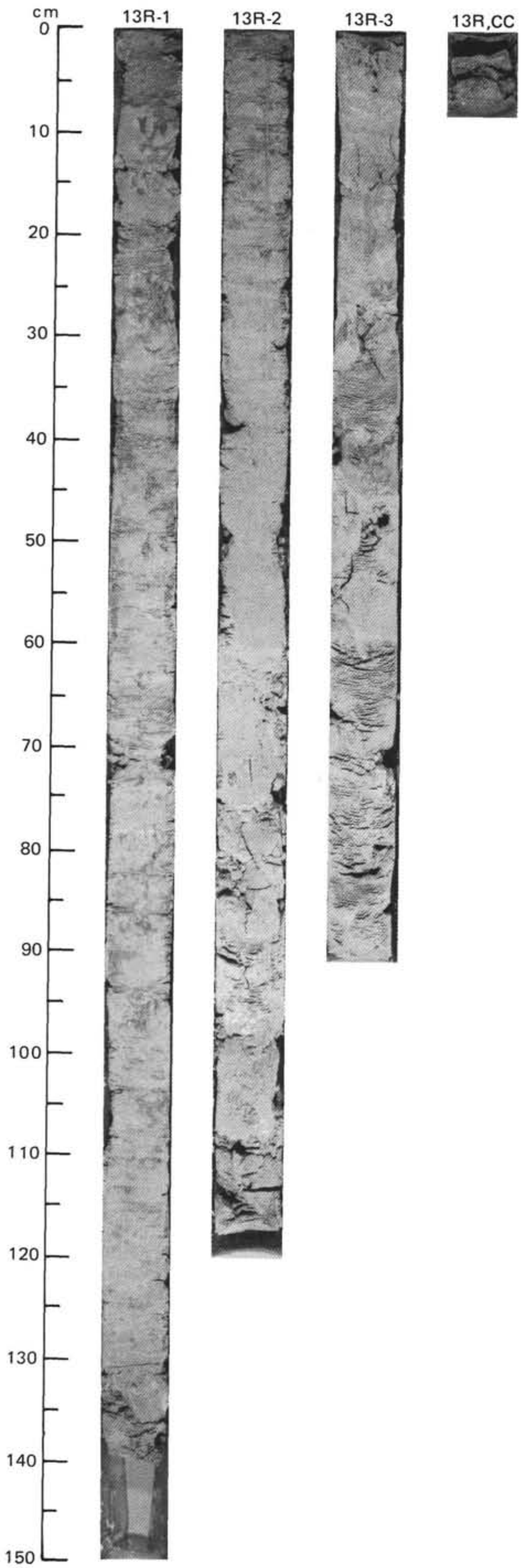
cm
0
10
20
30
40
50
60
70
80
90
100
110
120
130
140
150
13R-1
13R-2
13R-3
13R,CC

SITE 638 HOLE B CORE 14 R CORED INTERVAL 4785.6-4795.3 mbsl; 122.9-132.6 mbsf

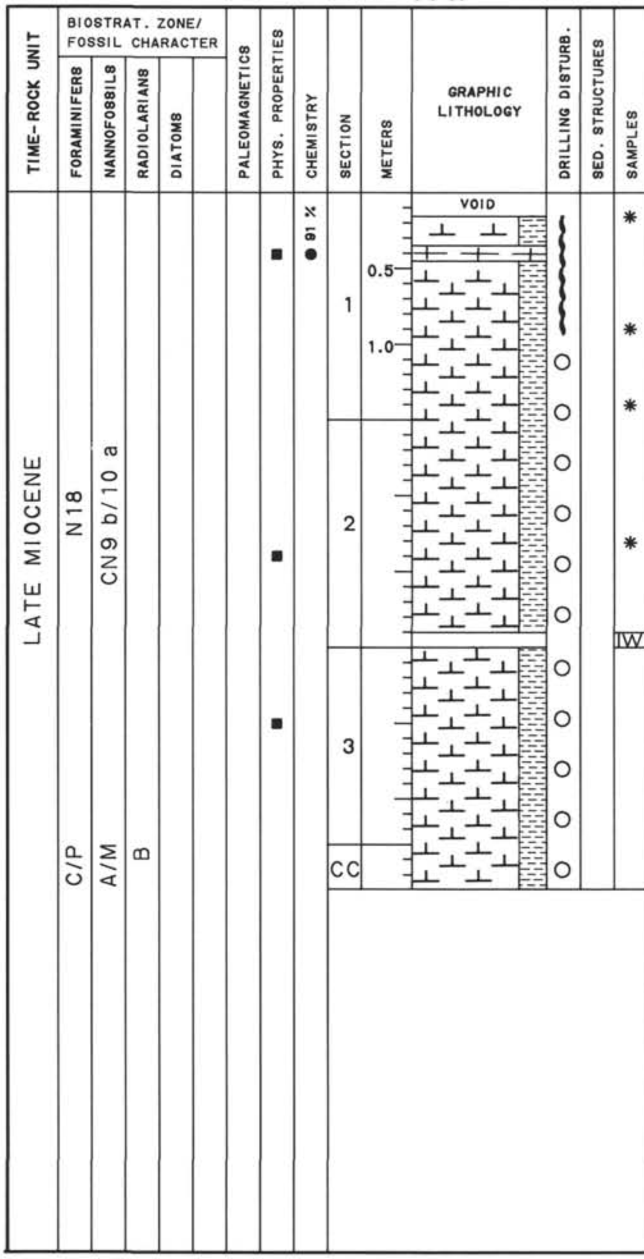

LITHOLOGIC DESCRIPTION

WHITE CLAYEY NANNOFOSSIL OOZE

Much of this core consists of a soupy drilling mixture of nannofossil ooze lumps. The upper part of Section 1 consists of stiff, white (5Y8/1) clayey nannofossil ooze. A band of pale yellow (2.5Y8/2) foraminiferal nannofossil ooze occurs at Section 1, 35-45 cm. Several clasts of dark greenish gray (5GY4/1) marl occur at Section 1, 133-140 cm. Drilling has destroyed any fine-scale structure.

SMEAR SLIDE SUMMARY (%):

	1,19 D	1,87 M	1,139 M	2,85 D
TEXTURE:				
Sand	–	5	Tr	–
Silt	10	35	15	7
Clay	90	60	85	93
COMPOSITION:				
Quartz	–	1	2	Tr
Mica	Tr	5	1	–
Clay	25	52	65	15
Calcite/Dolomite	–	5	Tr	–
Accessory Minerals (Opaques, Zeolites, Aggregrated clays= shale chips?)	Tr	2	5	–
Foraminifers	1	5	2	7
Nannofossils	74	30	25	78
Fish Remains	–	Tr	–	–

PHYSICAL PROPERTIES DATA:

	1,40	2,90	3,50
V_p (c)	1.71	–	–
ρ_b	1.94	–	–
T_c	–	2.80	2.86

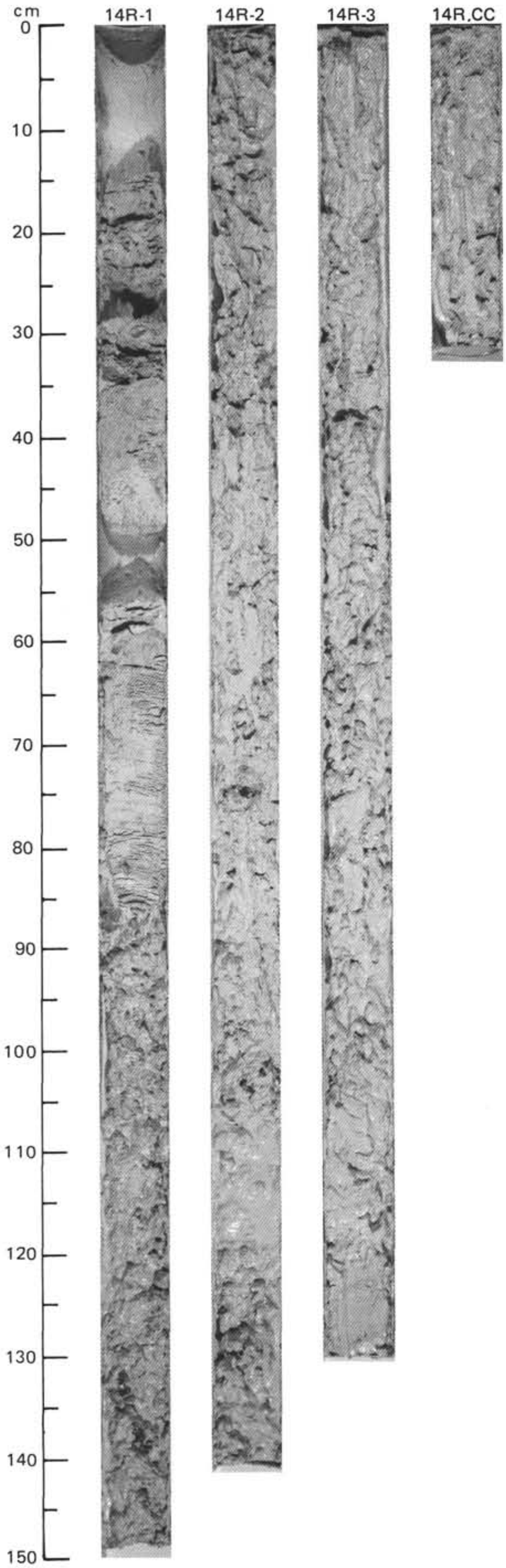
cm
0
10
20
30
40
50
60
70
80
90
100
110
120
130
140
150
14R-1
14R-2
14R-3
14R,CC

SITE 638 HOLE B CORE 15 R CORED INTERVAL 4795.3-4804.9 mbsl; 132.6-142.2 mbsf

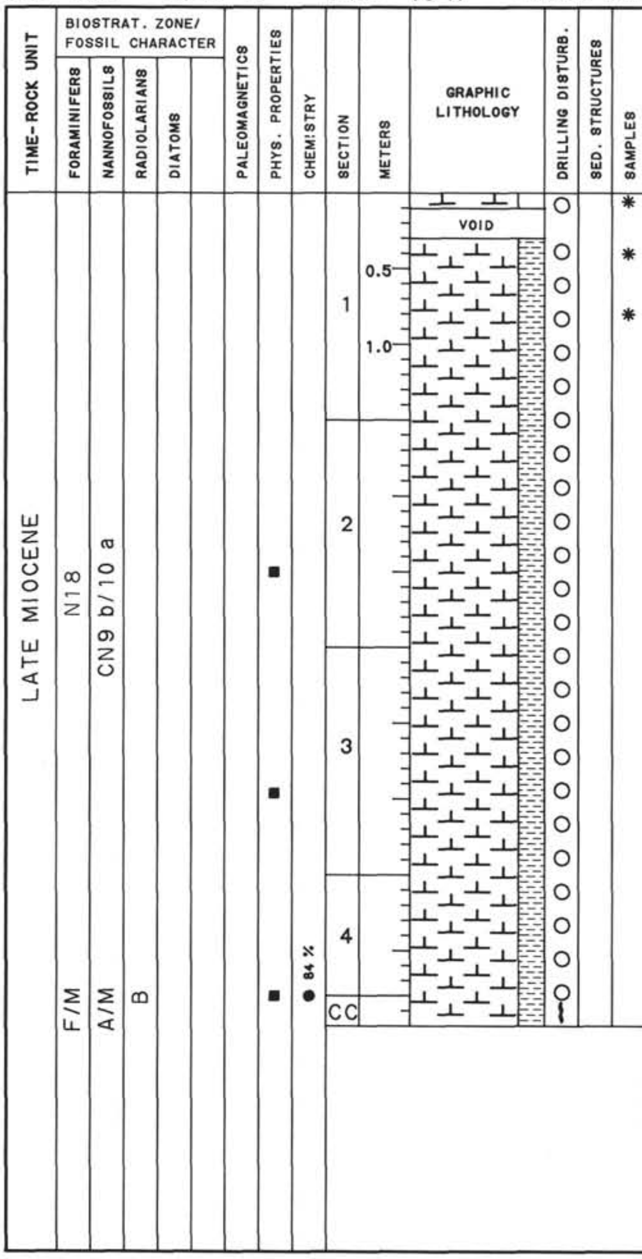

LITHOLOGIC DESCRIPTION

WHITE CLAYEY OOZE BRECCIA

This core consists of a soupy mixture of white (5Y8/1) clayey nannofossil ooze with scattered lumps of various lithologies: brownish marl, 'black shale', gray marl. No internal structure is discernable. This core (and Core 14) could be a drilling breccia composed of cavings or, conceivably, a debris flow further brecciated by drilling.

SMEAR SLIDE SUMMARY (%):

	1,2 M	1,42 M	1,80 D
TEXTURE:			
Sand	–	–	7
Silt	10	–	5
Clay	90	100	88
COMPOSITION:			
Quartz	Tr	–	–
Clay	90	97	15
Calcite/Dolomite	Tr	–	–
Accessory Minerals:			
Pyrite	Tr	–	–
Zeolites	10	1	Tr
Opaques	–	1	2
Foraminifers	–	–	10
Nannofossils	Tr	Tr	73
Radiolarians	–	Tr	–
Fish Remains	Tr	–	–
Plant Debris	–	1	–

PHYSICAL PROPERTIES DATA:

	2,100	3,95	4,81
V_p (c)	–	–	1.68
ρ_b	–	–	1.40
Tc	2.95	3.47	–

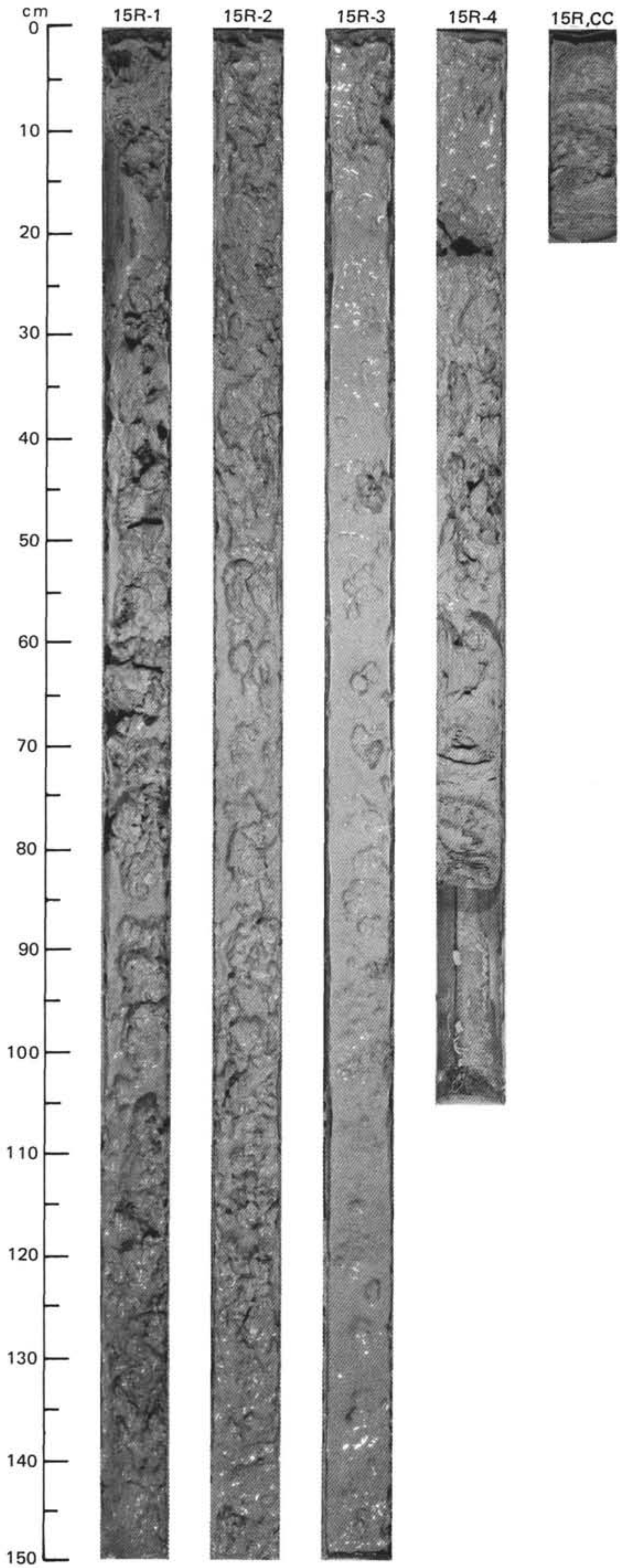
cm
15R-1
15R-2
15R-3
15R-4
15R,CC
0
10
20
30
40
50
60
70
80
90
100
110
120
130
140
150

SITE 638 HOLE B CORE 16 R CORED INTERVAL 4804.9-4814.5 mbsl; 142.2-151.8 mbsf

TIME-ROCK UNIT	FORAMINIFERS	NANNOFOSSILS	RADIOLARIANS	DIATOMS	PALEOMAGNETICS	PHYS. PROPERTIES	CHEMISTRY	SECTION	METERS	GRAPHIC LITHOLOGY	DRILLING DISTURB.	SED. STRUCTURES	SAMPLES
LATE MIOCENE	N18	CN9 b/10 a				■ ■ ■	● 81 %	1, 2, 3, CC	0.5, 1.0	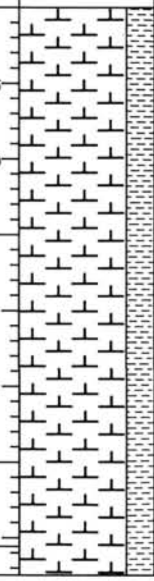			* *
	A/M	A/G	B										

WHITE CLAYEY OOZE

This core consists of stiff, white (2.5Y8/0) clayey nannofossil ooze, faintly laminated in greenish and grayish shades. Drilling disturbance is slight to moderate.

SMEAR SLIDE SUMMARY (%):

	1,78	2,90
	D	D
TEXTURE:		
Silt	30	5
Clay	70	95
COMPOSITION:		
Feldspar	Tr	Tr
Clay	–	5
Accessory Minerals (Zeolites, Opaques)	Tr	Tr
Foraminifers	5	5
Nannofossils	95	90

PHYSICAL PROPERTIES DATA:

	2,65	2,82	2,125
V_p (c)	–	1.75	–
ρ_b	–	2.03	–
γ	–	–	15.07
T_c	3.42	–	–

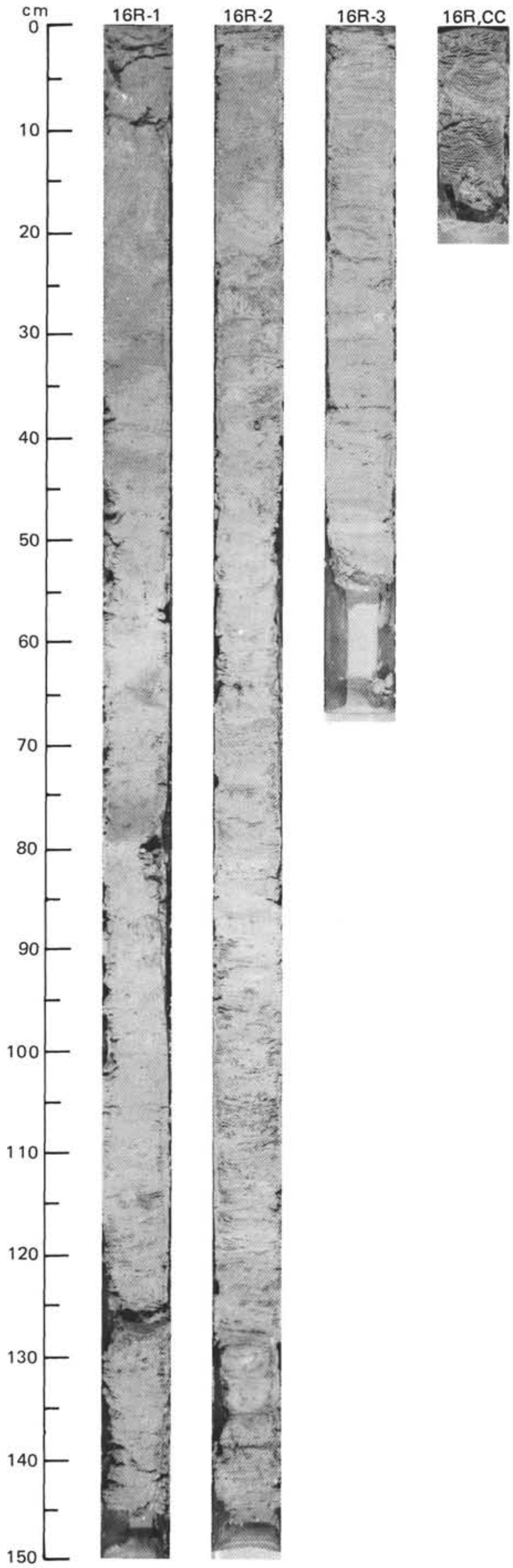
cm
16R-1
16R-2
16R-3
16R,CC
0
10
20
30
40
50
60
70
80
90
100
110
120
130
140
150

SITE 638 HOLE B CORE 17 R CORED INTERVAL 4814.5-4824.2 mbsl; 151.8-161.5 mbsf

TIME-ROCK UNIT	FORAMINIFERS	NANNOFOSSILS	RADIOLARIANS	DIATOMS	PALEOMAGNETICS	PHYS. PROPERTIES	CHEMISTRY	SECTION	METERS	GRAPHIC LITHOLOGY	DRILLING DISTURB.	SED. STRUCTURES	SAMPLES
LATE MIOCENE	N18 C/M	CN9 b C/M C/M	B			■	● % 85	1					**

LITHOLOGIC DESCRIPTION

GRAY CLAYEY OOZE

This core consists of 33 cm of pale gray (5Y7/11), structureless clayey nannofossil ooze. A 5 cm sandstone cobble was found at the bottom of the core resting in some patches of dark yellow-brown (10YR4/4) clay.

SMEAR SLIDE SUMMARY (%):

	1,16 D	CC D	CC M
TEXTURE:			
Silt	–	3	2
Clay	100	97	98
COMPOSITION:			
Quartz	–	–	1
Rock Fragments	–	–	1
Mica	Tr	–	88
Clay	5	20	–
Accessory Minerals (Pyrite, Zeolites)	–	2	Tr
Foraminifers	–	3	–
Nannofossils	95	75	10
Fish Remains	–	Tr	–

PHYSICAL PROPERTIES DATA:

	1,21
V_p (c)	1.67
ρ_b	1.98

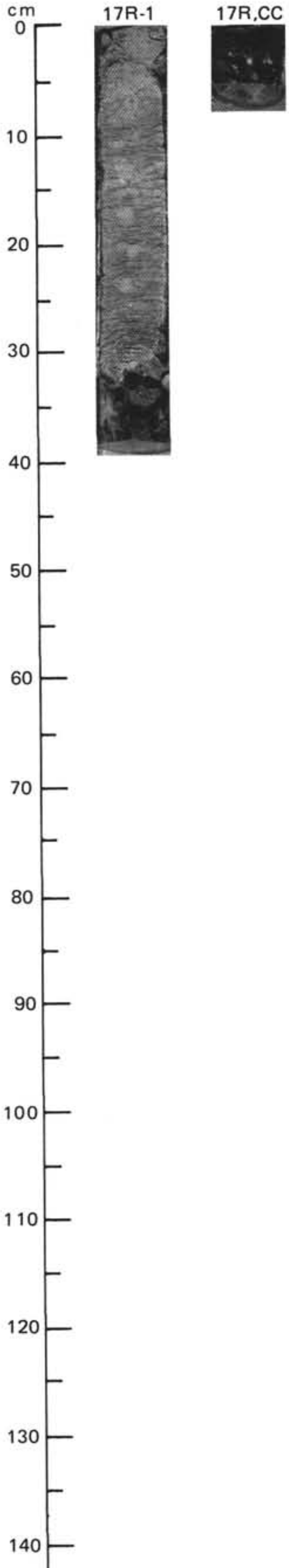
cm
17R-1
17R,CC
0
10
20
30
40
50
60
70
80
90
100
110
120
130
140
150

SITE 638 HOLE B CORE 18 R CORED INTERVAL 4824.2-4833.8 mbsl; 161.5-171.1 mbsf

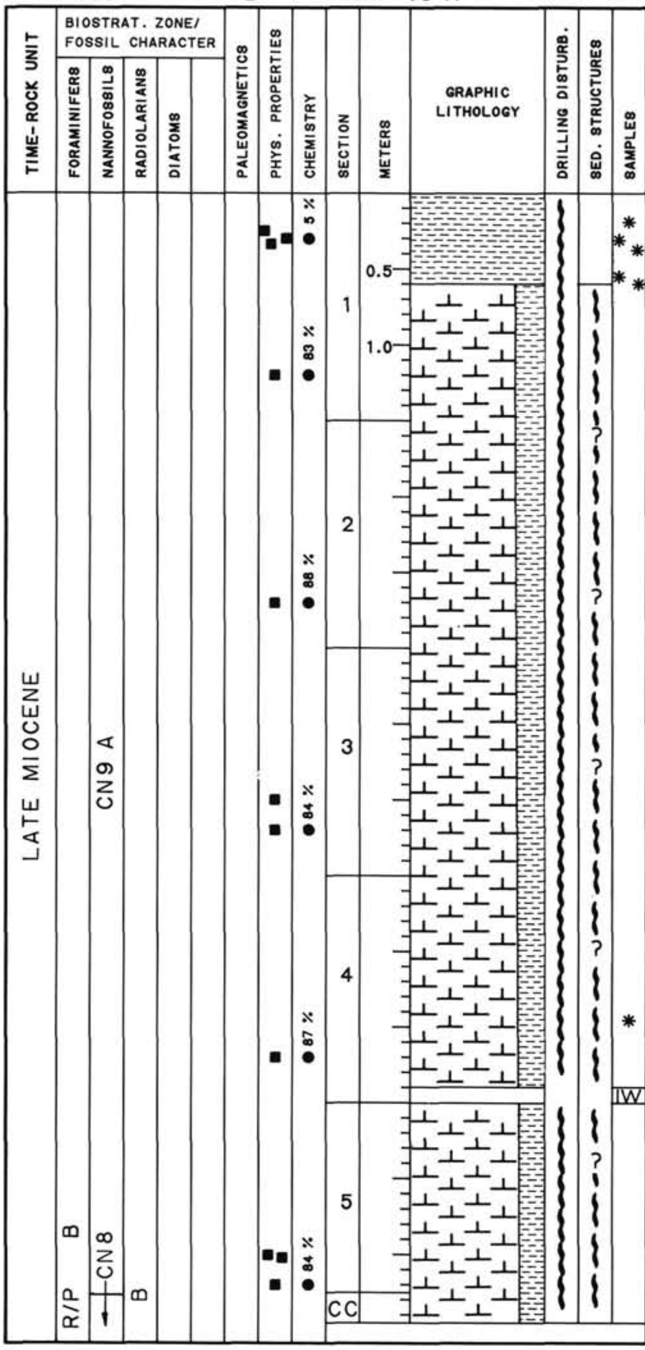

LITHOLOGIC DESCRIPTION

WHITE CLAYEY OOZE and BROWN CLAYSTONE

This core consists of 65 cm of reddish brown (10YR5/2) claystone overlying structureless, white (5GY8/1) clayey nannofossil ooze. In patches the ooze is sufficiently lithified to be considered a chalk.

SMEAR SLIDE SUMMARY (%):

	1,25 D	1,36 D	1,39 M	1,56 M	1,62 D	4,94 D
TEXTURE:						
Silt	10	10	10	10	30	15
Clay	90	90	90	90	70	85
COMPOSITION:						
Quartz	–	–	–	Tr	–	Tr
Feldspar	5	–	Tr	–	–	–
Mica	–	–	–	Tr	–	–
Clay	90	80	65	78	5	5
Volcanic Glass	–	–	5	–	–	–
Accessory Minerals (Fe Oxides, Zeolites)	5	20	10	2	–	Tr
Foraminifers	–	–	–	–	–	15
Nannofossils	–	Tr	20	20	95	80
Radiolarians	–	–	–	1	–	–

PHYSICAL PROPERTIES DATA:

	1,27	1,30	1,31	1,121	2,121	3,99
V_p (c)	–	–	2.22	1.11	–	–
ρ_b	–	–	1.79	1.86	1.93	–
γ	72.07	–	–	–	–	13.81
T_c	–	2.58	–	–	–	–

	3,121	4,121	5,99	5,100	5,121
V_p (c)	1.15	1.51	–	–	1.50
ρ_b	1.93	2.00	–	–	1.97
γ	–	–	45.70	–	–
T_c	–	–	–	3.40	–

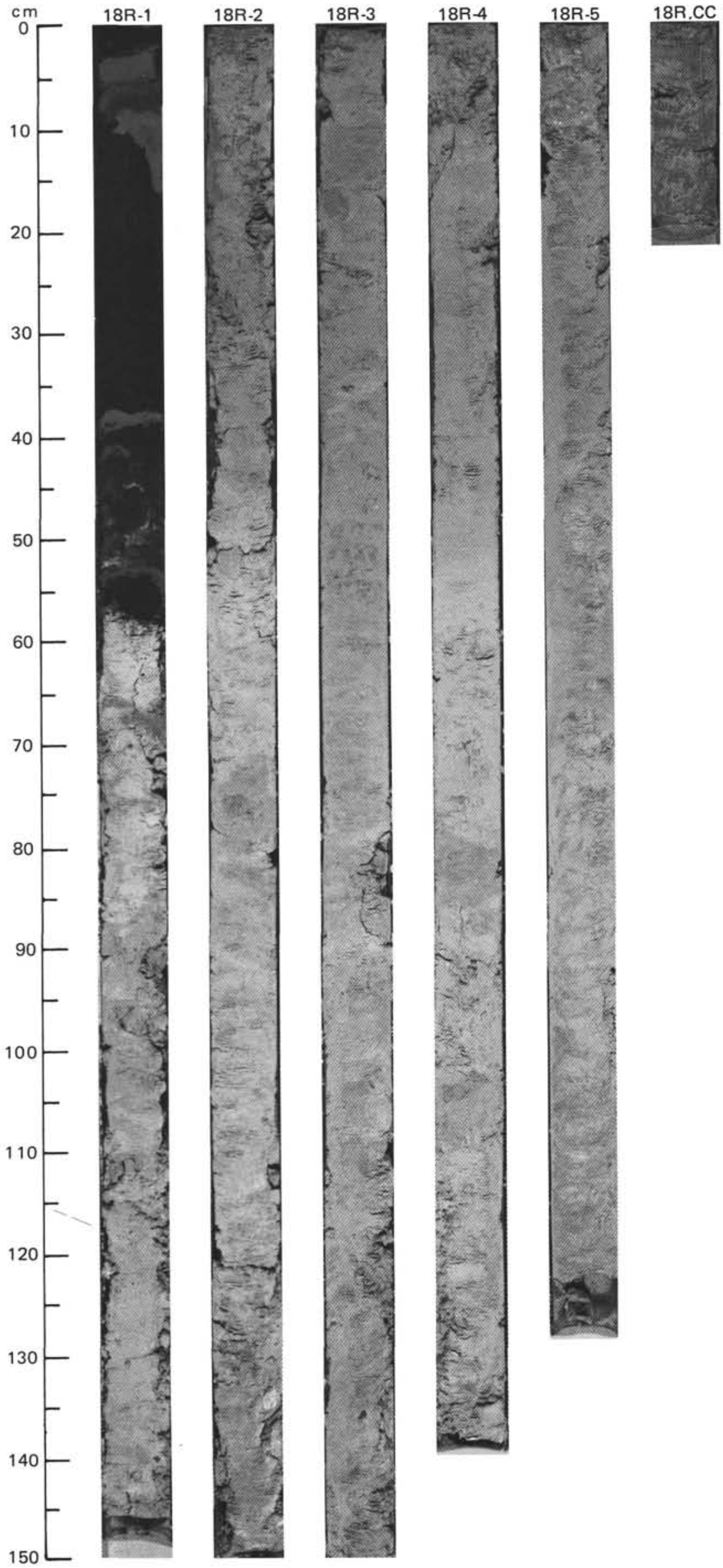
cm
0
10
20
30
40
50
60
70
80
90
100
110
120
130
140
150
18R-1
18R-2
18R-3
18R-4
18R-5
18R,CC

SITE 638 HOLE B CORE 19 R CORED INTERVAL 4833.8-4843.3 mbsl; 171.1-180.6 mbsf

TIME-ROCK UNIT	FORAMINIFERS	NANNOFOSSILS	RADIOLARIANS	DIATOMS		PALEOMAGNETICS	PHYS. PROPERTIES	CHEMISTRY	SECTION	METERS	GRAPHIC LITHOLOGY	DRILLING DISTURB.	SED. STRUCTURES	SAMPLES	LITHOLOGIC DESCRIPTION
LATE MIOCENE	N18 A/M	CN8 A/M	B				■	● 88 %	1 CC					*	

CLAYEY CHALK

This core consists of 35 cm of pale gray (5Y8/0) clayey nannofossil chalk with fine laminations dipping approximately 10 degrees.

SMEAR SLIDE SUMMARY (%):

	1,10
	D
TEXTURE:	
Silt	20
Clay	80
COMPOSITION:	
Calcite/Dolomite	45
Accessory Minerals (Pyrite)	5
Nannofossils	50

PHYSICAL PROPERTIES DATA:

	1,13
V_p	1.71
ρ_b	2.01

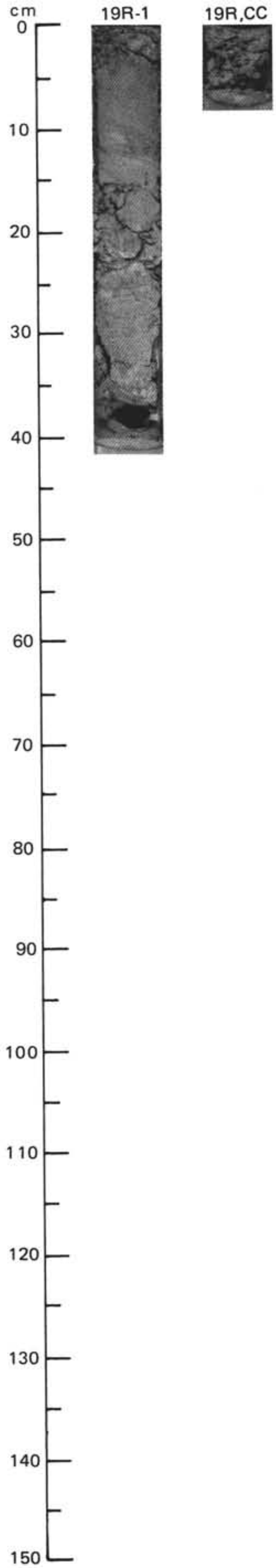
cm
19R-1
19R,CC
0
10
20
30
40
50
60
70
80
90
100
110
120
130
140
150

SITE 638 HOLE B CORE 20 R CORED INTERVAL 4843.3-4852.8 mbsl; 180.6-190.1 mbsf

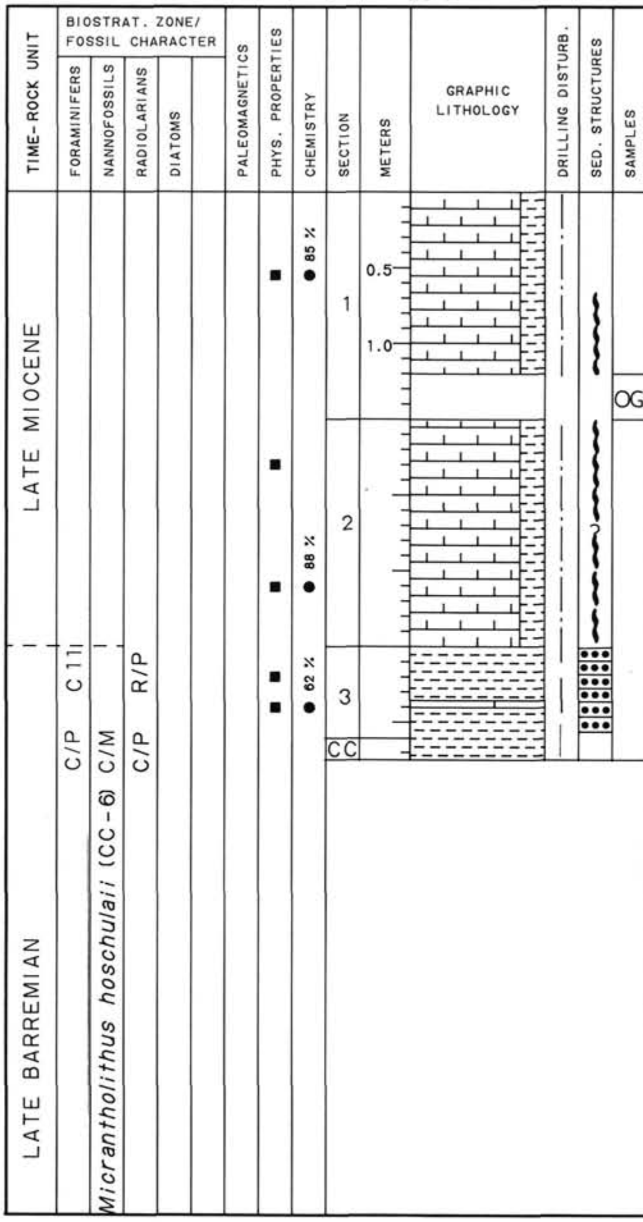

LITHOLOGIC DESCRIPTION

WHITE CLAYEY CHALK and GRAY CLASTIC TURBIDITES

This core shows a sequence of laminated, white (5Y7/1) clayey chalk overlying gray (5Y5/1), finely laminated turbidites. The laminations in the chalk dip ~15°. The turbidites consist of dark gray fine-silt layers that grade upwards into pale gray claystone and marl. Plant debris is common. The turbidites are horizontal laminated and are up to 4 cm thick. The contact between the turbidite unit and the overlying ooze is sharp with no sign of manganese pavement or a lag deposit.

PHYSICAL PROPERTIES DATA:

	1,55	2,30	2,109	3,20	3,39
$V\rho$ (c)	1.67	–	1.65	–	1.58
ρ_b	1.97	–	2.00	–	1.94
T_c	–	2.68	–	2.84	–

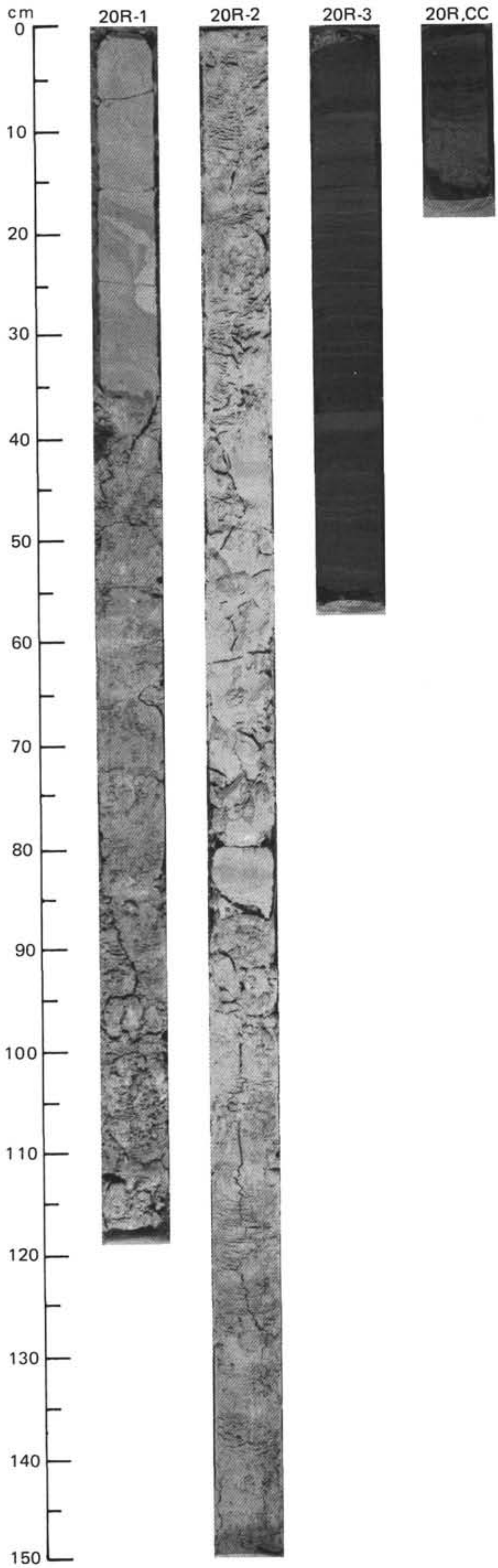
cm
0
10
20
30
40
50
60
70
80
90
100
110
120
130
140
150
20R-1
20R-2
20R-3
20R,CC

SITE 638 HOLE B CORE 21 R CORED INTERVAL 4852.8-4862.4 mbsl; 190.1-199.7 mbsf

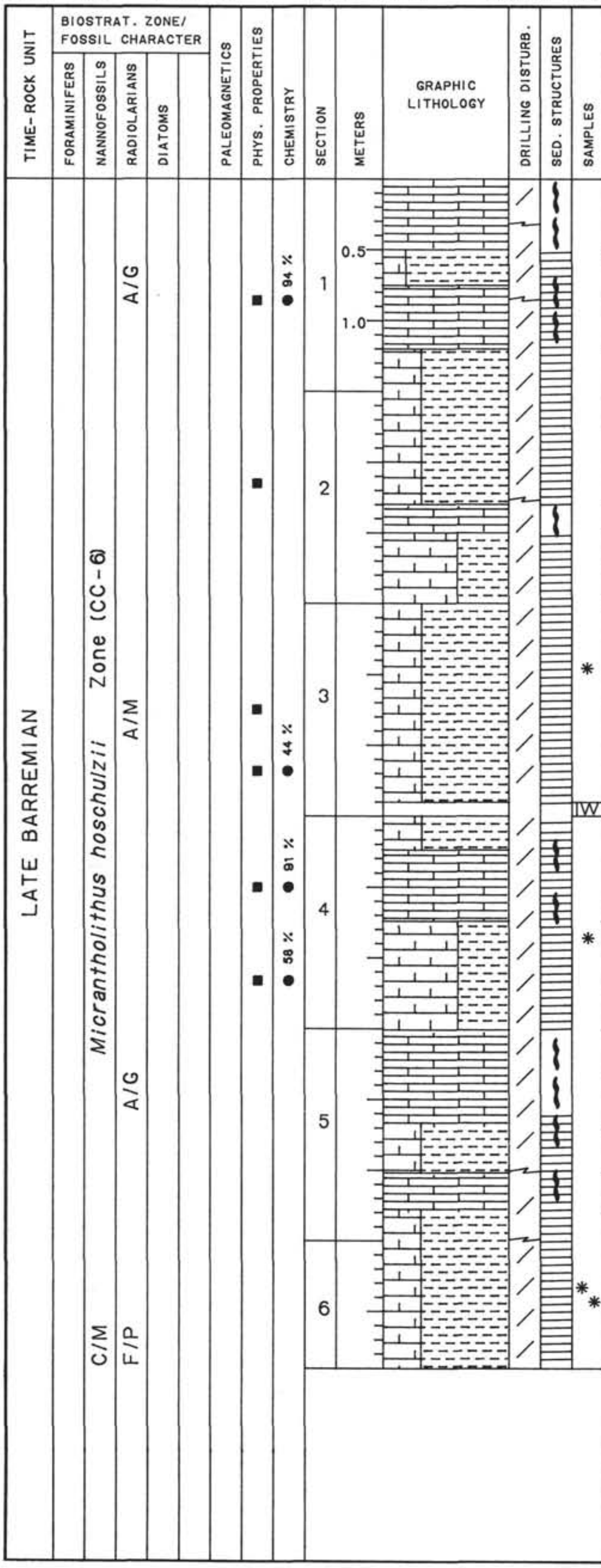

LITHOLOGIC DESCRIPTION

BIOTURBATED LIMESTONE, LAMINATED MARLSTONE and CLAYSTONE/MARLSTONE COUPLETS

The core consists of a regular alternation of the following lithologies: (the occurence of each lithology is indicated by a number on the right side of the "Samples" column)

1) Light gray (5Y7/1) micritic limestone and nannofossil marlstone, extensively bioturbated and locally showing faint banding and laminations.

2) Light gray to gray (5Y6/1 to 7/1) micritic limestone and calcareous claystone, vaguely laminated and weakly bioturbated.

3) Sequence of dark gray to dark olive gray (5Y4/1, 5Y3/2, 5Y4/2) calcareous claystone and light gray to light olive and greenish gray (5Y5/1 to 6/1, 5Y6/2, 5GY6/1) nannofossil marlstone couplets, parallel laminated and ranging in thickness from a few mm to 3-4 cm. Symbols given in 'Graphic lithology' column are schematic because thickness of couplets is too small to accurately display at this scale.

Lithologies 1 and 2 alternate in a generally cyclic fashion.

SMEAR SLIDE SUMMARY (%):

	3,46 M	4,85 M	6,36 M	6,38 M
TEXTURE:				
Sand	–	10	0	0
Silt	60	25	1	–
Clay	40	65	99	100
COMPOSITION:				
Quartz	–	10	1	–
Mica	–	1	–	–
Clay	35	50	56	66
Calcite/Dolomite	20	15	–	–
Accessory Minerals:				
Opaque Fe-Sulfide	1	–	Tr	2
Zeolites	–	4	1	1
Peloids	–	10	–	–
Foraminifers	–	Tr	2	–
Nannofossils	43	10	40	30
Plant Debris	1	–	Tr	1

PHYSICAL PROPERTIES DATA:

	1,85	2,65	3,72	3,119	4,54	4,116
V_p (a)	2.80	–	–	–	3.25	–
V_p (b)	3.01	–	–	–	3.36	–
V_p (c)	3.07	–	–	1.67	3.24	1.82
ρ_b	2.42	–	–	1.82	2.38	1.99
T_c	–	3.63	3.00	–	–	–

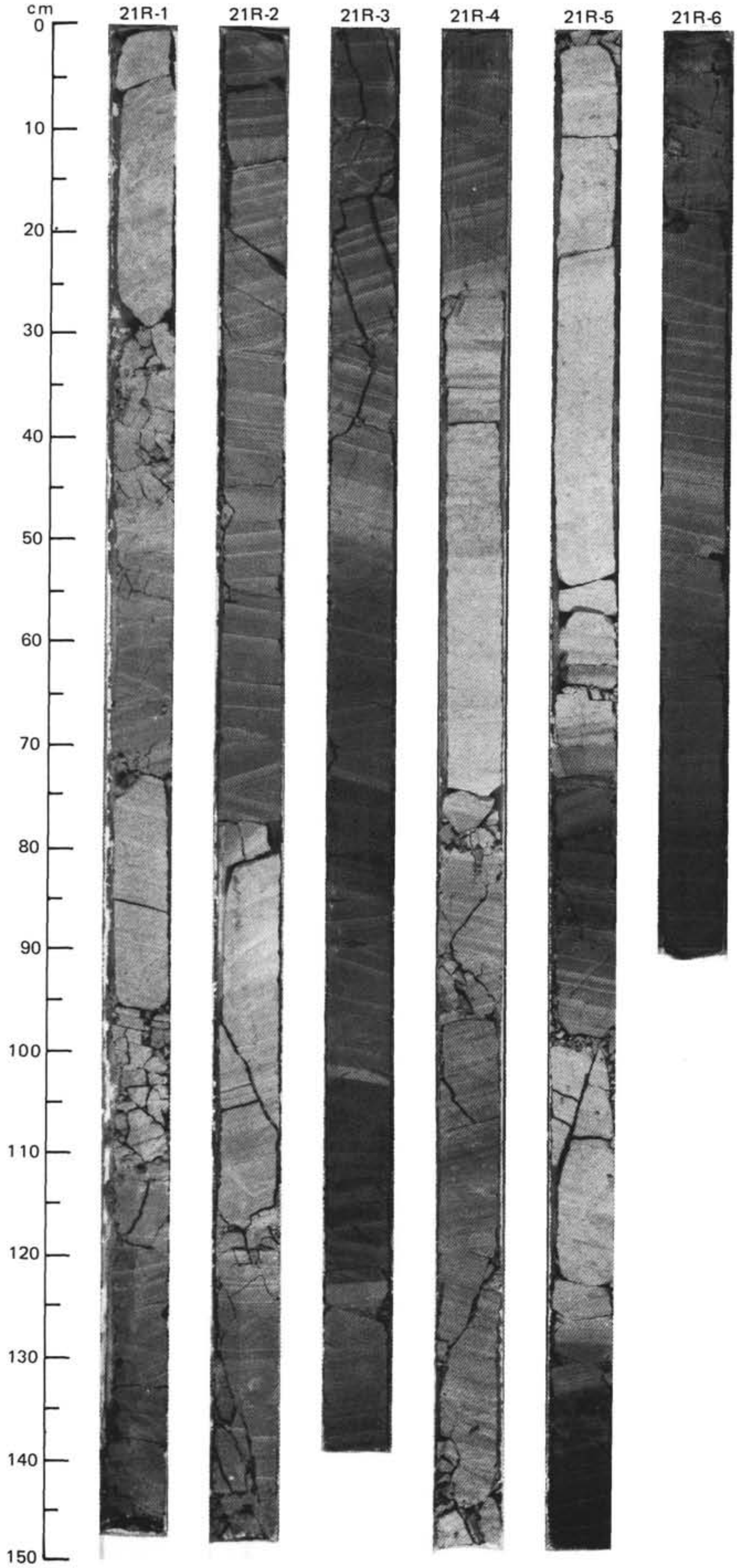
cm
0
10
20
30
40
50
60
70
80
90
100
110
120
130
140
150
21R-1
21R-2
21R-3
21R-4
21R-5
21R-6

SITE 638 HOLE B CORE 22 R CORED INTERVAL 4862.4-4872.0 mbsl; 199.7-209.3 mbsf

TIME-ROCK UNIT	BIOSTRAT. ZONE/ FOSSIL CHARACTER: FORAMINIFERS	NANNOFOSSILS	RADIOLARIANS	DIATOMS	PALEOMAGNETICS	PHYS. PROPERTIES	CHEMISTRY	SECTION	METERS	GRAPHIC LITHOLOGY	DRILLING DISTURB.	SED. STRUCTURES	SAMPLES
LATE BARREMIAN	C9-10	*Micrantholithus hoschulzii* Zone (CC-6)	C/M			■	● 93 %	1	0.5 1.0				#
						■■	● 53 %	2 3					#
						■	● 93 %	3					
						■		4					
								5					
	R/P	A/M	C/P					CC					

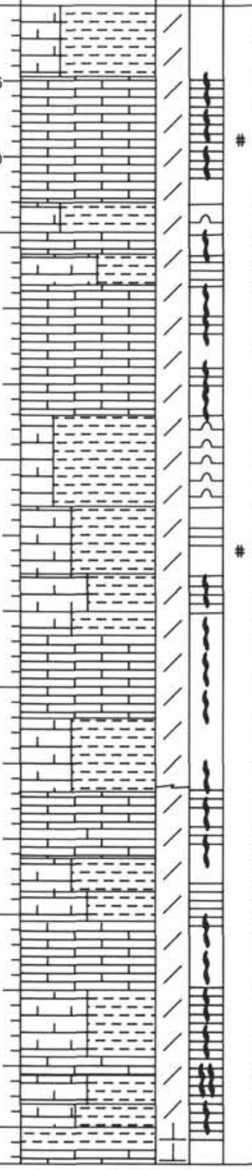

BIOTURBATED LIMESTONE, LAMINATED MARLSTONE, AND CLAYSTONE/MARLSTONE COUPLETS

The core consists of a regular alternation of the following lithologies: (the occurence of each lithology is indicated by a number on the right side of the "Samples" column)

1) Light gray (5Y7/1) micritic limestone and nannofossil marlstone, extensively bioturbated and locally showing faint banding and laminations.

2) Light gray to gray (5Y6/1 to 7/1) micritic limestone and calcareous claystone, vaguely laminated and weakly bioturbated.

3) Sequence of regular, dark gray to dark olive gray (5Y4/1, 5Y3/2, 5Y4/2) calcareous claystone and light gray to light olive and greenish gray (5Y5/1 to 6/1, 5Y6/2, 5GY6/1) nannofossil marlstone couplets, parallel laminated and ranging in thickness from a few mm to 3-4 cm. Symbols given in 'Graphic lithology' column are schematic, because thickness of couplets is too small to accurately display at this scale.

Lithologies 1 and 2 alternate in a generally cyclic fashion. Matrix-supported breccia layers occur in Section 1, 130-150 cm, and Section 2, 120 cm, to Section 3, 30 cm. One coarse-grained carbonate turbidite occurs in Section 3, 114 to 130 cm.

THIN SECTION SUMMARY (%):

	1,94-96 D
TEXTURE:	
Sand	5
Silt	15
Clay	80
COMPOSITION:	
Quartz	Tr
Accessory Minerals:	
Pyrite	1
Radiolarians (calcified)	18
Plant Debris	1
Micrite	80

PHYSICAL PROPERTIES DATA:

	1,113	3,57	3,60	3,135	4,60
V_p (a)	3.66	1.64	–	3.07	–
V_p (b)	3.47	–	–	3.25	–
V_p (c)	3.68	1.66	–	3.09	–
ρ_b	2.76	1.89	–	2.73	–
T_c	–	–	3.06	–	2.86

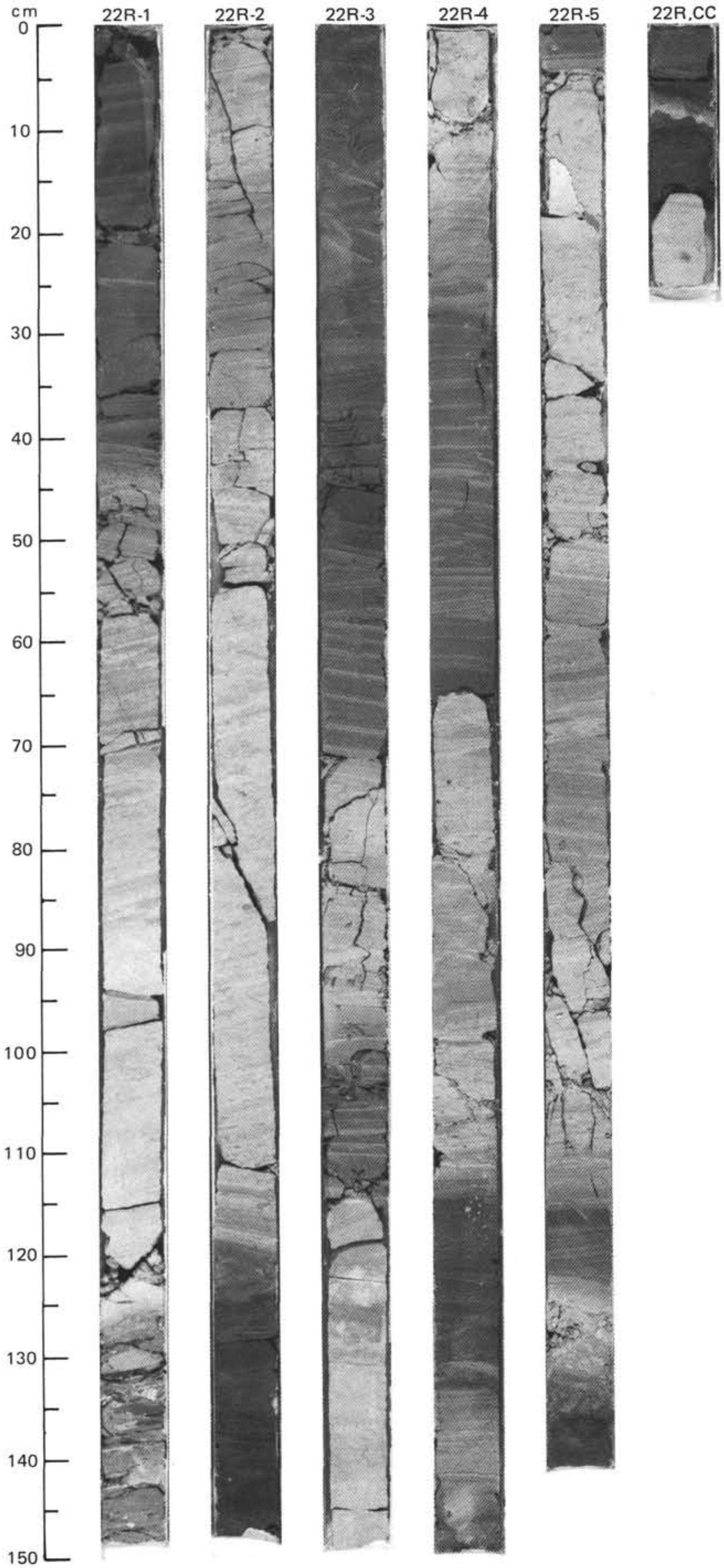
cm
0
10
20
30
40
50
60
70
80
90
100
110
120
130
140
150
22R-1
22R-2
22R-3
22R-4
22R-5
22R,CC

SITE 638 HOLE B CORE 23 R CORED INTERVAL 4872.0-4881.5 mbsl; 209.3-218.8 mbsf

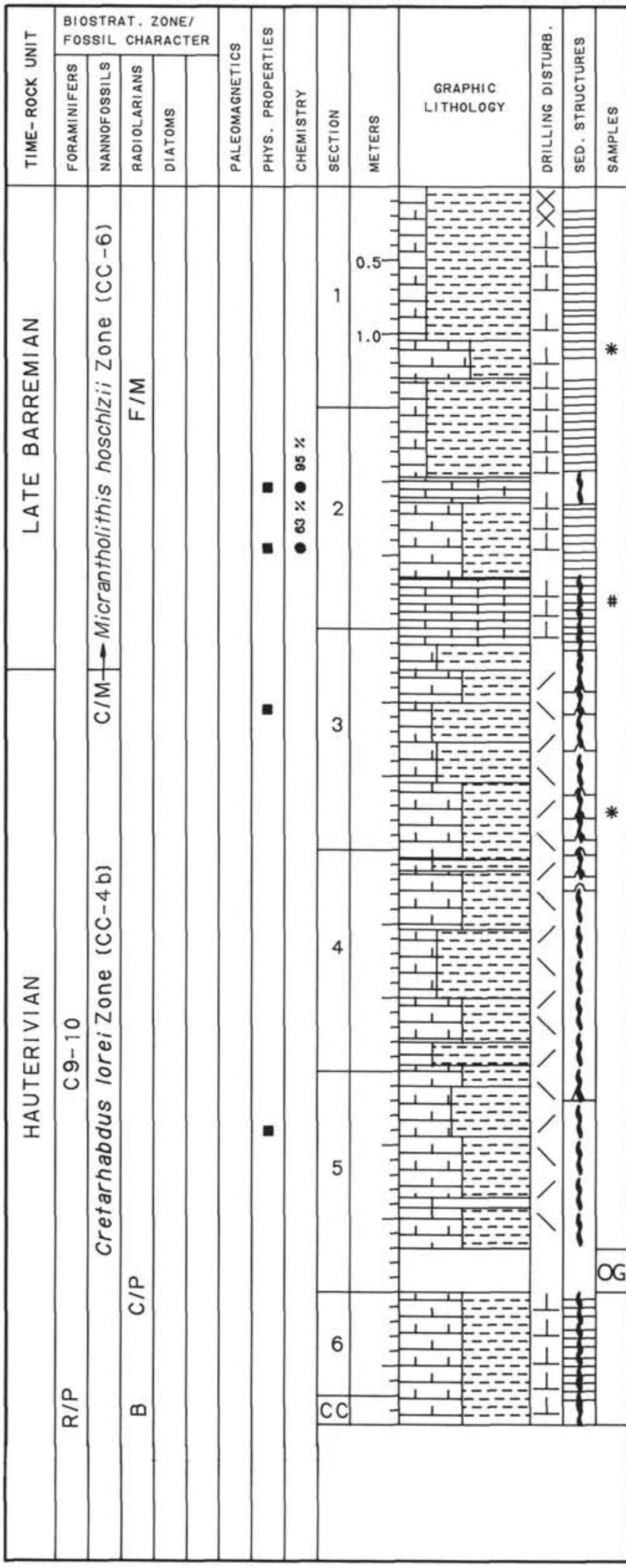

LITHOLOGIC DESCRIPTION

CALCAREOUS CLAYSTONE/MARLSTONE COUPLETS (Section 1, 0 cm, to Section 3, 27 cm)

Dark gray to dark olive gray (5Y4/1 to 6/1, 5Y3/2) calcareous claystone and light gray to light olive and greenish gray (5Y5/1 to 6/1, 5Y6/2, 5GY6/1) nannofossil marlstone couplets (turbidites), faintly graded and parallel laminated (equivalent to Lithology (3) of Cores 638B-21 and -22). Symbols given in 'Graphic lithology' column are schematic, because thickness of couplets is too small to accurately display at this scale. One thin layer of fine-grained, clayey sandstone is present in Section 1, 103-106 cm.

BIOTURBATED NANNOFOSSIL MARLSTONE (Section 3, 27 cm, to Section CC, 20 cm)

Dominantly light gray (N/5, N/6), faintly greenish (5G6/1 to 7/1), bioturbated nannofossil marlstone, convolute and plastically deformed (bed is slumped). Drilling deformation is severe throughout.

SMEAR SLIDE AND THIN SECTION SUMMARY (%):

	1,103 M	2,129-131 D	3,124 M
TEXTURE:			
Sand	30	5	–
Silt	18	10	2
Clay	52	85	98
COMPOSITION:			
Quartz	30	–	Tr
Rock Fragments	3	–	–
Mica	2	–	–
Clay	37	–	68
Calcite/Dolomite	–	–	Tr
Accessory Minerals:			
Opaques	1	1	2
Zeolites	Tr	–	–
Zircon	Tr	–	–
Foraminifers	Tr	–	–
Nannofossils	15	–	30
Radiolarians	Tr	15	–
Plant Debris	Tr	Tr	–
Micrite	12	84	–
Phosphatic Material	–	Tr	–
Ostracod? shell	–	Tr	–

PHYSICAL PROPERTIES DATA:

	2,53	2,93	3,51	5,40
V_p (a)	3.24	1.67	–	–
V_p (b)	3.44	1.76	–	–
V_p (c)	3.35	1.64	–	–
ρ_b	2.51	1.97	–	–
T_c	–	–	3.00	3.23

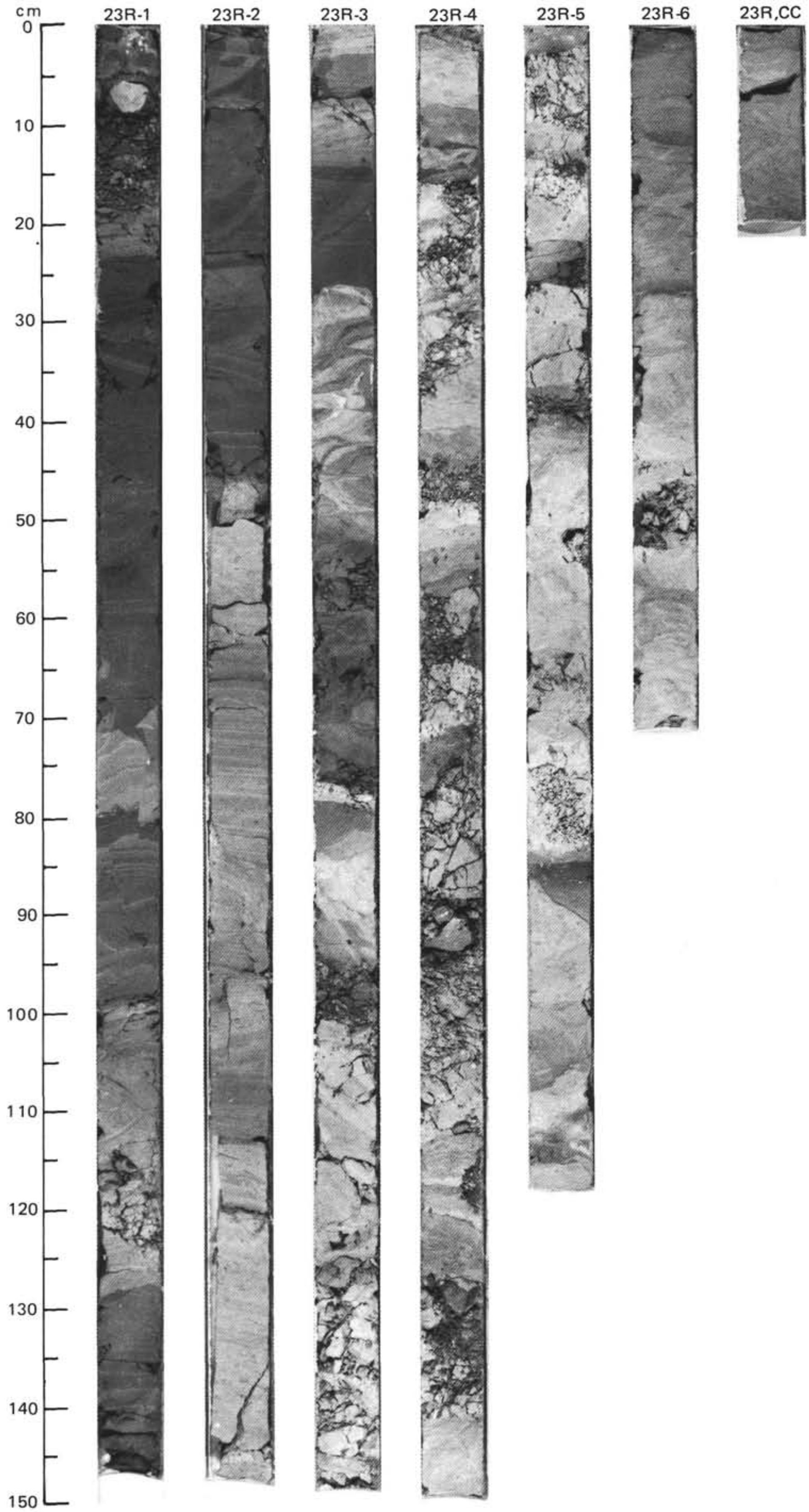
cm
0
10
20
30
40
50
60
70
80
90
100
110
120
130
140
150
23R-1
23R-2
23R-3
23R-4
23R-5
23R-6
23R,CC

SITE 638 HOLE B CORE 24 R CORED INTERVAL 4881.5-4891.1 mbsl; 218.8-228.4 mbsf

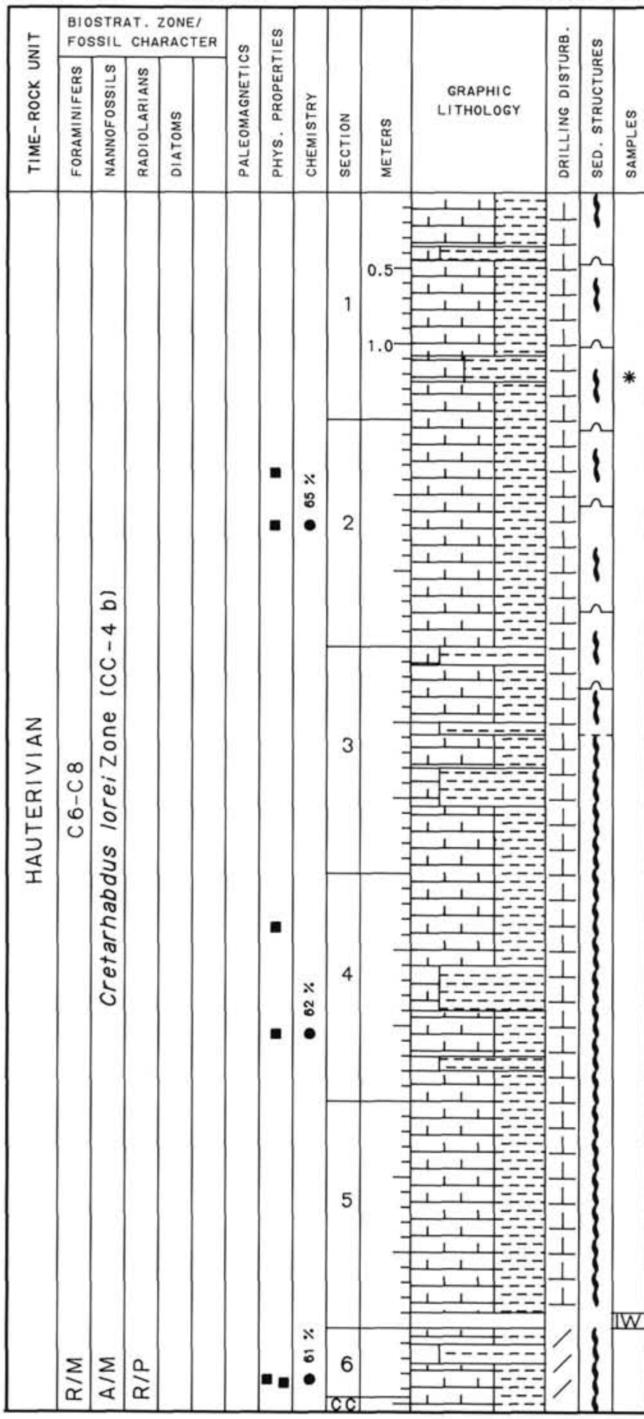

LITHOLOGIC DESCRIPTION

LIGHT GRAY, BIOTURBATED NANNOFOSSIL MARLSTONE

Light greenish to greenish gray (5Y4/1 to 5/1 to 6/1), bioturbated nannofossil marlstone and calcareous claystone, alternating in a cyclic fashion. Convolute and plastically deformed beds occur in Sections 1 and 2 (slumped bed). Drilling disturbance is severe throughout the core.

SMEAR SLIDE SUMMARY (%):

	1,120 M
TEXTURE:	
Clay	100
COMPOSITION:	
Quartz	Tr
Clay	62
Calcite/Dolomite	1
Accessory Minerals:	
Opaques	4
Nannofossils	33
Fish Remains	Tr

PHYSICAL PROPERTIES DATA:

	2,35	2,70	4,35	4,106	6,34	6,35
V_p (c)	–	1.74	–	1.68	1.75	–
ρ_b	–	2.00	–	1.98	2.05	–
T_c	3.43	–	3.50	–	–	3.44

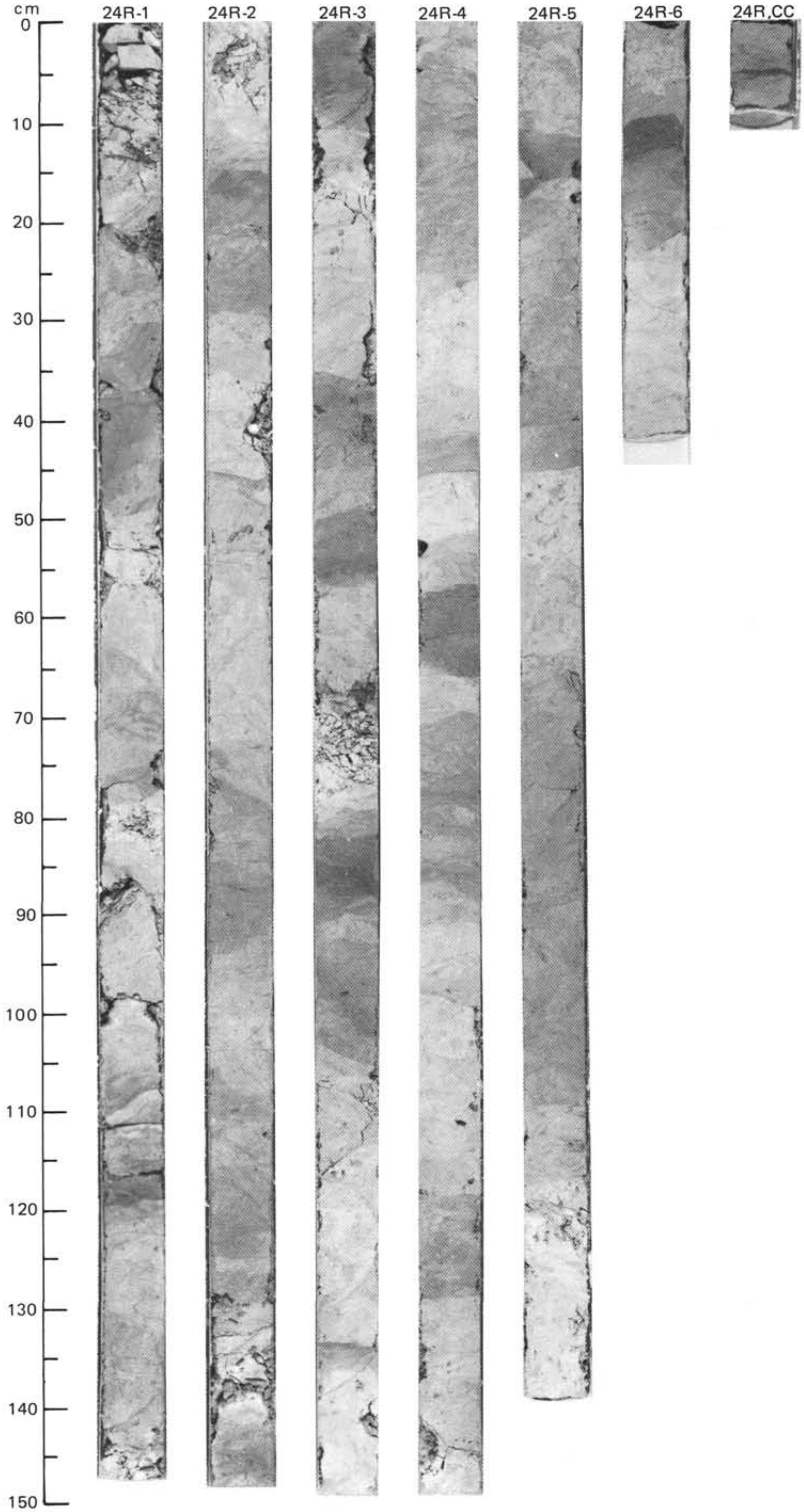

cm
0
10
20
30
40
50
60
70
80
90
100
110
120
130
140
150
24R-1
24R-2
24R-3
24R-4
24R-5
24R-6
24R,CC

SITE 638 HOLE B CORE 25 R CORED INTERVAL 4891.1-4900.8 mbsl; 228.4-238.1 mbsf

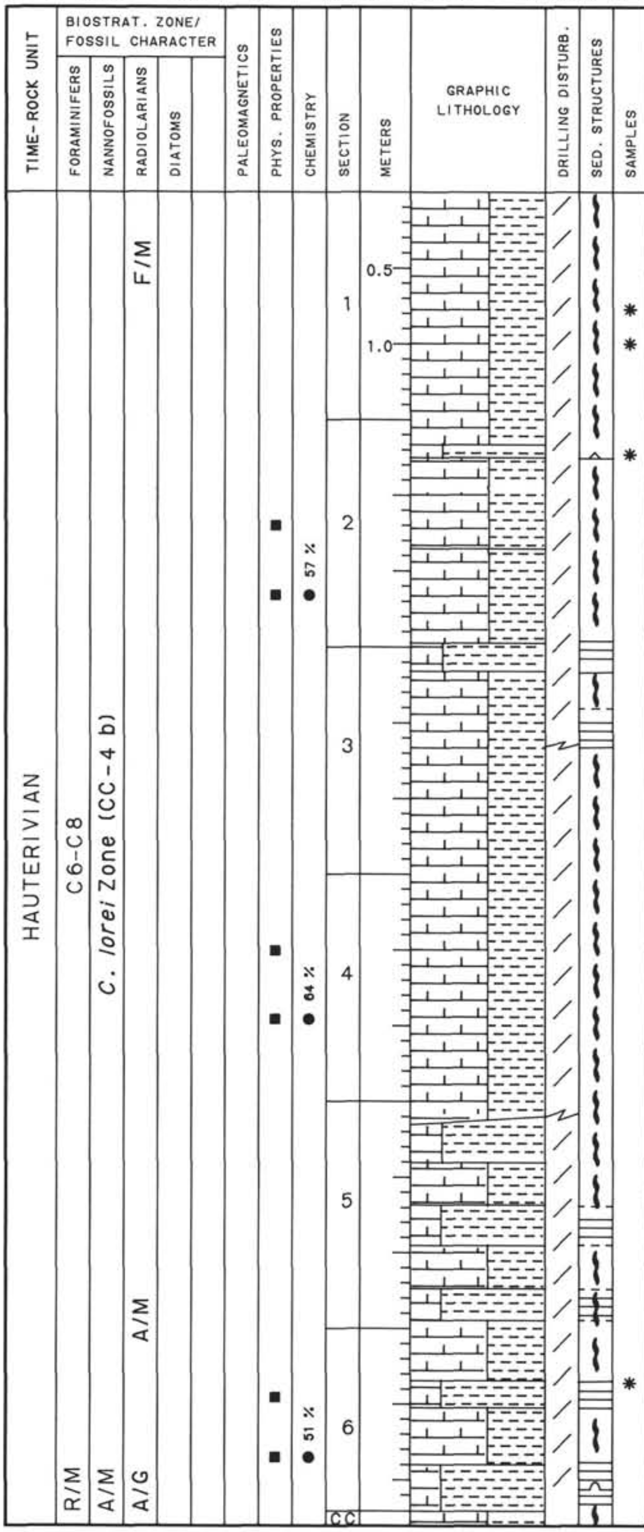

LITHOLOGIC DESCRIPTION

LIGHT GRAY, BIOTURBATED NANNOFOSSIL MARLSTONE

Dominantly light gray (N/4, N/5), faintly greenish (5G6/1 to 7/1), bioturbated nannofossil marlstone alternating in a cyclic fashion with dark gray (5Y4/1) calcareous claystone horizons. Local concentrations of very finely divided pyrite and detrital material (silt and wood fragments) are common. Several layers, a few centimeters thick, of calcareous claystone and graded silt occur in Section 2, 20 cm, 45 cm and 88 cm. A slumped bed is present in Section 6, 87 to 120 cm.

SMEAR SLIDE SUMMARY (%):

	1,80 D	1,100 M	2,23 D	6,42 M
TEXTURE:				
Sand	–	–	–	1
Silt	40	30	5	19
Clay	60	70	95	80
COMPOSITION:				
Quartz	–	–	–	2
Feldspar	–	–	Tr	Tr
Mica	–	–	2	Tr
Clay	40	30	71	77
Volcanic Glass	–	5	–	–
Calcite/Dolomite	–	5	2	4
Accessory Minerals:				
Opaques	–	–	3	3
Zeolites	–	10	5	Tr
Organic Matter	–	10	2	–
Nannofossils	60	40	15	10
Radiolarians	–	–	–	2
Fish Remains	–	–	–	1
Plant Debris	Tr	–	–	1

PHYSICAL PROPERTIES DATA:

	2,70	2,112	4,47	4,96	6,47	6,84
V_p (c)	–	1.76	–	1.75	–	1.69
ρ_b	–	2.06	–	1.99	–	1.97
T_c	3.64	–	3.21	–	3.06	–

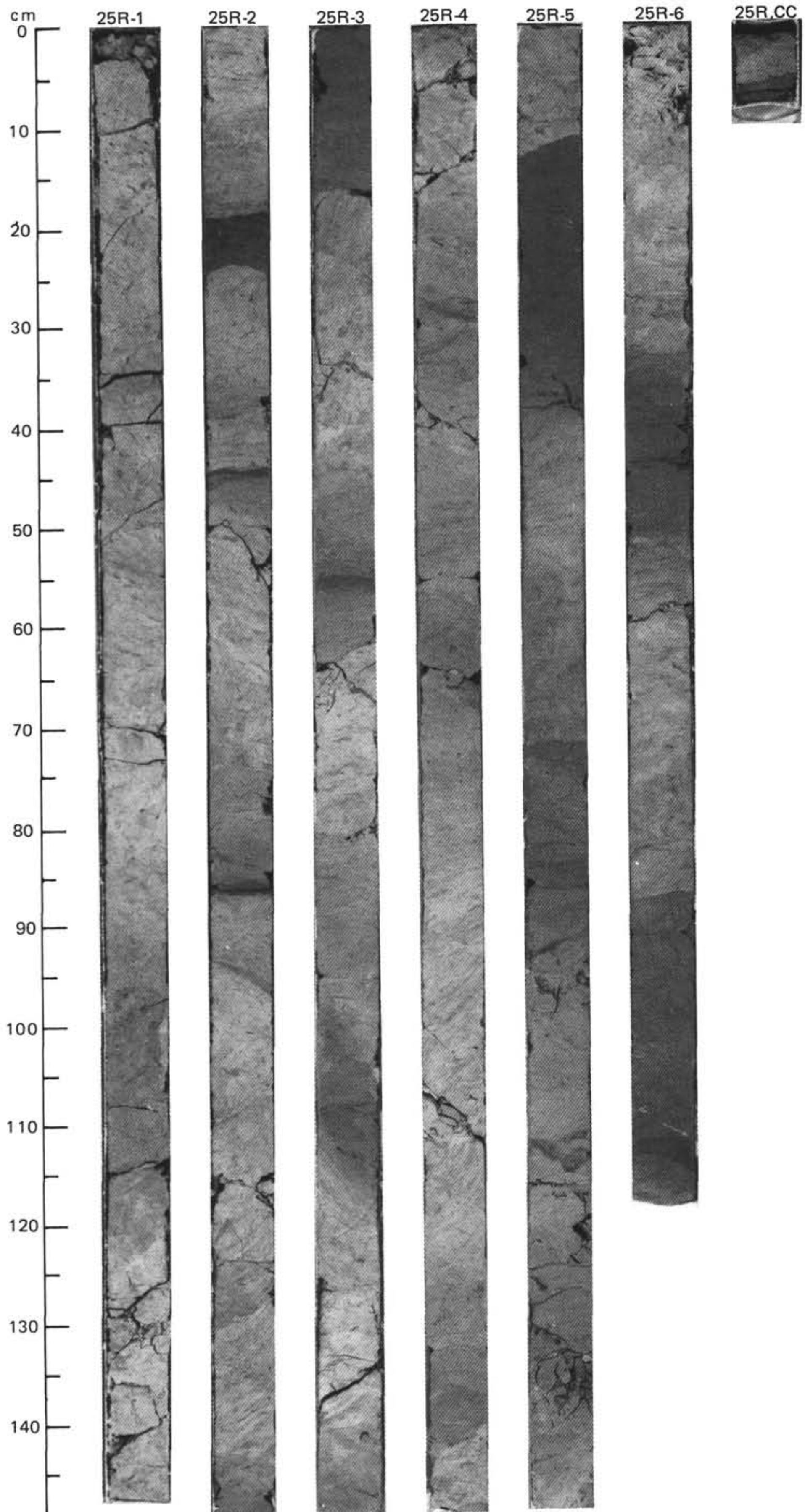
cm
0
10
20
30
40
50
60
70
80
90
100
110
120
130
140
150
25R-1
25R-2
25R-3
25R-4
25R-5
25R-6
25R,CC

SITE 638 HOLE B CORE 26 R CORED INTERVAL 4900.8-4910.4 mbsl; 238.1-247.7 mbsf

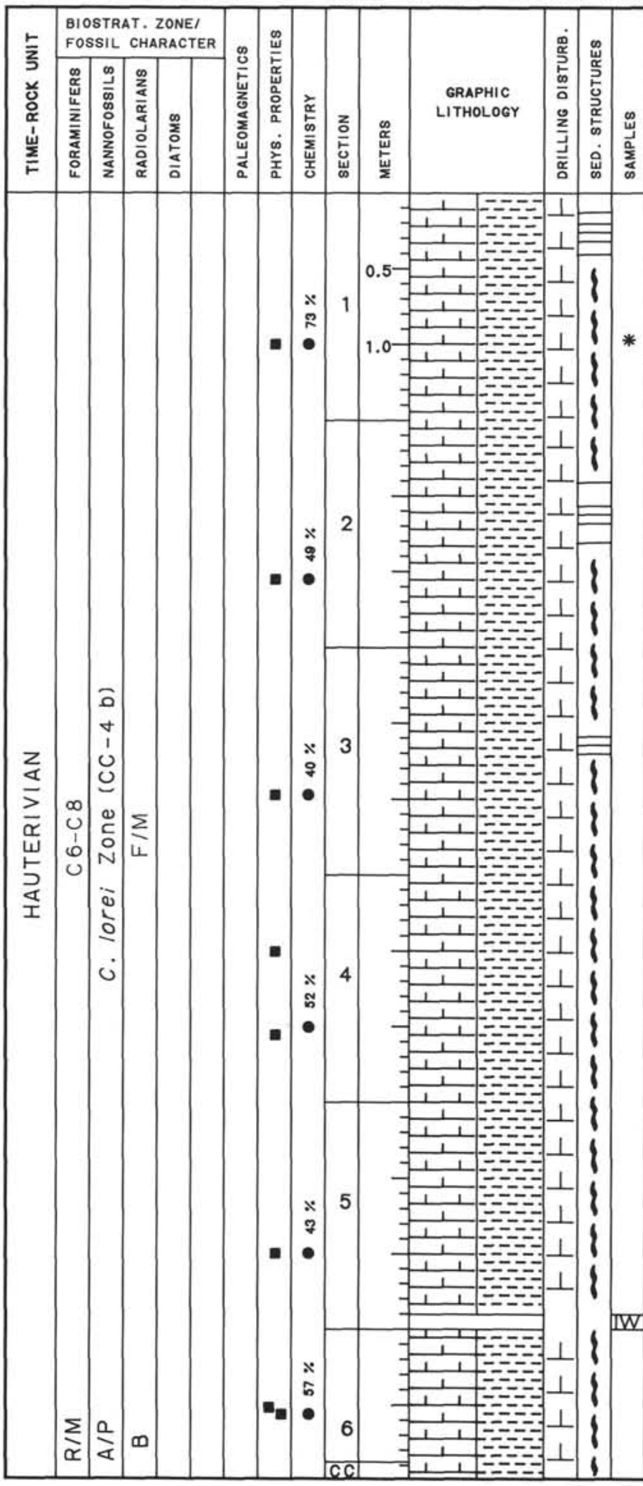

LITHOLOGIC DESCRIPTION

LIGHT GRAY, BIOTURBATED NANNOFOSSIL MARLSTONE

Dominantly gray to light gray (5Y5/1 to 5Y7/1), slightly greenish (5GY 5/1 to 6/1) nannofossil marlstone alternating in a cyclic fashion with minor dark gray (5Y4/1) laminated calcareous claystone. Bioturbation is moderate to strong. Chondrites burrows are locally present. Scattered, illite-rich patches and blebs occur locally. Drilling disturbance is severe and 'drilling-biscuit' deformation is extensive throughout. In places, disruption of the bedding and 'in situ' brecciation is possibly due to slumping.

SMEAR SLIDE SUMMARY (%):

	1,96
	M
TEXTURE:	
Silt	20
Clay	80
COMPOSITON:	
Mica	Tr
Clay	50
Accessory Minerals:	
Opaque-green	9
Pyrite	20
Zeolite	1
Nannofossils	20

PHYSICAL PROPERTIES DATA:

	1,107	2,107	3,98	4,50
$V\rho$ (c)	1.71	2.39	1.66	–
ρ_b	2.12	1.97	1.97	–
T_c	–	–	–	3.44

	4,106	5,101	6,50	6,51
$V\rho$ (c)	1.63	1.56	–	1.78
ρ_b	1.97	1.87	–	1.98
T_c	–	–	3.12	–

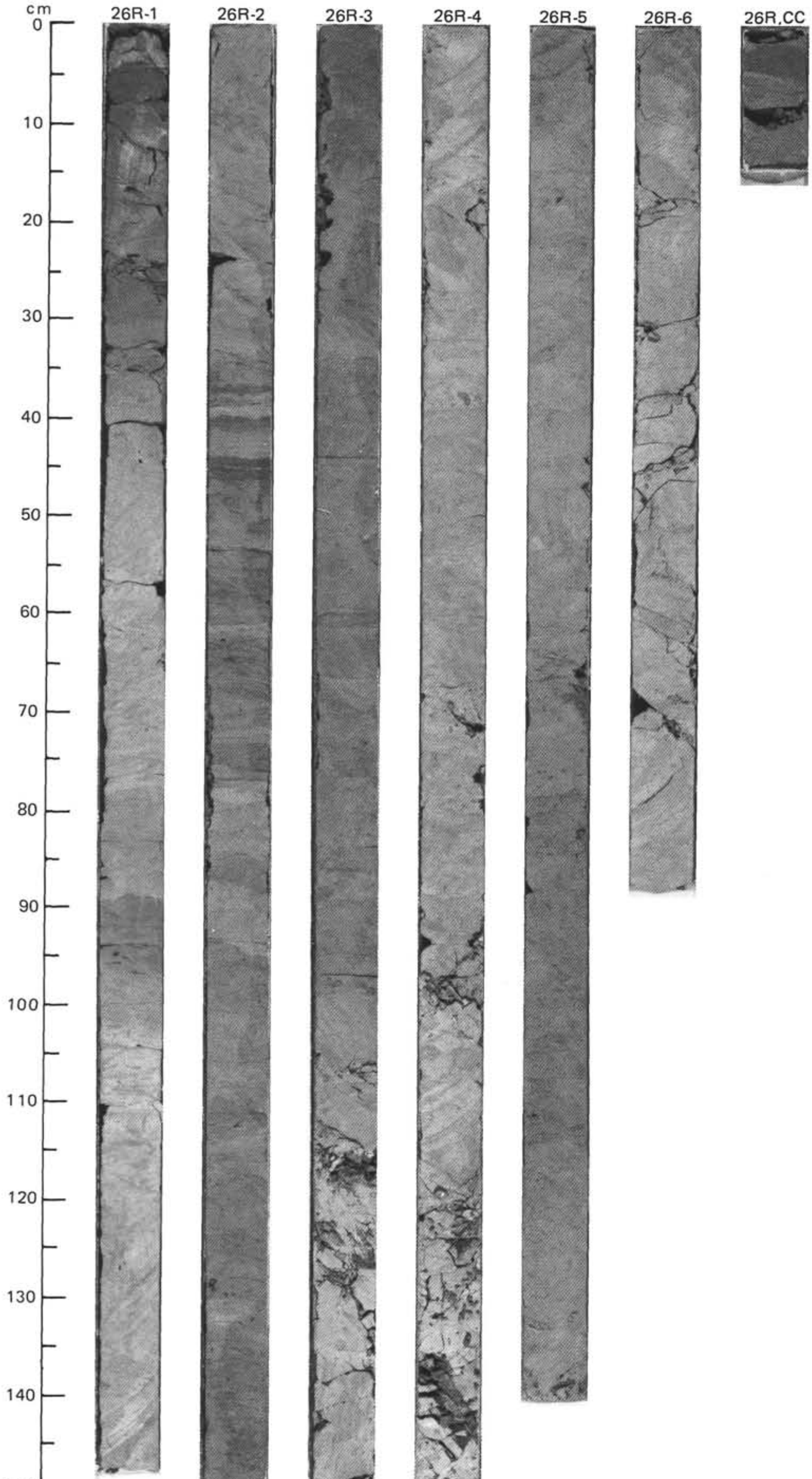
cm
0
10
20
30
40
50
60
70
80
90
100
110
120
130
140
150
26R-1
26R-2
26R-3
26R-4
26R-5
26R-6
26R,CC

SITE 638 HOLE B CORE 27 R CORED INTERVAL 4910.4-4920.0 mbsl; 247.7-257.3 mbsf

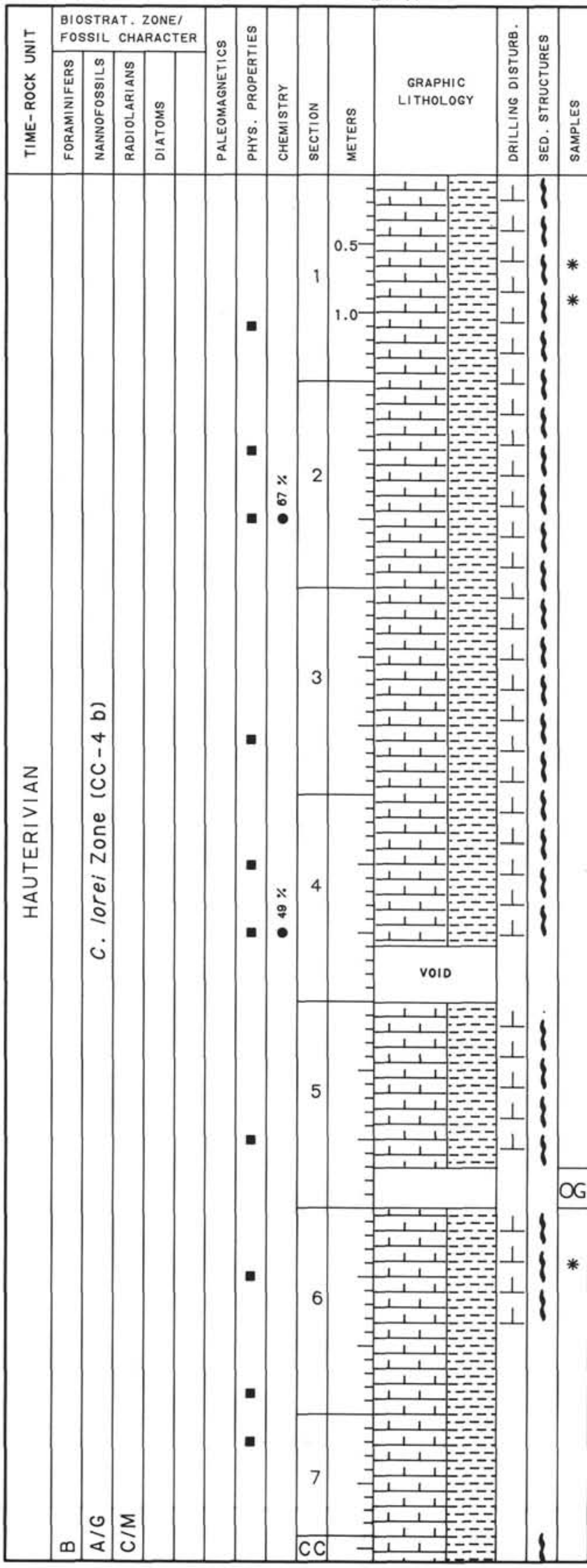

LITHOLOGIC DESCRIPTION

LIGHT GRAY, BIOTURBATED NANNOFOSSIL LIMESTONE

Dominantly gray to light gray (5Y6/1 to 7/1), slightly greenish (5GY5/1 to 6/1) nannofossil marlstone alternating in a cyclic fashion with a few, 10-cm-thick horizons of faintly laminated, darker gray (5Y5/1 to 4/1) clayey marlstone. Bioturbation is moderate to strong. Scattered, illite-rich green patches, specks and laminae occur. Pyrite-rich blebs, large wood fragments (up to 1 cm) and plant-material-rich layers are also present. Drilling disturbance is severe throughout.

SMEAR SLIDE SUMMARY (%):

	1,67 D	1,90 D	6,40 D
TEXTURE:			
Sand	–	10	–
Silt	40	30	30
Clay	60	60	70
COMPOSITION:			
Feldspar	Tr	–	10
Mica	5	–	10
Clay	40	35	30
Calcite/Dolomite	–	–	Tr
Accessory Minerals:			
Zeolites	5	–	–
Pyrite	–	5	Tr
Nannofossils	40	60	40
Plant Debris	10	–	10

PHYSICAL PROPERTIES DATA:

	1,111	2,50	2,99	3,113	4,50
V_p (c)	1.77	–	1.60	1.68	–
ρ_b	–	–	2.04	–	–
T_c	–	3.15	–	–	2.99

	4,99	5,101	6,50	6,136	7,119
V_p (c)	1.72	1.82	–	1.73	1.74
ρ_b	1.93	–	–	1.97	1.96
T_c	–	–	3.32	–	–

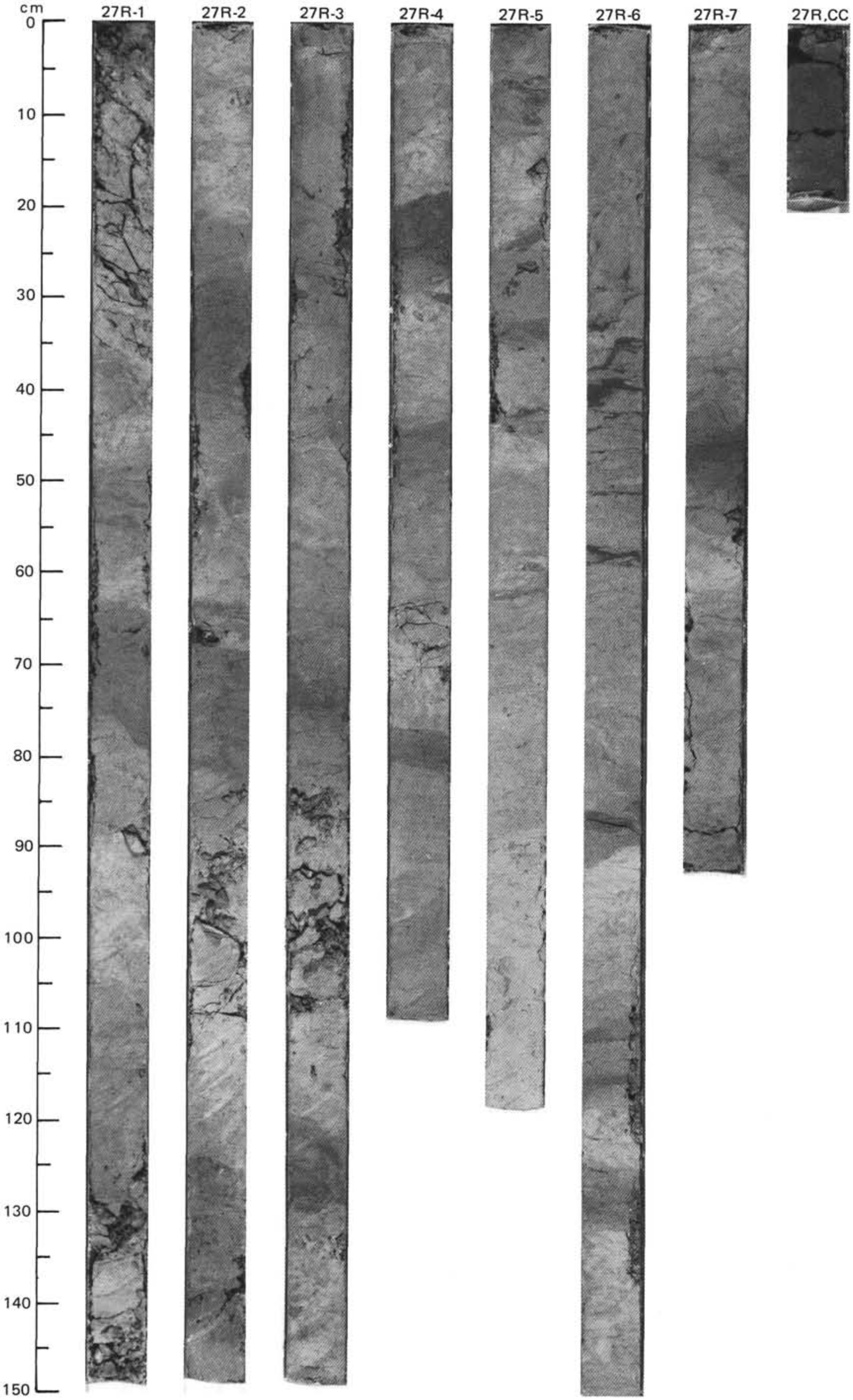
cm
0
10
20
30
40
50
60
70
80
90
100
110
120
130
140
150
27R-1
27R-2
27R-3
27R-4
27R-5
27R-6
27R-7
27R,CC

SITE 638 HOLE B CORE 28 R CORED INTERVAL 4920.0-4929.7 mbsl; 257.3-267.0 mbsf

TIME-ROCK UNIT	FORAMINIFERS	NANNOFOSSILS	RADIOLARIANS	DIATOMS	PALEOMAGNETICS	PHYS. PROPERTIES	CHEMISTRY	SECTION	METERS
HAUTERIVIAN	C3-C5	*C. lorei* Zone (CC-4 b)				■	● 44 %	1	0.5, 1.0
						■ ■	● 51 %	2	
						■	● 49 %	3	
						■ ■	● 58 %	4	
						■	● 63 %	5	
						■ ■		6	
	R/P	F/P	R/P			■		7	
								CC	

GRAPHIC LITHOLOGY / DRILLING DISTURB. / SED. STRUCTURES / SAMPLES

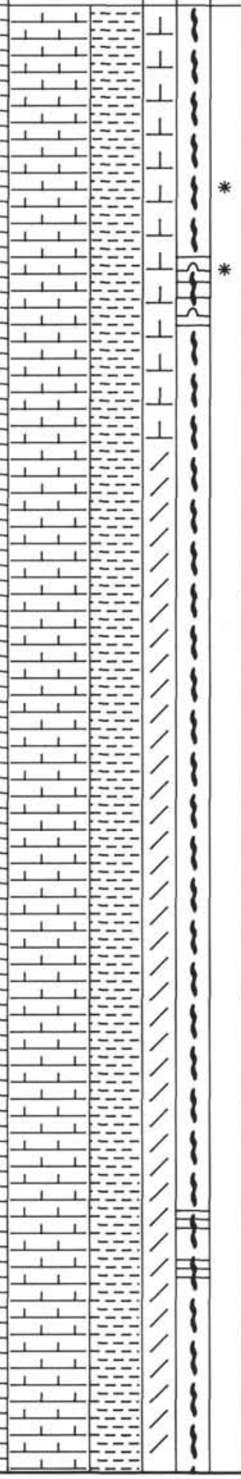

LITHOLOGIC DESCRIPTION

LIGHT GRAY, BIOTURBATED NANNOFOSSIL MARLSTONE

The core consists of extensively bioturbated light greenish gray (5Y-5GY 6/1, 5Y-5GY7/1) nannofossil marlstone, alternating in a cyclic fashion with darker gray horizons (5Y5/1) that are richer in clay and plant material. Darker horizons range in thickness from 10 to 20 cm. Pyrite-rich blebs and specks, as well as large coalified wood fragments are scattered throughout the core. Two slumped beds with convolute and plastically deformed layers occur in Sections 1, 115-135 cm and 2, 40-60 cm. Drilling deformation is intense; 'drilling biscuits' are present throughout the core.

SMEAR SLIDE SUMMARY (%):

	1,126 D	2,34 D
TEXTURE:		
Sand	10	–
Silt	30	30
Clay	60	70
COMPOSITION:		
Quartz	3	–
Feldspar	3	–
Mica	4	–
Clay	30	55
Nannofossils	40	40
Sponge Spicules	Tr	5
Plant Debris	20	Tr

PHYSICAL PROPERTIES DATA:

	1,133	2,50	2,133	3,133	4,50
V_p (c)	1.66	–	1.75	1.80	–
ρ_b	1.93	–	1.97	–	–
T_c	–	3.14	–	–	2.87

	4,141	5,141	6,50	6,141	7,40
V_p (c)	1.55	1.61	–	1.59	1.18
ρ_b	1.95	2.00	–	–	–
T_c	–	–	3.27	–	–

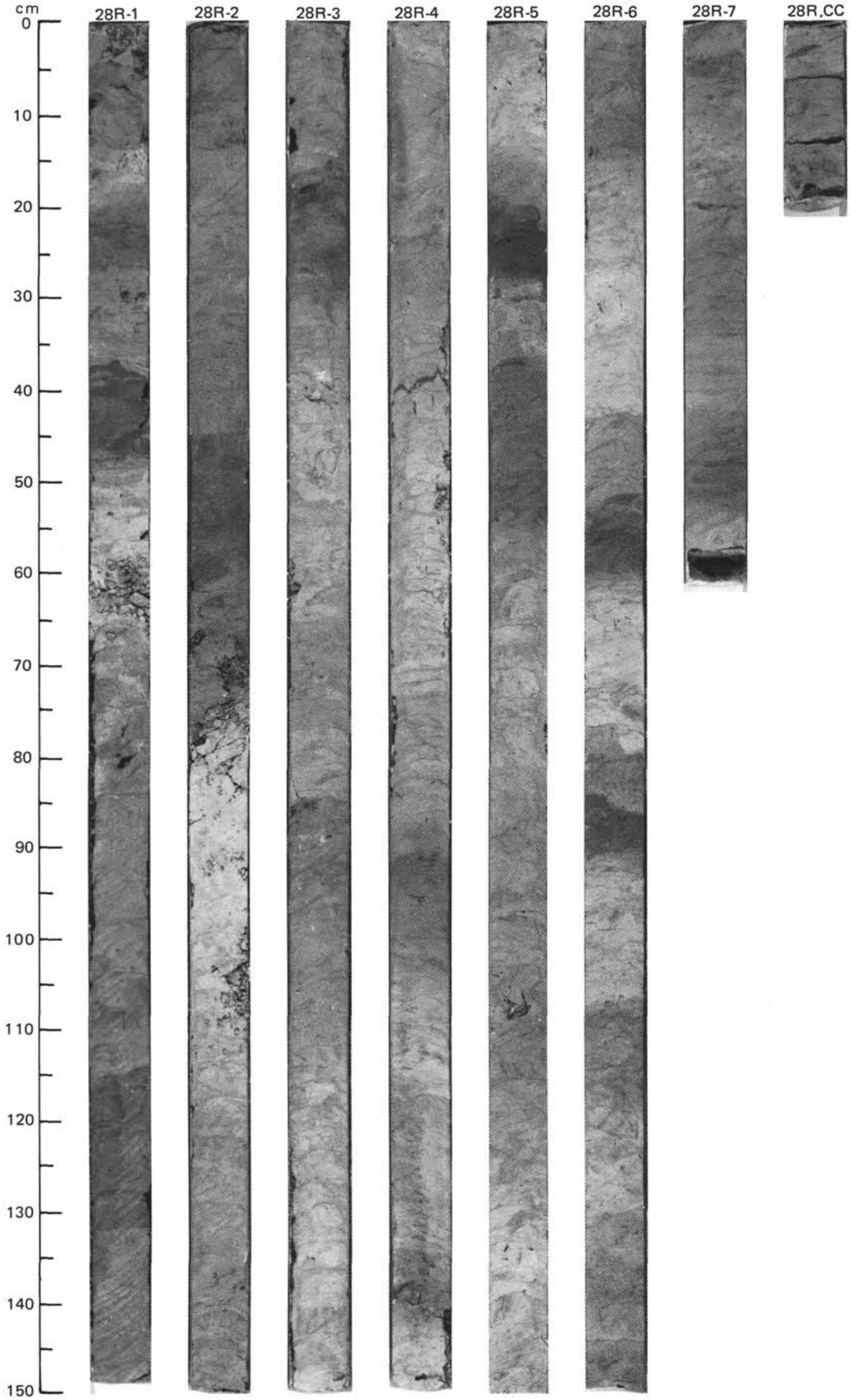
cm
0
10
20
30
40
50
60
70
80
90
100
110
120
130
140
150
28R-1
28R-2
28R-3
28R-4
28R-5
28R-6
28R-7
28R,CC

SITE 638 HOLE B CORE 29 R CORED INTERVAL 4929.7-4939.4 mbsl; 267.0-276.7 mbsf

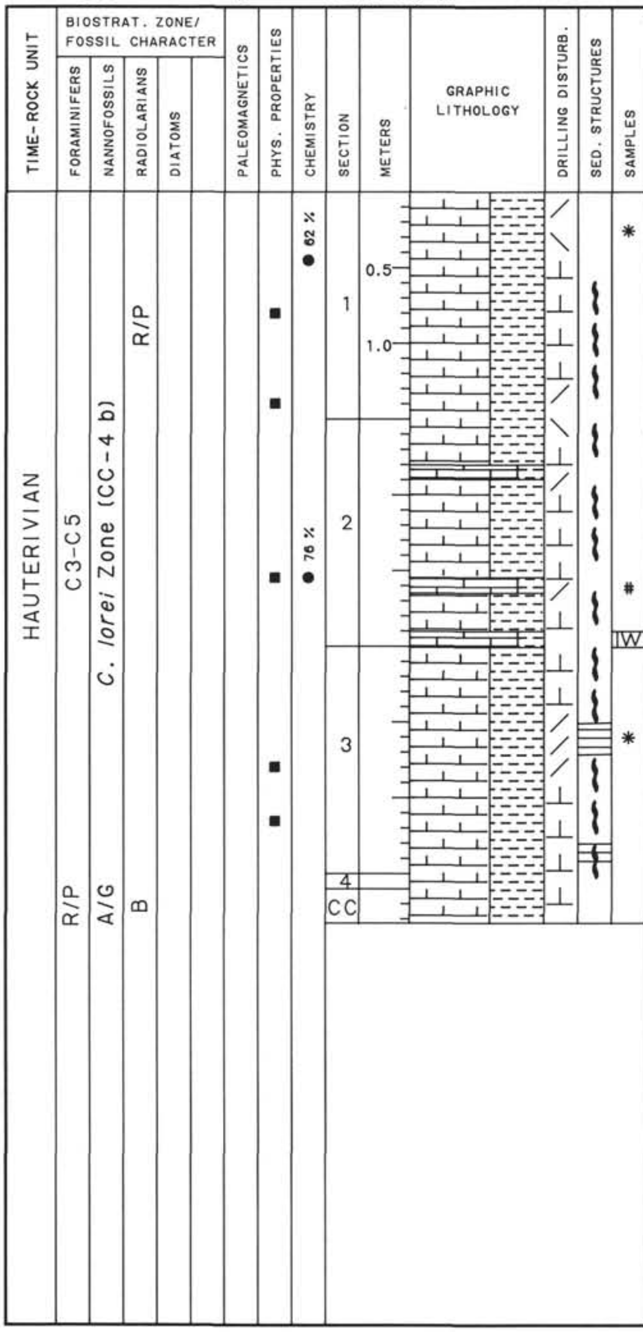

LITHOLOGIC DESCRIPTION

LIGHT GRAY, BIOTURBATED NANNOFOSSIL MARLSTONE

The core consists of extensively bioturbated light greenish gray (5Y-5GY6/1, 5Y-5GY7/1) nannofossil marlstone. Palygorskite-rich blebs and plant-rich layers, as well as large (up to 1 cm) coalified wood fragments are scattered throughout the core. Plastically deformed layers occur in Section 3, 10 to 20 cm. Drilling deformation is intense; 'drilling biscuits' are present throughout the core.

SMEAR SLIDE AND THIN SECTION SUMMARY (%):

	1,29 M	2,110-113 D	3,61 M
TEXTURE:			
Sand	–	10	–
Silt	10	–	10
Clay	90	90	90
COMPOSITION:			
Quartz	–	Tr	–
Feldspar	Tr	Tr	Tr
Mica	Tr	Tr	Tr
Clay	70	–	70
Volcanic Glass	3	–	Tr
Calcite/Dolomite	Tr	–	Tr
Accessory Minerals:			
Opaques	Tr	–	Tr
Zeolites	5	–	5
Nannofossils	15	–	20
Radiolarians	–	11	–
Plant Debris	6	1	5
Micrite	–	88	–
Glauconite	–	Tr	–

PHYSICAL PROPERTIES DATA:

	1,80	1,143	2,106	3,81	3,116
V_p (c)	–	1,87	3,10	–	1.47
ρ_b	–	2.19	2.45	–	1.99
T_c	3.13	–	–	3.07	–

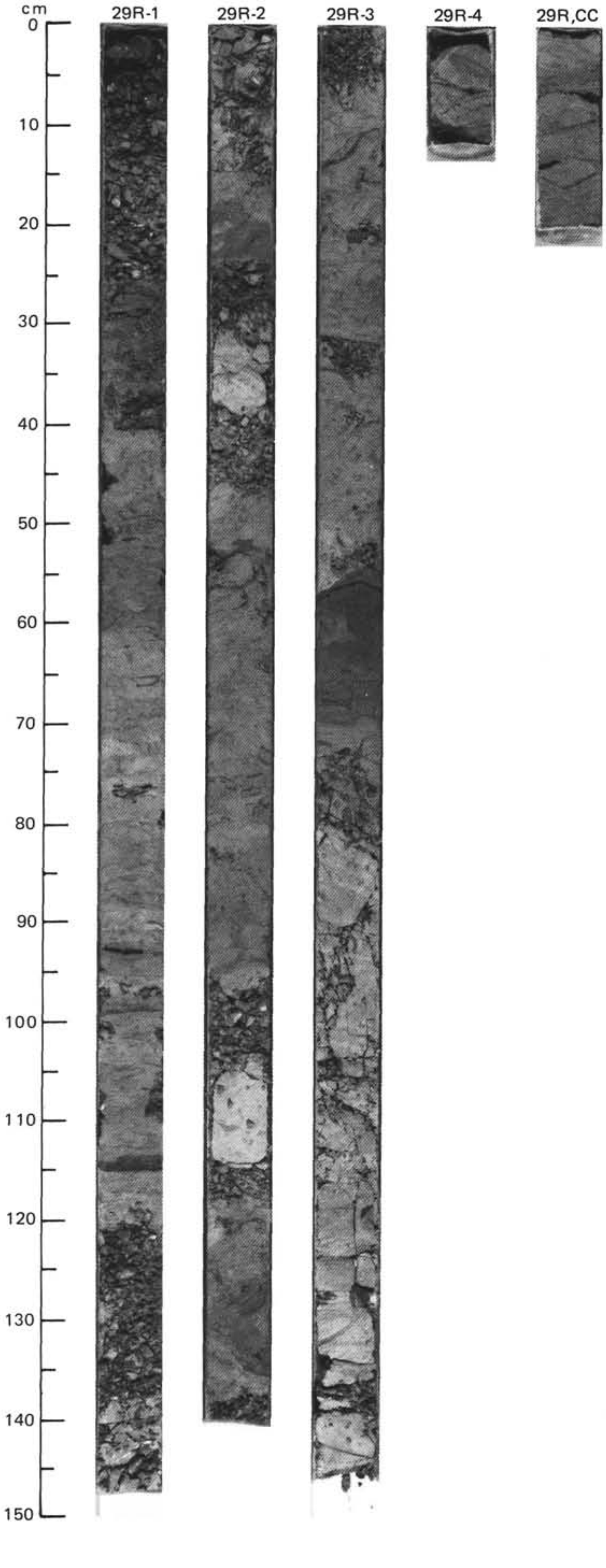
cm
0
10
20
30
40
50
60
70
80
90
100
110
120
130
140
150
29R-1
29R-2
29R-3
29R-4
29R,CC

SITE 638 HOLE B CORE 30 R CORED INTERVAL 4939.4-4949.0 mbsl; 276.7-286.3 mbsf

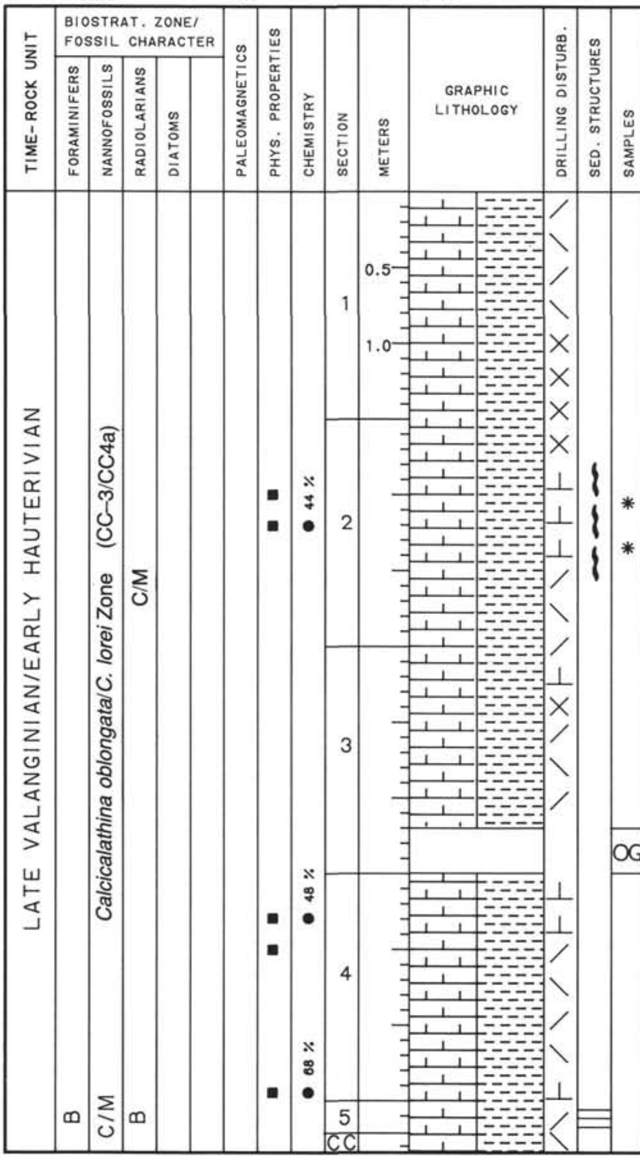

LITHOLOGIC DESCRIPTION

LIGHT GRAY, BIOTURBATED NANNOFOSSIL MARLSTONE

The core consists of variegated light gray (5Y6/1 to 7/1) and gray (5Y5/1), bioturbated nannofossil marlstone. The core is highly disturbed by drilling. The rocks are either crushed or intensely fractured. Brittle deformation seems to be chiefly related to the process of coring, while folding of layers seems to be a syn-sedimentary slump feature (Sections 2, 70 to 90 cm; Section 3, 115 to 120 cm; Section 4, 30 to 38 cm).

SMEAR SLIDE SUMMARY (%):

	2,53 M	2,87 D
TEXTURE:		
Silt	–	5
Clay	100	95
COMPOSITION:		
Clay	40	60
Accessory Minerals:		
Zeolites	–	Tr
Opaques	–	2
Nannofossils	51	35
Plant Debris	1	3
Micrite	8	–

PHYSICAL PROPERTIES DATA:

	2,50	2,68	4,32	4,50	4,145
V_p (c)	–	1.67	1.71	–	2.05
ρ_b	–	1.91	1.92	–	2.21
T_c	3.44	–	--	3.22	–

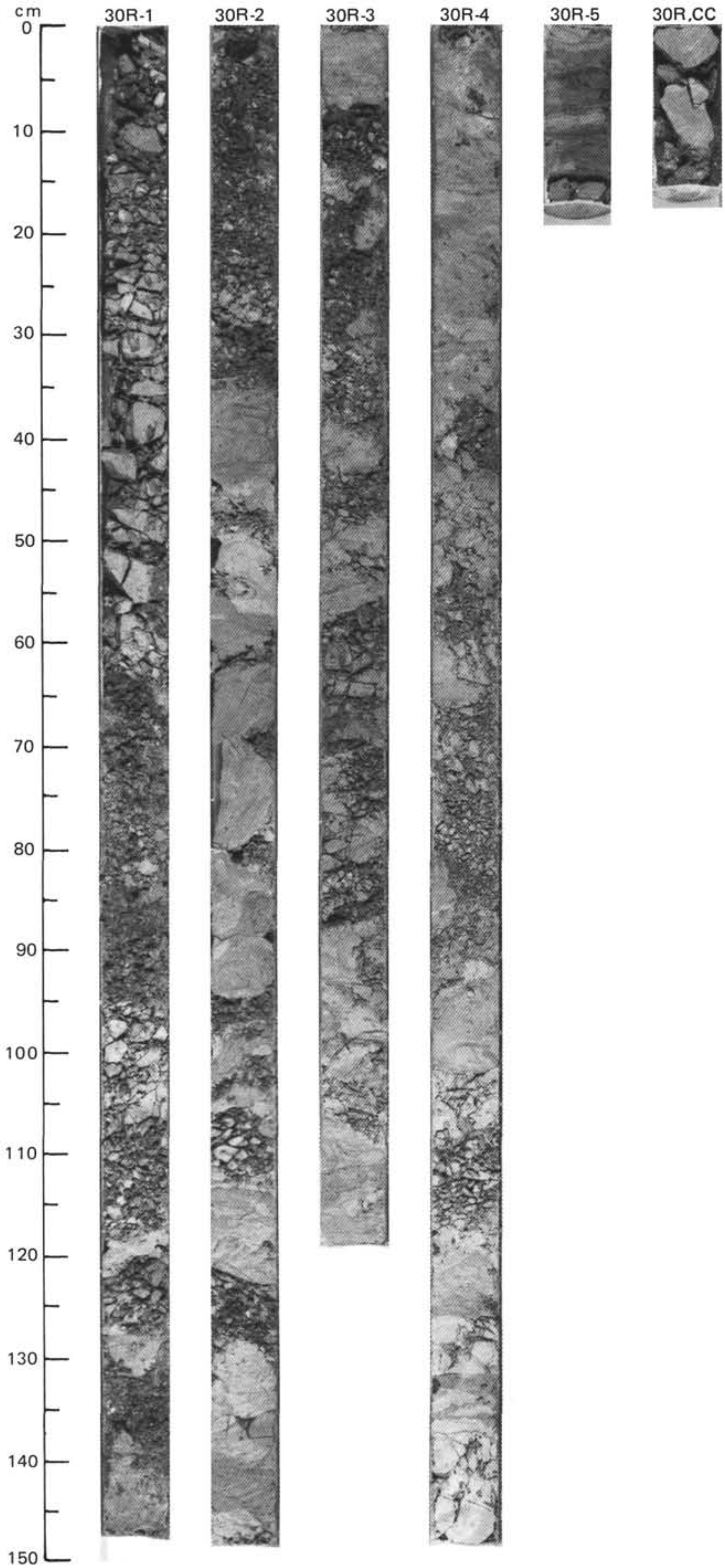
cm
0
10
20
30
40
50
60
70
80
90
100
110
120
130
140
150
30R-1
30R-2
30R-3
30R-4
30R-5
30R,CC

SITE 638 HOLE B CORE 31 R CORED INTERVAL 4949.0-4958.7 mbsl; 286.3-296.0 mbsf

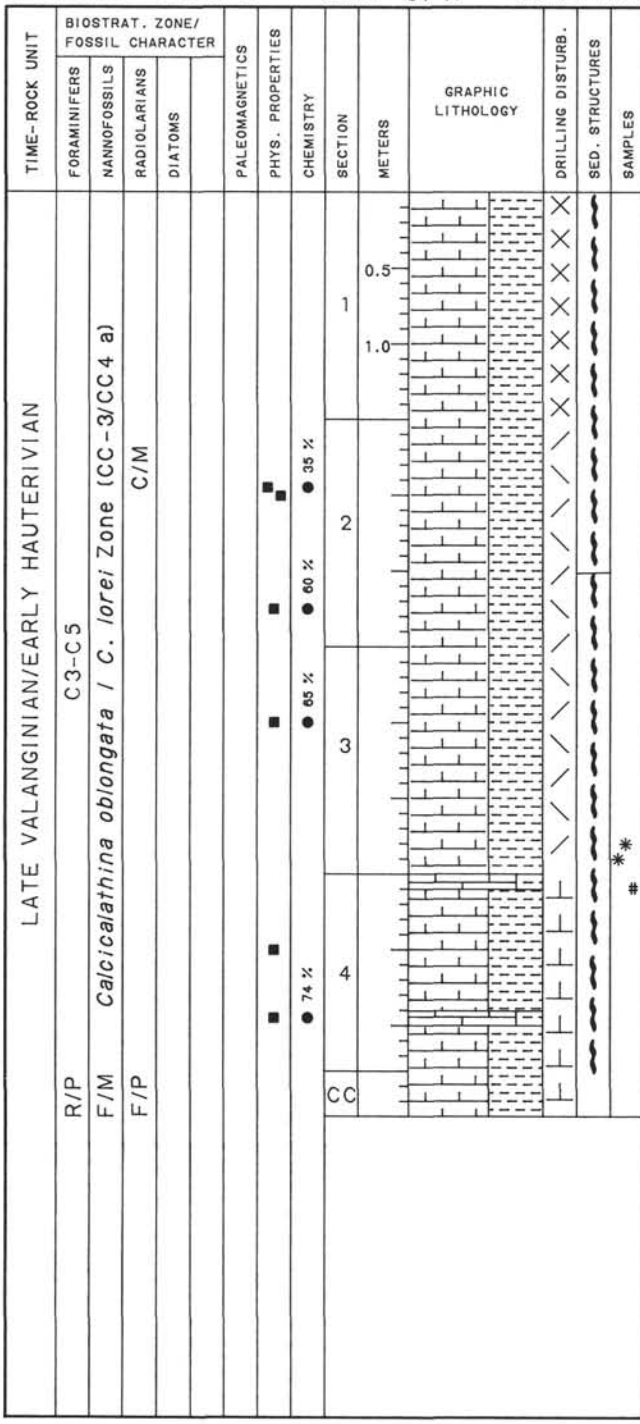

LITHOLOGIC DESCRIPTION

LIGHT GRAY, BIOTURBATED NANNOFOSSIL MARLSTONE

The core consists of variegated light gray (5Y6/1 to 7/1), slightly greenish and gray (5Y5/1) bioturbated nannofossil marlstone. The core is highly disturbed by drilling; the rocks are either crushed or intensely fractured. Brittle deformation seems to be chiefly related to the process of coring while folding of layers seems to be a syn-sedimentary slump feature (Section 1, 135-140 cm; Section 2, 60-90 cm; Section 3, 0-150 cm). Concentrations of silt-sized pyrite framboids occur at Section 3, 132-133 cm.

SMEAR SLIDE AND THIN SECTION SUMMARY (%):

	3,132 M	3,147 D	4,1-3 D
TEXTURE:			
Sand	87	–	5
Silt	–	25	15
Clay	13	75	80
COMPOSITION:			
Quartz	7	15	Tr
Mica	1	–	Tr
Clay	3	50	–
Calcite/Dolomite	–	Tr	–
Accessory Minerals:			
Pyrite	79	2	Tr
Nannofossils	5	23	–
Radiolarians	–	–	20
Fish Remains	–	–	Tr
Plant Debris	5	2	Tr
Micrite	–	8	80

PHYSICAL PROPERTIES DATA:

	2,43	2,50	2,123	3,48	4,50	4,95
V_p (c)	1.27	–	1.42	1.66	–	2.10
ρ_b	1.87	–	1.90	2.00	–	2.55
T_c	–	3.55	–	–	3.49	–

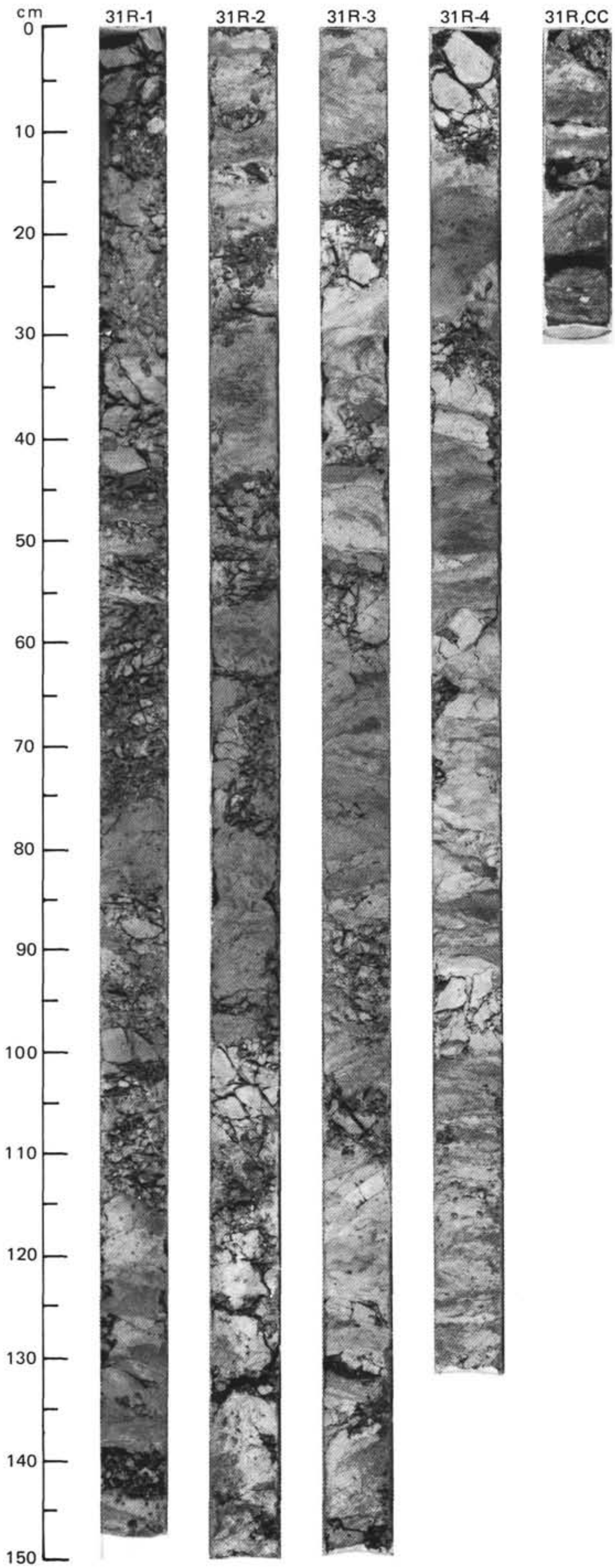
cm
0
10
20
30
40
50
60
70
80
90
100
110
120
130
140
150
31R-1
31R-2
31R-3
31R-4
31R,CC

SITE 638 HOLE B CORE 32 R CORED INTERVAL 4958.7-4968.3 mbsl; 296.0-305.6 mbsf

TIME-ROCK UNIT	FORAMINIFERS	NANNOFOSSILS	RADIOLARIANS	DIATOMS	PALEOMAGNETICS	PHYS. PROPERTIES	CHEMISTRY	SECTION	METERS
LATE VALANGINIAN/EARLY HAUTERIVIAN	R/P	CC-3 / CC4 a C/M	F/P			■ ■ ■	● 25 % ● 74 %	1 2 CC	0.5 1.0

BIOSTRAT. ZONE/ FOSSIL CHARACTER

GRAPHIC LITHOLOGY

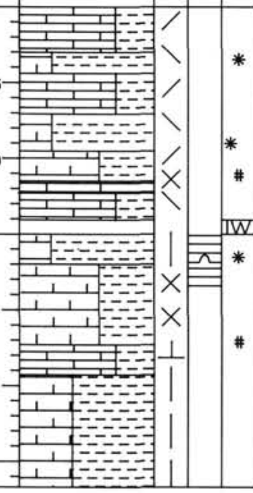

DRILLING DISTURB. SED. STRUCTURES SAMPLES

LITHOLOGIC DESCRIPTION

INTERBEDDED CLAYEY LIMESTONE, MARLSTONE AND CALCAREOUS CLAYSTONE

The core is highly disturbed by drilling: about 50% of it consists of drilling breccia; the remainder contains isolated blocks of the above-mentioned lithologies. The calcareous claystone and marlstone are gray to dark gray in color (5Y4/1, 5Y5/1), locally with a brownish tint (5Y4/2). Lamination is broadly parallel, frequently plastically deformed. Clayey limestone is light gray in color (5Y6/1, 5Y7/1), bioturbated and sometimes fractured, with veins filled with calcite.

Interpretation of apparent syn-sedimentary, soft-sediment deformation is ambiguous due to high drilling disturbance.

SMEAR SLIDE AND THIN SECTION SUMMARY (%):

	1,37 M	1,91 D	2,17 M	1,119-121 M	2,81-82 M
TEXTURE:					
Sand	3	—	—	—	—
Silt	18	5	15	1	1
Clay	79	95	85	99	99
COMPOSITION:					
Quartz	12	Tr	5	Tr	1
Mica	—	Tr	1	—	—
Clay	52	82	76	—	—
Calcite/Dolomite	Tr	2	1	—	—
Accessory Minerals:					
Opaques	4	1	2	1	2
Zircon, rutile	—	—	Tr	—	—
Phosphate	—	—	Tr	—	—
Nannofossils	25	15	15	—	5
Radiolarians	—	—	—	2	2
Plant Debris	2	—	—	Tr	—
Micrite	5	—	—	97	90

PHYSICAL PROPERTIES DATA:

	1,78	2,78	2,104
V_p (a)	—	3.52	—
V_p (b)	—	3.58	—
V_p (c)	1.68	3.30	—
ρ_b	1.96	2.61	—
T_c	—	—	3.29

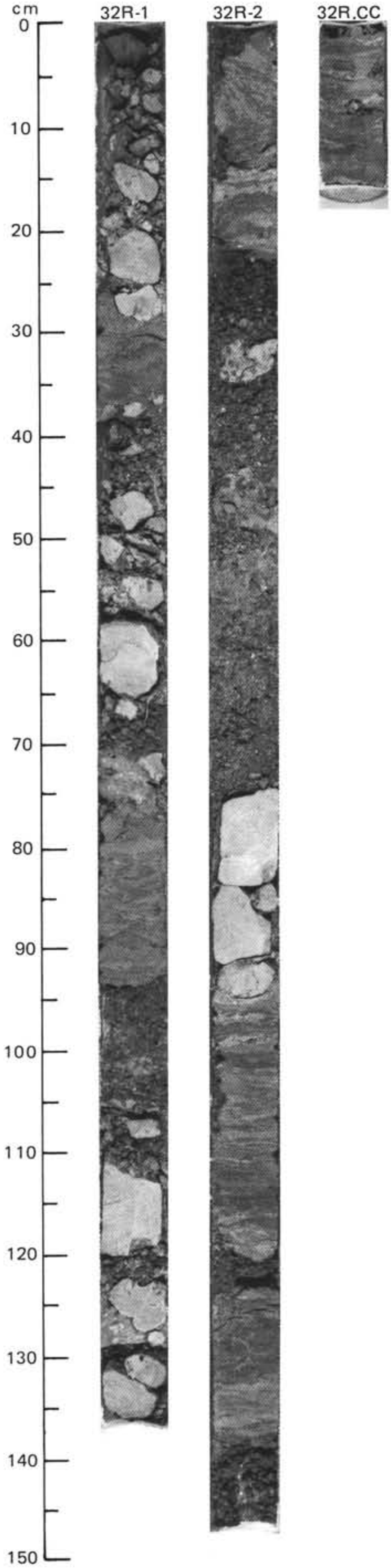
cm
0
10
20
30
40
50
60
70
80
90
100
110
120
130
140
150
32R-1
32R-2
32R,CC

SITE 638 HOLE B CORE 33 R CORED INTERVAL 4968.3-4978.0 mbsl; 305.6-315.3 mbsf

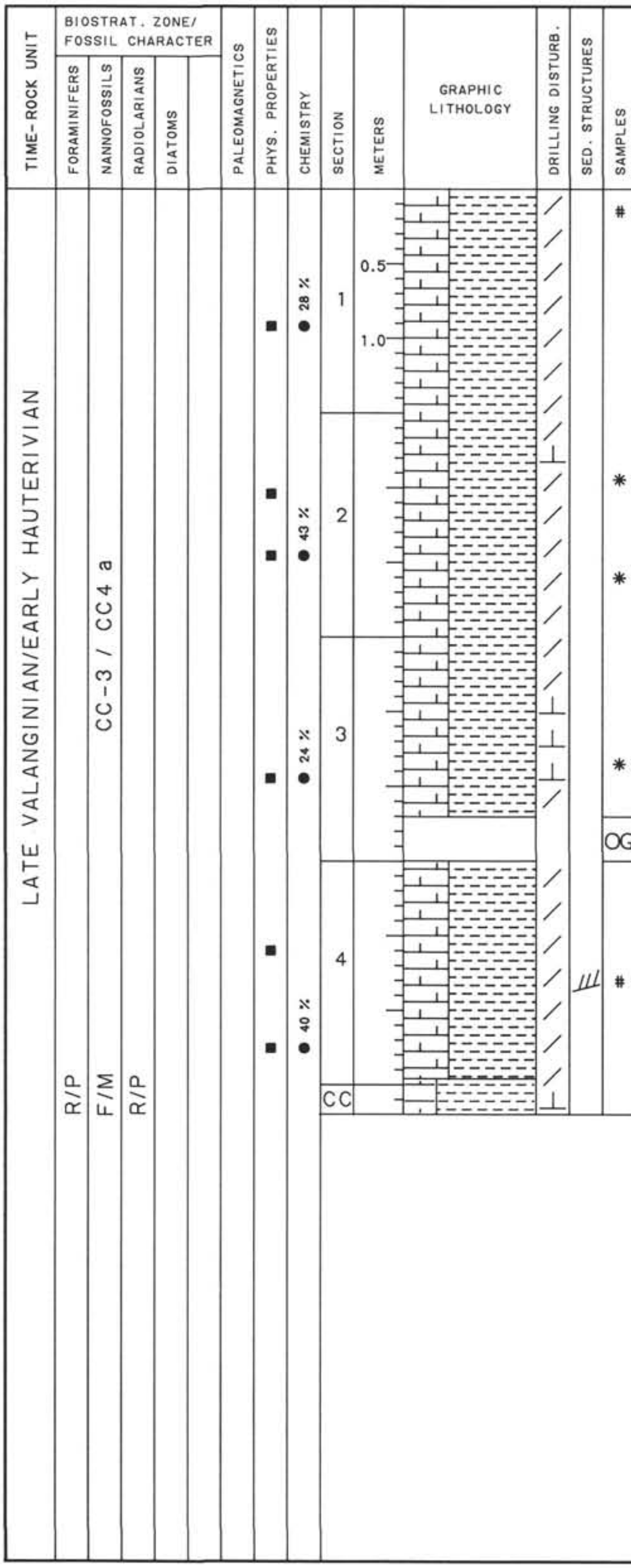

LITHOLOGIC DESCRIPTION

INTERBEDDED CALCAREOUS CLAY and MARL

The core consists of centimeter-scale alternations of gray (5Y5/1), locally silty calcareous clay and light olive gray (5Y6/2) marl (symbols given in 'Graphic lithology' column are schematic, because thickness of couplets is too small to accurately display at this scale). Bioturbation is moderate. Contacts between layers are sharp, frequently crinkled, crenulated or folded. Drilling deformation is intense; microfaulting is extensive throughout the core. A few blocks, 6 to 7 cm in length, of dark gray (5Y3/1, 5Y4/1), fine-grained carbonate-cemented sandstone, rich in wood fragments and showing parallel laminations, are scattered throughout the core. A single undisturbed layer of the same sandstone, showing high-angle oblique laminae occurs in Section 4, 80 to 90 cm.

SMEAR SLIDE AND THIN SECTION SUMMARY (%):

	1,15-18 M	2,43 D	2,112 M	3,88 D	4,82-86 D
TEXTURE:					
Sand	–	4	–	2	65
Silt	5	21	5	23	–
Clay	95	75	95	75	35
COMPOSITION:					
Quartz	Tr	12	–	1	30
Feldspar	–	1	–	–	15
Mica	Tr	6	–	1	27
Clay	–	60	60	55	–
Calcite/Cement	–	3	Tr	6	25
Accessory Minerals:					
Opaques	2	5	2	2	1
Zeolites	–	–	1	–	–
Chert	–	–	–	–	Tr
Nannofossils	–	12	30	35	–
Radiolarians	3	–	–	–	–
Fish Remains	–	Tr	Tr	–	–
Plant Debris	2	1	3	–	–
Micrite	93	–	4	–	–
Ostracod?	Tr	–	–	–	–
Echinoid Spicule	–	–	–	–	Tr
Rock Fragments:					
Chl & Sericite Schist	–	–	–	–	1
Acid Plutonic	–	–	–	–	1
Micrite Intraclasts	–	–	–	–	Tr

PHYSICAL PROPERTIES DATA:

	1,91	2,56	2,91	3,91	4,57	4,126
V_p (c)	1.76	–	1.69	1.70	–	1.73
ρ_b	2.11	–	2.01	2.00	–	2.03
T_c	–	3.90	–	–	4.81	–

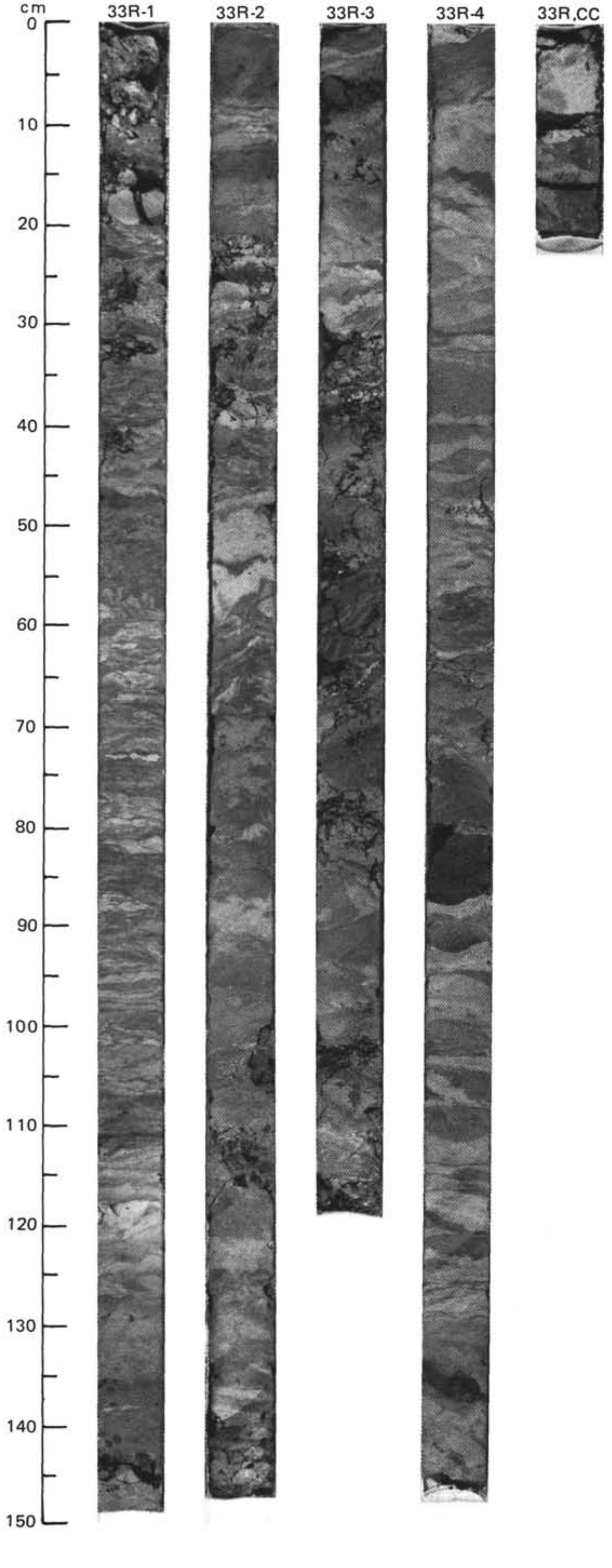

cm
0
10
20
30
40
50
60
70
80
90
100
110
120
130
140
150
33R-1
33R-2
33R-3
33R-4
33R,CC

SITE 638 HOLE B CORE 34 R CORED INTERVAL 4978.0-4987.6 mbsl; 315.3-324.9 mbsf

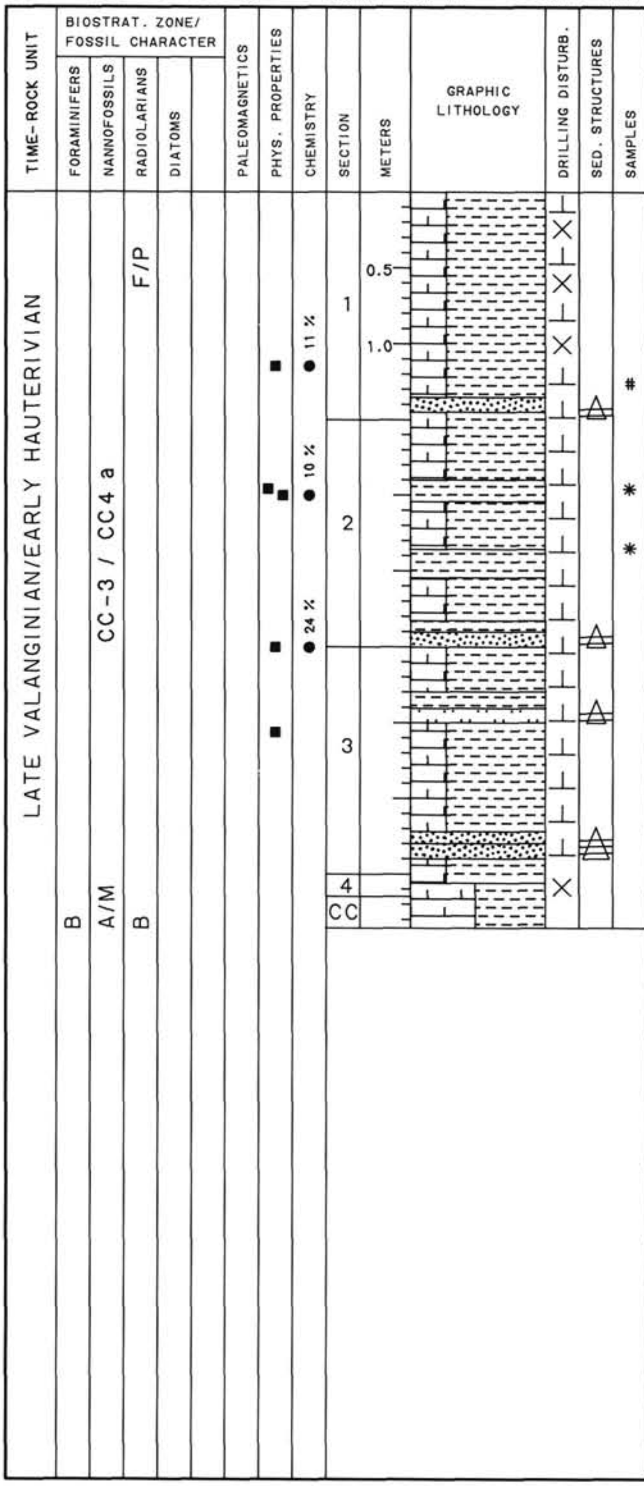

LITHOLOGIC DESCRIPTION

INTERBEDDED DARK GRAY CLAYSTONE and LIGHT GREENISH GRAY MARLSTONE

The core contains alternating, cm-thick layers of dark gray (N/4) claystone and silty claystone and light greenish gray (5Y6/1) nannofossil marlstone, intensely deformed and microfaulted by drilling. (symbols given in 'Graphic lithology' column are schematic, because thickness of couplets is too small to accurately display at this scale). Drilling deformation is chiefly brittle and includes a) 'biscuiting' and b) small-scale microfaulting within each biscuit. Other sediment deformation is interpreted as a syn-sedimentary feature related to slumping or 'creeping'. Medium- to fine-grained, wood-fragment-rich sandstone/claystone couplets, 5 to 20 cm thick, showing normal size grading and parallel lamination at their base (Ta-e and Tb-e beds of the Bouma sequence), occur. Sand/shale ratio is 1:4.

SMEAR SLIDE AND THIN SECTION SUMMARY (%):

	1,136-138 D	2,48 D	2,82 D
TEXTURE:			
Silt	40	15	40
Clay	60	85	60
COMPOSITION:			
Quartz	30	3	–
Feldspar	7	2	Tr
Mica	–	3	Tr
Clay	–	73	40
Volcanic Glass	–	Tr	–
Calcite/Dolomite	–	2	–
Accessory Minerals:			
Zeolites	–	Tr	Tr
Opaques	–	Tr	Tr
Zircon	Tr	–	–
Nannofossils	–	10	60
Sponge Spicules	–	–	Tr
Plant Debris	3	7	Tr
Microspar and Clay	60	–	–

PHYSICAL PROPERTIES DATA:

	1,115	2,45	2,47	2,146	3,56
V_p (a)	1.40	–	–	3.68	–
V_p (b)	1.67	–	–	4.18	–
V_p (c)	1.71	–	1.69	4.16	–
ρ_b	2.05	–	2.02	2.65	–
T_c	–	3.59	–	–	3.56

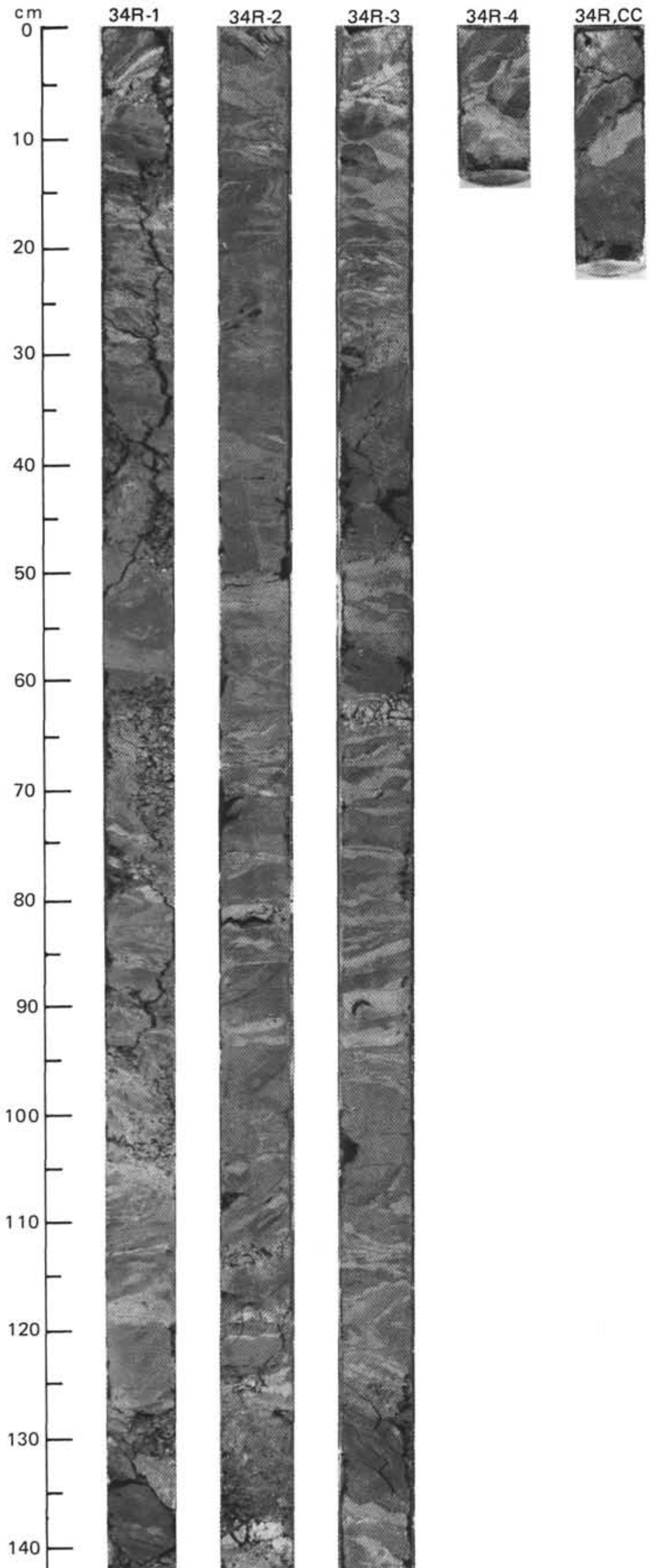
cm
0
10
20
30
40
50
60
70
80
90
100
110
120
130
140
150
34R-1
34R-2
34R-3
34R-4
34R,CC

SITE 638 HOLE B CORE 35 R CORED INTERVAL 4987.6-4997.2 mbsl; 324.9-334.5 mbsf

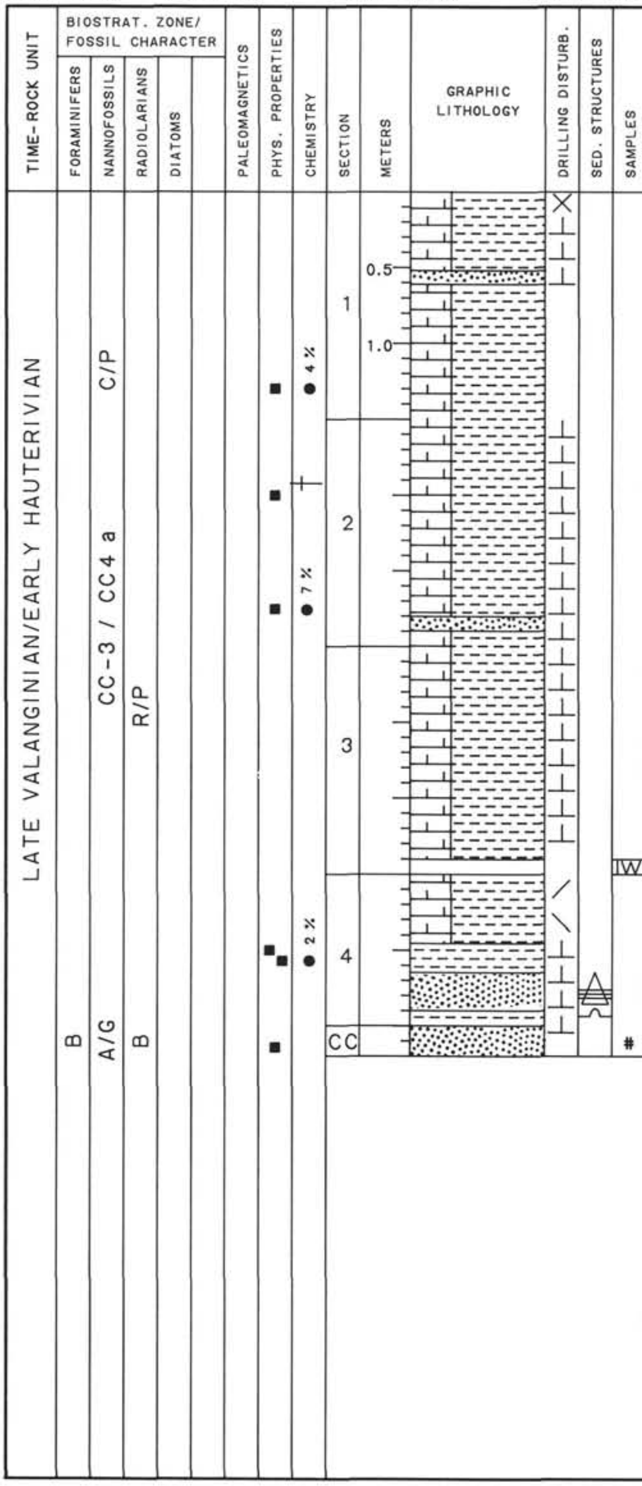

LITHOLOGIC DESCRIPTION

INTERBEDDED DARK GRAY CLAYSTONE and LIGHT GREENISH GRAY MARLSTONE

The core contains alternating, cm-thick layers of dark gray (N/4) claystone and greenish gray (5Y4/1 to 6/1) nannofossil marlstone, intensely deformed and microfaulted by drilling. (symbols given in 'Graphic lithology' column are schematic, because thickness of couplets is too small to accurately display at this scale). Drilling deformation is chiefly brittle and includes a) 'biscuiting' and b) small-scale microfaulting within each biscuit. Extensive crenulation of bedding planes and folding is interpreted to be produced by slumping or downslope 'creeping' of sediments. A few, dark gray (N/3) medium- to fine-grained, wood-fragment-rich sandstone/claystone couplets, 5 to 20 cm thick, occur. Sandstone beds show normal size grading and parallel lamination at their base (Ta-e and Tb-e beds of the Bouma sequence). Sand/shale ratio is 1:4.

THIN SECTION SUMMARY (%):

	CC,11-13
	D
TEXTURE:	
Sand	80
Silt	20
COMPOSITION:	
Quartz	44
Feldspar	23
Rock Fragments:	
Mica Schist	Tr
Acid Plutonic	1
Intraclasts-Micritic with Pyrite	2
Mica	5
Calcite Cement	25
Accessory Minerals:	
Epidote	Tr
Sphene	Tr

PHYSICAL PROPERTIES DATA:

	1,129	2,50	2,124	4,50	4,57	CC,14
V_p (c)	1.68	–	1.73	–	1.63	4,14
ρ_b	2.09	–	2.16	–	2.08	2.61
T_c	–	3.67	–	3.75	–	–

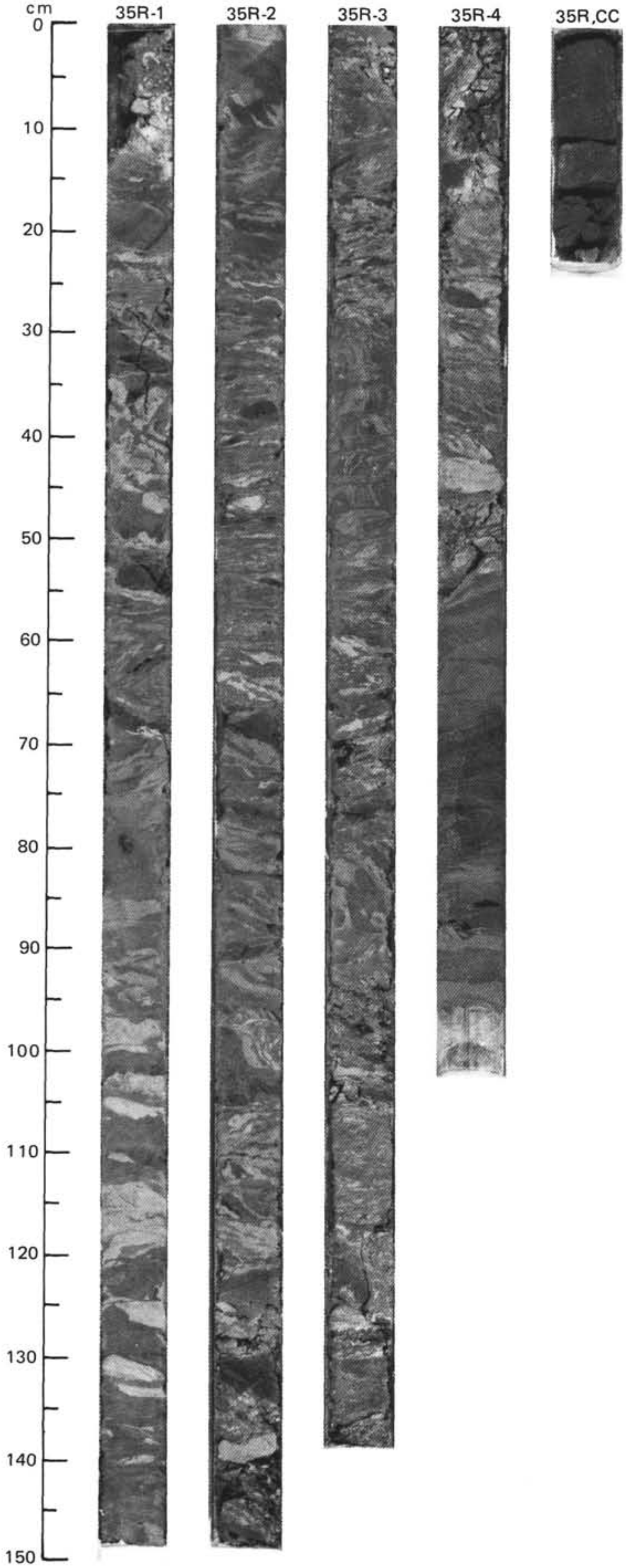
cm
0
10
20
30
40
50
60
70
80
90
100
110
120
130
140
150
35R-1
35R-2
35R-3
35R-4
35R,CC

SITE 638 HOLE B CORE 36 R CORED INTERVAL 4997.2-5006.9 mbsl; 334.5-344.2 mbsf

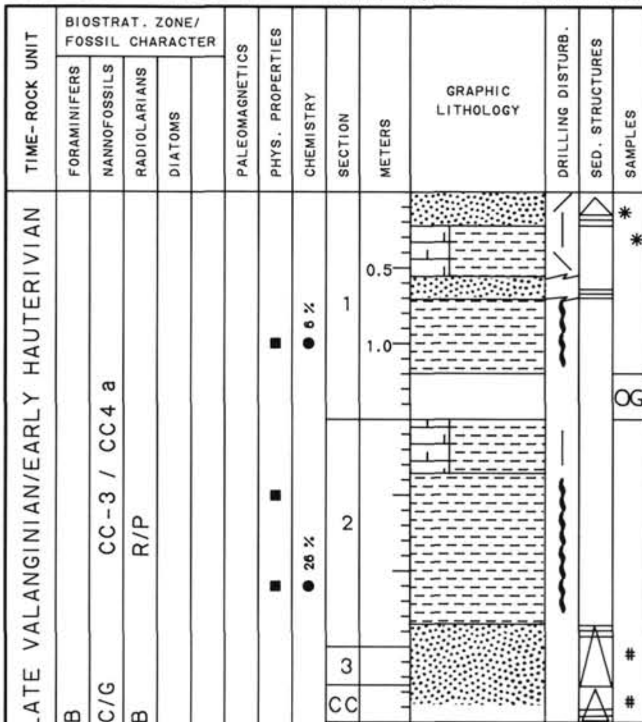

LITHOLOGIC DESCRIPTION

INTERBEDDED SANDSTONE and CLAYSTONE/MARLSTONE COUPLETS

The core consists of thin-bedded siltstone and fine- to medium-grained sandstone turbidites in alternating claystone, silty claystone and marlstone background sediments (symbols given in 'Graphic lithology' column are schematic, because thickness of couplets is too small to accurately display at this scale). Sandstone beds are dark gray (N/4), dark greenish and bluish gray (5Y4/1, 5B4/1), contain large amounts (up to 7%) of terrestrial plant debris and are carbonate cemented. They are normally graded, either massive or parallel laminated at the base and grade upwards to structureless or finely laminated dark greenish gray claystone (Bouma sequences Ta-e and Tb-e). These sandstones range in thickness from a few to 40 cm, but there are indications that there are uncemented portions which have been largely washed by drilling (recovery less than 30%). Background sediments are cm-scale alternations of dark gray (N/4) claystone and light greenish gray to greenish gray (5Y6/1, 5Y5/1) nannofossil marlstone (microturbidites). Sandstone/shale ratio is about 2:5.

SMEAR SLIDE AND THIN SECTION SUMMARY (%):

	1,11	1,30	3,7-8	CC,4-5
	D	D	D	D
TEXTURE:				
Sand	–	–	80	80
Silt	10	20	20	20
Clay	90	80	–	–
COMPOSITION:				
Quartz	Tr	Tr	40	45
Feldspar	–	–	23	20
Mica	3	5	4	5
Clay	80	45	–	–
Volcanic Glass	2	5	–	–
Calcite Cement	–	–	25	25
Accessory Minerals:				
Epidote	–	–	–	Tr
Pyrite	5	–	Tr	–
Rutile	–	–	Tr	–
Heavy Minerals	–	–	–	Tr
Foraminifers	–	–	Tr	–
Nannofossils	10	45	–	–
Sponge Spicules	–	Tr	–	–
Plant Debris	–	Tr	–	–
Rock Fragments:				
Mica Schist	–	–	3	1
Acid Plutonic	–	–	3	1
Quartzite	–	–	Tr	Tr
Micrite	–	–	2	2
Bioclasts	–	–	–	1

PHYSICAL PROPERTIES DATA:

	1,98	2,50	2,111	CC,25
V_p (a)	–	–	–	4.52
V_p (b)	–	–	–	4.21
V_p (c)	1.68	–	1.54	4.21
ρ_b	2.02	–	1.97	3.04
Tc	–	3.79	–	–

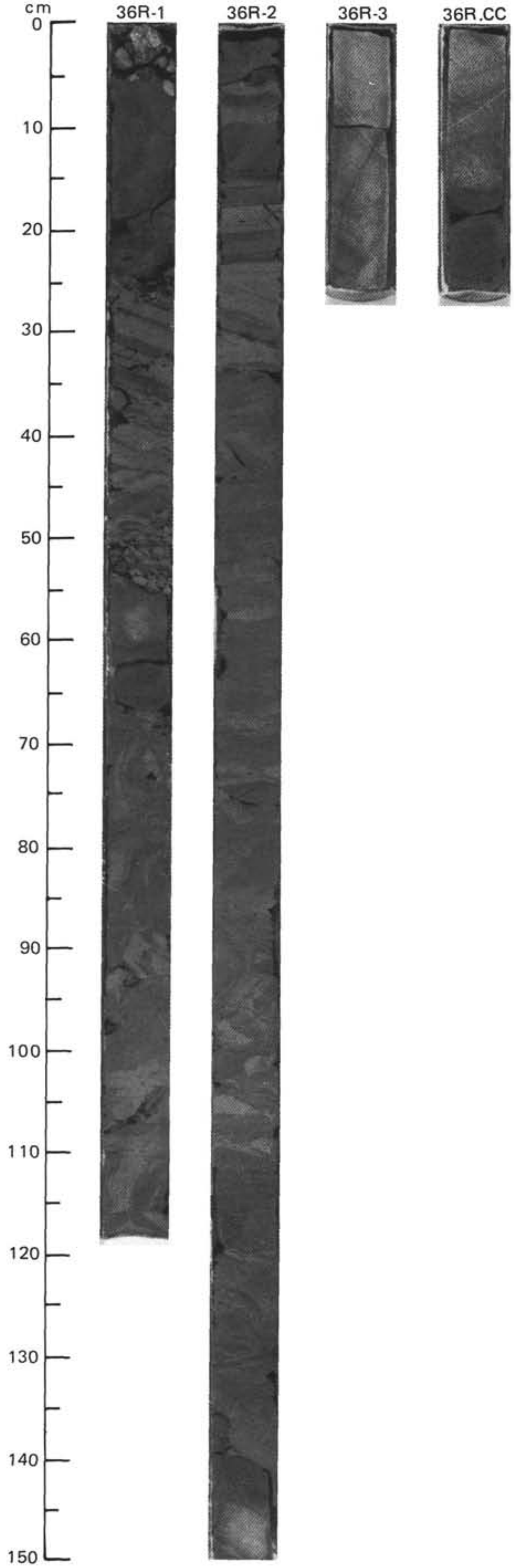
cm
0
10
20
30
40
50
60
70
80
90
100
110
120
130
140
150
36R-1
36R-2
36R-3
36R,CC

SITE 638 HOLE B CORE 37 R CORED INTERVAL 5006.9-5016.5 mbsl; 344.2-353.8 mbsf

TIME-ROCK UNIT	FORAMINIFERS	NANNOFOSSILS	RADIOLARIANS	DIATOMS		PALEOMAGNETICS	PHYS. PROPERTIES	CHEMISTRY	SECTION	METERS	GRAPHIC LITHOLOGY	DRILLING DISTURB.	SED. STRUCTURES	SAMPLES
LATE VALANGINIAN/EARLY HAUTERIVIAN	B	CC-3 / CC4 a F/M	B R/P				■ ■ ■ ■	24 % ●	1 CC	0.5	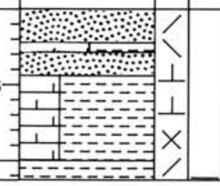			# * *

BIOSTRAT. ZONE/ FOSSIL CHARACTER

LITHOLOGIC DESCRIPTION

SANDSTONE, CLAYSTONE and NANNOFOSSIL MARLSTONE

The above-mentioned lithologies are randomly distributed in the single section recovered. Sandstone beds are dark gray (N/4), dark greenish and bluish gray (5Y4/1, 5B4/1), contain large amounts (up to 7%) of terrestrial plant debris and are carbonate cemented. They are normally graded, either massive or parallel laminated at the base and grade upward to structureless or finely laminated dark greenish gray claystone (Bouma sequences Ta-e and Tb-e). Gaps occur between sandstone blocks and there are indications that uncemented sandy portions have been largely washed by drilling (recovery less than 15%). The dark gray (N/4) claystone alternates with light greenish gray (5Y6/1) nannofossil marlstone. Both are intensely disturbed by drilling.

SMEAR SLIDE AND THIN SECTION SUMMARY (%):

	1,3-5 D	1,49 D	1,56 D
TEXTURE:			
Sand	80	–	–
Silt	20	–	8
Clay	–	100	92
COMPOSITION:			
Quartz	44	Tr	5
Feldspar	22	–	–
Mica	4	Tr	1
Clay	–	60	82
Calcite/Dolomite	–	Tr	–
Calcite Cement	25	–	–
Accessory Minerals:			
Iron Oxides	–	–	Tr
Pyrite Framboids	–	–	1
Zeolites	–	–	Tr
Nannofossils	–	40	10
Plant Debris	–	–	1
Rock Fragments:			
Acid Plutonic	1	–	–
Schist and Hornfels	2	–	–
Micrite/Peloid Intraclasts	2	–	–

PHYSICAL PROPERTIES DATA:

	1,4	1,23	1,49
V_p (a)	4.01	–	–
V_p (b)	3.93	–	–
V_p (c)	3.75	1.65	–
ρ_b	2.76	2.08	–
T_c	–	–	3.87

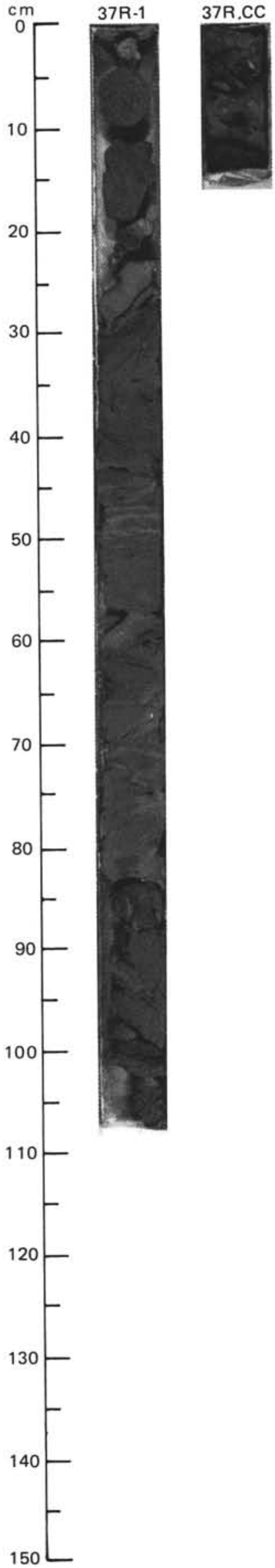
cm
37R-1
37R,CC
0
10
20
30
40
50
60
70
80
90
100
110
120
130
140
150

SITE 638 HOLE B CORE 38 R CORED INTERVAL 5016.5-5026.2 mbsl; 353.8-363.5 mbsf

TIME-ROCK UNIT	FORAMINIFERS	NANNOFOSSILS	RADIOLARIANS	DIATOMS	PALEOMAGNETICS	PHYS. PROPERTIES	CHEMISTRY	SECTION	METERS	GRAPHIC LITHOLOGY	DRILLING DISTURB.	SED. STRUCTURES	SAMPLES
LATE VALANGINIAN/EARLY HAUTERIVIAN	R/P	F/P CC-3 / CC4 a	B				45 % ● 19 %	1	0.5	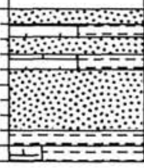			#
								CC					

(BIOSTRAT. ZONE/FOSSIL CHARACTER: FORAMINIFERS, NANNOFOSSILS, RADIOLARIANS, DIATOMS)

LITHOLOGIC DESCRIPTION

SANDSTONE, CLAYSTONE and NANNOFOSSIL MARLSTONE

The above-mentioned lithologies are randomly distributed in the single section recovered in this core. Pieces are not in order. The core consists of dark gray (N/4), dark greenish and bluish gray (5Y4/1, 5B4/1) sandstone, containing large amounts (up to 7-8%) of terrestrial plant debris. Pieces are normally graded, either massive or parallel laminated and are carbonate cemented.

THIN SECTION SUMMARY (%):

	1,58-62 D
TEXTURE:	
Sand	80
Silt	20
COMPOSITION:	
Quartz	32
Feldspar	20
Rock Fragments	10
Mica	10
Cement-Calcite	15
Foraminifers	Tr
Plant Debris	12
Bioclasts	Tr
Micritic Intraclasts	1

PHYSICAL PROPERTIES DATA:

	1,30	1,33
V_p (a)	3.31	2.76
V_p (b)	3.91	3.22
V_p (c)	3.81	2.63
ρ_b	2.59	2.49

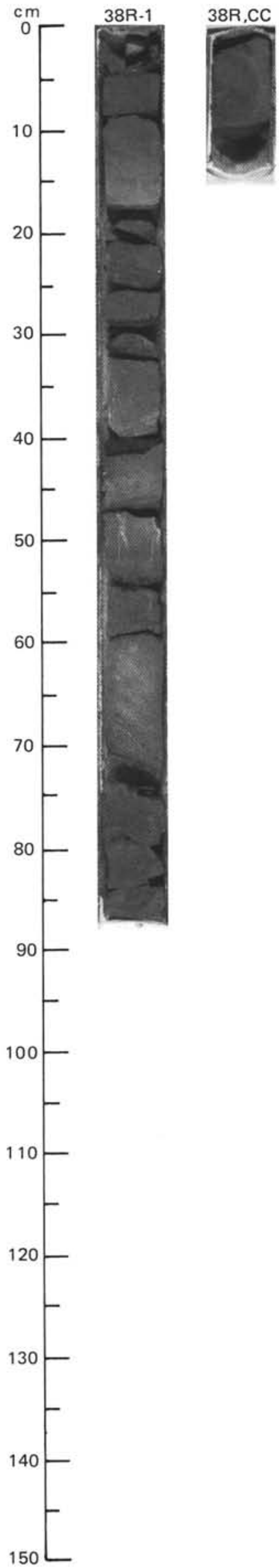
cm
38R-1
38R,CC
0
10
20
30
40
50
60
70
80
90
100
110
120
130
140
150

SITE 638 HOLE B CORE 39 R CORED INTERVAL 5026.2-5035.8 mbsl; 363.5-373.1 mbsf

TIME-ROCK UNIT	FORAMINIFERS	NANNOFOSSILS	RADIOLARIANS	DIATOMS	PALEOMAGNETICS	PHYS. PROPERTIES	CHEMISTRY	SECTION	METERS	GRAPHIC LITHOLOGY	DRILLING DISTURB.	SED. STRUCTURES	SAMPLES
LATE VALANGINIAN/EARLY HAUTERIVIAN	B	CC-3 / CC 4 a F/P	B			■	● 14 %	1 / CC					* #

LITHOLOGIC DESCRIPTION

SANDSTONE, CLAYSTONE and NANNOFOSSIL MARLSTONE

The above-mentioned lithologies are present in the 40-cm section recovered in this core. Sandstone beds are coarse grained and dark gray (N/4, 2.5Y4/1), contain terrestrial plant debris in amounts up to 8% and are carbonate cemented. They are graded and without bedding structures. It is likely that uncemented portions of sandstone beds or softer clay and marl have been largely lost during drilling as the recovery was less than 5%. Dark gray (N/4) claystone alternating with light greenish gray (5Y 6/1) nannofossil marlstone is also present.

SMEAR SLIDE AND THIN SECTION SUMMARY (%):

	1,10 M	1,14-15 M	1,19-25 D
TEXTURE:			
Sand	—	—	90
Silt	30	2	10
Clay	70	98	—
COMPOSITION:			
Quartz	10	Tr	45
Feldspar	Tr	—	15
Rock Fragments	—	—	15
Mica	15	Tr	7
Clay	49	—	—
Calcite/Dolomite	15	—	—
Cement:			
Calcite/Trace QTZ	—	—	15
Tourmaline	—	—	Tr
Opaques	1	1	—
Pyrite	1	—	—
Zircon,Rutile	Tr	—	Tr
Nannofossils	7	—	—
Fish Remains	Tr	—	—
Plant Debris	2	1	3
Bioclasts	—	Tr	—
Micrite	—	98	—

PHYSICAL PROPERTIES DATA:

	1,35
V_p (a)	4.05
V_p (b)	4.34
V_p (c)	3.87
ρ_b	2.67

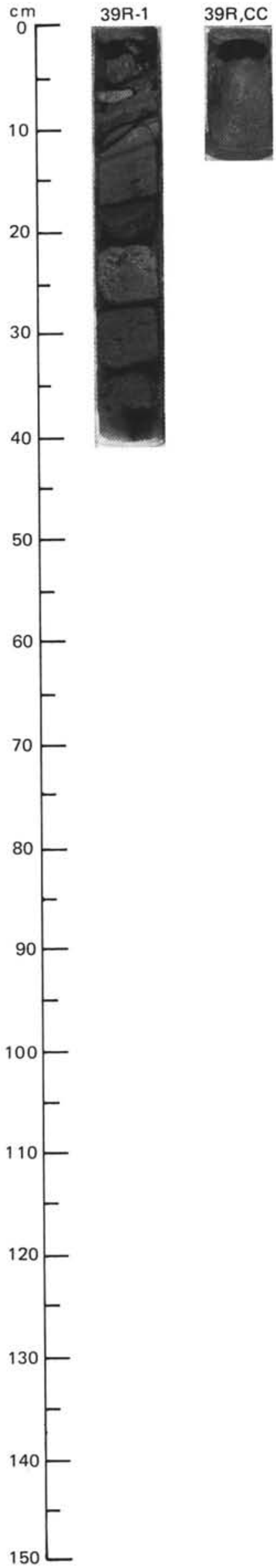
cm
39R-1
39R,CC
0
10
20
30
40
50
60
70
80
90
100
110
120
130
140
150

SITE 638 HOLE B CORE 40 R CORED INTERVAL 5035.8–5045.5 mbsl; 373.1–382.8 mbsf

TIME-ROCK UNIT	FORAMINIFERS	NANNOFOSSILS	RADIOLARIANS	DIATOMS	PALEOMAGNETICS	PHYS. PROPERTIES	CHEMISTRY	SECTION	METERS	GRAPHIC LITHOLOGY	DRILLING DISTURB.	SED. STRUCTURES	SAMPLES	LITHOLOGIC DESCRIPTION
LATE VALANGINIAN/EARLY HAUTERIVIAN	B	CC-3 / CC4 a F/M	B			■	● 17 %	1 CC						

BIOSTRAT. ZONE/ FOSSIL CHARACTER

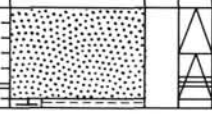

SANDSTONE and CLAYSTONE

Core 40 consists of a few pieces of coarse-grained arkosic sandstone rich in plant debris. The sandstone beds display normal grading, parallel and ripple laminae pertaining respectively to the divisions a, b, and c of the Bouma sequence. They are intercalated with gray calcareous claystone also of turbidite origin.

PHYSICAL PROPERTIES DATA:

1,53

$V\rho$ (a)	2.63
$V\rho$ (b)	1.79
$V\rho$ (c)	3.32
ρ_b	2.46

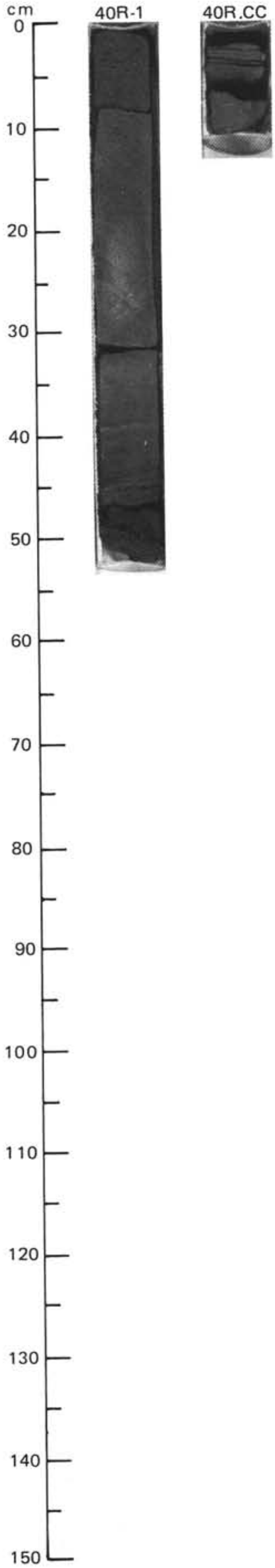
cm
0
10
20
30
40
50
60
70
80
90
100
110
120
130
140
150
40R-1
40R.CC

SITE 638 HOLE B CORE 41 R CORED INTERVAL 5045.5-5055.2 mbsl; 382.8-392.5 mbsf

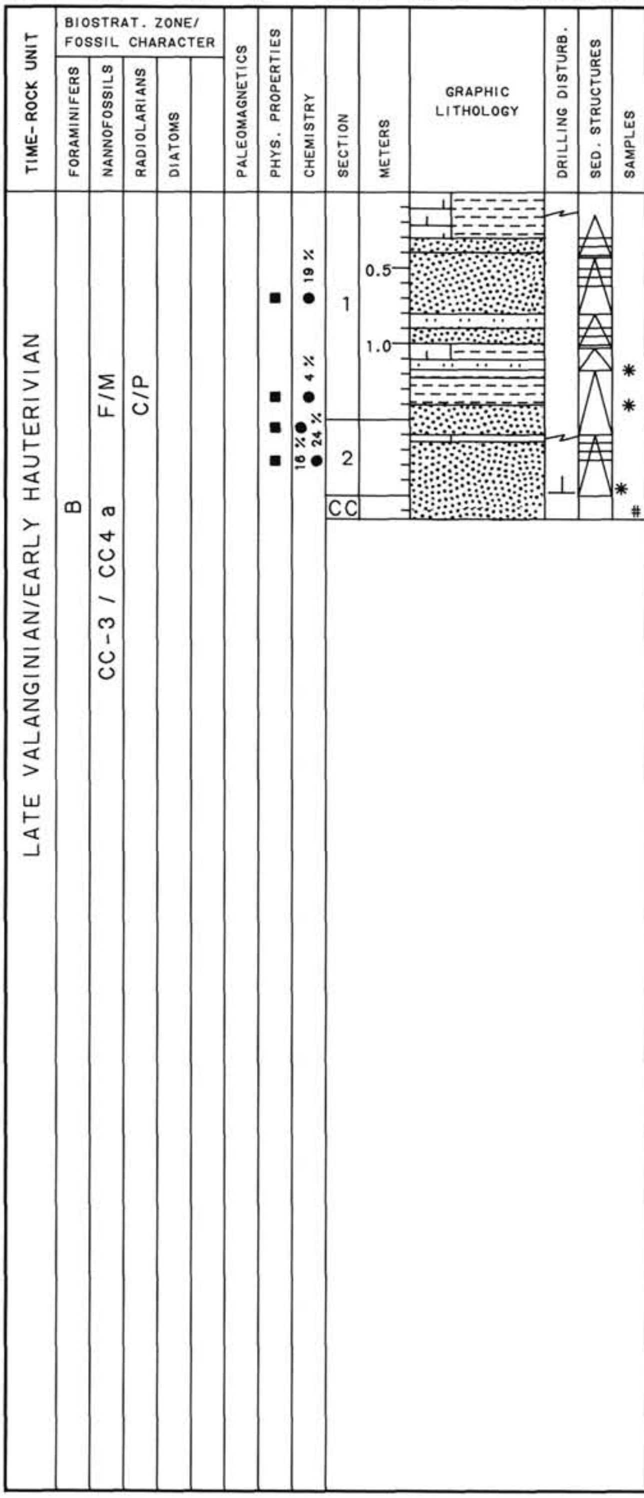

LITHOLOGIC DESCRIPTION

SANDSTONE and CLAYSTONE

This core consists of a sequence of graded sandstone beds, ranging in thickness from 30 to 50 cm. The sandstone is gray to very dark gray (5Y4/1), coarse to medium grained, and bears terrestrial plant debris in considerable amounts (up to 8%). It grades upwards to siltstone and may be capped by a relatively thin, dark gray (5Y4/1) or grayish brown (2.5Y5/2) claystone layer (Bouma sequences Td and Te). The sandstone beds are either massive (Ta) or parallel laminated (Tb) and may contain claystone clasts, a few centimeters in diameter, in their basal portions (e.g. Sample 2, 40 to 45 centimeters). Pelagic sediment is virtually absent. Recovered portions are fairly undeformed although washing of significant amounts of unconsolidated sediment (chiefly sand) is presumed because of the overall low percentage of core recovery.

SMEAR SLIDE AND THIN SECTION SUMMARY (%):

	1,119 M	1,133 D	2,44 M	CC,10-13 D
TEXTURE:				
Sand	–	–	–	100
Silt	–	23	10	–
Clay	100	77	90	–
COMPOSITION:				
Quartz	–	10	Tr	38
Feldspar	Tr	–	–	20
Rock Fragments	–	–	–	3
Mica	Tr	2	1	12
Clay	68	59	79	–
Calcite/Dolomite	Tr	10	10	–
Cement-Calcite	–	–	–	27
Accessory Minerals:				
Pyrite	Tr	1	Tr	Tr
Zircon	–	–	–	Tr
Apatite	–	–	–	Tr
Nannofossils	30	15	10	–
Plant Debris	2	3	–	–

PHYSICAL PROPERTIES DATA:

	1,71	1,135	2,5	2,28
V_p (a)	4.49	–	–	4.54
V_p (b)	4.62	–	–	4.70
V_p (c)	4.41	1.79	2.13	4.76
ρ_b	2.69	2.11	2.35	2.66

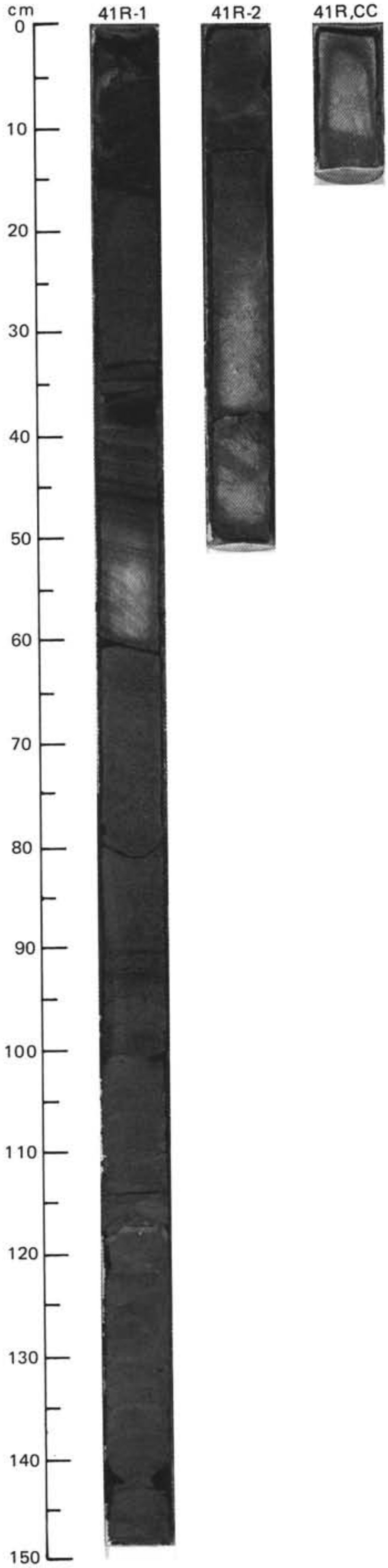
cm
0
10
20
30
40
50
60
70
80
90
100
110
120
130
140
150
41R-1
41R-2
41R,CC

SITE 638 HOLE B CORE 42 R CORED INTERVAL 5055.2-5064.9 mbsl; 392.5-402.2 mbsf

TIME-ROCK UNIT	FORAMINIFERS	NANNOFOSSILS	RADIOLARIANS	DIATOMS	PALEOMAGNETICS	PHYS. PROPERTIES	CHEMISTRY	SECTION	METERS	GRAPHIC LITHOLOGY	DRILLING DISTURB.	SED. STRUCTURES	SAMPLES
LATE VALANGINIAN/EARLY HAUTERIVIAN	B	CC-3 / CC4 a C/M	R/P			■ ■ ■ ■ ■	● 20 % ● 7 %	1 2 CC	0.5 1.0				

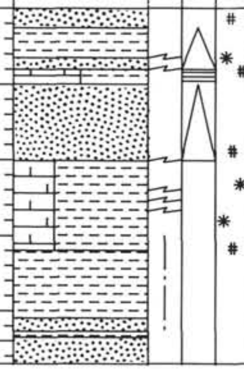

LITHOLOGIC DESCRIPTION

SANDSTONE and CLAYSTONE

This core consists of a sequence of graded sandstone beds, ranging in thickness from 30 to 50 cm. The sandstone is gray to very dark gray (5Y4/1), coarse to medium grained, and contains considerable amounts (up to 10%) of terrestrial plant debris. Sandstone beds grade upwards to siltstone and may be capped by a relatively thin, dark gray (5Y4/1) or grayish brown (2.5Y5/2) claystone layer (Bouma sequences Td and Te). Sandstone beds are either massive (Ta) or parallel laminated (Tb). Pelagic sediment is rare. Several intercalations of olive gray calcareous claystone and marlstone couplets/turbidites occur (symbols given in 'Graphic lithology' column are schematic, because thickness of couplets is too small to accurately display at this scale). Recovered portions are fairly undeformed although loss of significant amounts of unconsolidated sediment (chiefly sand) is presumed.

SMEAR SLIDE AND THIN SECTION SUMMARY (%):

	1,3-5 D	1,35 D	1,42-43 D	1,97-101 D	1,114 D	1,141 D	2,1-3 D
TEXTURE:							
Sand	75	10	–	75	–	–	5
Silt	25	35	15	25	15	20	45
Clay	–	55	85	–	85	80	50
COMPOSITION:							
Quartz	49	20	5	50	10	Tr	20
Feldspar	29	5	–	15	–	–	5
Rock Fragments	–	Tr	–	8	–	–	–
Acid Plutonic	2	–	–	–	–	–	–
Mica Schist	2	–	–	–	–	–	–
Low Grade Meta Sandstone	3	–	–	–	–	–	–
Micritic Intraclasts	1	–	5	Tr	–	–	–
Quartzite	1	–	–	–	–	–	–
Mica	4	7	1	2	3	Tr	12
Clay	–	45	35	–	61	64	20
Calcite/Dolomite	–	5	–	Tr	10	20	2
Calcite Cement	9	–	7	25	–	–	–
Accessory Minerals:							
Opaques	–	2	2	–	1	Tr	1
Zircon, Rutile, Pyrox, and Amphibole	Tr	1	–	–	Tr	–	Tr
Phosphatic Material	–	Tr	Tr	–	–	–	–
Foraminifers	–	–	–	–	–	Tr	–
Nannofossils	–	15	–	–	15	15	–
Plant Debris	–	–	10	–	–	1	20
Micrite	–	–	35	–	–	–	2

PHYSICAL PROPERTIES DATA:

	1,63	1,113	2,12	2,27	2,43
V_p (a)	4.70	–	–	1.78	–
V_p (b)	5.30	–	–	1.70	–
V_p (c)	4.76	1.71	–	1.66	–
ρ_b	2.71	2.11	–	2.14	–
T_c	–	–	3.65	–	3.78

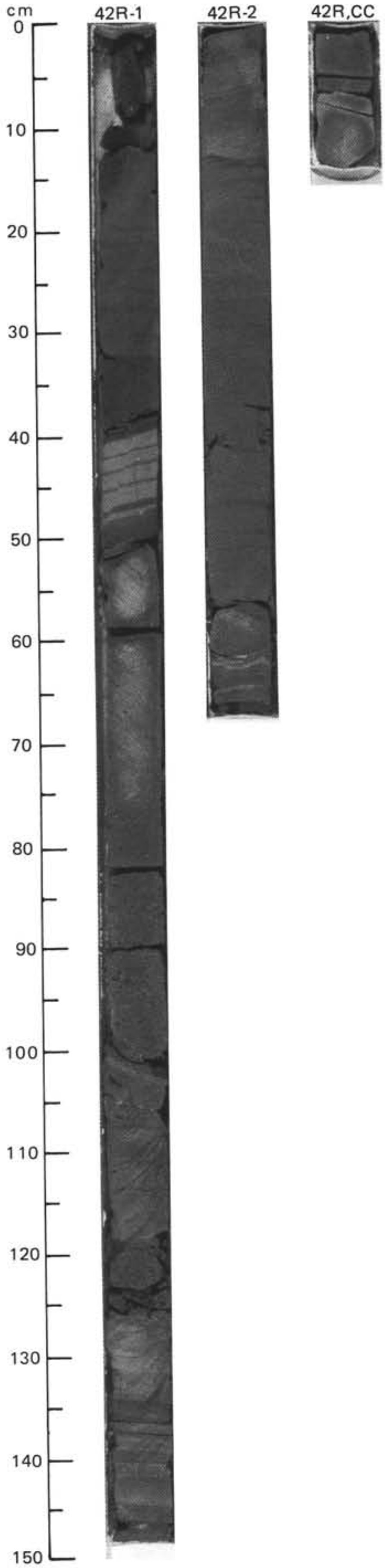
cm
42R-1
42R-2
42R,CC
0
10
20
30
40
50
60
70
80
90
100
110
120
130
140
150

SITE 638 HOLE B CORE 43 R CORED INTERVAL 5064.9- 5074.6 mbsl; 402.2-411.9 mbsf

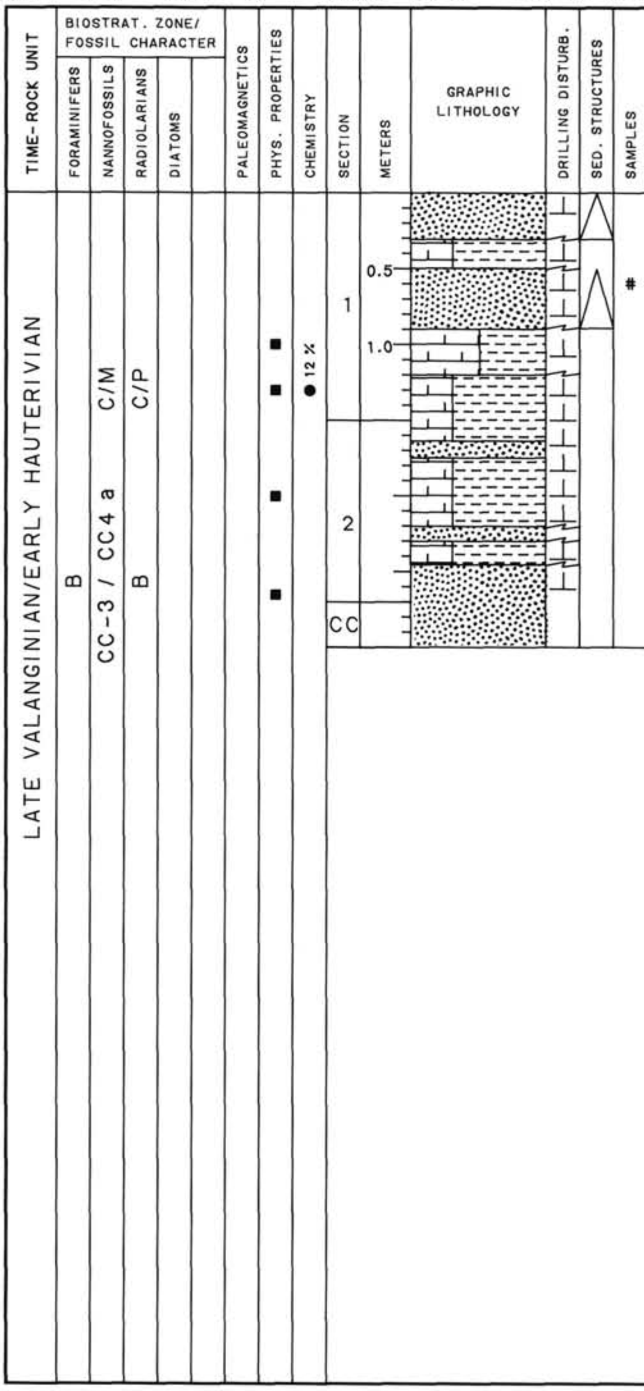

LITHOLOGIC DESCRIPTION

SANDSTONE and CLAYSTONE/MARLSTONE COUPLETS

The core consists of graded sandstone beds, ranging in thickness from 30 to 50 cm, interbedded with thin bedded gray (2.5Y5/1) claystone and light greenish gray (5Y6/1) nannofossil marlstone couplets of turbiditic origin (symbols given in 'Graphic lithology' column are schematic, because thickness of couplets is too small to accurately display at this scale). Sandstone beds are gray to very dark gray (5Y4/1), very coarse to medium grained, and contain considerable amounts (up to 10%) of terrestrial plant debris. Only cemented basal portions of the beds are recovered; these are massive (Ta) and rarely show faint parallel laminae (Tb). Recovered portions are fairly undeformed although loss of significant amounts of unconsolidated sediment (chiefly sand) is presumed.

THIN SECTION SUMMARY (%):

	1,66-70 M
TEXTURE:	
Clay	100
COMPOSITION:	
Quartz	1
Mica	Tr
Accessory Minerals:	
Pyrite	2
Organic Matter	1
Micrite	96
Bioclasts	Tr

PHYSICAL PROPERTIES DATA:

	1,100	1,131	2,50	2,116
V_p (a)	–	–	–	4.39
V_p (b)	–	–	–	4.22
V_p (c)	–	1.67	–	3.96
ρ_b	–	2.06	–	2.71
T_c	4.07	–	3.45	–

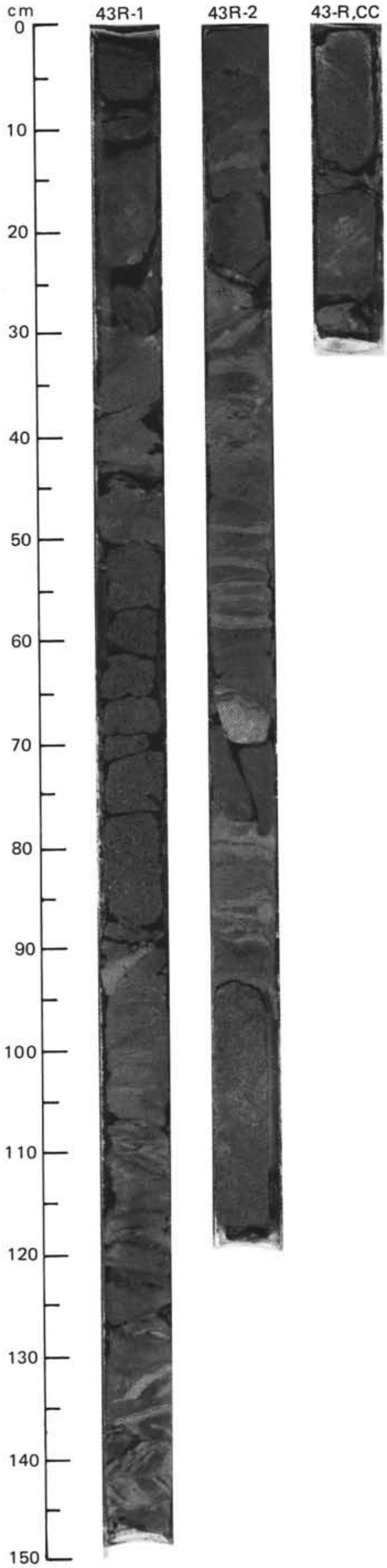
cm
0
10
20
30
40
50
60
70
80
90
100
110
120
130
140
150
43R-1
43R-2
43-R,CC

SITE 638 HOLE B CORE 44 R CORED INTERVAL 5074.6-5084.2 mbsl; 411.9-421.5 mbsf

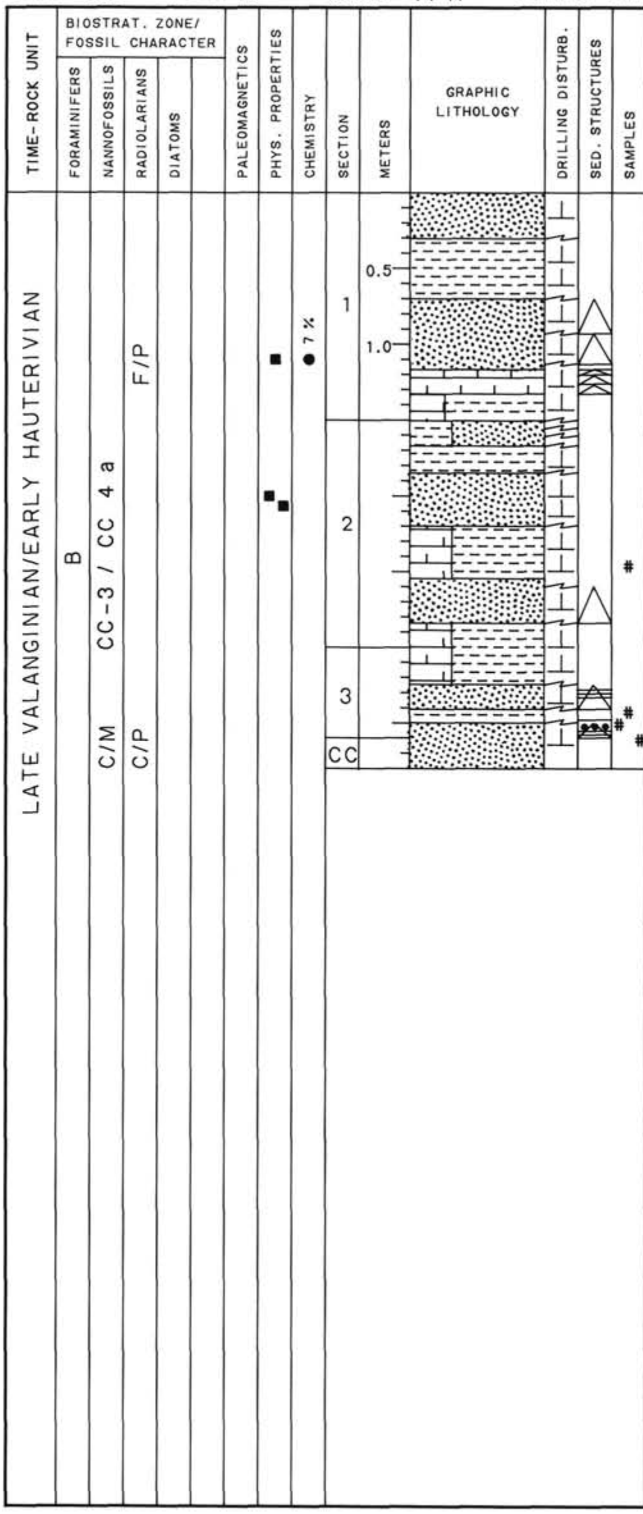

LITHOLOGIC DESCRIPTION

SANDSTONE and CLAYSTONE/MARLSTONE COUPLETS

The core consists of graded sandstone beds, ranging in thickness from 30 to 50 cm, interbedded with thin-bedded gray (2.5Y4/1) claystone and light greenish gray (5Y5/1) nannofossil marlstone couplets. (symbols given in 'Graphic lithology' column are schematic, because thickness of couplets is too small to accurately display at this scale). Sandstone beds are gray to very dark gray (N/4), very coarse to medium grained, and considerable amounts (up to 10%) of terrestrial plant debris. They are massive (Ta) of the Bouma sequence, rarely showing faint parallel laminae (Tb) and ripple laminae (Tc). Claystone rip-up clasts may be present at the base of the beds (Section 2, 0-60 cm). Most of the fine-grained divisions of major turbidite beds appear to have been washed out of the core during drilling and were not recovered.

THIN SECTION SUMMARY (%):

	2,98-102 (a)	(b)	3,51-53	3,55-57	3,59-61
	D	D	D	D	D
TEXTURE:					
Sand	–	–	90	90	90
Silt	90	90	5	10	10
Clay	10	10	5	–	–
COMPOSITION:					
Quartz	40	15	30	47	48
Feldspar	3	1	20	15	15
Rock Fragments	1	Tr	4	5	10
Mica	20	15	12	5	5
Clay	Tr	10	8	Tr	Tr
Cement Calcite	26	29	25	25	20
Accessory Minerals	Tr	Tr	Tr	–	Tr
Plant Debris	5	20	1	3	2
Micritic Intraclasts	5	10	Tr	–	–

PHYSICAL PROPERTIES DATA:

	1,111	2,49	2,56
V_p (a)	–	–	3.55
V_p (b)	–	–	3.81
V_p (c)	1.75	–	3.91
ρ_b	2.15	–	2.63
T_c	–	3.65	–

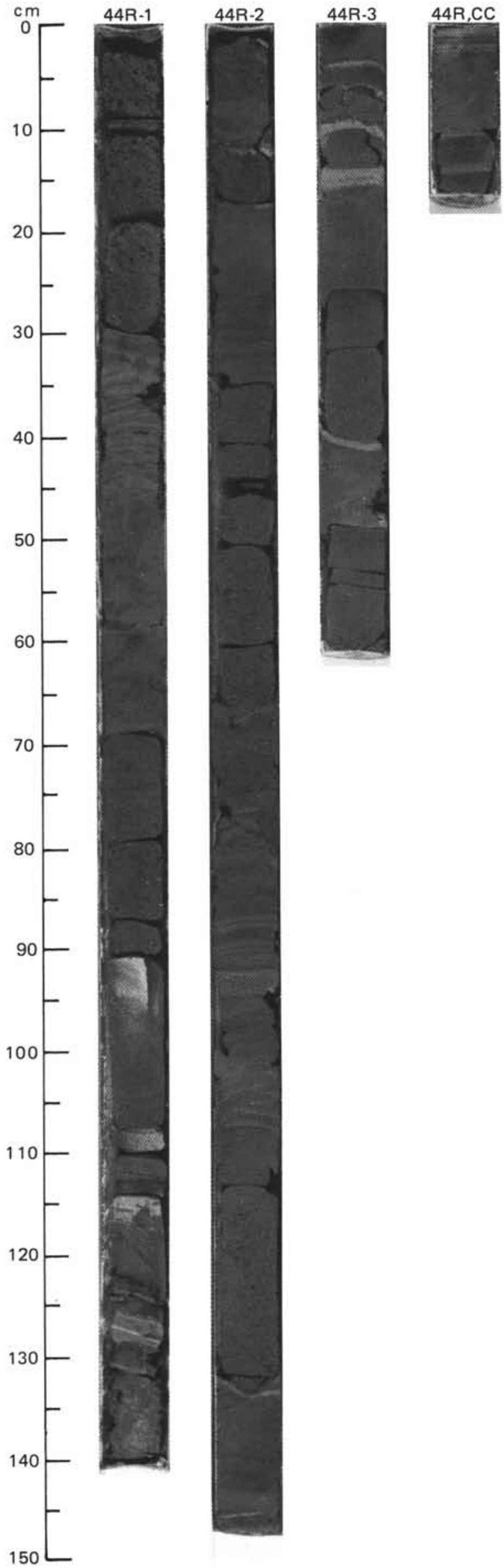
cm
0
10
20
30
40
50
60
70
80
90
100
110
120
130
140
150
44R-1
44R-2
44R-3
44R,CC

SITE 638 HOLE B CORE 45 R CORED INTERVAL 5084.2-5093.8 mbsl; 421.5-431.1 mbsf

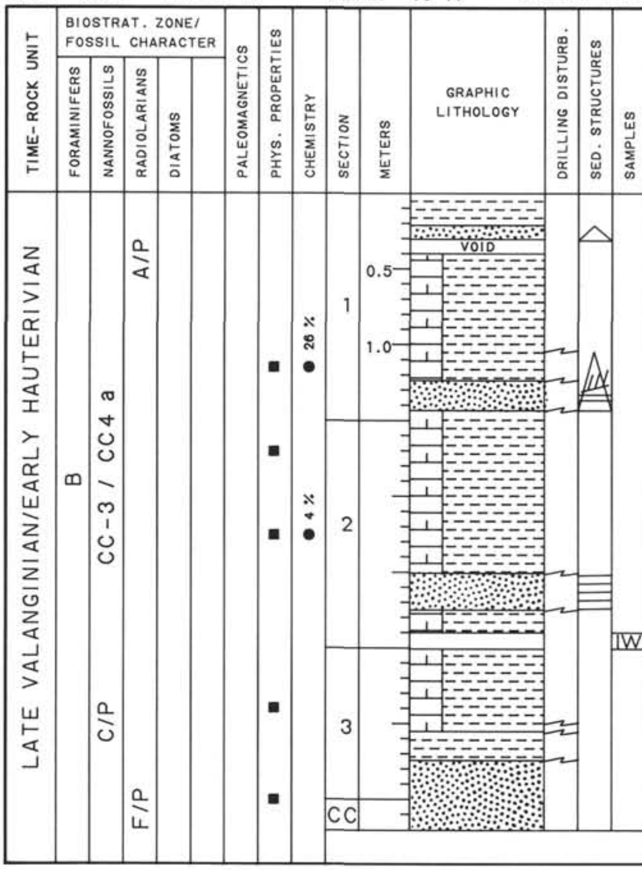

LITHOLOGIC DESCRIPTION

SANDSTONE and CLAYSTONE/MARLSTONE COUPLETS

The core consists of graded sandstone beds, ranging in thickness from 30 to 50 cm, interbedded with thin-bedded gray (2.5Y4/1, 5GY4/1) siltstone/claystone and light greenish gray (5Y5/1) nannofossil marlstone couplets (turbidites) (symbols given in 'Graphic lithology' column are schematic, because thickness of couplets is too small to accurately display at this scale). Sandstone beds are gray to very dark gray (N/4), very coarse to medium grained, and contain considerable amounts (up to 10%) of terrestrial plant debris. The sands are massive (Ta) of the Bouma sequence, rarely show faint parallel laminae (Tb) and ripple laminae (Tc). Recovered portions are fairly undeformed although loss of significant amounts of unconsolidated sediment (chiefly sand) is presumed.

PHYSICAL PROPERTIES DATA:

	1,116	2,19	2,75	3,41	3,101
Vp (a)	–	–	–	–	3.30
Vp (b)	–	–	–	–	3.38
Vp (c)	1.80	–	1.80	–	3.03
ρ_b	2.30	–	2.19	–	2.58
T_c	–	3.42	–	3.46	–

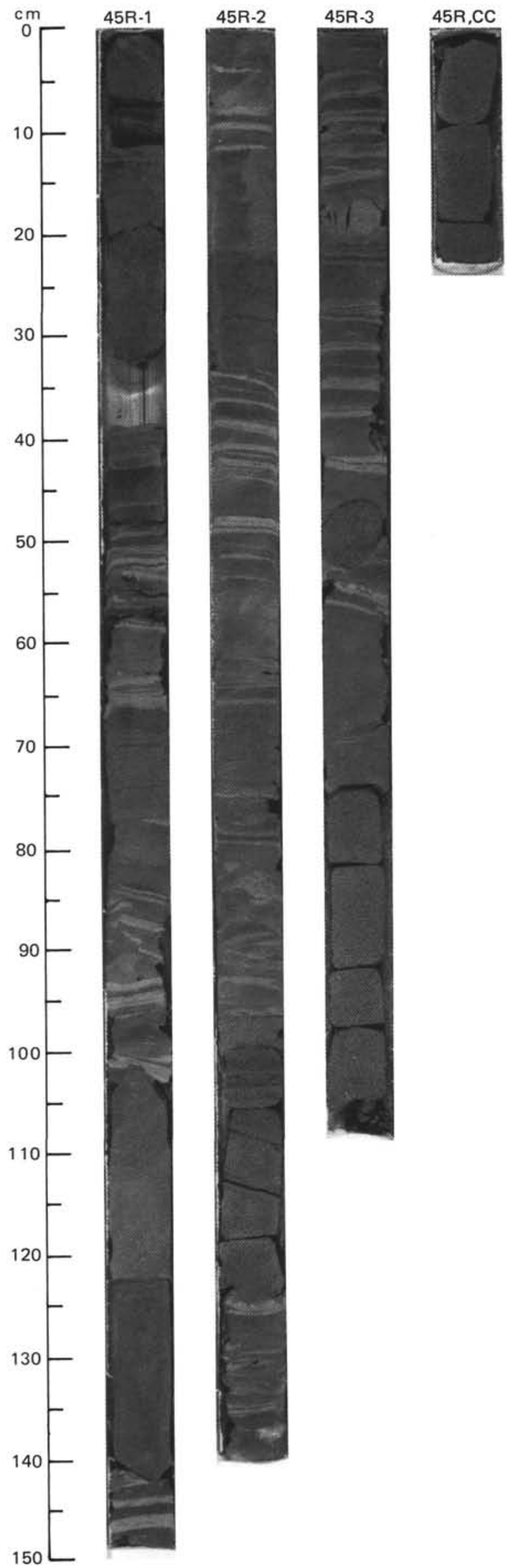
cm
0
10
20
30
40
50
60
70
80
90
100
110
120
130
140
150
45R-1
45R-2
45R-3
45R,CC

SITE 638 HOLE C CORE 1 R CORED INTERVAL 5074.4-5084.0 mbsl; 411.9-421.5 mbsf

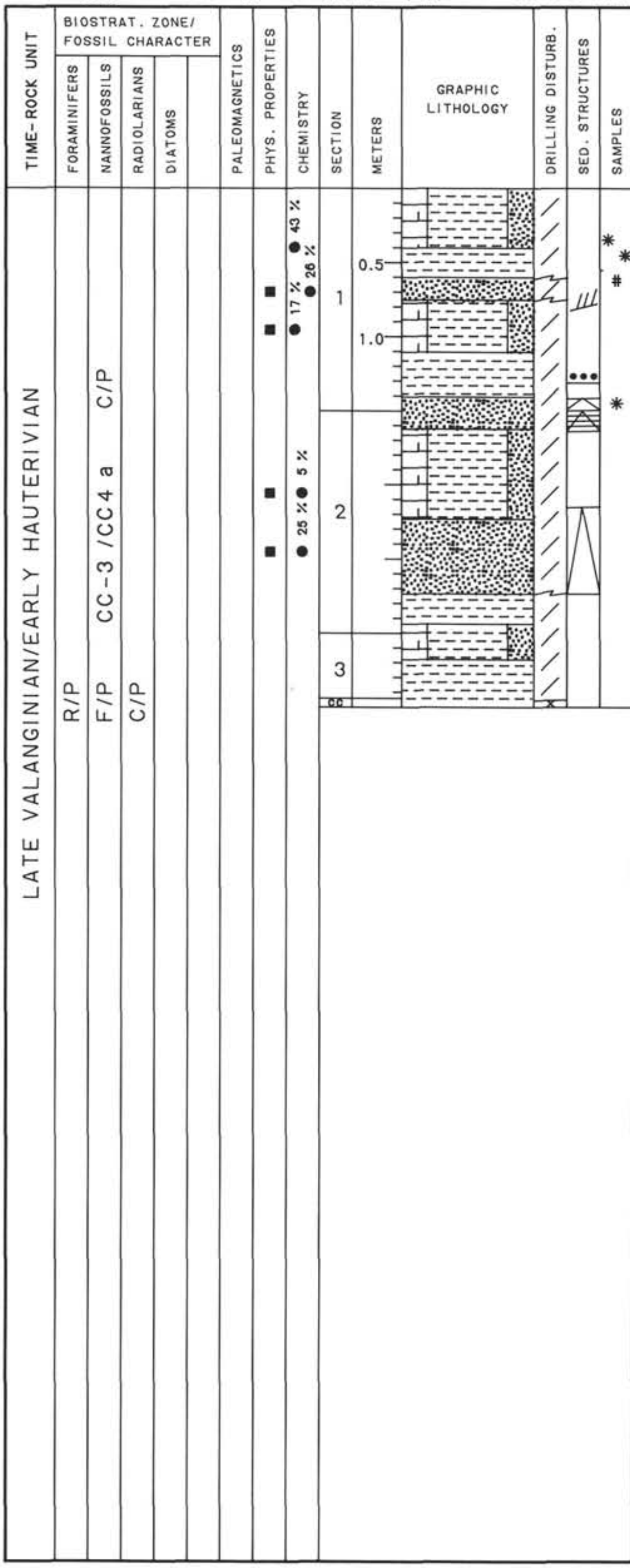

LITHOLOGIC DESCRIPTION

SANDSTONE, CLAYSTONE and MARLSTONE

This core consists of alternations of the following lithologies:

(1) Dark gray (N/4, N/5), coarse- to fine-grained arkosic sandstone, which is calcite cemented and, in places, rich in coalified wood fragments. Sandstone beds generally show normal size grading and parallel laminations (Tb of the Bouma sequence). The coarser grained sandstone beds are generally massive. Thickness varies from 20 to 40 cm.

(2) Dark gray to dark greenish gray (N/4, 5Y4/1, 5Y4/2) faintly laminated (Td) or massive (Te) claystone layers, typically from a few cm up to 20 cm thick. A silty clay horizon is commonly present at the base. Rare, light brownish gray (2.5Y5/1) siderite-rich layers, grading upwards to claystone occur in this lithology (Section 1, 56-60 cm).

(3) Light greenish and olive gray (5Y6/1, 5Y7/1 and 5Y6/2), parallel-laminated, nannofossil marlstone layers, averaging 1 cm in thickness.

Lithologies (1) and (2) are turbidites; lithology (3) is pelagic. Sandstone beds occur with a frequency of 2-3 per section and are interbedded in microturbidite sequences consisting of small-scale alternation of lithologies (2) and (3). Lithology (3) constitutes about 5-10% of the core.

SMEAR SLIDE AND THIN SECTION SUMMARY (%):

	1,40 M	1,56 D	1,26 M	1,39 M	1,142 D
TEXTURE:					
Silt	–	20	40	29	35
Clay	–	80	60	71	65
COMPOSITION:					
Quartz	Tr	10	10	–	–
Mica	–	1	1	Tr	3
Clay	–	38	52	50	53
Calcite/Dolomite	96	45	2	29	15
Accessory Minerals:					
Pyrite, Opaques	1	Tr	–	1	–
Amphibole	–	Tr	–	–	–
Zeol, Pyr, FeOx	–	–	–	–	3
Nannofossils	–	–	10	20	5
Radiolarians	Tr	Tr	–	–	–
Plant Debris	–	–	25	–	1

PHYSICAL PROPERTIES DATA:

	1,69	1,93	2,54	2,95
V_p (a)	4.20	–	–	4.24
V_p (b)	4.42	–	–	4.29
V_p (c)	4.39	1.83	1.79	4.36
ρ_b	2.78	2.67	2.17	2.64

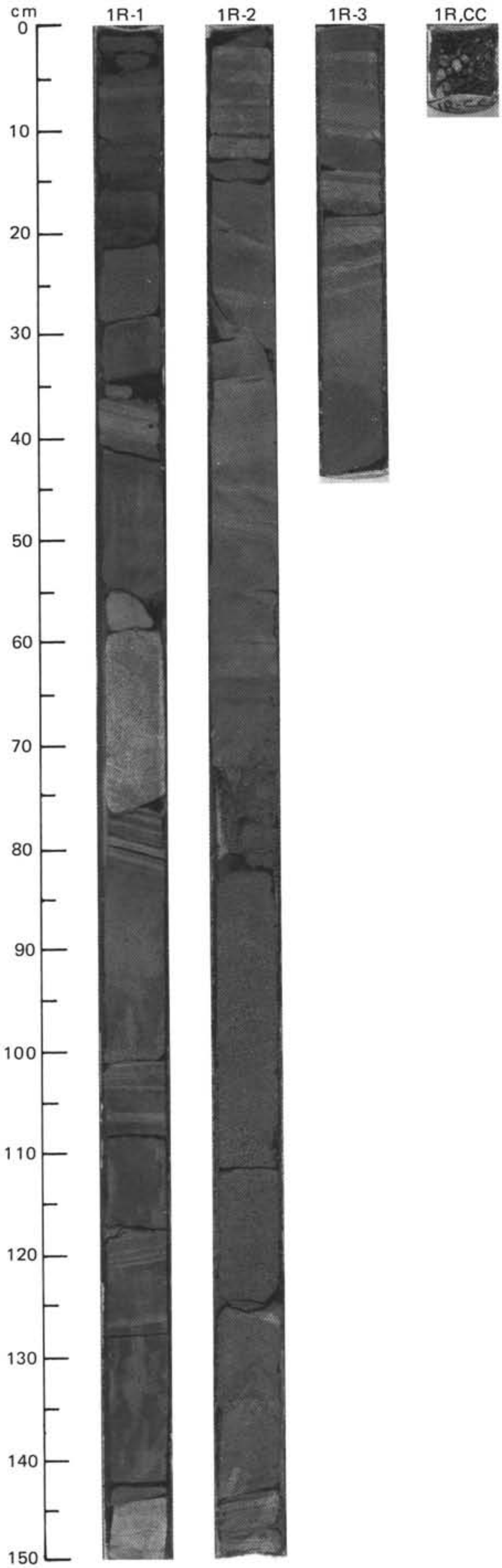
cm
0
10
20
30
40
50
60
70
80
90
100
110
120
130
140
150
1R-1
1R-2
1R-3
1R,CC

SITE 638 HOLE C CORE 2 R CORED INTERVAL 5084.0-5093.7 mbsl; 421.5-431.2 mbsf

TIME-ROCK UNIT	FORAMINIFERS	NANNOFOSSILS	RADIOLARIANS	DIATOMS		PALEOMAGNETICS	PHYS. PROPERTIES	CHEMISTRY	SECTION	METERS	GRAPHIC LITHOLOGY	DRILLING DISTURB.	SED. STRUCTURES	SAMPLES
									1			/		#

LITHOLOGIC DESCRIPTION

SANDSTONE WITH MARLSTONE

This core consists of a few unoriented pieces of dark gray (N/4),medium-grained sandstone, normally graded and faintly parallel laminated. A fragment of greenish gray (5Y5/1) nannofossil marlstone occurs in Sample 1, 6-8 cm.

THIN SECTION SUMMARY (%):

	1,4 D
TEXTURE:	
Silt	45
Clay	50
COMPOSITION:	
Quartz and feldspars	20
Mica	1
Clay	24
Micrite	50
Opaques, organic matter	5
Radiolarians	Tr

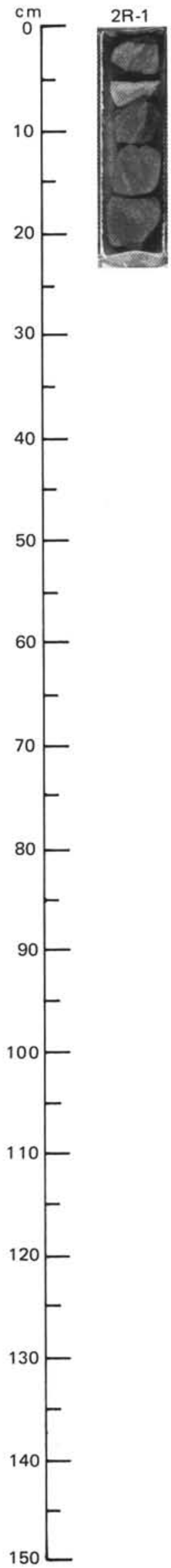
cm
2R-1
0
10
20
30
40
50
60
70
80
90
100
110
120
130
140
150

SITE 638 HOLE C CORE 3 R CORED INTERVAL 5093.7-5103.4 mbsl; 431.2-440.9 mbsf

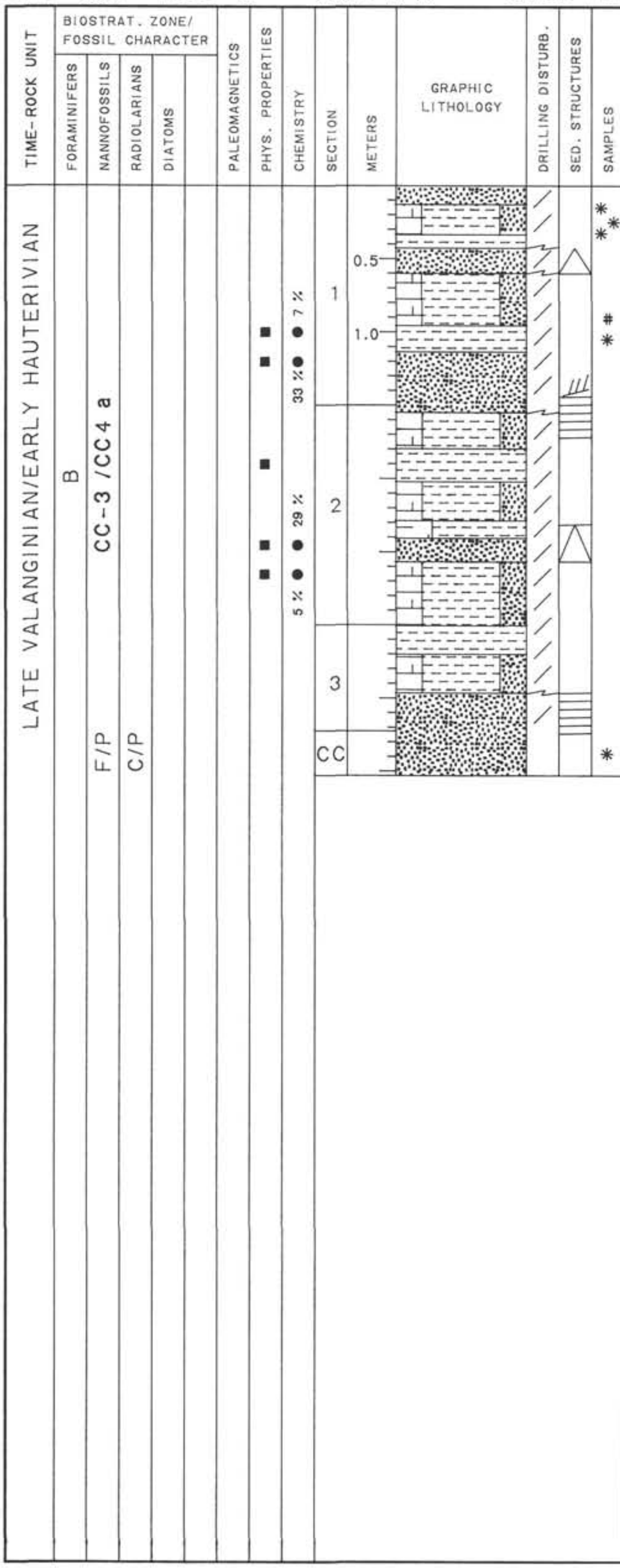

LITHOLOGIC DESCRIPTION

SANDSTONE, CLAYSTONE and MARLSTONE

This core consists of alternations of the following lighologies:

(1) Dark gray (N4/, N5/), coarse- to fine-grained arkosic sandstone, which is calcite cemented and in places rich in coalified wood fragments. Sandstone beds generally show normal size grading and parallel laminations (Tb of the Bouma sequence). Large-scale, tabular, oblique laminae, dipping 30 degrees, occur in a sandstone bed in Sample 1, 130-140 cm. Dewatering structures are present (Sample 2, 95 cm), though not common. Coarse-grained sandstone beds are generally massive. Thickness varies from 20 to 50 cm.

(2) Dark gray to dark greenish gray (N4/, 5Y4/1, 5Y4/2) faintly laminated (Td) or massive (Te) claystone layers, typically from a few to 10 cm thick. A silty claystone horizon is commonly present at the base. A few light brownish gray (2.5Y6/2), carbonate-rich microturbidite layers, occur. Planolites- and Chondrites burrows occur at several levels.

(3) Light greenish and olive gray (5Y6/1, 5Y7/1 and 5Y6/2), parallel-laminated, nannofossil marlstone layers, averaging 1 cm thick.

Lithologies (1) and (2) are turbidites; lithology (3) is pelagic. Sandstone beds occur with a frequency of 2-3 per section and are interbedded in microturbidite sequences consisting of small-scale alternations of lithologies (2) and (3). Lithology (3) constitutes about 10-15% of the core.

SMEAR SLIDE AND THIN SECTION SUMMARY (%):

	1,22 D	1,24 M	1,28 M	1,90 D	1,92 M
TEXTURE:					
Sand	3	–	–	–	–
Silt	25	–	5	–	50
Clay	72	100	95	–	50
COMPOSITION:					
Quartz	25	–	5	10	10
Mica	4	Tr	–	7	Tr
Clay	52	30	30	35	40
Calcite/Dolomite (Siderite 1,92)	Tr	1	53	38	40
Accessory Minerals:					
Pyrite, Fe oxide	1	1	1	10	–
Zircon	Tr	–	Tr	–	–
Phosph. Min.	Tr	–	–	–	–
Nannofossils	15	67	10	–	10
Radiolarians	–	–	–	Tr	–
Plant Debris	2	Tr	1	–	–
Micrite	1	–	–	–	–
Intraclasts (peloidal)	–	1	–	–	–
Spores	–	Tr	–	–	–
Bioclasts	–	–	Tr	–	–

PHYSICAL PROPERTIES DATA:

	1,99	1,119	2,40	2,98	2,119
V_p (a)	–	4.05	–	3.91	–
V_p (b)	–	4.14	–	4.17	–
V_p (c)	1.81	4.08	–	4.27	1.85
ρ_b	2.14	2.68	–	2.70	2.12
T_c	–	–	3.35	–	–

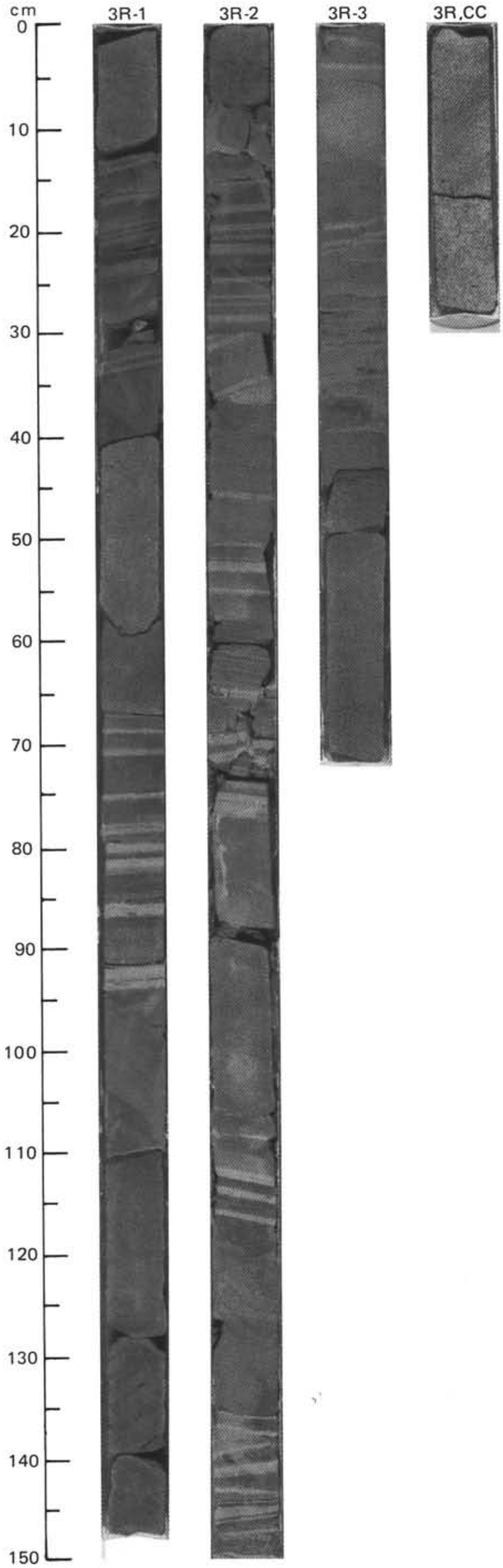
cm
0
10
20
30
40
50
60
70
80
90
100
110
120
130
140
150
3R-1
3R-2
3R-3
3R,CC

SITE 638 HOLE C CORE 4 R CORED INTERVAL 5103.4-5113.1 mbsl; 440.9-450.5 mbsf

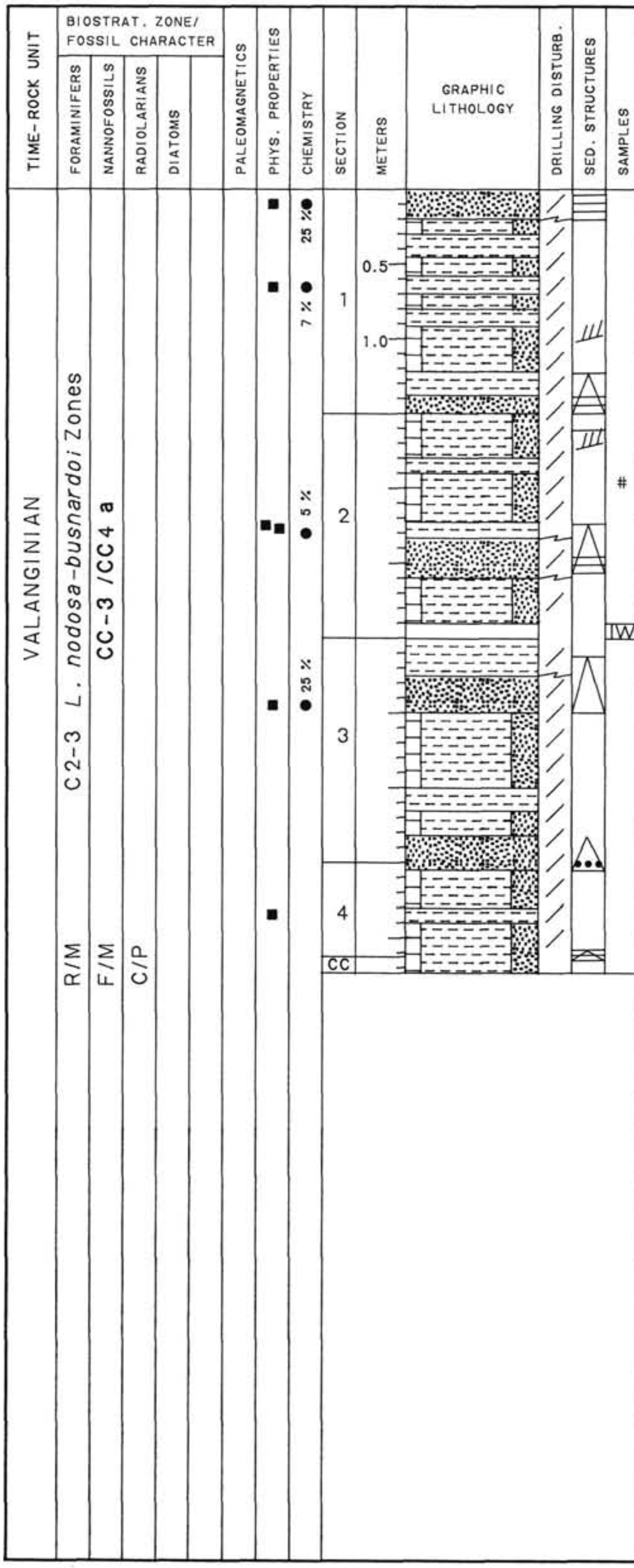

LITHOLOGIC DESCRIPTION

SANDSTONE, CLAYSTONE and MARLSTONE

This core consiste of alternations of the following lithologies:

(1) Dark gray (N4/), coarse- to fine-grained arkosic sandstone, which is calcite cemented and in places rich in coalified wood fragments. Sandstone beds generally show normal size grading and parallel laminations (Tb of the Bouma sequence) and range from 20 to 30 cm thick. The coarser grained sandstone beds are generally massive. A few layers, several centimeters thick, of fine-grained, ripple- to convolute-laminated sand occur in Sections 2 and 3 (Tc).

(2) Dark gray to dark greenish gray (N/4, 5Y4/1, 5Y4/2) faintly laminated (Td) or massive (Te) claystone layers, typically from a few to 10 cm thick. A silty clay horizon is commonly present at the base of these clay layers. Planolites and Chondrites burrows occur at several levels.

(3) Light greenish and olive gray (5Y6/1, 5Y7/1 and 5Y6/2), parallel-laminated, nannofossil marlstone layers, averaging 1 cm thick.

Lithologies (1) and (2) are turbidites, lithology (3) is pelagic. Sandstone beds occur with a frequency of 2 per section and are interbedded in microturbidite sequences consisting of small-scale alternations of lithologies (2) and (3). Normal microfaults occur at Sample 1, 121-127 cm. Lithology (3) constitutes about 10-15% of the core.

THIN SECTION SUMMARY (%):

	2,47
	D
TEXTURE:	
Silt	100
COMPOSITION:	
Quartz, feldspars	45
Mica	10
Clay and microspar	40
Accessory minerals:	
Pyrite, opaques	4
Zircon	Tr
Radiolarians	Tr
Fish remains	Tr
Plant debris	Tr
Peloid grains	Tr

PHYSICAL PROPERTIES DATA:

	1,11	1,69	2,76	2,78	3,47	4,36
V_p (a)	3.27	–	–	–	3.62	–
V_p (b)	3.10	–	–	–	3.47	–
V_p (c)	3.29	1.84	–	1.86	3.50	–
ρ_b	2.57	2.23	–	2.24	1.23	–
T_c	–	–	3.41	–	–	3.42

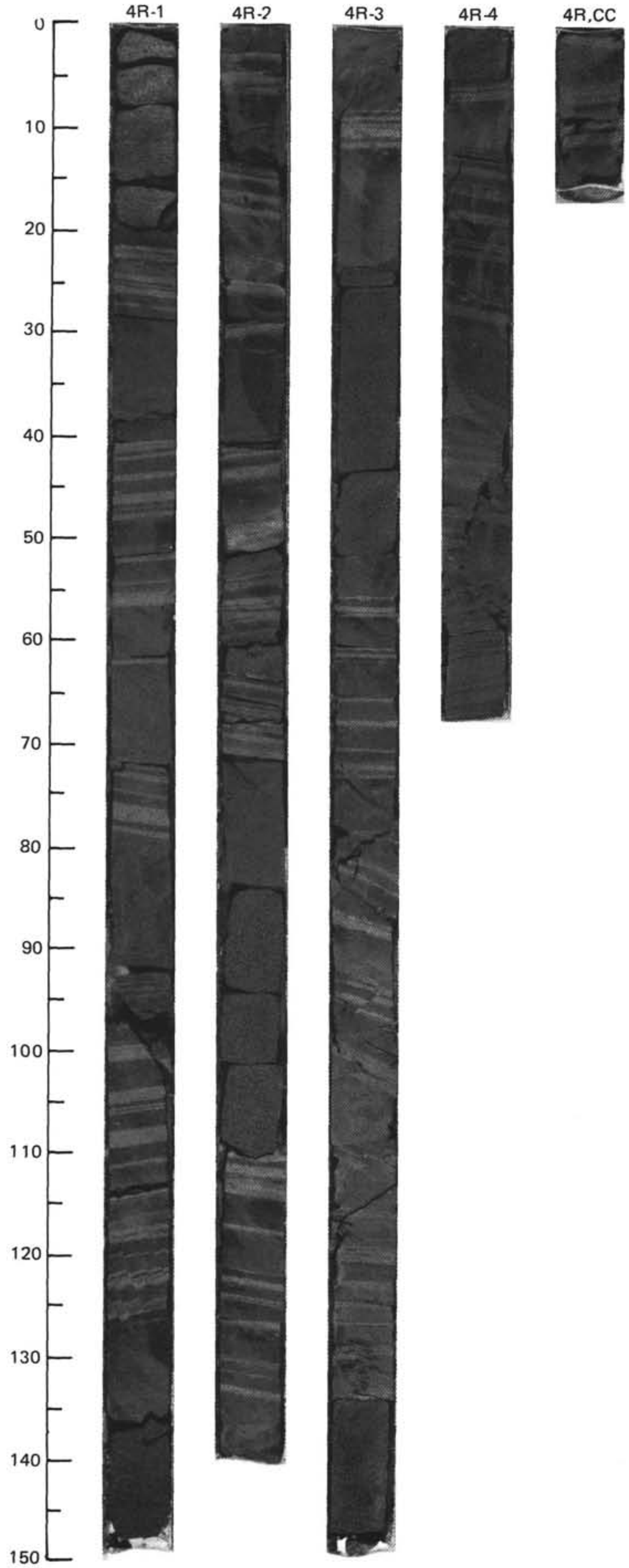
4R-1
4R-2
4R-3
4R-4
4R,CC
0
10
20
30
40
50
60
70
80
90
100
110
120
130
140
150

SITE 638 HOLE C CORE 5 R CORED INTERVAL 5113.1-5122.7 mbsl; 450.5-460.2 mbsf

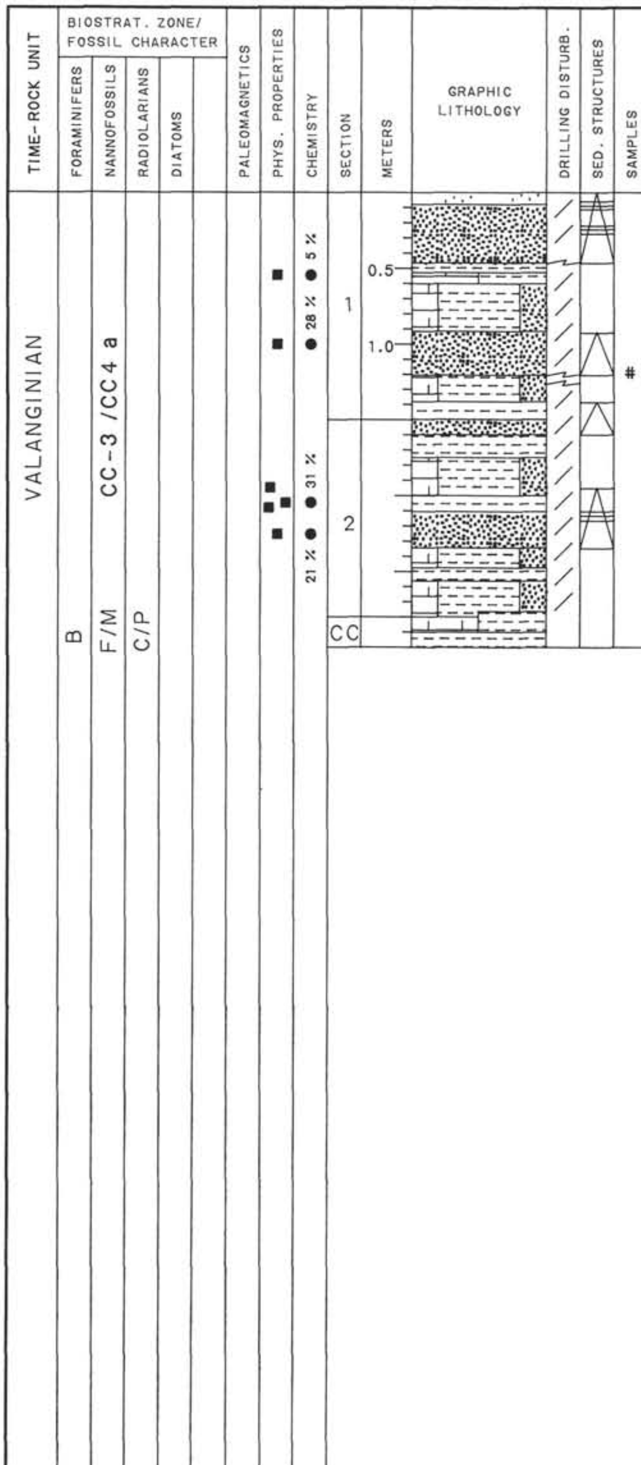

LITHOLOGIC DESCRIPTION

SANDSTONE, CLAYSTONE and MARLSTONE

This core consists of alternations of the following lithologies:

(1) Dark gray (N4/, N5/), coarse- to fine-grained arkosic sandstone, which is calcite cemented and in places rich in coalified wood fragments. Sandstone beds generally show normal size grading and parallel laminations (Tb of the Bouma sequence) at the top. The coarser grained sandstone beds are generally massive. Sandstone beds are 20 to 50 cm thick.

(2) Dark greenish gray (N4/, 5Y4/1) faintly laminated (Td) or massive (Te) claystone layers, typically from a few to 10 cm thick. A silty horizon is commonly present at the base.

(3) Light greenish gray (5Y6/1, 5Y6/2 and 5Y7/1), parallel-laminated, nannofossil marlstone layers, averaging 1 cm thick.

Lithologies (1) and (2) are turbidites; lithology (3) is pelagic. Sandstone beds occur with a frequency of 2 per section and are interbedded in microturbidite sequences consisting of small-scale alternations of lithologies (2) and (3). Lithology (3) constitutes about 10% of the core.

THIN SECTION SUMMARY (%):

	1,120 D
COMPOSITION:	
Quartz,	50
Feldspar	10
Mica	5
Calcite/Dolomite	33
Accessory Minerals:	
Opaques, pyrite	2

PHYSICAL PROPERTIES DATA:

	1,55	1,99	2,48	2,51	2,53	2,76
V_p (a)	–	4.76	–	–	–	4.47
V_p (b)	–	5.12	–	–	–	4.71
V_p (c)	1.78	4.93	–	1.98	–	4.81
ρ_b	2.18	2.63	–	2.29	–	2.69
Tc	–	–	6.70	–	4.19	–

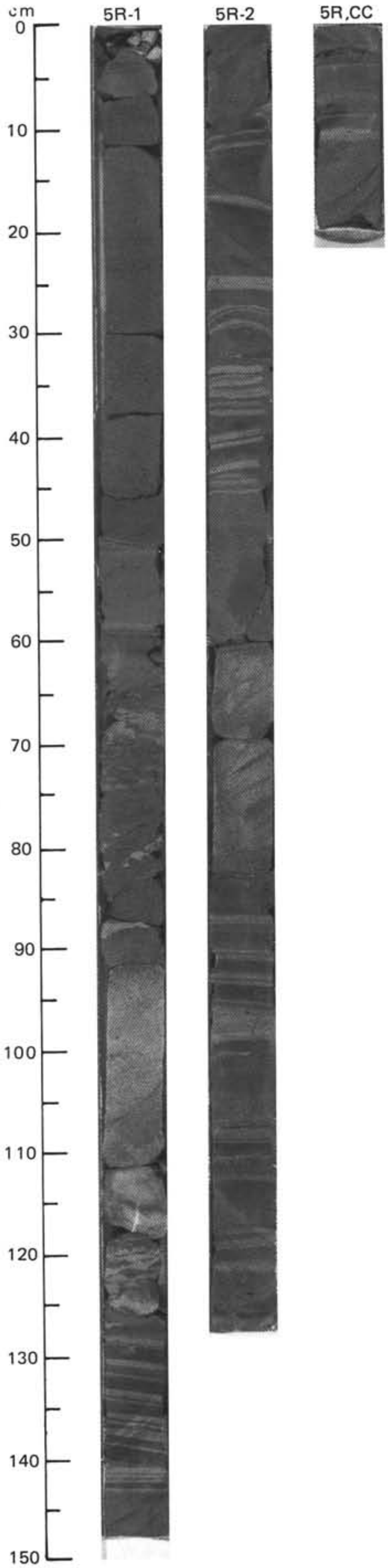
cm
5R-1
5R-2
5R,CC
0
10
20
30
40
50
60
70
80
90
100
110
120
130
140
150

SITE 638 HOLE C CORE 6 R CORED INTERVAL 5122.7-5132.4 mbsl; 460.2-469.9 mbsf

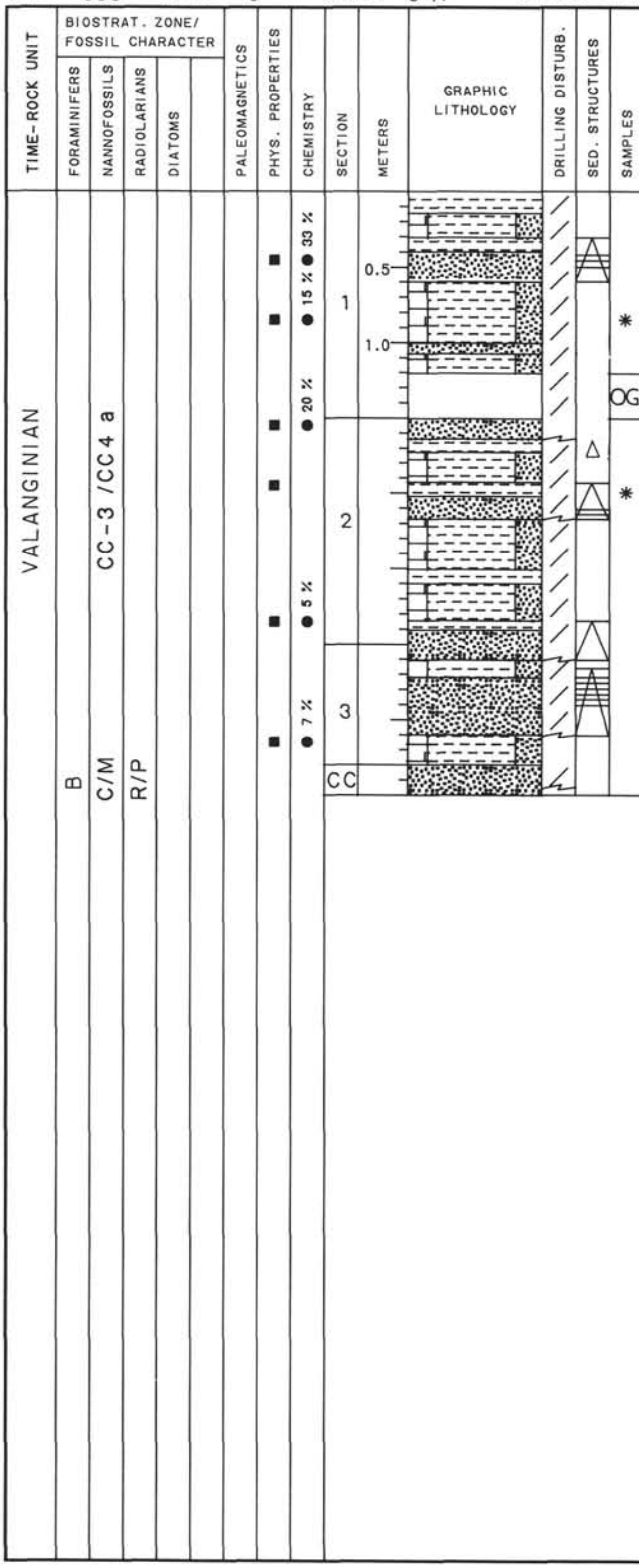

LITHOLOGIC DESCRIPTION

SANDSTONE, CLAYSTONE and MARLSTONE

This core consists of alternations of the following lithologies:

(1) Dark gray (N4/), coarse- to fine-grained arkosic sandstone, which is calcite cemented and in places rich in coalified wood fragments. Sandstone beds generally show normal size grading, parallel laminations (Tb of the Bouma sequence) and ripple laminae (Tc) at the top. The coarser grained sandstone beds are generally massive. Sandstone beds are 10 to 20 cm thick.

(2) Dark greenish gray (5Y4/1) faintly laminated (Td) or massive (Te of the Bouma sequence) claystone layers, typically from a few to 10 cm thick. A silty horizon is commonly present at the base of these layers.

(3) Light greenish gray (5Y6/1), parallel-laminated, nannofossil marlstone layers, averaging 1 cm thick.

Lithologies (1) and (2) are turbidites. Lithology (3) is pelagic. Sandstone beds occur with a frequency of 2-3 per section and are interbedded in microturbidite sequences consisting of small-scale alternations of lithologies (2) and (3). A siderite-rich layer occurs at Sample 2, 128 cm. Lithology (3) constitutes about 10-15% of the core.

SMEAR SLIDE SUMMARY (%):

	1,85	2,50
	D	D
TEXTURE:		
Silt	10	15
Clay	90	85
COMPOSITION:		
Quartz	2	10
Feldspar	–	2
Mica	–	5
Clay	40	72
Calcite/Dolomite	5	2
Accessory Minerals:		
Pyrite	2	–
Opaques+Zircon	–	1
Nannofossils	50	5
Plant Debris	Tr	3

PHYSICAL PROPERTIES DATA:

	1,45	1,83	2,3	2,44	2,134	3,66
V_p (c)	4.56	1.78	3.70	–	1.78	1.75
ρ_b	2.83	2.13	2.54	–	2.14	2.19
Tc	–	–	–	3.21	–	–

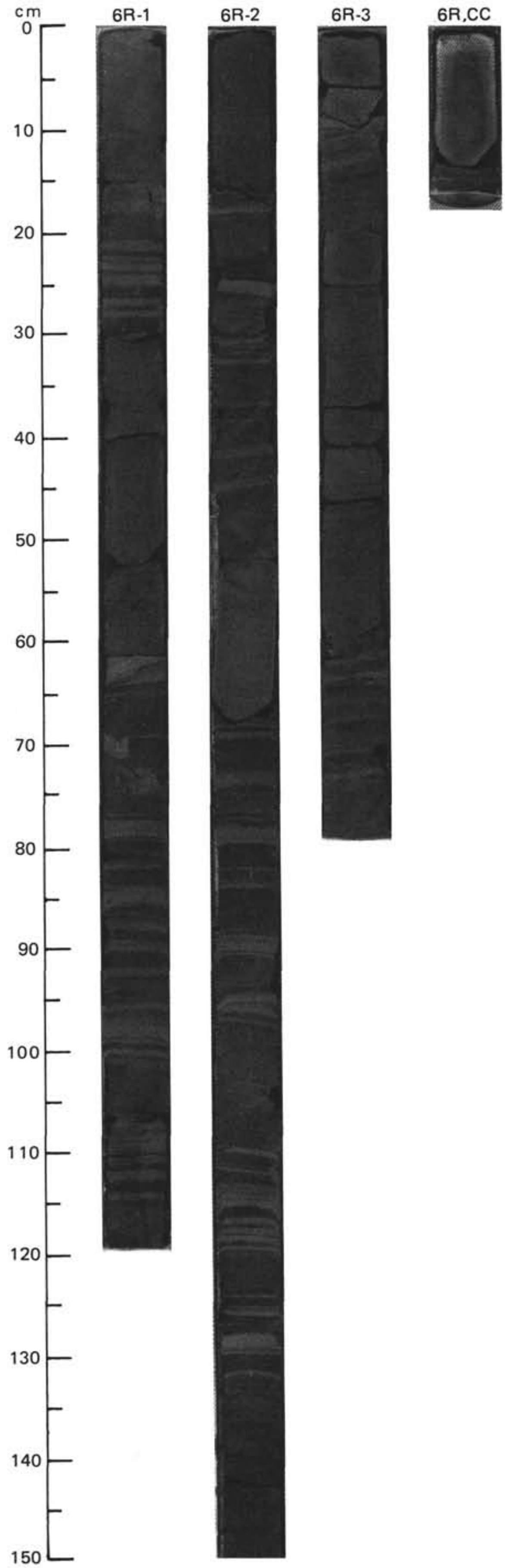
cm
0
10
20
30
40
50
60
70
80
90
100
110
120
130
140
150
6R-1
6R-2
6R-3
6R,CC

SITE 638 HOLE C CORE 7 R CORED INTERVAL 5132.4-5142.0 mbsl; 469.9-479.5 mbsf

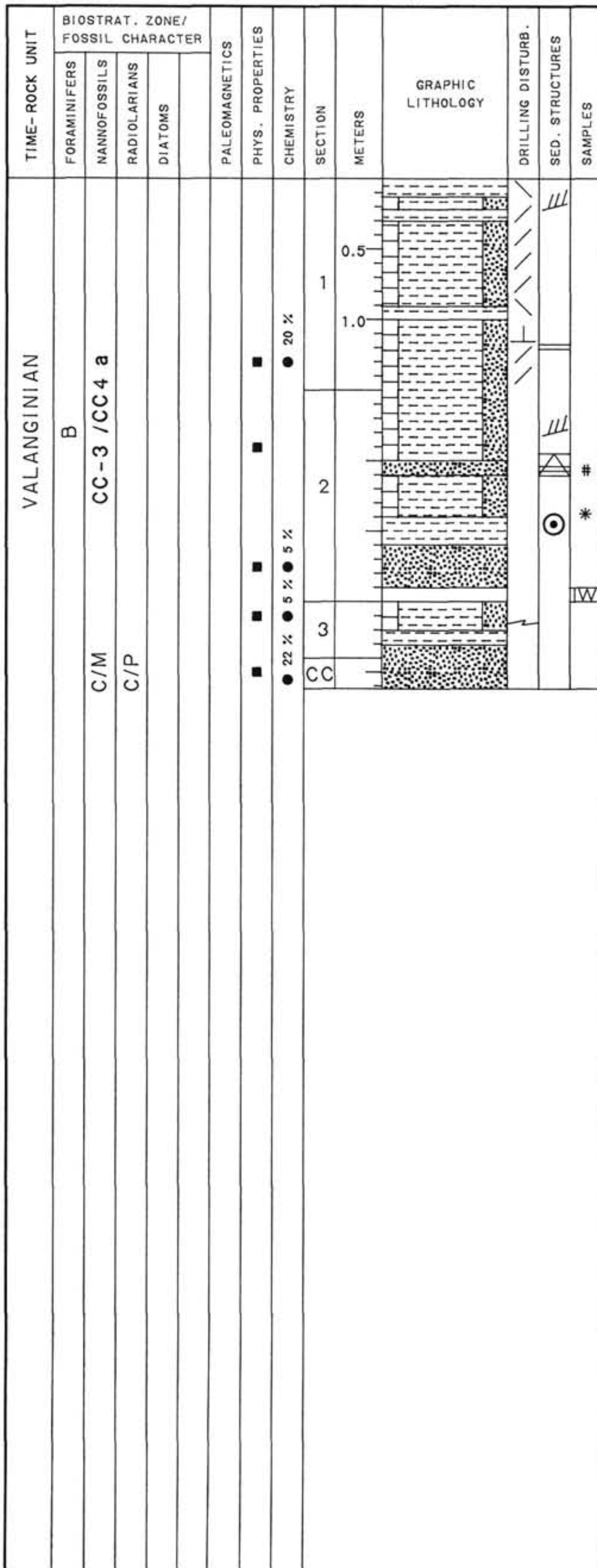

LITHOLOGIC DESCRIPTION

CLAYSTONE and MARLSTONE WITH SAND LAYERS

This core mainly consists of centimeter-scale alternations of lithologies (2) and (3):

(2) Dark gray to greenish gray (N/4, 5Y4/1) faintly laminated (Td) or base. Siderite-rich horizons at the base of claystone layers are rare; their color is olive gray (5Y5/2).

(3) Light greenish gray (5Y6/1), parallel-laminated, nannofossil marlstone layers, averaging 1 cm in thick.

Several medium- to fine-grained sand layers, poorly cemented to uncemented, a few to 20 cm thick are present. The sand is clay rich and contains wood fragments. Coarser sands are massive or parallel laminated (Ta and Tb of the Bouma sequence); finer and thinner layers show ripple and convolute laminae (Tc). Sands and sandstones correspond to Lithology (1) of the previous cores. A siderite concretionary layer, a few mm thick occur in Section 2 at 95 cm. Lithologies (1) and (2) are turbidites. Lithology (3) is pelagic. Sandstone beds occur with a frequency of 2-3 per section. Lithology (3) constitutes about 20% of the core.

SMEAR SLIDE AND THIN SECTION SUMMARY:

	2, 57 D	2, 86 M
TEXTURE:		
Sand	90	–
Silt	10	30
Clay	–	70
COMPOSITION:		
Quartz	38	2
Clay	–	2
Siderite	–	95
Nannofossils	–	Tr
Feldspar	20	–
Rock fragments	5	–
Mica	5	–
Calcite/Dolomite	30	–
Accessory minerals:		
Organic matter, coal fragment	2	–
Bioclast	Tr	–
Intraclast	Tr	–

PHYSICAL PROPERTIES DATA:

	1,127	2,37	2,126	3,10	CC,7
V_p	1.82	–	–	1.83	3.72
ρ_b	2.16	–	2.20	2.16	2.50
Tc	–	3.59	–	–	–

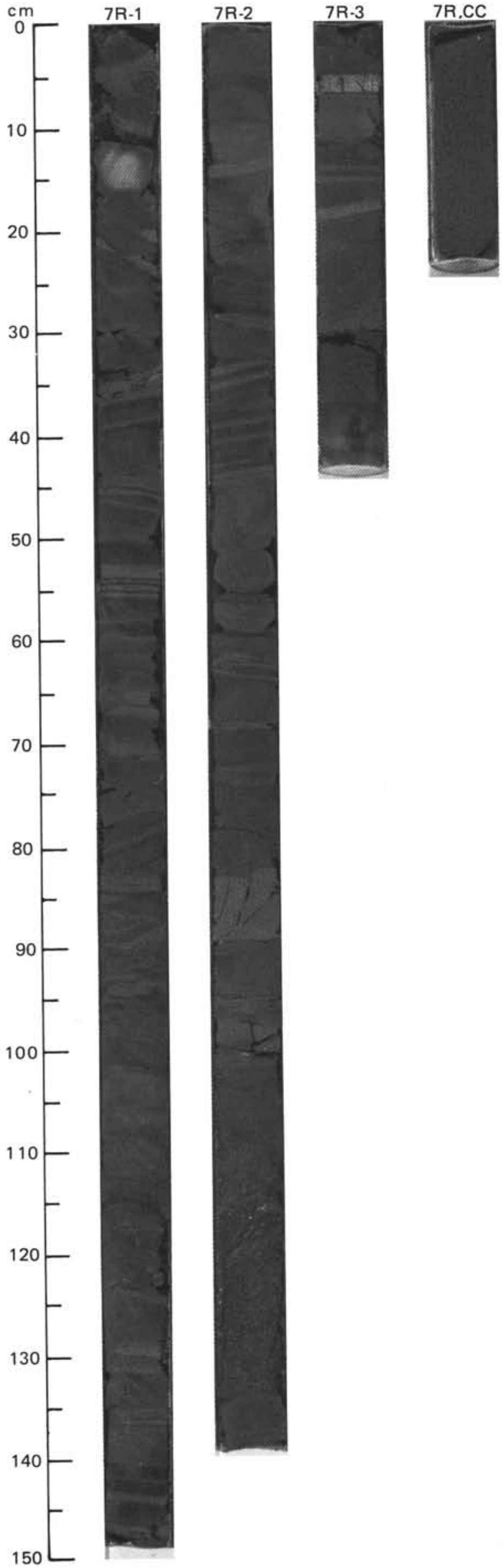
cm
7R-1
7R-2
7R-3
7R,CC
0
10
20
30
40
50
60
70
80
90
100
110
120
130
140
150

SITE 638 HOLE C CORE 8 R CORED INTERVAL 5142.0-5151.7 mbsl; 479.5-489.2 mbsf

TIME-ROCK UNIT	FORAMINIFERS	NANNOFOSSILS	RADIOLARIANS	DIATOMS	PALEOMAGNETICS	PHYS. PROPERTIES	CHEMISTRY	SECTION	METERS	GRAPHIC LITHOLOGY	DRILLING DISTURB.	SED. STRUCTURES	SAMPLES	LITHOLOGIC DESCRIPTION
VALANGINIAN	B	C/P; F/M; CC-3 /CC4 a	B			■ ■ ■ ■ ■	● 19 %; ● 64 %; ● 16 %	1; 2; CC	0.5; 1.0	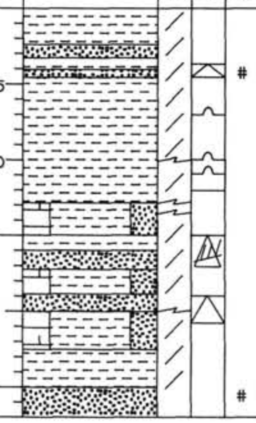			#; #	see below

SANDSTONE, CLAYSTONE and MARLSTONE

This core consists of alternations of the following lithologies:

(1) Dark gray (N4/), coarse- to fine-grained, calcite cemented, arkosic sandstone. A few laminae and a thick layer (Sample 1, 37-42 cm) contain very abundant, coarse, coalified plant debris. Sandstone beds generally show normal size grading, parallel laminations (Tb of the Bouma sequence) and, less commonly, ripple laminations (Tc) at the top. Coarse-grained to granule-sized sandstone beds (recovered in the CC) are generally massive. In Sample 2, 11-22 cm, claystone 'rip-up' clasts are present at the boundary between the massive division (Ta) and ripple-laminated division (Tc of the Bouma sequence). Sandstone beds are a few to 10 thick.

(2) Dark gray to dark greenish gray (N4/, 5Y4/1) faintly laminated (Td) or massive (Te of the Bouma sequence) claystone layers, typically from a few to 10 cm thick. A silty horizon is commonly present at the base.

(3) Light greenish gray (5Y6/1, 5Y5/1), parallel-laminated nannofossil marlstone layers, averaging 2-3 cm in thickness.

Lithologies (1) and (2) are turbidites. Lithology (3) is pelagic. Sandstone beds occur with a frequency of 2 per section and are interbedded in microturbidite sequences consisting of small-scale alternation of Lithologies (2) and (3). Slump structures are present at Sample 1, 50 to 130 cm. Light olive gray (2.5Y6/2) siderite-rich layers and nodules occur in Section 1 at 20, 50 and 90-95 cm. Lithology (3) constitutes about 5% of the core.

THIN SECTION SUMMARY (%):

	1,46	CC,8
	D	D
TEXTURE:		
Sand	–	50
Silt	5	25
Clay	95	25
COMPOSITION:		
Quartz	5	40
Feldspar	–	28
Rock Fragments	–	4
Clay	95	–
Mica	–	2
Calcite	–	25
Plant debris	1	–
Radiolarians	Tr	–
Accessory Minerals:		
Pyrite	1	–
Zeolite	Tr	–

PHYSICAL PROPERTIES DATA:

	1,53	1,142	2,27	2,48	CC,9
V_p (a)	–	–	2.49	–	3.82
V_p (b)	–	–	2.56	–	3.96
V_p (c)	–	1.88	2.64	–	3.62
ρ_b	–	2.20	2.41	–	2.68
T_c	3.63	–	–	3.81	–

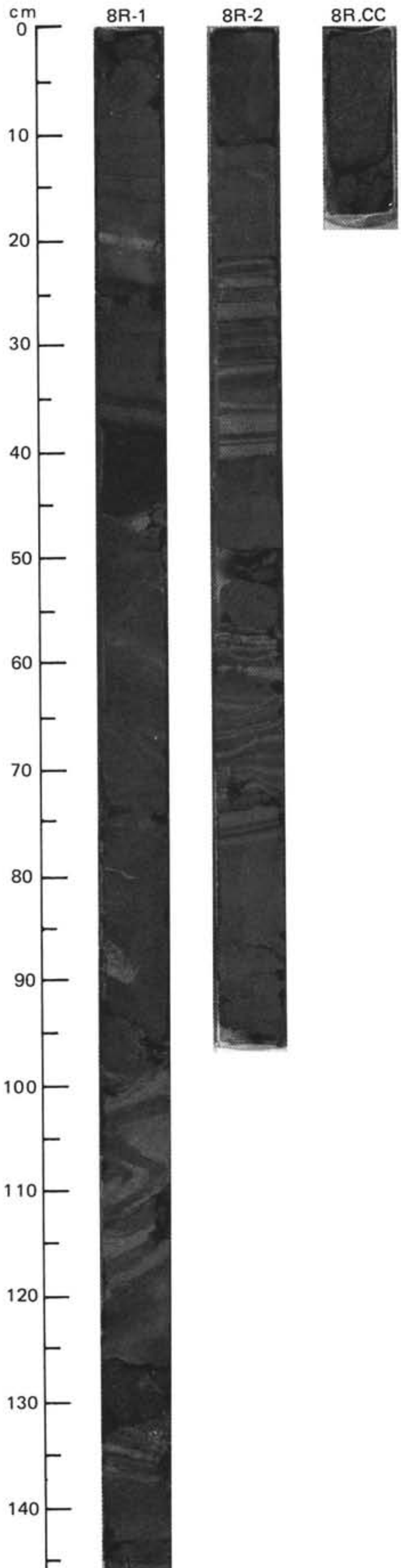
cm
0
10
20
30
40
50
60
70
80
90
100
110
120
130
140
150
8R-1
8R-2
8R,CC

SITE 638 HOLE C CORE 9 R CORED INTERVAL 5151.7-5161.4 mbsl; 489.2-498.9 mbsf

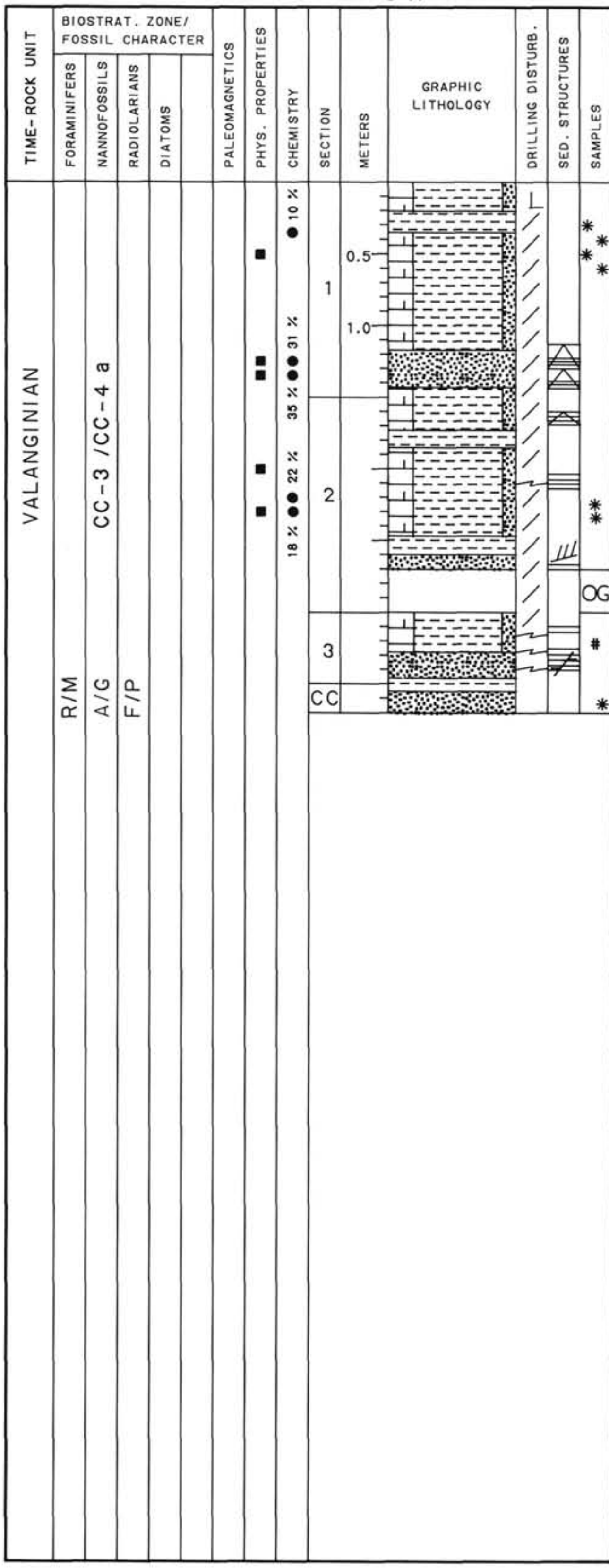

LITHOLOGIC DESCRIPTION

SANDSTONE, CLAYSTONE and MARLSTONE

This core consists of alternations of the following lithologies:

(1) Dark gray to dark greenish gray (N4/, N5/, 5Y4/1), medium- to fine-grained, calcite cemented, arkosic sandstone beds showing normal size grading, parallel laminations (Tb of the Bouma sequence) and ripple laminations (Tc) at the top. Sandstone beds, a few to 10 cm thick, show microfaults which are sealed and cut by calcite-filled veins (Section 3, 30-40 cm), and water-escape structures (Sections 2, 116-118 cm).

(2) Dark greenish gray (5Y4/1) faintly laminated (Td) or massive (Te) claystone layers, typically a few cm thick. A silty clay- or siderite-rich horizon generally occurs at the base of claystone layers.

(3) Light greenish gray (5Y6/1), parallel-laminated, nannofossil marlstone layers, averaging 1 cm in thickness, either with sharp or gradational boundaries with the underlying claystone.

Lithologies (1) and (2) are turbidites. Lithology (3) is pelagic. Sandstone beds occur with a frequency of 2-3 per section and are interbedded in microturbidite sequences consisting of small-scale alternations of Lithologies (2) and (3). Lithology (3) constitutes about 10% of the core.

SMEAR SLIDE AND THIN SECTION SUMMARY (%):

	1,31	1,33	1,48	1,55	2,73	2,79	CC,17
	D	M	M	D	D	M	D
TEXTURE:							
Sand	–	Tr	–	–	–	5	35
Silt	25	20	18	30	5	20	15
Clay	75	80	82	70	95	75	50
COMPOSITION:							
Quartz	10	12	15	8	1	7	35
Feldspar	5	–	–	2	–	–	–
Mica	2	2	10	2	–	–	Tr
Clay	76	41	55	67	35	33	25
Calcite/Dolomite	2	2	–	1	3	15	15
Accessory Minerals:							
Opaques (Pyrite +Hematite)	Tr	2	2	1	–	3	–
Phosphatic Material	–	Tr	–	–	–	–	–
Zircon, Amphibole, Rutile, Tourmaline	Tr	Tr	Tr	–	Tr	Tr	Tr
Nannofossils	1	40	15	15	60	40	25
Fish Remains	–	–	–	–	–	Tr	–
Plant Debris	4	1	3	4	1	2	–
Spores	Tr	–	–	–	–	–	–
Zeolites	–	–	–	–	Tr	–	–

PHYSICAL PROPERTIES DATA:

	1,50	1,121	1,134	2,50	2,78
V_p (a)	–	4.46	2.25	–	1.83
V_p (b)	–	5.02	–	–	–
V_p (c)	–	4.76	–	–	–
ρ_b	–	2.67	2.45	–	2.23
T_c	3.46	–	–	3.87	–

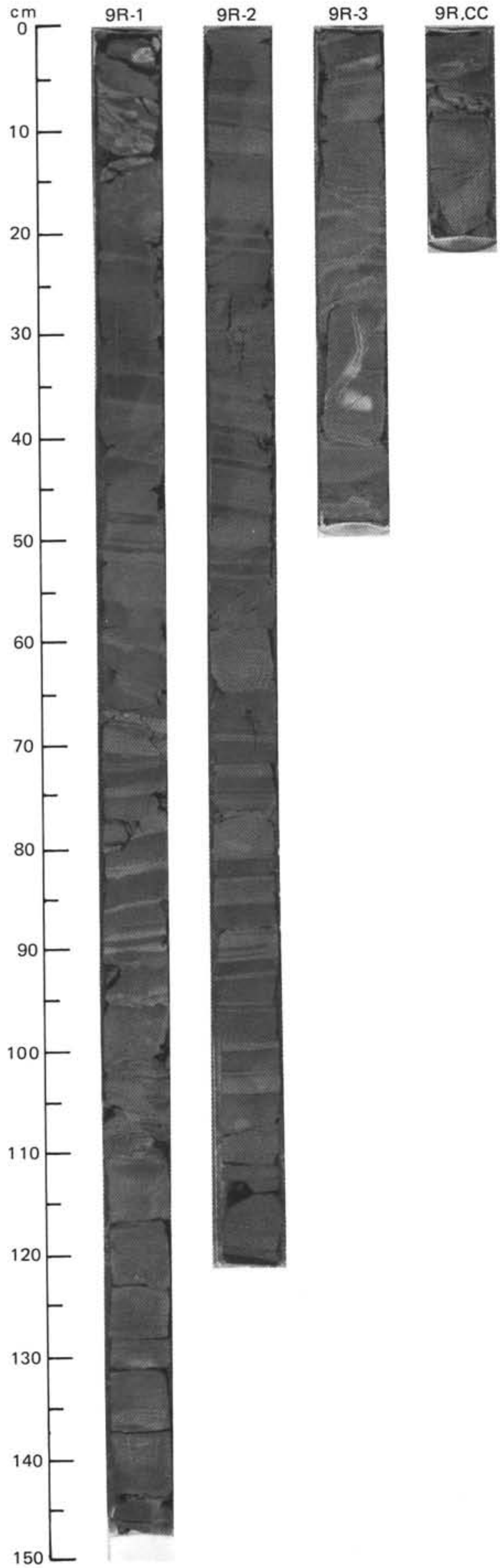
cm
0
10
20
30
40
50
60
70
80
90
100
110
120
130
140
150
9R-1
9R-2
9R-3
9R,CC

SITE 638 HOLE C CORE 10 R CORED INTERVAL 5161.4-5171.0 mbsl; 498.9-508.5 mbsf

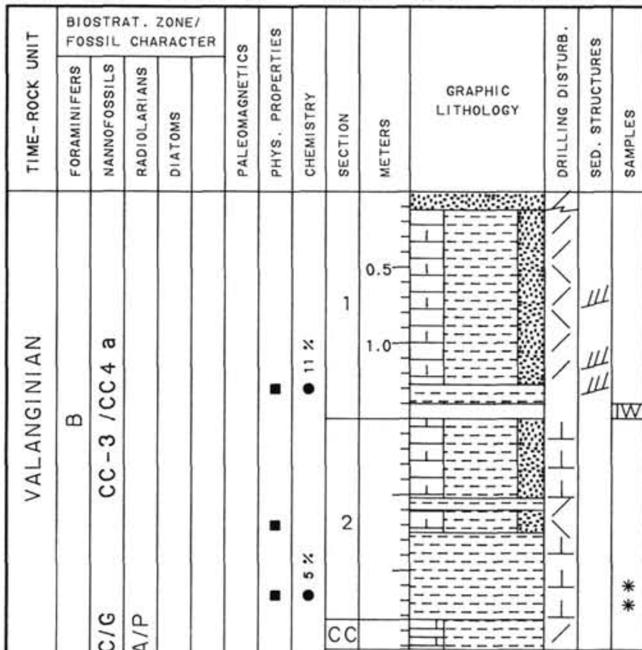

LITHOLOGIC DESCRIPTION

CLAYSTONE and MARLSTONE WITH SANDSTONE BEDS

This core consists of alternations of the following lithologies:

(1) Dark gray (N4/, N5/) medium- to fine-grained, calcite cemented arkosic sandstone beds, averaging 10 cm in thickness and showing normal size grading, a massive texture (Ta) and parallel laminations (Tb). Fine-grained, thin sandstone beds, averaging 1 cm thick, with sharp, planar boundaries and showing ripple laminae, occur in Section 1.

(2) Dark greenish gray (5Y4/1) faintly laminated (Td of the Bouma sequence) or massive (Te) claystone layers, typically a few cm thick (Section 1). In Sample 2, 40-150 cm, massive silty claystone beds averaging 20 cm thick, are present. A silty clay horizon generally occurs at the base of most beds.

(3) Light greenish gray (5Y6/1), parallel-laminated, nannofossil marlstone layers, typically averaging 1 cm thick, either with sharp or gradational boundaries with the underlying claystone.

Lithologies (1) and (2) are turbidites. Lithology (3) is pelagic. Thicker sandstone beds occur with a frequency of 1 per section and are interbedded in microturbidite sequences consisting of small-scale alternations of Lithologies (2) and (3). Lithology (3) constitutes about 10% of the core.

SMEAR SLIDE SUMMARY (%):

	2,116 D	2,133 M
TEXTURE:		
Silt	20	35
Clay	80	65
COMPOSITION:		
Quartz	3	15
Feldspar	Tr	1
Mica	10	10
Clay	75	60
Calcite/Dolomite	2	3
Accessory Minerals	1	3
Opaques	2	2
Siderite?	2	2
Nannofossils	3	3
Fish Remains	1	–
Plant Debris	1	1

PHYSICAL PROPERTIES DATA:

	1,130	2,71	2,118
V_p (a)	1.78	–	1.91
ρ_b	2.18	–	2.24
T_c	–	4.26	–

CORE 11 R NO RECOVERY

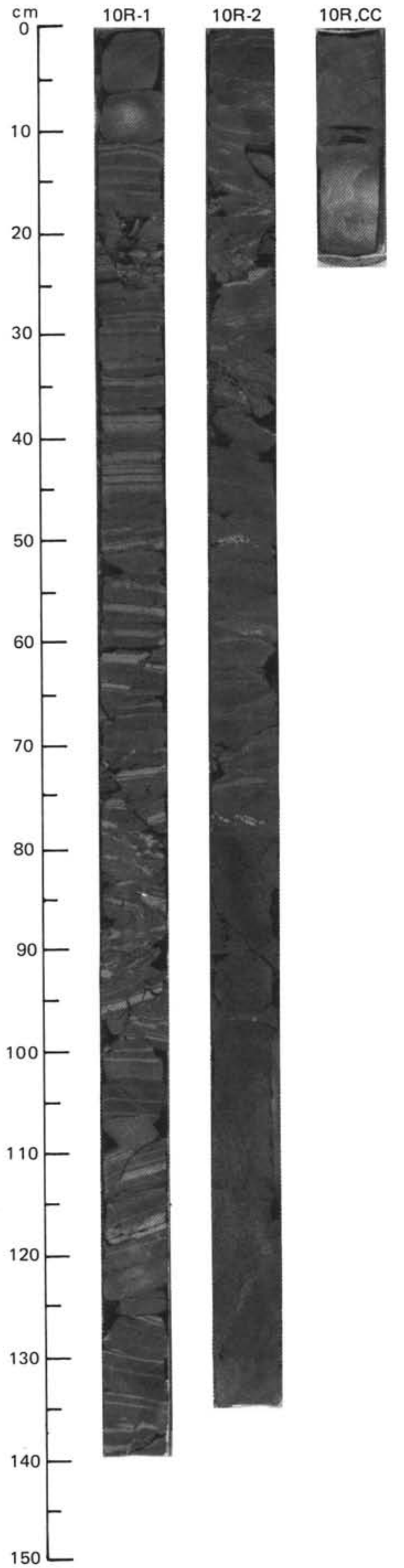
cm
0
10
20
30
40
50
60
70
80
90
100
110
120
130
140
150
10R-1
10R-2
10R,CC

SITE 638 HOLE C CORE 12 R CORED INTERVAL 5180.7-5190.4 mbsl; 518.2-527.9 mbsf

TIME-ROCK UNIT	FORAMINIFERS	NANNOFOSSILS	RADIOLARIANS	DIATOMS	PALEOMAGNETICS	PHYS. PROPERTIES	CHEMISTRY	SECTION	METERS	GRAPHIC LITHOLOGY	DRILLING DISTURB.	SED. STRUCTURES	SAMPLES
VALANGINIAN	B	CC-3 /CC-4 a F/M	B			■ ■	● 11 %	1 CC	0.5	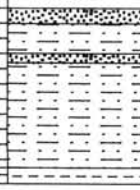			#

LITHOLOGIC DESCRIPTION

SILTY CLAY and MARLSTONE WITH SANDSTONE BEDS

The core consists of dominantly dark gray and dark greenish gray (N4/, 5Y4/1) silty clay, massive or faintly graded and ranging in thickness from a few mm up to a few cm. Silty clay beds alternate with mm-thick laminae of light greenish gray (5Y5/1), nannofossil marlstone. A few layers, up to 5 cm thick, of fine-grained, parallel- and ripple-laminated sandstone occur. A high percentage (up to 20%) of coalified plant remains occur in the sandstone and dark gray claystone.

THIN SECTION SUMMARY (%):

	1,2 D
TEXTURE:	
Silt	40
Clay	60
COMPOSITION:	
Quartz	30
Mica	10
Clay	50
Accessory minerals:	
Opaques	10

PHYSICAL PROPERTIES DATA:

	1,71	1,91
$V\rho$ (a)	–	1.84
ρ_b	–	2.17
T_c	4.24	–

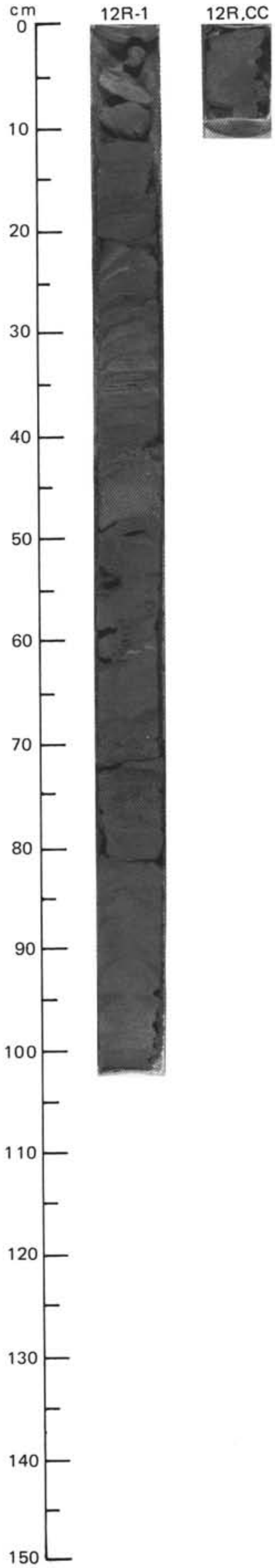
cm
0
10
20
30
40
50
60
70
80
90
100
110
120
130
140
150
12R-1
12R,CC

SITE 638 HOLE C CORE 13 R CORED INTERVAL 5190.4-5200 mbsl; 527.9-537.5 mbsf

TIME-ROCK UNIT	BIOSTRAT. ZONE/ FOSSIL CHARACTER: FORAMINIFERS	NANNOFOSSILS	RADIOLARIANS	DIATOMS	PALEOMAGNETICS	PHYS. PROPERTIES	CHEMISTRY	SECTION	METERS	GRAPHIC LITHOLOGY	DRILLING DISTURB.	SED. STRUCTURES	SAMPLES
VALANGINIAN	B	A/M CC-3 /C C-4 a B	B			■	● 5 %	1 CC					

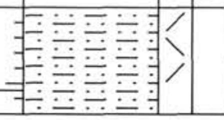

SILTY CLAY and CLAY WITH SANDSTONE BEDS

The core consists of a highly disturbed mixture of clay and silty clay, with sandy stringers and blebs. Sand ranges from medium- to fine-grained. Graded silty clay to clay layers, with thin laminations at base, are present throughout. Siderite-rich clay layers, 1-2 mm thick, light gray to pale yellow (2.5Y7/2 and 2.5Y7/4) occur at Section 1, 43, 46, 47 and 49 cm. Pyrite specks occur in the dark gray claystone.

PHYSICAL PROPERTIES DATA:

	1,36	CC,7
V_p (a)	1.97	–
ρ_b	2.21	–
T_c	–	4.30

SITE 638 HOLE C CORE 14 R CORED INTERVAL 5200-5209.7 mbsl; 537.5-547.2 mbsf

TIME-ROCK UNIT	BIOSTRAT. ZONE/ FOSSIL CHARACTER: FORAMINIFERS	NANNOFOSSILS	RADIOLARIANS	DIATOMS	PALEOMAGNETICS	PHYS. PROPERTIES	CHEMISTRY	SECTION	METERS	GRAPHIC LITHOLOGY	DRILLING DISTURB.	SED. STRUCTURES	SAMPLES
?	R/P	B	F/P			■ ■ ■ ■	● 10 % ● 28 % ● 5 %	1 2 CC	0.5 1.0				

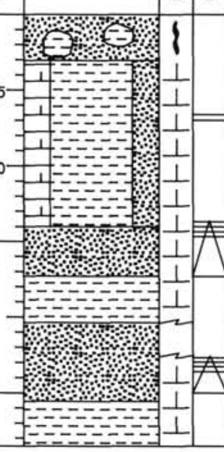

SANDSTONE, CLAYSTONE and MARLSTONE

The core consists of alternations of the following lithologies:

(1) Dark gray (N4/), either uncemented or calcite cemented, coarse- to medium-grained sandstone, massive (Ta), parallel laminated (Tb) and ripple laminated (Tc).

(2) Dark greenish gray (5Y4/1, 5Y5/1), massive and faintly laminated claystone, slightly bioturbated. Claystone layers range from a few to 6-7 cm in thickness.

(3) Thin layers (1 to 5 mm thick) of light greenish gray (5Y6/1) and olive gray (5Y6/3), laminated nannofossil marlstone. Lithologies (2) and (3) alternate at a centimeter scale in Sample 1, 40 to 120 cm and are interpreted as microturbidites. Sandstone constitutes about 25% of the core; pelagic marlstone (Lithology 3), less than 10%.

PHYSICAL PROPERTIES DATA:

	1,50	1,119	2,5	2,48
V_p (a)	–	–	4.35	–
V_p (b)	–	–	3.67	–
V_p (c)	–	1.68	4.00	1.94
ρ_b	–	2.05	2.85	2.16
T_c	3.54	–	–	–

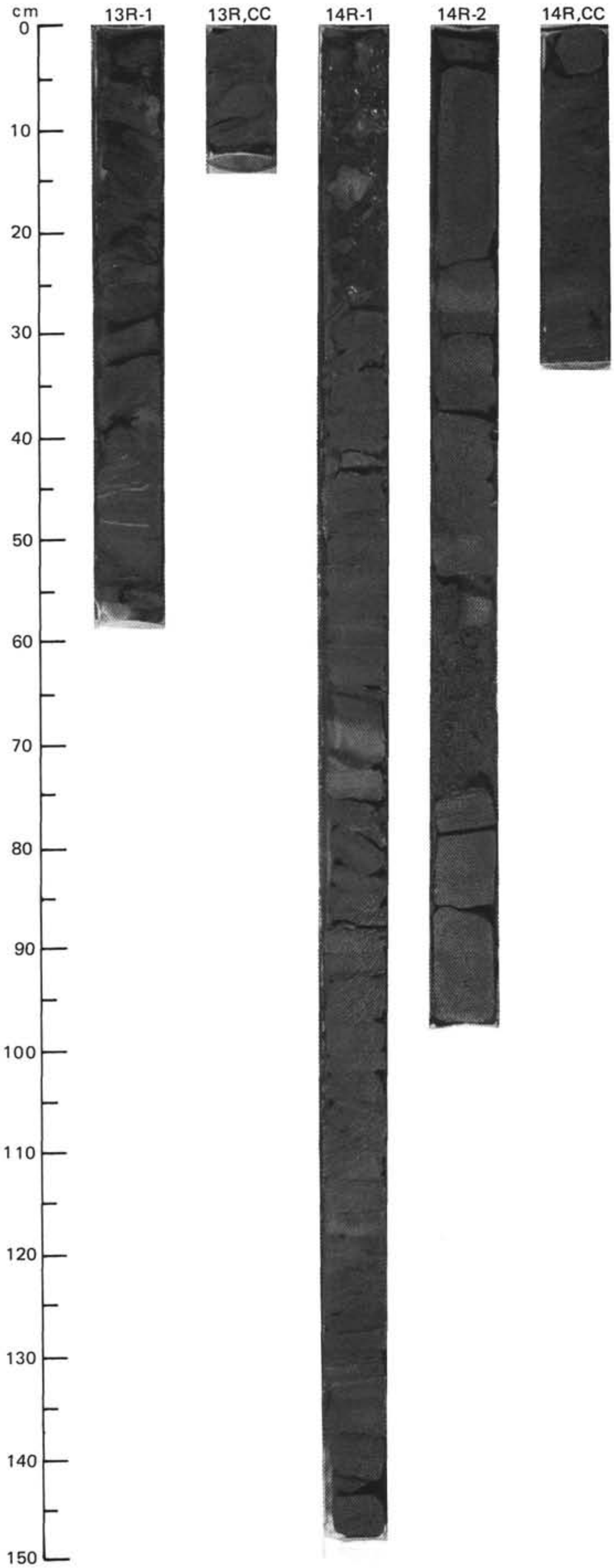
cm
13R-1
13R,CC
14R-1
14R-2
14R,CC
0
10
20
30
40
50
60
70
80
90
100
110
120
130
140
150